



**DEVELOPMENT OF NON-LINEAR BOND
STRESS-SLIP MODELS FOR REINFORCED
CONCRETE STRUCTURES IN FIRE**

By
Jamal Khalaf

A Thesis Submitted in Partial Fulfilment of the Requirements for the
Degree of Doctor of Philosophy

Department of Mechanical, Aerospace and Civil Engineering

College of Engineering, Design and Physical Sciences

Brunel University London

March 2017

DECLARATION

The work in this thesis is based upon the research carried out at the Department of Mechanical, Aerospace and Civil Engineering, Brunel University. Except where specific references have been made to the work of others, this thesis is the result of my own work. No part of this thesis has been submitted elsewhere for any other degree or qualification.

Jamal Khalaf

ACKNOWLEDGEMENT

Firstly, I would like to thank my lord Almighty Allah who helped me to finish this work.

Thanks to my supervisors Dr Zhaohui Huang and Professor Mizi Fan for their guidance, support, encouragement and patience throughout the completion of this research.

Thanks to my family especially my wonderful wife who supports me during my research, and my sons Harith and Layth and my lovely daughter Dema.

Thanks to my parents and extend my appreciation and gratitude to all my family members (brothers, sisters and all relatives).

Thanks to my friends for their support and continuous encouragement.

Gratefully acknowledges the financial support of the Ministry of Higher Education and Scientific Research of Iraqi Government for this PhD project.

PUBLICATIONS

Published Journal Papers

- [1] Khalaf J. & Huang Z. (2016). 'Behaviour of the bond between prestressed strands and concrete under fire conditions'. *Construction & Building Materials*, Volume 128, pp. 12-23.
- [2] Khalaf J., Huang Z. & Fan M. (2016). 'Analysis of bond-slip between concrete and steel bar in fire'. *Computers and Structures*, Volume 162, pp. 1-15.
- [3] Khalaf J. & Huang Z. (2017). 'Parametric study on the bond behaviour between concrete and reinforcement at elevated temperatures ' (under review).

Published Conference Papers

- [1] Khalaf, J. and Huang, Z. (2016) 'Modelling of bond-slip between prestressed strands and concrete at elevated temperatures', *9th International Conference on Structures in Fire*. Princeton, USA. 1 - 10 June.
- [2] Khalaf, J., Huang, Z. and Fan, M. (2015) 'A robust model to predict the interaction between concrete and steel bar in fire', *First International Conference on Structural Safety under Fire & Blast*. Glasgow, Scotland, UK. 2-4 September. ASRANet Ltd, pp. 538 - 549.
- [3] Khalaf, J., Huang, Z. and Fan, M. (2014) 'Modelling the bond characteristic between concrete and steel bar in fire' , *8th International Conference on Structures in Fire*. Shanghai, China. 11 - 13 June. Tongji University Press, pp. 483 - 490.

ABSTRACT

Exposure of concrete structures to high temperatures leads to significant losses in mechanical and physical properties of concrete and steel reinforcement as well as the bond characteristics between them. Degradation of bond properties in fire may significantly influence the load capacity of concrete structures. Therefore the bond behaviours need to be considered for the structural fire engineering design of reinforced concrete structures. At present, the information about the material degradations of concrete and reinforcing steel bars at elevated temperatures are generally available. However, the research on the response of the bond characteristic between concrete and reinforcing steel bar at elevated temperatures is still limited. Due to the lack of robust models for considering the influence of the bond characteristics between the concrete and steel bar at elevated temperatures, the majority of the numerical models developed for predicting the behaviour of reinforced concrete structures in fire was based on the full bond interaction. Hence, the main purpose of this research is to develop robust numerical models for predicting the bond-slip between concrete and the reinforcement under fire conditions. Therefore, the bond-slip between the concrete and reinforcement for conventional and prestress concrete structures at both ambient and elevated temperatures has been investigated in this research.

Two models have been developed in this study: the first model is to simulate the behaviour of bond-slip of deformed steel bars in normal concrete at room temperature and under fire conditions. The model is established based on a partly cracked thick-wall cylinder theory and the smeared cracking approach is adopted to consider the softening behaviour of concrete in tension. The model is able to consider a number of parameters: such as different concrete properties and covers, different steel bar diameters and geometries. The proposed model has been incorporated into the Vulcan program for 3D analysis of reinforced concrete structures in fire.

The second robust model has been developed to predict the bond stress-slip relationship between the strand and concrete of prestressed concrete structural members. In this model, two bond-slip curves have been proposed to represent the bond-slip characteristics for the three-wire and seven-wire strands. This model

considers the variation of concrete properties, strands' geometries and the type of strand surface (smooth or indented). The degradation of materials and bond characteristic at elevated temperatures are also included in the model. The proposed models have been validated against previous experimental results at both ambient and elevated temperatures and good agreements have been achieved.

A comprehensive parametric study has been carried out in this research to examine the influence of bond-slip model on the structural behaviours of normal reinforced concrete structures. The study investigated the most important factors that can affect the bond characteristics between concrete and steel reinforcement at elevated temperatures. These factors are: the concrete cover, spalling of concrete, concrete compressive and tensile strengths.

LIST OF CONTENTS

DECLARATION	i
ACKNOWLEDGEMENT	ii
PUBLICATIONS	iii
ABSTRACT	iv
LIST OF CONTENTS	vi
LIST OF FIGURES	x
LIST OF TABLES	xvii
NOTATIONS	xviii
Chapter 1 Introduction	1
1.1 Structural fire engineering	1
1.1.1 Fire curves used in structural fire engineering design	2
1.1.2 Design of structures under fire condition	6
1.2 Reinforced concrete structures and the bond between concrete and reinforcement in fire	8
1.3 Research background	10
1.4 Research objectives	13
1.5 Outline of the thesis.....	15
Chapter 2 Literature review on the bond behaviour under fire conditions	17
2.1 Introduction	17
2.2 Mechanism of bond stress-slip in reinforced concrete	18
2.2.1 Bond mechanism for normal reinforced concrete.....	18
2.2.2 Bond mechanism for prestressed concrete.....	21
2.3 Factors affecting on the bond behaviour	25
2.3.1 Effect of concrete on the bond behaviour	25
2.3.2 Effect of reinforcement on the bond behaviour	26
2.3.3 Effect of the environment on the bond behaviour	27
2.4 Design codes related to the bond of reinforced concrete	28
2.5 Effect of high temperatures on the properties of reinforced concrete structures	30

2.5.1 The properties of concrete at elevated temperatures	31
2.5.1.1 Thermal properties of concrete	31
2.5.1.2 Mechanical properties of concrete	33
2.5.2 The properties of reinforcement (steel bar and strand) at elevated temperatures	36
2.5.2.1 Thermal properties of reinforcement	36
2.2.2.2 Mechanical properties of reinforcement	37
2.5.3 The bond behaviour at elevated temperatures	39
2.6 Finite element method	47
2.6.1 Modelling the structures under fire conditions	47
2.6.2 Introduction to software VULCAN	48
2.7 Conclusion	51
Chapter 3 Analysis of bond-slip between concrete and steel bar in fire	52
3.1 Introduction	52
3.2 Analytical model	54
3.2.1 Uncracked stage	56
3.2.2 Partly cracked stage	57
3.2.3 Entirely cracked stage	61
3.3 Incorporated bond stress–slip model into Vulcan software	65
3.4 Validations	69
3.4.1 Validations of the bond stress–slip model	69
3.4.1.1 Bond stress–slip curve at ambient temperature	69
3.4.1.2 Bond stress–slip curve at elevated temperatures	73
3.4.2 Validations of the bond-link element with new developed bond stress–slip model	78
3.4.2.1 Modelling pull-out test at ambient temperature	78
3.4.2.2 Modelling simply supported RC beam at ambient temperature	81
3.4.2.3 Modelling fire tests of RC beams	83
3.5 Conclusions	89
Chapter 4 Behaviour of the bond between prestressed strands and concrete in fire	90

4.1 Introduction	90
4.2 Analytical model	92
4.3 Effect of elevated temperatures on the bond strength	100
4.4 Incorporating the bond stress-slip model into Vulcan software.....	102
4.5 Validations.....	105
4.5.1 Bond stress–slip curve at ambient and elevated temperatures.....	105
4.5.1.1 Transfer and flexural bonds at ambient temperature.....	105
4.5.1.2 Bond stress–slip for seven-wire smooth and indented strands at ambient temperature.....	106
4.5.1.3 Bond stress–slip for three-wire indented and smooth strands at ambient temperature.....	108
4.5.1.4 Bond stress–slip curves at elevated temperatures	110
4.5.2 Structural behaviour of prestressed concrete members	111
4.5.2.1 Modelling of simply supported PC beams at ambient temperature .	111
4.5.2.2 Modelling fire tests of simply supported PC slabs	115
4.6 Conclusions	122
Chapter 5 Parametric study on the bond behaviour at elevated temperatures	
.....	123
5.1 Introduction	123
5.2 Modelling background	124
5.3 Modelling isolated simply supported reinforced concrete beam.....	128
5.3.1 Yielding effect of reinforcing steel bars on the bond behaviour	130
5.3.2 The effect of concrete cover on the bond behaviour	132
5.3.3 The effect of concrete spalling on the behaviour of the beam.....	140
5.3.4 The effect of concrete strength on the bond	145
5.4 Modelling isolated simply supported reinforced concrete slab.....	149
5.4.1 The effect of concrete cover on the behaviour of the slab.....	150
5.4.2 The effect of concrete strength on the behaviour of the slab.....	155
5.5 Modelling of reinforced concrete frame structure in fire	159
5.6 Conclusions	163
Chapter 6 Conclusions and recommendations for future works.....	165

6.1 Summary of thesis contributions	165
6.1.1 Development of a robust model to simulate the bond stress-slip between concrete and steel bars at elevated temperatures.....	165
6.1.2 Development of a new model to simulate bond stress-slip between the concrete and prestressed strands in fire.....	166
6.1.3 Parametric study on the bond behaviour at elevated temperatures.....	166
6.2 Conclusions	167
6.3 Recommendations for future studies	168
REFERENCES.....	170

LIST OF FIGURES

Figure 1.1 Phases of real fire development	3
Figure 1.2 ISO 834 (ISO-834, 1975) and ASTM E119 (ASTM E119, 2000) standard fire curves.....	3
Figure 1.3 Temperature-time curves used for design of structures under fire condition.....	4
Figure 2.1 Local bond stress-slip law	18
Figure 2.2 Wedge action between the steel bar and concrete (Tepfers 1979)	19
Figure 2.3 Bond stress in reinforced concrete for deformed bar.....	20
Figure 2.4 Bond stress-slip for plain wire and plain seven-wire strand (CEB-FIP- Bulletin10, 2000).....	21
Figure 2.5 Push-in test apparatus	23
Figure 2.6 Transfer bond length and flexural bond length before and after member loading	24
Figure 2.7 Expansion of concrete due to corrosion of the embedded steel (Kumar & Paulo, 2006)	28
Figure 2.8 Thermal conductivity of concrete at elevated temperatures	32
Figure 2.9 Specific heat capacity of concrete at elevated temperatures.....	32
Figure 2.10 Thermal expansion of concrete at elevated temperatures (CEN 2004) .	33
Figure 2.11 Degradation of concrete compressive strength at elevated temperatures	34
Figure 2.12 Degradation of concrete tensile strength at elevated temperatures.....	35
Figure 2.13 Thermal strains of reinforcing steel bar and strand	37
Figure 2.14 Degradation of steel bars at elevated temperatures	38
Figure 2.15 Degradation of strands at elevated temperatures	39
Figure 2.16 Bond stress-slip relationship of cold deformed steel at elevated temperatures (Diederichs & Schneider 1981).....	41
Figure 2.17 Bond stress-slip relationship of prestressing steel at elevated temperatures (Diederichs & Schneider 1981).....	41
Figure 2.18 Bond stress-slip relationship of rusted plain round bars at elevated temperatures (Diederichs & Schneider 1981).....	42

Figure 2.19 Relative bond strength of various reinforcing bars as a function of temperatures (Diederichs & Schneider 1981).....	42
Figure 2.20 Residual bond stress-slip for various temperatures (16 mm steel bar diameter, 55 mm concrete cover and 3.7 MPa initial stress) (Morley & Royles 1983)	43
Figure 2.21 Residual bond stress-slip curves at various temperatures (16 mm deformed bar diameter, 55 mm concrete cover with no initial stress) (Morley 1982)	44
Figure 2.22 Residual bond stress-slip for different concrete cover and various temperatures	45
Figure 2.23 Variation of maximum bond stress with temperature for different covers (16 mm diameter of deformed bar) (Morley & Royles 1983)	45
Figure 2.24 Residual bond strength versus temperature for modified specimens prepared with different FRC mixtures (Haddad et al. 2008)	46
Figure 2.25 Average bond stress-slip curve defined by CEB-FIP Model Code 1990	48
Figure 2.26 Reinforced concrete beam: plain concrete, reinforcing steel bar and 3D bond-link elements (Huang 2010)	50
Figure 3.1 Mechanical action between the steel bar and concrete	55
Figure 3.2 Partly cracked concrete cylinder	55
Figure 3.3 Uncracked elastic stage.....	56
Figure 3.4 (a) Stress-strain curve of concrete in tension (b) Concrete tensile stress-strain curves at different temperatures	58
Figure 3.5 Influence of β on the current model at different temperatures: (a) At 500°C, (b) At 300°C	60
Figure 3.6 Proposed curves: (a) Bond stress-slip curve (b) Bond stress - R_i curve	63
Figure 3.7 The relationship between the slip and R_i	64
Figure 3.8 Bond-link element: (a) 2-D Coordinates (b) 3-D Coordinates	66
Figure 3.9 Comparison of predicted and measured bond stress-slip curves at ambient temperature.....	73
Figure 3.10 Comparison of predicted and measured bond stress-slip curves at elevated temperatures	76

Figure 3.11 Comparison between the predicted and tested stress distributions along anchored reinforcing steel bar (Viwathanatepa et al. 1979)	80
Figure 3.12 Predicted bond stress distributions corresponding to different end-slips for test (Viwathanatepa et al. 1979).....	80
Figure 3.13 Predicted end-slips vs pull-out force for the test (Viwathanatepa et al. 1979)	81
Figure 3.14 Details of J4 beam tested at ambient temperature (Burns & Siess 1962)	82
Figure 3.15 Comparison of predicted and measured mid-span deflections of J4 beam (Burns & Siess 1962).....	82
Figure 3.16 Details of tested beams in fire (Lin et al. 1987).....	83
Figure 3.17 Comparison of predicted and measured temperatures of four main reinforcing steel layers for Beam 1 (Lin et al. 1987).....	84
Figure 3.18 Comparison of predicted and measured temperatures of four main reinforcing steel layers for Beam 5 (Lin et al. 1987).....	85
Figure 3.19 Comparison of predicted and measured maximum deflections of Beam1 (ASTM Fire) (Lin et al. 1987)	86
Figure 3.20 Comparison of predicted and measured maximum deflections of Beam3 (ASTM Fire) (Lin et al. 1987)	87
Figure 3.21 Comparison of predicted and measured maximum deflections of Beam5 (SDHI Fire) (Lin et al. 1987)	88
Figure 3.22 Comparison of predicted and measured maximum deflections of Beam6 (SDHI Fire) (Lin et al. 1987)	88
Figure 4.1 Transfer length and flexural length before and after loading	Error!
Bookmark not defined.	
Figure 4.2 The interaction between the outer wires of the strand and concrete.....	93
Figure 4.3 Parabolic Mohr Envelope (Curtis 2011).....	97
Figure 4.4 Bond stress-slip curve: (a) Three-wire strands and indented seven wire strands, (b) Seven-wire smooth strands.....	98
Figure 4.5 Comparison of predicted and tested bond stress–slip curves for the seven-wire smooth strand at ambient temperature (Vázquez-Herrero et al. 2013)	107

Figure 4.6	Comparison of predicted and tested load–slip curves for the pull-out seven-wire indented strands at ambient temperature (Lundgren 2002)	108
Figure 4.7	Comparison of predicted and tested load–slip curves for the three-wire push-in test at ambient temperature (Gustavson 2004)	109
Figure 4.8	Comparison of predicted and tested load-slip curves for the three-wire pull-out test at ambient temperature (Gustavson 2004)	109
Figure 4.9	Comparison of predicted and tested bond strength degradation with different concrete compressive strengths at elevated temperatures (Moore 2008): (a) 77.4 MPa; (b) 98.8 MPa	111
Figure 4.10	Details of tested T-beam Z-1 (Cowen & VanHorn 1967) (all dimensions in mm)	112
Figure 4.11	Comparison of the predicted and tested load versus mid-span deflections curves for T-beam Z-1 (Cowen & VanHorn 1967)	113
Figure 4.12	Details of the tested T-girder (T-6-1.5h-A) (Tadros & Morcouc 2011) (all dimensions in mm)	114
Figure 4.13	Comparison of the predicted and tested load versus mid-span deflections curves for the tested T-girder (Tadros & Morcouc 2011)	114
Figure 4.14	Details of PC Slab TB3 (Bailey & Ellobody 2009) (all dimensions in mm)	115
Figure 4.15	Comparison between the predicted and tested temperature histories (Bailey & Ellobody 2009)	116
Figure 4.16	Comparison of predicted and measured mid-span deflections of Slab TB3 (Bailey & Ellobody 2009)	117
Figure 4.17	Comparison of predicted and tested longitudinal expansion for Slab TB3 (Bailey & Ellobody 2009)	118
Figure 4.18	Details of PC Slab PSS-1 (Zheng & Hou 2008)	119
Figure 4.19	Heating curve used in the analysis (Zheng & Hou 2008)	119
Figure 4.20	The predicted and tested temperature histories for Slab PSS-1 (Zheng & Hou 2008)	120
Figure 4.21	Comparison of predicted and measured mid-span deflections of Slab PSS-1 (Zheng & Hou 2008)	121
Figure 5.1	Whole floor layout of reinforced concrete structure	125

Figure 5.2 Division of reinforced concrete building into beam-column, slab, reinforcement and bond link elements (Huang 2010).....	126
Figure 5.3 Isolated simply supported beam heated by ISO 834 standard fire	128
Figure 5.4 The cross-sectional details of the isolated reinforced concrete beam (all dimensions in mm)	128
Figure 5.5 Influence of steel strains on local bond-stress slip relationship (CEB-FIP 2010).....	131
Figure 5.6 Yielding effect of reinforcing steel bar on the bond behaviour	132
Figure 5.7 Segmentation of the beam cross-section.....	133
Figure 5.8 Temperature histories of the steel bar (Bar 1) for the beam subjected to ISO 834 standard fire with different thicknesses of concrete cover	134
Figure 5.9 Temperature histories of the steel bar (Bar 2) for the beam subjected to ISO 834 standard fire with different thicknesses of concrete cover	134
Figure 5.10 Temperature histories of the steel bar (Bar 3) for the beam subjected to ISO 834 standard fire with different thicknesses of concrete cover ...	135
Figure 5.11 Comparison between full-bond and partial-bond for the concrete cover of 10 mm	136
Figure 5.12 Comparison between full-bond and partial-bond for concrete cover of 20 mm	137
Figure 5.13 Comparison between full-bond and partial-bond for concrete cover of 30 mm	137
Figure 5.14 Comparison between full-bond and partial-bond for concrete cover of 40 mm	138
Figure 5.15 Comparison between full-bond and partial-bond for concrete cover of 50 mm	138
Figure 5.16 Influence of concrete cover on the structural behaviour of a simply supported beam modelled with partial bond.....	140
Figure 5.17 Temperature histories of the reinforcing bars for the beam exposed to ISO 834 standard fire	141
Figure 5.18 Influence of concrete spalling on the behaviour of the beam modelled as full or partial bond	142
Figure 5.19 Comparison of the behaviour of the beam modelled as full bond or partial bond (all elements spalled)	143

Figure 5.20	Comparison of the behaviour of the beam modelled as full bond or partial bond (elements 1&5 spalled).....	143
Figure 5.21	Comparison of the behaviour of the beam modelled as full bond or partial bond (elements 2&4 spalled).....	144
Figure 5.22	Comparison of the behaviour of the beam modelled as full bond or partial bond (element 3 spalled).....	144
Figure 5.23	Time-temperature histories for the reinforcing steel bars of the beam subjected to IOS 834 standard fire.....	145
Figure 5.24	Comparison of the behaviour of the beam modelled with full bond and partial bond using concrete compressive strength of 20 MPa	146
Figure 5.25	Comparison of the behaviour of the beam modelled with full bond and partial bond using concrete compressive strength of 30 MPa	147
Figure 5.26	Comparison of the behaviour of the beam modelled with full bond and partial bond using concrete compressive strength of 40 MPa	147
Figure 5.27	Comparison of the behaviour of the beam modelled with full bond and partial bond using concrete compressive strength of 45 MPa	148
Figure 5.28	Influence of concrete compressive strength on the behaviour of the beam modelled with full bond	148
Figure 5.29	Influence of concrete compressive strength on the behaviour of the beam modelled with partial bond.....	149
Figure 5.30	Details of the isolated slab modelled	150
Figure 5.31	The cross-section of the slab modelled.....	150
Figure 5.32	Time-temperature histories of the reinforcing steel bars with different concrete covers under ISO 834 fire	151
Figure 5.33	Comparison of the central deflections of the slab modelled as full bond or partial bond using concrete cover of 10 mm	152
Figure 5.34	Comparison of the central deflections of the slab modelled as full bond or partial bond using concrete cover of 15 mm	153
Figure 5.35	Comparison of the central deflections of the slab modelled as full bond or partial bond using concrete cover of 20 mm	153
Figure 5.36	Comparison of the central deflections of the slab modelled as full bond or partial bond using concrete cover of 25 mm	154
Figure 5.37	Comparison of the central deflections of the slab modelled as full bond or partial bond using concrete cover of 30 mm	154

Figure 5.38 Influence of different concrete covers on the central deflections of the slab modelled as partial bond.....	155
Figure 5.39 Time-temperature history of the reinforcing steel bars within the slab exposed to ISO 834 fire	156
Figure 5.40 Comparison of the central deflections of the slab modelled as full bond or partial bond using concrete compressive strength of 20MPa.....	156
Figure 5.41 Comparison of the central deflections of the slab modelled as full bond or partial bond using concrete compressive strength of 30MPa.....	157
Figure 5.42 Comparison of the central deflections of the slab modelled as full bond or partial bond using concrete compressive strength of 40MPa.....	157
Figure 5.43 Comparison of the central deflections of the slab modelled as full bond or partial bond using concrete compressive strength of 45MPa.....	158
Figure 5.44 Influence of different concrete strengths on the central deflections of the slab modelled as partial bond.....	158
Figure 5.45 Floor layout of the building with different locations of the fire compartments.....	160
Figure 5.46 The deflections of the floor slabs at the position a, b and c under whole floor fire	161
Figure 5.47 Comparison of the central deflections of the floor slabs for different fire compartments.....	161
Figure 5.48 Comparison of the deflections at Position a for compartment fire FC-1 and whole floor fire, together with the central deflection of isolated simply supported slab.	162
Figure 5.49 Comparison of the deflections at Position b for compartment fire FC-2 and whole floor fire, together with the central deflection of isolated simply supported slab.	162
Figure 5.50 Comparison of the deflections at Position a for compartment fire FC-3 and whole floor fire, together with the central deflection of isolated simply supported slab.	163

LIST OF TABLES

Table 3.1 Details of pull-out test in previous experiments at ambient temperature.....	70
Table 3.2 Details of pull-out tests in previous experiments at elevated temperatures.....	74
Table 4.1 Values of C and μ used in the proposed model.....	95
Table 4.2 Three-wire strands parameters.....	100
Table 4.3 Seven-wire strands parameters.....	100
Table 4.4 Comparison between the predicted and measured bond stresses for push-in tests.....	106
Table 4.5 Comparison between the predicted and measured bond stresses for pull-out tests.....	106

NOTATIONS

The following symbols are used in this thesis:

u	moisture content of concrete weight
σ_r	radial stress
$\sigma_{i,T}$	tangential stress at elevated temperatures
P_T^i	total radial pressure at elevated temperatures
$P_{i,T}$	pressure resistance of the elastic outer zone at elevated temperatures
r	radius from the centre of the rebar
R_s	radius of the steel bar
R_c	radius of concrete cylinder = R_s + the least thickness of concrete cover
R_i	radius of the uncracked inner face
$\varepsilon_{u,T}$	smear strain of concrete at elevated temperatures when tensile stress equal to zero
$\varepsilon_{t,0}$	smear tangential strain at the rebar interface
f_{ct}	tensile strength of concrete at ambient temperature
$E_{0,T}$	initial elastic modulus of concrete at elevated temperatures
τ_T^i	bond stress at elevated temperatures
α	effective face angle
$f_{ct,T}$	degradation of the concrete tensile strength at elevated temperatures
C	concrete cover
S_{\max}	maximum slip at the maximum bond stress point τ_{\max}
$F_{T,x}^i$	bonding force between the concrete and the steel bar
A	the contact area between the concrete and the reinforcing steel bar
U	perimeter of the steel bar

L	length of the steel bar which contributes to the node connected by the bond element
$\Delta \mathbf{F}$	nodal force increment vector
$\Delta \mathbf{u}$	nodal displacement increment vector
k_1^i	tangent stiffness coefficients of the bond connector
l_b	embedded length of the rebar inside the specimens
d_b	diameter of the rebar
V_c	Shear force resistance of the concrete in front of strand ridges
v_c	shear strength of the shear keys in the concrete mass
A_{sh}	shear area of the cracked surface
d_w	diameter of the outer wires
l_w	length of the wires
d_s	nominal strand diameter
F	force along the length of the wires
C	cohesion between the concrete and steel
μ	coefficient of friction
θ	pitch angle of the outer wires
τ	peak shear strength ($v_c = \tau$)
f_c'	concrete compressive strength
f_t	concrete tensile strength
σ_n	normal stress perpendicular to the strand axes
P_1	initial tension force on the strand usually equal to $0.75 f_u$ (0.75 ultimate stress)
P_2	force after the stress released from the strand
A_s	nominal area of the strand
E_s	modulus of elasticity of the strand
ν	Poisson ratio of the steel equal to 0.3
ε_{s1}	first strain of the strand at P_1
ε_{s2}	second strain of the strand at P_2
ε_c	strain of the concrete due to the lateral pressure of strand.

T_b	maximum bond force in the direction of strand
τ	average bond stress
τ_{\max}	maximum bond stress
S	slip between strand and concrete.
A_b	contact area between the strand and concrete
τ_T	bond stress at elevated temperatures
$\tau_{\max,T}$	maximum bond stress at elevated temperatures

Chapter 1 Introduction

1.1 Structural fire engineering

Fire can cause massive losses in lives and properties. Hence, the implementation of fire safety becomes an important part from the building regulation. The Building Regulation 2000 states that in the Approved Document B, the objectives of ensuring fire safety in buildings are: maintaining the structural stability for a reasonable period under fire conditions, restricting the growth and spread of fire, and provision of safeness, which means evacuation of the occupants and the rescue operation of the firefighters (ODBM 2000). It is essential for life safety to ensure that the integrity of the building be maintained during fire. This integrity means that occupants should have sufficient means and time to escape without being affected by heat or smoke, and fighting operations have enough time to ensure that the neighbouring buildings are not affected. The fire resistance of a structure in Eurocodes is expressed by three failure criteria which are: load bearing capacity by maintaining sufficient strength in the required duration, insulation by limiting the increase of temperature across separating elements and integrity to maintain structural integrity against penetration of hot gases (Lin, 2014). Two types of fire protection methods are used in structures, active and passive. Active fire protection procedure is a system depends on the automatic devices such as fire alarms and detecting system or sprinklers. However, passive fire protection method deals with the structure itself, by ensuring the stability of the structure during a reasonable time and controlling the spread of fire. This passive fire protection can be obtained by controlling the building materials and dimensions, compartments and using fire protection materials (Phan et al. 2010). The fire starts when the combustible materials get ignited for some reasons. With low average temperature at the beginning of a fire in a compartment, it is possible to control the growth of fire by using active fire protection systems like sprinkler systems and fire extinguishers. However, when the fire is fully developed to 'post-flashover' and the flames spread out, active fire protection systems cannot control the fire. Therefore, the risk of structural collapse can be great, unless sufficient fire resistance and fire protection are provided to the structural members during building design (passive fire protection).

Generally, reinforced concrete structure has a good fire resistance. Concrete does not support combustion, rather it prevents spread a fire to other parts of building and adjoining structures. Reinforced concrete structure can retain its structural integrity during a fire, also has good thermal insulation property to keep the unexposed surface relatively cool (Morley 1982; Kodur 2014).

1.1.1 Fire curves used in structural fire engineering design

Fire resistance of structural elements can be described as the period of time under standard fire exposer until the failure of the element occurs (Huang 2010). A real fire depends on the ignition source, sufficient combustible material and oxygen. The development of a nature fire within a compartment involves three phases as shown in Figure 1.1. The first phase (pre-flashover) starts when the combustible materials are ignited. In this phase the average temperature is low and the active fire protection can control the growth of the fire. However, if the active fire protection systems fail to contain the fire, the second phase of the nature fire will start at the point of flash-over (see Figure 1.1). The growth of fire in the second phase depends on the availability of the fuel and oxygen as well as the ventilation for the small compartments. After flash over, passive fire protection becomes very important by designing the structure to prevent the spread of the fire and structural collapse. The third phase starts after the fire temperature reaches to the maximum, then the temperature decreases due to the reduction of the combustion rate of the fuel. At this point, the cool phase will start and the fire curve will drop. The risk of a fire on the building can be raised during the cooling phase because of the thermal contraction of the beams can generate large tensile deformation on the connections between beams and columns, which leads to local failure or even structural collapse.

The test of structural members under fire condition follows the standard codes such as ISO 834 standard fire (ISO-834 1975), ASTM E119 (ASTM E119 2000) and Eurocode (CEN 2002). The standard fire curves in ISO 834 and ASTM E119 depend only on the time of fire exposer, as shown in Figure 1.2, without taking in account the building characteristics such as compartment size, ventilation condition, available of combustible material (fire load), and the material of surrounding surfaces.

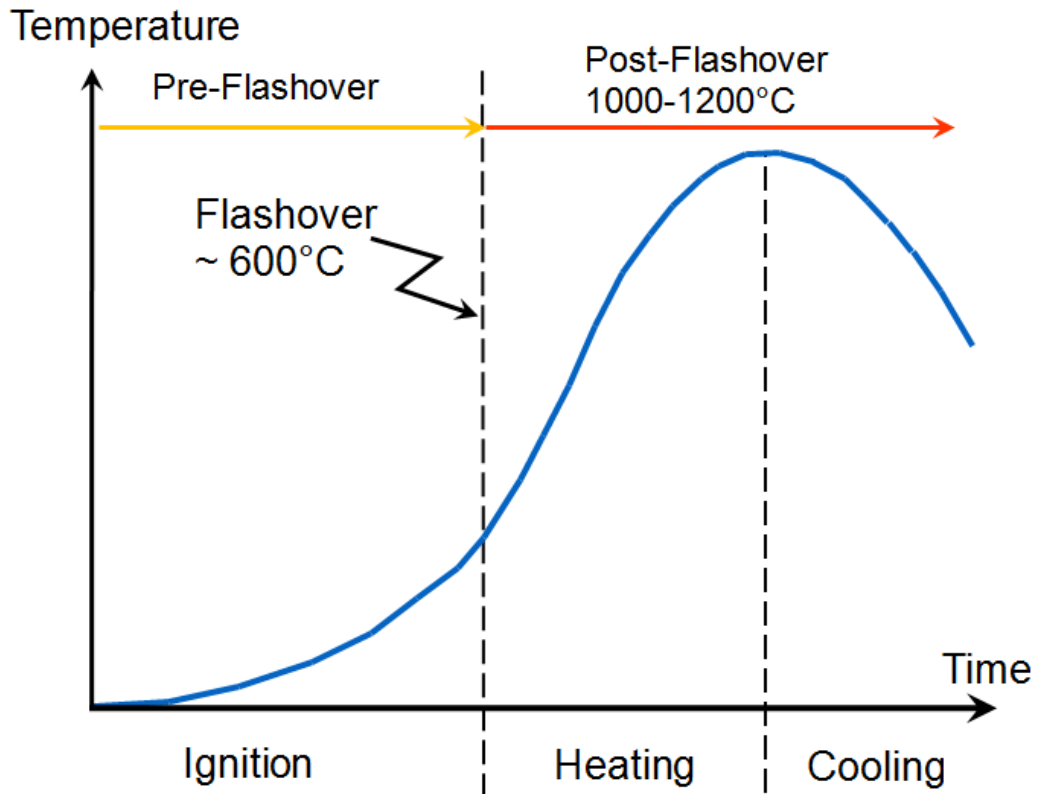


Figure 1.1 Phases of real fire development

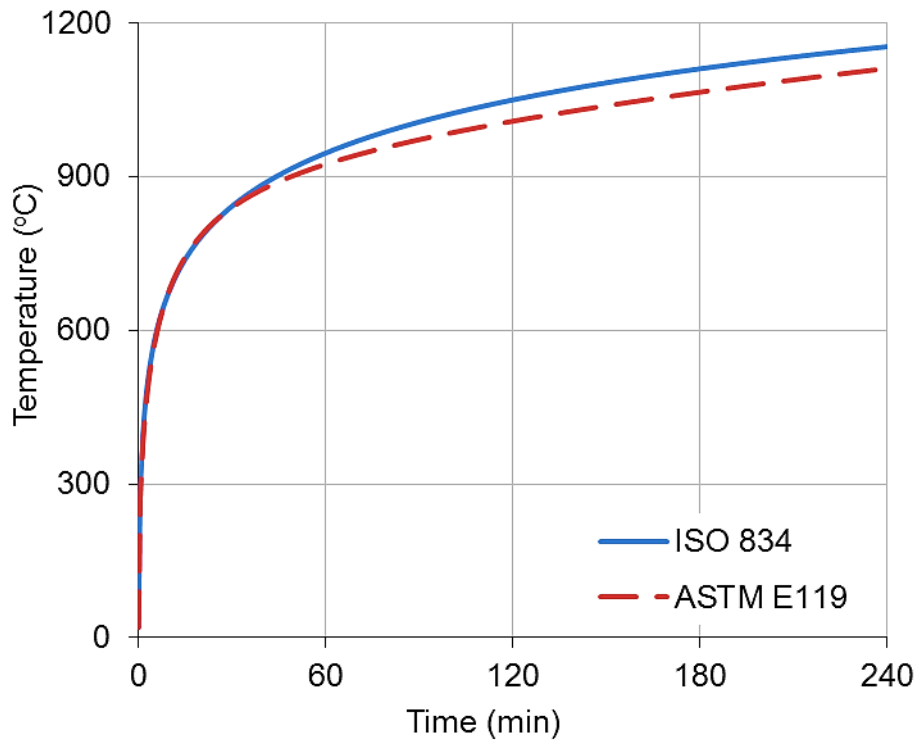


Figure 1.2 ISO 834 (ISO-834, 1975) and ASTM E119 (ASTM E119, 2000) standard fire curves.

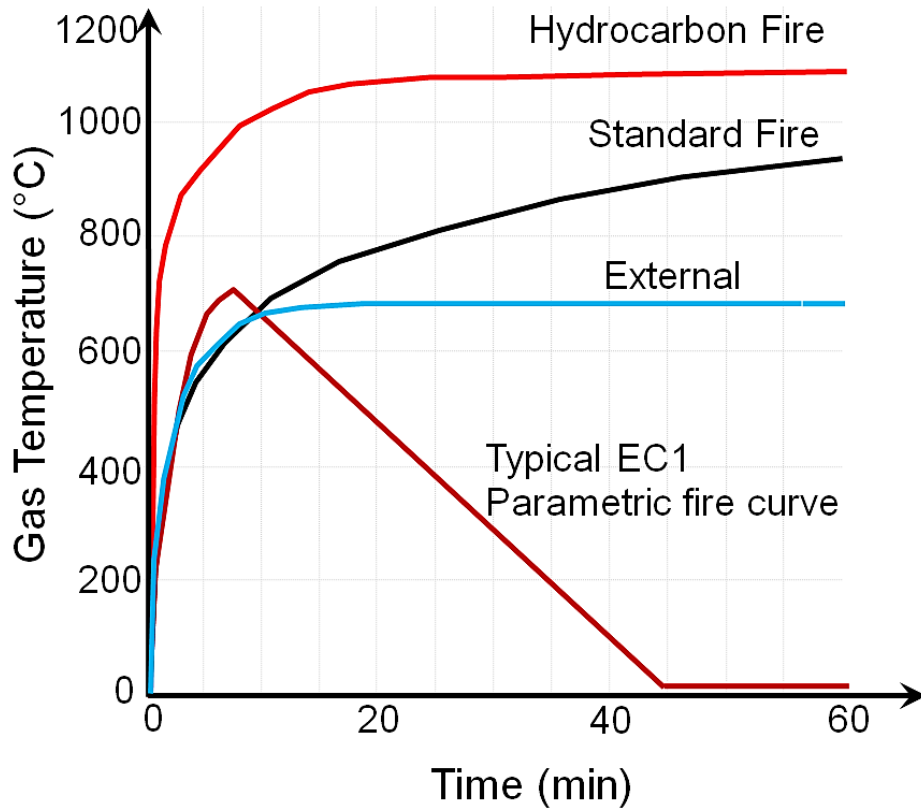


Figure 1.3 Temperature-time curves used for design of structures under fire condition

Figure 1.3 gives different fire curves based on the type of combustible materials and the position of the structural member inside or outside of the building.

Standard temperature-time curve is used for design the members located inside a building and given by Equation (1.1):

$$\theta_g = 20 + 345 \log_{10}(8t + 1) \tag{1.1}$$

where: θ_g is the gas temperature in the fire compartment or furnace (°C), and t is the time in minutes (ISO-834, 1975).

External fire curve is used for design the members located outside a building and follows Equation 1.2:

$$\theta_g = 660(1 - 0.687e^{-0.32t} - 0.313e^{-3.8t}) + 20 \tag{1.2}$$

Hydrocarbon time-temperature curve is used for design the structure that contains chemical materials and follows Equation (1.3):

$$\theta_g = 1080 (1 - 0.3257e^{-0.167t} - 0.675e^{-2.5t}) + 20 \quad (1.3)$$

For Equations (1.2) and (1.3): θ_g is the gas temperature in the fire compartment or the furnace ($^{\circ}\text{C}$), and t is the time in minutes (CEN 2002).

Parametric temperature-time curves:

The parametric time-temperature curve specified in Eurocode EN 1991-1-2 (CEN 2002) provides an estimation of a real fire curve by taking the compartment characteristics into consideration, such as compartment size, ventilation condition, available combustible material, fire load, and the material of surrounding surfaces. This fire curve is valid for fire compartments up to 500 m² of floor area and height of 4 m without openings in the roof. The gas temperature θ_g inside a compartment during heating phase can be determined using Equation (1.4):

$$\theta_g = 20 + 1325 \left(1 - 0.324e^{-0.2t^*} - 0.204e^{-1.7t^*} - 0.472e^{-19t^*} \right) \quad (1.4)$$

where,

$$t^* = t \cdot \Gamma \quad (1.5)$$

where t is the time in hour.

$$\Gamma = \frac{(O/b)^2}{(0.04/1160)^2} \quad (1.6)$$

where, b is the thermal absorptivity depending on the density ρ , specific heat c and thermal conductivity λ of the boundary of an enclosure, which can be calculated as:

$$b = \sqrt{(\rho c \lambda)} \quad (1.7)$$

And O is the opening factor, expressed as:

$$O = \frac{A_v \sqrt{h_{eq}}}{A_t} \quad 0.02 \leq O \leq 0.2 \quad (1.8)$$

where, A_v is the total area of vertical openings on all walls, h_{eq} is the weighted average of window heights on all walls, A_t is the total area of enclosure (walls, ceiling and floor, including openings). Equation (1.4) approximates the standard time-temperature curve in case of $\Gamma = 1$.

For the cooling phase, the calculation of temperature-time curve is given in EN1991-1-2 (CEN 2002) as:

$$\theta_g = \begin{cases} \theta_{\max} - 625(t^* - t_{\max}^* \cdot x) & t_{\max}^* \leq 0.5 \\ \theta_{\max} - 250(3 - t_{\max}^*)(t^* - t_{\max}^* \cdot x) & 0.5 < t_{\max}^* < 2 \\ \theta_{\max} - 250(t^* - t_{\max}^* \cdot x) & t_{\max}^* \geq 2 \end{cases} \quad (1.9)$$

where, θ_{\max} is the maximum temperature during the heating phase at $t^* = t_{\max}^*$.

$x = 1.0$ if $t_{\max} > t_{\lim}$; or $x = t_{\lim} \cdot \Gamma / t_{\max}^*$ if $t_{\max} = t_{\lim}$

$$t_{\max} = \max \left[\frac{0.2 \times 10^{-3} \times q_{t,d}}{O}; t_{\lim} \right] \quad (1.10)$$

$$t_{\max}^* = t_{\max} \times \Gamma \quad (1.11)$$

where $q_{t,d}$ is the design fire load density related to the surface area A_t ; t_{\lim} is the time for maximum gas temperature in case of a fuel controlled fire; In the case of slow fire growth rate, $t_{\lim} = 25$ min; in the case of medium fire growth rate, $t_{\lim} = 20$ min and in the case of fast fire growth rate, $t_{\lim} = 15$ min (CEN 2002).

Although, parametric time-temperature curve specified in Eurocode EN 1991-1-2 (CEN 2002) provides better prediction to a real fire curve, the standard fire curves are commonly used for structural fire design and standard fire tests.

1.1.2 Design of structures under fire condition

Codes for fire resistance design differ from country to country around the world, but all of them have the objectives of protecting the life and property from fire. The main differences between the fire design and normal temperature design are: the strengths of materials reduce at elevated temperatures, the cross section areas reduce by

charring or spalling, internal forces may be induced by thermal expansion, the applied load may be changed, the deflections may be important as they may affect the global stability, and also different failure mechanisms need to be considered (Phan et al. 2010). The essential point in structural fire design is to ensure that the real fire resistance of a structure is greater than the design required fire resistance of the structure. Two methods are used in structural fire design: Prescriptive Fire Resistance Design and Performance-Based Design for Fire. The first method is a traditional approach by considering the standard fire curve rather than a real fire. The structural response in fire is represented by using isolated members tested in the furnace under standard fire curve (Phan et al. 2010). Hence, the behaviours of real buildings under real fire conditions cannot be properly considered in this design method. This is because the standard fire curve cannot accurately represent the real fires and the performance of isolated structural members is considerably different with those members within the whole building due to the restraints and interactions provided by the surrounding structures. Normally this design approach will produce more conservative fire resistance design. The second design method is the Performance-Based Design for Fire. In this method designers can take a rational approach to ensure satisfactory performance of a building in fire by any acceptable solutions to make economic savings without affecting the fire safety of the building. For instance, using the parametric fire curve specified in Eurocode (CEN 2002) for design to take into account different factors that affect on time-temperature curve and considering the cooling phase of the fire, which may generate thermal contraction in the beams, resulted larger tensile forces acting on the connections between beams and columns (Bisby 2012).

Structural fire design in Eurocodes like (CEN 2002) and (CEN 2004) allow designers to treat the fire as one of the basic design limit states, taking into account some factors such as, non-uniform heating because of partial protection, realistic stress-strain properties of structural materials at high temperatures and the level of loading at fire limit state (Huang 2010). The codes specify minimum required fire endurance time for building by using acceptable solutions which called “deemed-to-satisfy solution” to reduce the fire protection cost without undermining the fire safety of the building. This requirement can be achieved by allowing methods for

determining the fire endurance time such as qualification tests and analytical methods (Phan et al. 2010).

At present, there are three applicable levels of structural fire engineering design, that are: tabulated data which is used for member analysis by applying standard fire only; simplified calculation methods which are used for analysis of the parts of the structure by applying the standard or parametric fire curves; advanced calculation models for global structural analysis by applying the standard or parametric fire curves (Law 2016).

1.2 Reinforced concrete structures and the bond between concrete and reinforcement in fire

Exposure of concrete structures to high temperatures results in significant losses in mechanical and physical properties of concrete and steel reinforcement as well as the bond characteristics between them. Degradation of the bond properties in fire may significantly influence the moment capacity or flexibility of the reinforced concrete structures. Therefore the bond behaviour should be considered for the structural fire engineering design of reinforced concrete structures (Pothisiri & Panedpojaman 2013). Right now, information about material degradations such as concrete and steel reinforcement is generally available at elevated temperatures. However, investigation about bond behaviour between concrete and rebar at elevated temperatures is still limited because of complexity, and also the research on the bond characteristic of prestressed concrete member is very limited.

Failure of concrete in tension is known as a brittle failure; hence concrete members require an additional support in tension region. This support can be established using reinforcing steel bars for normal concrete and strands in prestressed concrete constructions. Concrete and reinforcement need to build a good interaction between them. This interaction is known as bond stress which must be sufficient to anchor the rebar. Conventionally, design of reinforced concrete structure is based on the assumption of strain compatibility as the strain in the concrete and steel bar are the same at sections under the maximum load. This assumption requires a good bond between the concrete and rebar and the maximum bond stress can be reasonably determined (CEB-FIP-Bulletin10 2000). The quality of the bond controls the

needed anchorage length of the rebar. Good bond between the concrete and reinforcing bars can decrease the construction cost by reducing the anchorage length of the rebar, and obtaining the full capacity of the concrete members. In fact, bond between the concrete and steel reinforcing bars is important not only for concrete and steel to work together as a composite material, but also important to provide the ductility for the concrete structures. For structural safety, bond gives good mechanical properties for the structures at local level. Likewise ductility requires a good bond to resist the large strain of the steel along the anchorage of the rebar when bending cracks initiated (CEB-FIP-Bulletin10 2000).

From this point of view, it is important to understand the factors that can effect on the bond performance in order to achieve high bond quality between the concrete and reinforcement. There are considerable experimental and analytical studies on the bond characteristics have been conducted. Previous research indicated that many factors can effect the bond characteristics between the concrete and reinforcement, such as concrete compressive and tensile strengths; concrete cover; geometric of reinforcement; bars diameter; transverse reinforcement and direction of casting (Brown et al. 1993).

Prestressed concrete (PC) members can be constructed utilizing unbonded or bonded strands. For bonded members, the bond is essential for the success of prestressing system. Forces are transferred from strands to concrete through end anchors together with the bond between strand and concrete. Therefore bonded PC beams are more robust structural members at ambient temperature. However, previous research indicated that compared to normal reinforcing steel, prestressed steel wires are more sensitive to elevated temperatures due to the stress level in prestressing wires is very high (Hou et al. 2015).

Structural fire safety is one of the most important considerations in building applications as mentioned before. The conventional approach of evaluating fire resistance through fire tests is expensive, time consuming and limited to study different parameters. Also, it is difficult to perform a full scale fire test such as whole building with include different fire compartment within the building. Therefore, an alternative to fire testing is the use of numerical modelling for evaluating fire resistance of reinforced concrete structural members. Numerical methodology allows

to incorporating various parameters in an efficient and cost-effective way (Kodur & Shakya 2014). Hence, the experimental data obtained from the tests can be used for validating of the proposed models before using these models in actual applications.

1.3 Research background

The first attempts for using reinforcement in concrete were during the 19th century, in which smooth bars were used to support the concrete in tension. Because of limited bond stress between the smooth bars and concrete, end hooks were suggested to increase the anchorage capacity. At the beginning of 20th century, deformed bars were introduced to increase the capacity of bond between the concrete and reinforcement (CEB-FIP-Bulletin10 2000). Many studies since early of the 20th century about the bond of deformed bars had been done. The results indicated that using deformed bars with small rib spacing and high ribs can improve the resistance to slip and increase the ultimate bond strength (Lutz 1970; Goto 1971). Increasing the roughness of the steel bar improves the bond strength, but splitting resistance of the concrete surrounding the steel bar limits the bond capacity. Hence, there is no much point in additional roughness unless extra confinement is provided to the concrete (CEB-FIP-Bulletin10 2000). The usual way to study the bond between the concrete and steel bar is pull-out tests. Pull-out test can be done by embedding the bar inside a prismatic concrete specimen and pull the bar out of the concrete at the time of test. Short embedded length is usually used in pull-out test to achieve a uniform bond stress distribution along the embedded bar length (Watstein 1947). Different theories have been proposed to analyse the state of stress in pull-out specimens. The theory of elasticity was proposed by Osterman (1951) to calculate the bond stress distribution between the concrete and steel bars. This theory was established based on the circumferential stresses and radial stresses surround the steel bar, which can briefly explained as the transfer load between the rebar and concrete is achieved by bearing the bar ribs on the concrete. The resultant is a compressive forces acting on the ribs, which are generated due to the confinement of the surrounding concrete to the reinforcement. The compressive forces are decomposed into parallel and perpendicular to the rebar. The reaction forces acting on the concrete due to the perpendicular components of the compressive forces acting on the ribs create circumferential tension stresses in the concrete surrounding

the steel bar. If these tensile stresses exceed the tensile strength of concrete, splitting failure occurs due to cracking of concrete (Wang & Liu 2003). Another theory for analysing the bond stress distribution is the modulus of displacement (K-value). This theory is built based on the assumption that the bond stress is directly proportional to the relative displacement between the concrete and reinforcement (Losberg 1964; Tepfers 1980). An empirical formula was proposed by Lutz (1970) to calculate the bond strength based on the test results. The effects of concrete and transverse reinforcement are taken into account in this formula. Parameters like beam width and number of bars are also considered (Lutz 1970).

Investigation about the bond between strand and concrete in prestress concrete members was conducted by Welsh and Sozen (1969). The result from this study indicated that the bond is provided by two mechanisms that is the interlocking and friction. Parameters such as shrinkage, lateral pressure and concrete settlement were investigated in this study. Finite elements method had been used to calculate the stress distribution in the concrete key. Also, the bond as a function of the twist angle of the strand was investigated in this study (Welsh & Sozen 1968).

During the past decades, numerous models have been developed to calculate bond stress at ambient temperature. Tepfers (1979) proposed an analytical solution based on the theory of elasticity (Timoshenko & Goodier 1951) for modelling the bond of deformed bars. This model was developed based on the propagation of circumferential cracks of concrete along the rebar which defined as the thick wall cylinder theory. Two stages were assumed in this theory for modelling the bond: a lower bond or elastic stage when the concrete surrounding the bar is partly cracked and upper bond plastic stage when the surrounding concrete is entirely cracked. Modulus of slip theory was used in this model to analyse the distribution of stresses along the anchored bar (Tepfers 1979). This analytical solution has been developed by many researchers to take in consideration many aspects, such as the strain-softening of concrete in tension to calculate the maximum radial stress and maximum bond stress (Wang & Liu 2003).

At present, information about the bond between concrete and reinforcement at ambient temperature are generally available. However, investigation about the bond characteristic between concrete and reinforcing steel bar at elevated temperatures is

still limited. Effect of high temperatures on the bond was studied by Diederichs and Schneider (1981). The range of temperature was 20-800°C and three different types of steel reinforcement were used in that study (plain round bars, deformed bars and strands). The conclusion from the study was that the bond strength is affected by the test procedure and bar's shape, in which the smooth bar shows sharper decrease in bond strength than the deformed bar. Also the study indicated that, degradation of the bond strength at high temperatures is more than the degradation of concrete compressive strength. Another study was conducted by Morley & Royles (1983) about the response of the bond to high temperature. Deformed bars were used in this test with a range of temperatures 20-750°C. The results indicated that the bond performance depends upon the concrete strength and the specimens tested during heating give lower bond strength than others tested after cooling. The effect of elevated temperature on the bond between deformed rebar and fiber reinforced concrete was studied by Haddad et al. (2008). In this investigation, the concrete was mixed with fibres to minimize the damage in the interface between concrete and reinforcement and this enhances the bond performance at elevated temperatures.

Study of the bond behaviour between concrete and strands for PC structures at elevated temperatures is more complicated than normal reinforced concrete. A hollow concrete slab was tested under fire condition by Fellingner et al. (2003) to study the behaviour of bond for prestressed strands at elevated temperatures. This study indicated that the bond-slip relation cannot be precisely defined by temperature alone, whereas this relationship depends on other factors such as thermal expansion during fire exposure and the support conditions of the member. Experimental study was carried out by Moore (2008) about the performance of prestressed concrete bridges under fire condition. Pull-out tests were conducted to study the behaviour of bond between strands and concrete in prestressed concrete at elevated temperatures. Two sizes of seven wire strands (12.7 mm & 9.5 mm) and two concrete mix design (75.8 MPa & 96.5 MPa) with range of temperatures 20-704 °C were used in this experiment. It can be concluded from this study that the bond strength depends on some factors such as cracks induced by heating, in which the bond strength was greater for samples with fewer cracks. Also, the average bond strength was greater for higher concrete compressive strength and the failure was brittle, while for lower

compressive strength ductile failure was observed. Finally, the smaller strand's diameter shows better bond strength.

During the past decades, numerous models have been developed to calculate bond stress at ambient temperature. The majority of these models are empirical and based on a statistical methodology. Thus, these models are highly dependent on the test data, which may limit their validity in different situations (Huanzi 2009).

Currently, there are limited numbers of numerical models available for modelling bond characteristics at elevated temperatures. Huang (2010) adopted the CEB-FIP bond-slip model at ambient temperature (CEB-FIP Model code 90 1991) and considered the degradation of bond strength at elevated temperatures by using the experimental results generated by (Bazant & Kaplan 1996). Huang's model was the first development of the bond characteristics in fire. Pothisiri and Panedpojaman (2013) have proposed a mechanical bond-slip model at elevated temperatures based on the theory of thick-wall cylinder and smeared crack of concrete in tension. However, this model was established to calculate the bond-slip based on the correlation between the experimental slip obtained from previous tests.

Modelling of bond-slip relationship for prestressed concrete at ambient temperature is limited. These models take in consideration limited parameters and limited cases. A model was proposed by Benitez & Galvez (2011) to simulate the bond during the prestressing force release. This model was developed based on thick wall cylinder theory and considered a single wire (indented bar) without taking in account the spiral effect of strands. Bolmsvik & Lundgren (2006) used finite element software DIANA to simulate the bond-slip within the interface between concrete and three-wire strands only. Different parameters were considered in this study such as adhesion, friction and mechanical interlocking. Modelling the bond-slip for prestress structures at elevated temperature was difficult to find in literature.

1.4 Research objectives

As mentioned before, the conventional approach of evaluating fire resistance through fire tests is expensive, time consuming and there are limitations to study different parameters. Therefore, an alternative to fire testing is the use of numerical models for evaluating structural fire resistance of concrete structural members. Numerical

models allow researchers to take into account various parameters with an efficient and cost-effective way.

Due to the lack of robust models for considering the influence of the bond characteristics between concrete and reinforcement at elevated temperatures, the majority of the numerical models developed for predicting the behaviour of reinforced concrete structures in fire were based on the assumption of full bond interaction (Huang 2010). Hence, the main objectives of this research are to:

- Develop a robust numerical model for predicting the bond stress-slip between concrete and reinforcing ribbed bars for normal reinforced concrete structures at elevated temperatures. The calculation in this numerical model is based on the constitutive equations of concrete and geometric properties of the rebar and concrete cover to find the bond-slip relationship under fire conditions.
- Incorporate the bond-slip model proposed above into **VULCAN** software for 3D analysis of reinforced concrete structures under fire conditions using bond-link element approach.
- Validate the proposed model against previous test results. The validation consists of two stages: the first stage is to validate bond-slip models for ribbed bar and strand at both ambient and elevated temperatures; the second stage is to validate the bond-link element with the developed bond-slip models, which involves modelling structural members at both ambient and elevated temperatures.
- Develop a robust model for modelling the bond stress-slip between concrete and strands for prestressed concrete structures under fire conditions. This model is developed based on the constitutive equations of concrete and geometric properties of seven-wire and three-wire strands. Also, incorporate this model into **VULCAN** software and validate it against previous test results.
- Conduct a comprehensive parametric study to identify the most important factors which can effect on the bond characteristics between concrete and steel reinforcement for reinforced concrete beam and slab at elevated temperatures.

1.5 Outline of the thesis

This PhD thesis consists of six chapters as the following:

Chapter 1 gives an introduction to the structural fire engineering and structural design under fire conditions; also gives an introduction and background on the topic of bond stress-slip between concrete and reinforcing steel bars and prestressed strands for normal reinforced concrete and prestressed concrete structures under fire conditions. The research background and the main objectives of this PhD project are presented in this chapter.

Chapter 2 presents a literature review on the bond-slip between concrete and reinforcement. This chapter starts with definition of the bond stress between concrete and reinforcement. Then mechanisms of the bond stress-slip for normal and prestressed reinforced concrete are explained. Also, factors affecting on the bond characteristic and influence of the bond on the behaviour of concrete structures are discussed. Codes related to the bond of reinforced concrete are also considered in this chapter. Then, degradations of the materials and the bond stress at elevated temperatures are discussed. Finally, a brief introduction about the finite elements method and **VULCAN** software for 3D modelling of structures under fire condition are presented.

Chapter 3 presents the development of the bond-slip model between concrete and deformed steel bars for normal reinforced concrete under fire condition. This model is incorporated into **VULCAN** program using bond-link element approach. Then, the validation of the model is performed by comparing the predicted results with experimental data.

Chapter 4 illustrates the development of the bond-slip model between concrete and strands in prestressed concrete structures at elevated temperatures. The analytical bond stress-slip model is for modelling the bond with three and seven wire strands at ambient and elevated temperatures. The developed model is also incorporated into **VULCAN** program and validated against the previous test data.

Chapter 5 presents a comprehensive parametric study on the bond between the concrete and steel bar at elevated temperatures. The study is dedicated to identify the most important factors that effect on bond behaviour between concrete and

reinforcement steel bars for beam and slab members at elevated temperatures. The parameters include steel bar yielding, concrete cover, concrete spalling, concrete compressive and tensile strengths.

Chapter 6 gives the conclusions based on the research reported in this PhD thesis and provides some recommendations for future research works.

Chapter 2 Literature review on the bond behaviour under fire conditions

As mentioned in Chapter 1, the structural fire engineering is one of the most important subjects, which is directly related into human lives and ownerships. Therefore, it is important to design the structures which have sufficient fire resistance in case of fire. Although it is commonly known that reinforced concrete structures have good fire resistance. However, fire can cause a great reduction in the strength and stiffness of concrete and reinforcement as well as the bond strength between them. Hence, this chapter will focus on the bond stress-slip between concrete and steel rebar for normal concrete structures and the bond stress-slip between concrete and strands for prestressed concrete structures under fire conditions.

2.1 Introduction

Reinforced concrete can be considered as a composite material which consists of concrete and reinforcement. Composite material is a result from combined two or more different materials to produce a new material which has superior characteristic. Usually, the components of this material are strengthened each other to avoid the weakness of each ones. Reinforced concrete consists of concrete matrix and reinforcement. Plain concrete is strong to resist the compressive stresses but it is weak in tension, whereas the steel has high tensile strength. Therefore, in reinforced concrete elements, concrete provides the resistance to the compression load and the rebar is placed at where tensile load is predicted; and sometimes in compression. The load is transferred from the concrete to rebar through the bond between them. This bond may become the weakest part within the concrete member, and it becomes weaker when the member is exposed to severe environment, such as high temperatures or fires. Therefore, it is important to understand the behaviour of the bond between concrete and reinforcement, especially under fire condition, which may dominate the failure of concrete members.

2.2 Mechanism of bond stress-slip in reinforced concrete

Previous researchers indicated that, when the reinforced concrete members are loaded, the stresses in the interface between concrete and steel bar increase. The capacity of the interface to transmit stress starts to deteriorate at a particular load level, and this deterioration becomes worse at elevated temperatures (Pothisiri & Panedpojaman 2012). The damage at the interface or bond gradually spreads to the surrounding concretes. The development of this process results in a slip between the steel and concrete due to the steel strain differs from concrete strain. This strain difference is the result of relative displacement between concrete and reinforcement. The mechanism to transfer stresses between concrete and reinforcement can be represented by adhesion, mechanical interlock, friction and Poisson's effect. This mechanism can be classified based on the type of reinforcement.

2.2.1 Bond mechanism for normal reinforced concrete

The interaction between concrete and steel rebar during pull-out process is classified into different stages based on the level of cracking in the concrete surrounding the rebar as shown in Figure 2.1 (CEB-FIP-Bulletin10 2000).

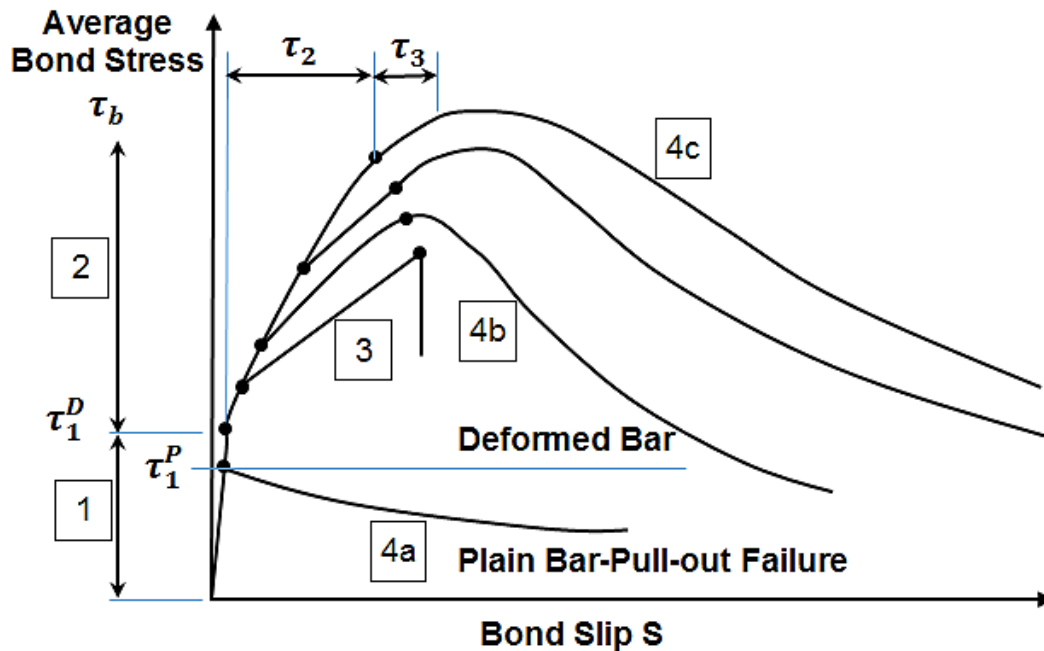


Figure 2.1 Local bond stress-slip law

Stage-1: the concrete is in elastic (uncracked) phase and the bond stress τ_b is less than τ_1 (τ_1^P for plain or smooth bar and τ_1^D for deformed bar) in this stage. The bond

is represented by chemical adhesion between the concrete and steel bar. In this stage, the concrete surrounding the bar is uncracked and no slip occurs between the concrete and rebar. The chemical adhesion is accompanied by micro mechanical interaction that is provided from the rough steel surface. This chemical and mechanical interaction is broken when the bond stress increases and is followed by the slip of the bar. Then, a dry friction initiates between the concrete and rebar, which is strongly affected by the transverse pressures. Bar displacement may occur because of the bar slip at the interface and the shear deformations. Hence, the slip in **Stage-1** (see Figure 2.1) comes from the localized strains at the interface due to the shear deformation, not from the relative slip between the concrete and steel bar. In the case when plain bar is used, the bond stress-slip curve is as shown in curve 4a. **Stage-4a** is provided by friction, bar roughness, effect of transvers pressure and concrete shrinkage until the interface deteriorating due to slippage of the bar.

Stage-2 starts when bond stress for deformed bar $\tau_b > \tau_1^D$ as shown in Figure 2.1. Great bearing stresses in the concrete are induced by the bar ribs after breaking the adhesion. The transverse micro-cracks start to appear at the tips of the bar ribs. It is indicated that the steel bars with large ribs and small ribs spacing have a greater anchorage capacity. Also, the rib face should be inclined at 45° or more to the bar axis in order to achieve crushing of the concrete in front of the ribs during the pull-out of the bar (Hertz 1982).

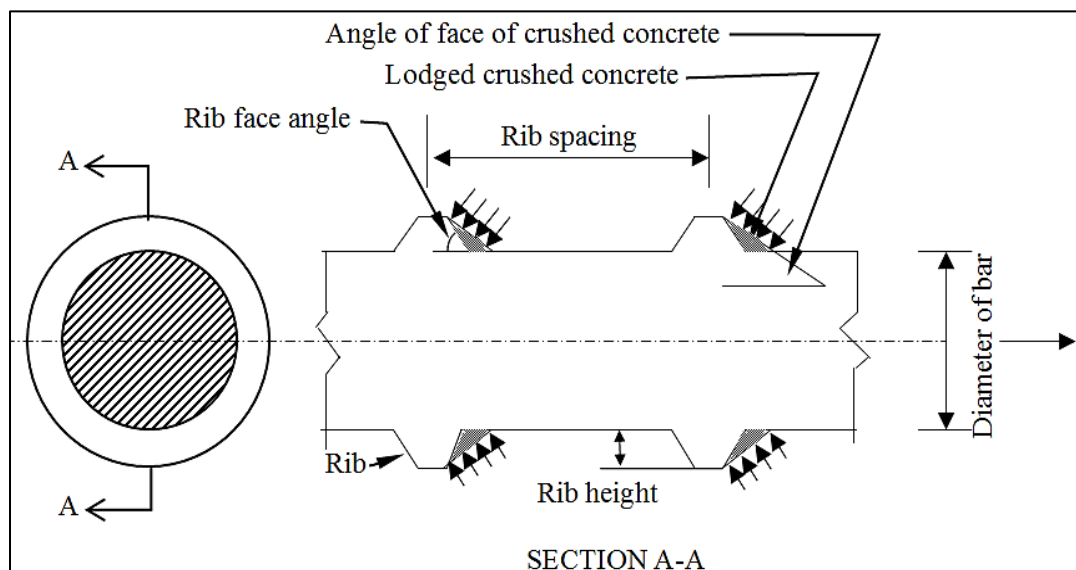


Figure 2.2 Wedge action between the steel bar and concrete (Tepfers 1979)

Stage-3 is the most important and complicated phase. This stage begins when the transverse cracks radially spread from the interface through the concrete cover due to wedging action and crushing the concrete in front of the bar ribs (see Figure 2.2 and 2.3). The transfer of the load between the reinforced bar and concrete is achieved by bearing of the ribs on the concrete interface. The resultant force acting on the rib is a compressive force generated due to the restraint of the surrounding concrete. As shown in Figure 2.3, the compressive forces P^* acting on the ribs, resulted from the pull out load, are decomposed into two directions, parallel and perpendicular to longitudinal axis of the reinforcing bar σ_l and σ_r , respectively. The reaction forces acting on the concrete due to the perpendicular components of P^* , create circumferential tension stresses σ_c in the concretes surrounding the steel bar. If these tensile stresses exceed the tensile strength of concrete, splitting failure occurs (see **Stage-4b** and τ_3 in Figure 2.1) (Tepfers 1979; CEB-FIP-Bulletin10 2000; Wang & Liu 2003).

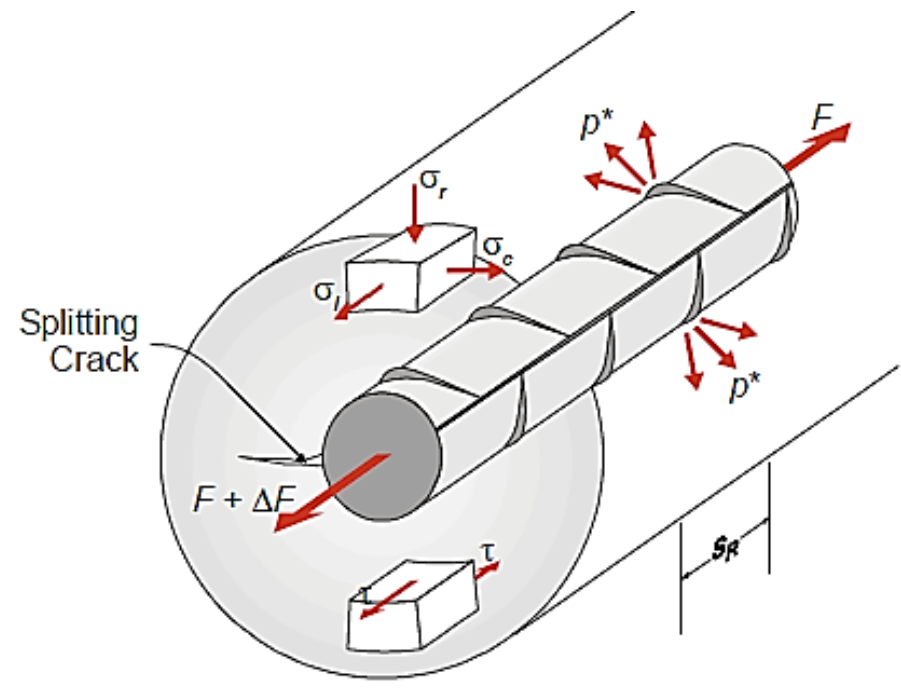


Figure 2.3 Bond stress in reinforced concrete for deformed bar

In the case of high confinement is provided from the concrete cover and the transverse reinforcement, a pull-out failure of bond occurs instead of splitting failure (**Stage-4c** in Figure 2.1). The type of bond failure due to the level of confinement effects may be defined as a ‘splitting-induced pull-out failure’ when the level of

confinement is moderate, or ‘pull-out failure’ if the level of confinement is high. In the pull-out failure the transfer of force mechanism changes from rib bearing to friction after crushing all concrete in front of the ribs. Finally, the bond will finish when the interface is flattened because of the wear and compaction. All these stages represent the local behaviour of the bond. However, the global behaviour of the bond is a result from the superimposition of the various stages (CEB-FIP-Bulletin10 2000).

2.2.2 Bond mechanism for prestressed concrete

Mechanism of the bond in prestressed concrete (PC) member depends on type of the prestress reinforcement (one wire or strand). Figure 2.4 illustrates the relation between the bond stress versus slip for the plain wire and strand. As shown from the figure the bond strength in strand does not drop after a small slip and that attributes to the mechanical interlocking.

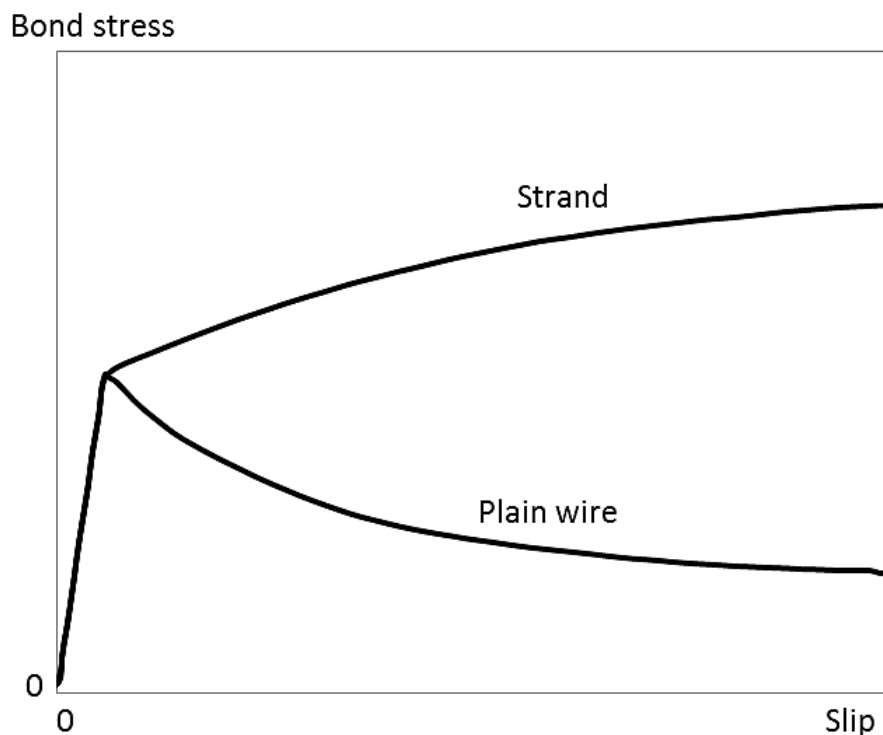


Figure 2.4 Bond stress-slip for plain wire and plain seven-wire strand (CEB-FIP-Bulletin10, 2000)

One high tension steel wire can be found as a plain or indented wire. For the plain wire, the bond mechanism is attributed to the adhesion and friction as well as the effect of Poisson’s ratio. Adhesion contributes by a minor value of the bond, as this

adhesion bond will disappear after a very small slip between the concrete and wire. Then, the pull-out force is transferred by friction. The friction between the steel and concrete is affected by many factors such as roughness of the interface and radial compressive stress (CEB-FIP-Bulletin10 2000). The radial stresses are generated as a result from shorten of concrete and Poisson's effect, in which the diameter of the wire will increase due to Poisson's effect after releasing the pretension force from the wire. This expansion in the diameter improves the bond by increasing the confinement. When the stress in steel increases as a result from the member loading, the Poisson's effect will decrease because of the reduction of wire diameter. As a consequence, the bond resistance decreases sharply until losing the bond stress when large slip occurs.

For the indented wire, some researchers proposed the mechanical interlocking between the indentations and concrete to work like the ribs in deformed bars. The theory of thick wall cylinder is adopted by (Benitez & Galvez 2011) to model the bond between the indented wire and concrete. This model can be used just in case of splitting failure of bond when thin concrete cover is used. The bond strength in this model is strongly affected by the shape and the size of indentation.

Strand is known as a group of wires (two, three or seven wires) are twisted to form the prestressing strand. Generally, the bond between the concrete and strand in PC member is categorized as transfer bond and flexural bond (Abrishami & Mitchell 1993). During PC manufacture, strands are initially pretensioned by using jacks at the ends abutments. The concrete is cast and cured then the strands are cut. Initial tensioning of the strands causes a reduction of the strands diameter due to Poisson's effect. After concrete reaches sufficient strength, the strands are released from the abutments, and the stresses in the strands at the free ends of the member return to zero. With this reduction of the strands stresses, the diameter of the strand expands along the transfer length and wedging action caused by lateral expansion (called Hoyer effect) results in improving the bond performance over the transfer bond length (Abrishami & Mitchell 1993). From the literature, to determine the bond stress for the flexural bond length, normal pull-out tests have been conducted by cast the concrete surrounding the strand then the strand is pulled from the concrete with measuring the pull-out force versus the slip. However, the bond for the transfer bond

length can be obtained by using push-in test. This test can be carried out by applying initial prestress on the strand between points A and B, and then casting the concrete at point C until the time of test, then releasing the stress from the strand at point A gradually toward point B with recording of the stress released versus the slip. This process is illustrated in Figure 2.5 (Abrishami & Mitchell 1993; CEB-FIP-Bulletin10 2000).

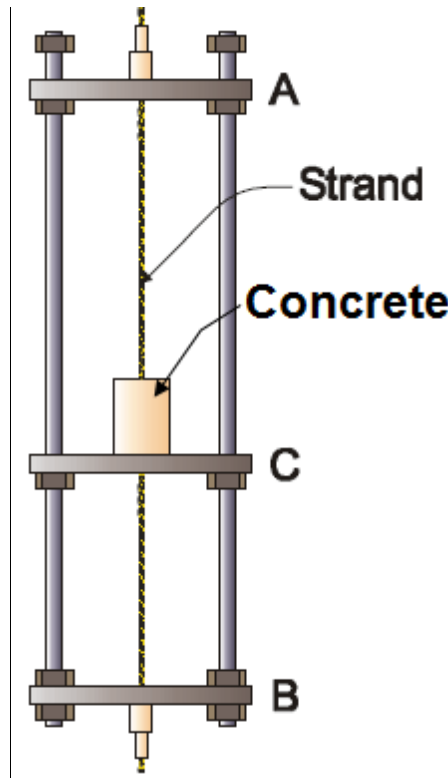


Figure 2.5 Push-in test apparatus

Figure 2.6 explains the difference between the transfer bond length and flexural bond length before and after member loading. Figure 2.6(b) shows the variation of stresses in the pretensioned strand along the beam after release the prestress from the strand and before loading. Figure 2.6(c) shows the variation of stresses in the strand for the same beam that is subjected to external load. The transfer bond length l_t , as shown in Figure 2.6(b) is the distance from the end of the concrete where the strand stress is zero to the point where the strand stress reaches to the maximum level for an unloaded beam. The flexural bond length l_f starts from the end of the transfer bond length to the point in which the ultimate stress can be developed after loading (see Figure 2.6(c)).

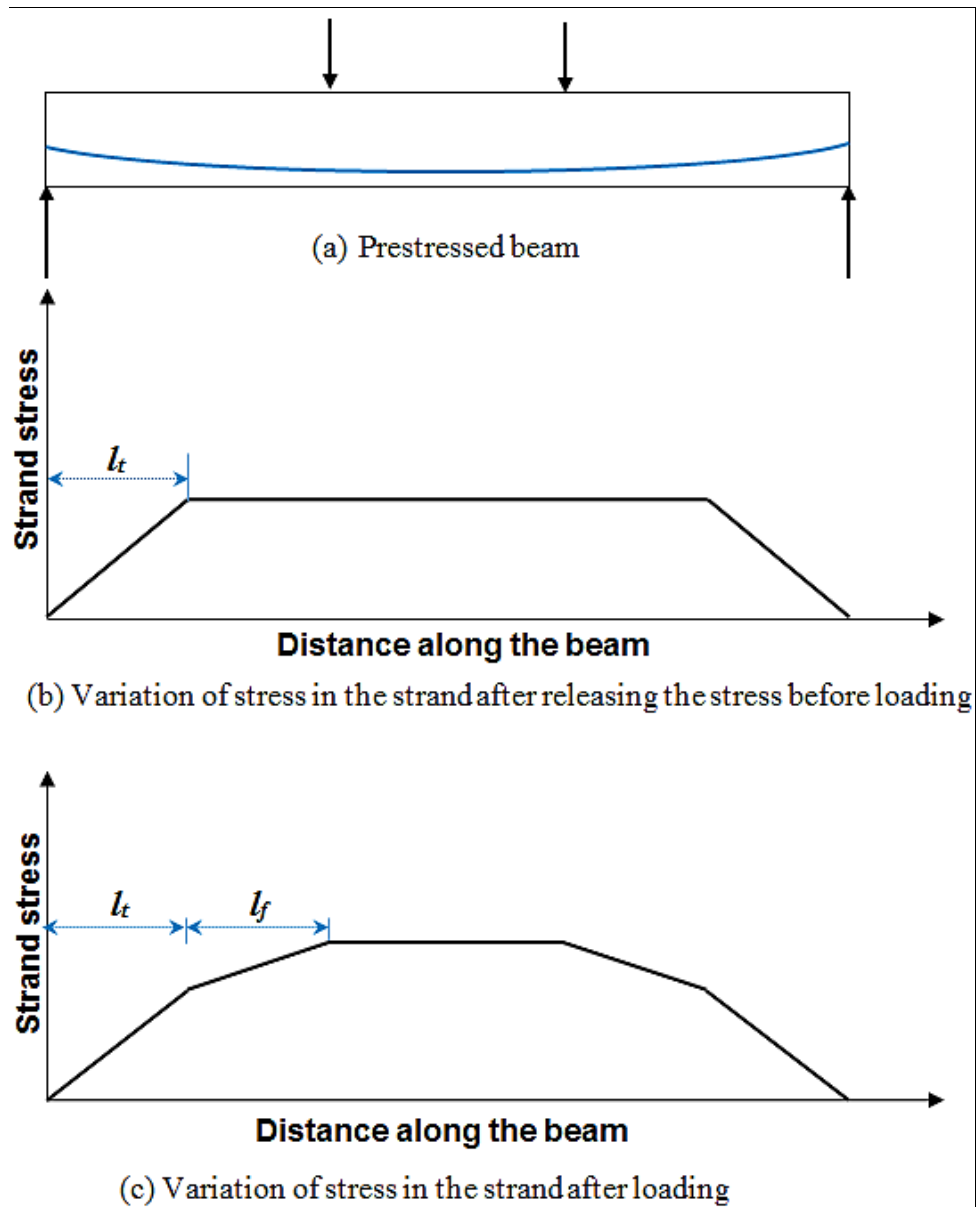


Figure 2.6 Transfer bond length and flexural bond length before and after member loading

The mechanism that contributes to the bond between prestressed strand and surrounding concrete is known as chemical adhesion, friction and mechanical interlocking between the outer wires of the strand and concrete. Adhesion bond has a small effect on the total bond which can be lost in the early stage after little slippage in the strand. Then, the main dominant factors to the bond mechanism are the dry friction and mechanical interlocking (Marti-Vargas et al. 2013). As mentioned before, concrete shortening and Poisson's effect provide the confinement to the reinforcement, which contributes in increasing the friction bond strength. However, a reduction in the diameter of the strand can occur after member loading, resulting in

decreasing the effect of friction due to confinement reduction. Hence, the mechanical interlocking becomes the main provider to the bond strength.

When concrete is casted around the strands in prestressed concrete members, the concrete forms an envelope or sleeve surrounding the strand. The hardened concrete mimics the shape of strand. When the strand is pulled through the concrete, the movement is resisted by the concrete keys acting on the outside wires of the strand. The mechanical interlocking is the largest contributor to the bond, especially in cracked regions. When the cracks are formed in the concrete surrounding the strand, the slip of the strand occurs for some small finite distance on either side of the crack to preserve the compatibility of the strand (Russel & Burns 1993). When the slip occurs, the mechanical interlocking is activated by the interlocking reaction of the outside wires of the strand with the concrete envelope. The slip is caused mainly by crushing of the concrete in front of the strand's ridges. The high pressure on the concrete in front of the ridges causes tensile stresses in the concrete surrounding the strand, which in turn create internal inclined cracks. These inclined cracks are initiated at relatively low bond stresses at the point of contact between the strand and concrete. Growing of the stress in the strand leads to increasing the slip, and the concrete in front of the ridges will be crushed. More slip can occur due to more local crushing takes place. Thereafter, shear cracks will initiate within the concrete keys between the strand ridges. After reaching the maximum bond resistance, these concrete keys are sheared off and deterioration of the bond will start (Russel & Burns 1993; Choi et al. 2010).

2.3 Factors affecting on the bond behaviour

Bond behaviours of normal and prestressed concrete structures are affected by different factors and parameters. Type of concrete and reinforcement in addition to the external environment and affect the state of stresses are the main factors that influence on the bond behaviour.

2.3.1 Effect of concrete on the bond behaviour

The quality of concrete is one of the most important factors affecting the bond characteristics. As mentioned before, the bond action is a result from the pressure that formed in front of the bar ribs and the shear forces of the concrete in the

interface between the concrete and rebar. Therefore, the capacity of bond strength is directly affected by the concrete compressive and tensile strengths. Also, the cast direction of the concrete with respect to bar orientation is another factor which effects on the bond performance. The bond behaves better when the bars placed horizontally close to the bottom of the concrete member, and for the vertical bars the cast of the concrete in the direction against bar loading gives better bond strength (CEB-FIP-Bulletin10 2000). Concrete cover plays a significant role in bond performance. Increasing the concrete cover provides the confinement to the rebar and increases the level of the circumference stresses within the concrete cylinder surrounding the steel bar. The state of these stresses can weaken the bond strength and can change the bond failure from pull-out to splitting failure.

2.3.2 Effect of reinforcement on the bond behaviour

The geometry of reinforcing bar can control the behaviour of bond. In case of deformed bar is used in reinforced concrete structures, the bond is strongly affected by the rib height h , rib spacing S_R and the bar's diameter d_b . The bond index f_R can be calculated based on these factors as:

$$f_R = \frac{A_R}{\pi \cdot d_b \cdot S_R} \quad (2.1)$$

where: A_R is the area of the two side of the projection rib. Generally, the bond index is in the range of 0.05-0.1, which can give a good indication about the bond performance (CEB-FIP-Bulletin10 2000).

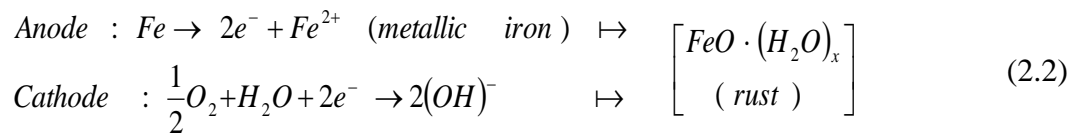
Yielding the steel in the plastic range has a severe effect on the bond strength (similar to the effect of splitting). A reduction in the steel diameter can occur due to steel yielding. This bar contraction leads to a great reduction in the friction between the concrete and rebar, and also affect the geometry of the bar ribs (bond index) (CEB-FIP-Bulletin10 2000).

For prestressed concrete members indented strands perform better than smooth strands in terms of bond, but it could be dangerous when thin prestressed members are used due to splitting failure. Typically, increasing the outer wires diameters and reducing the pitch angle of them result in higher bond strength. Poisson's ratio

(Hoyer effect) has an important effect on the bond strength within the transfer length of the prestressed member when the steel is in the elastic range (Russel & Burns 1993).

2.3.3 Effect of the environment on the bond behaviour

Environment can significantly affect the concrete and the reinforcement in the concrete constructions and consequently affect the bond between them. The most typical effect is the rust of the steel bars. The steel may gain the rust resulting initially from cooling after rolling temperature; exposed to the atmospheric humidity, pollution and condensation. The small initial rust has a positive effect on the bond, since it can increase the friction between concrete and reinforcement. However, more steel corrosion leads to reduction in the dimension of the bar ribs and the cross-section of the rebar itself. Corrosion of reinforcement steel bar is a result from penetration of the chloride ions, carbon dioxide and the oxygen into the concrete and act with the concrete and steel bar. Chemical reaction between carbon dioxide from the air and the hydration products of cement in concrete causes a reduction in the alkalinity of concrete and consequently in its ability to protect the steel reinforcement from corrosion (Burkan & Ghani 2004). The action of the iron oxide is an electrochemical process in which a part from the rebar becomes anodic and the other part works as cathodic as illustrated bellow (Kumar & Paulo 2006):



The transformation of metallic iron to rust is accompanied by volume expansion as shown in Figure 2.7. This expansion causes cracking of the concrete surrounding the steel bar, which consequently weakens the bond between the rebar and concrete, as well as splitting and spalling of the concrete cover. The best way to resist the corrosion is to reduce penetration of the chloride and other ions. This can be achieved by increasing the concrete cover and control the permeability of the concrete by reducing water-cement ratio, adequate cement content and control the aggregate size and grading, as well as using admixtures like fly ash. Another way to resist the corrosion in reinforced concrete structures is by coating the steel bar and using cathodic protection (Kumar & Paulo 2006).

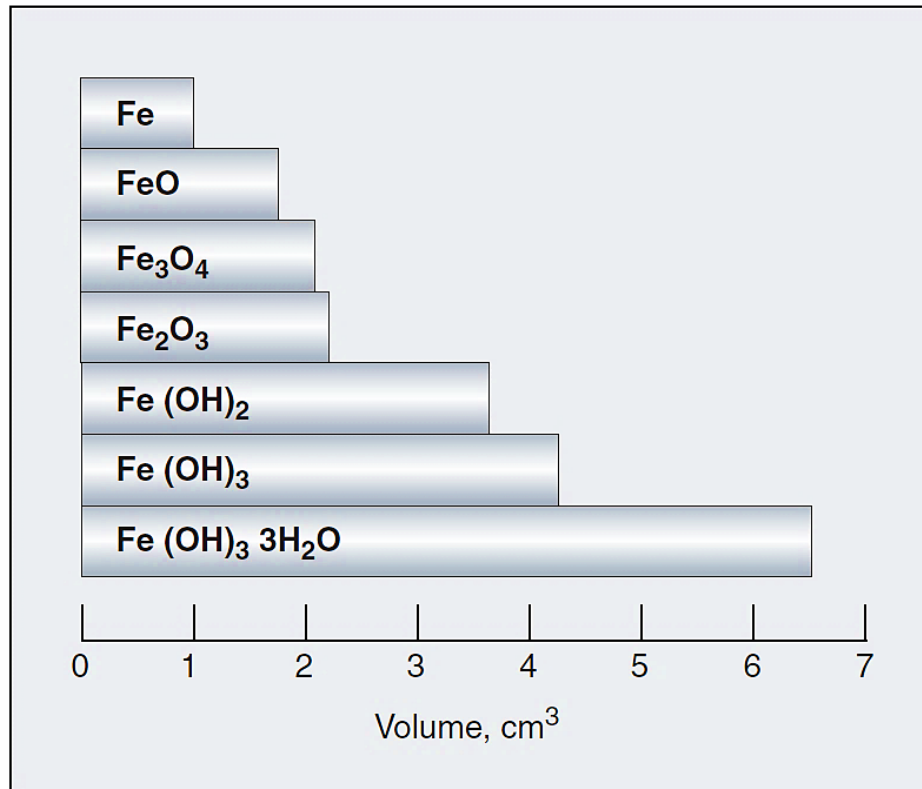


Figure 2.7 Expansion of concrete due to corrosion of the embedded steel (Kumar & Paulo, 2006)

Another environmental factor effect on the bond is the low and high temperature. Generally, low temperature has a favourable effect on concrete by increasing the compressive strength, the tensile strength and the modulus of elasticity of the concrete (CEB-FIP 2010). Hence, the bond strength for reinforced concrete members at low temperature is usually higher than that at room temperature, and the bond failure can be shifted from splitting to shear failure at -40°C (CEB-FIP-Bulletin10 2000). The effect of high temperatures on the bond is intensively explained in Section 2.5.3.

2.4 Design codes related to the bond of reinforced concrete

The development of economical and reliable concrete structure system depends on the improvement of design codes. The codes are usually developed based on the knowledge of designers, researchers, contractors as well as the codes' written bodies themselves. The rules in the code have to be general and widely applicable in different scenarios. Also, the rules should be simple and easy to apply and the most important thing is to be robust and conservative. Generally, for reinforced concrete structures, strain compatibility between concrete and reinforcement is the main

factor that should be maintained, thus the components act as a composite structure. Design codes such as European standard (EN), American Concrete Institute (ACI) and *fib* (CEB-FIP) follow the research community by taking the information in form of test data, formulas and recommendation. Then rules are set for designers for structural design (CEB-FIP-Bulletin10 2000). Bond performance is affected by a lot of parameters such as material properties, concrete confinement and bar spacing. The majority of bond formulations in the current design codes are empirical based on a statistical methodology. Thus, these formulations are highly dependent on the test data, which may limit their validity in the different situations (Huanzi 2009). Therefore, the newer form of analysis involves complicated examination using nonlinear finite element calculations to give more details about the bond phenomena (Phan et al. 2010). Lots of national codes are to represent a particular national view and philosophy, for example American Concrete Institute (ACI), Germany Industry Norm (DIN), British Standards (BS) and Japanese Society of Civil Engineering (JSCE). However, few codes are considered as multinational codes such as the Eurocodes (EN) and CEB-FIP Code. These multinational codes have been developed based on the collective experience of researchers and designers all over the world (CEB-FIP-Bulletin10 2000).

It is important to know the way that codes explain the bond. Designing for bond in codes is explained based on the traditional capacity design approach. Hence, actual bond stress is not necessarily to be calculated; rather the anchorage length should be computed to the point of bar yielding, which can be done by giving the materials and the geometric properties of the anchorage. Formulations of bond stress in codes are empirical relationship based on the test data of bond strength. These bond formulas in the design codes are found to be simple and can be used for the hand calculation of anchorage length. However for more complicated situations, such as earthquake or blast, a computer program is needed to perform the analysis by using finite element methods.

The accurate evaluation of the performance of reinforced concrete structures depends on the ability of the designer to model the constituent materials as well as the bond between the concrete and steel bars (Phan et al. 2010). The most popular bond-slip model is the one in the CEB-FIP Model Code 90 (CEB-FIP Model code 90 1991).

For the bond strength it is generally supposed that increasing the bond strength result in improving the performance of the reinforced concrete structure itself. However, this opinion is not always supported by the experimental data. This is because that the failure mode of the bond can change from pull-out to splitting failure, which decreases the ductility of the member. In such case, increasing the capacity of splitting bond in the member can be done by providing additional confinement to the bar, which can be achieved by providing extra transvers steel. From this point of view, extra cost to increase the bond strength is not needed and the performance of the structure still acceptable even there is a small slippage in the bar (CEB-FIP-Bulletin10 2000).

2.5 Effect of high temperatures on the properties of reinforced concrete structures

The behaviour of reinforced concrete structural element exposed to fire depends on the thermal and mechanical properties of its component (concrete, steel and bond between them). Previous researches indicated that concrete structures begin losing strength rapidly when temperature reaches higher than 300°C. Typically, when temperature exceeds 1000 °C the concrete compressive strength reduces by about 90% and the modulus of elasticity reduces by 70% compared to the values at ambient temperature. The strength of reinforcing steel bars is intensively decreased after temperature of 300 °C. At temperature about 600°C, the strength of reinforcement is only about 35-45% of the corresponding strength at ambient temperature. Also the reduction of the bond strength between the concrete and steel bar is about 30-50% of its ambient temperature strength at temperature of 400°C-500 °C. All these reductions in material strengths cause degradation in the stiffness of reinforced concrete structural member (Morley 1982; Griffin & Beavis 1992; CEN 2004a; Elghazouli et al. 2009; Rivera et al. 2016).

On the other hand, at elevated temperatures cracking and spalling of concrete can also take place due to different rate of longitudinal thermal expansion of steel and concrete. The spalling of concrete cover causes buckling of reinforcement due to directly exposed to fire. Also, concrete member cannot fulfil its structural requirements if the bond between concrete and reinforcement is lost because of the

high temperatures. As a result, the concrete element loses its load carrying capacity and failure can take place. However, when the whole structure is considered under fire conditions two notes should be taken in consideration for design: the first note is the capacity of the concrete members will change due to the redistribution of forces and bending moments within a continuous structure, and the second note is the restraint of the member by the surrounding cooling structure may give an increase in fire resistance (Morley 1982). Therefore it is important to study the effect of elevated temperatures on the thermal and mechanical properties of concrete and reinforcement as well as the bond between them.

2.5.1 The properties of concrete at elevated temperatures

2.5.1.1 Thermal properties of concrete

Thermal properties of concrete such as thermal conductivity K_c and specific heat $C_{p,c}$ are strongly affected at elevated temperatures. Thermal conductivity of concrete is influenced by many factors such as moisture and mix characteristics of concrete. Generally, thermal conductivity of air is much lower than thermal conductivity of water. Therefore the loss of moisture, when concrete is exposed to high temperature, leads to replace the free water with air, which results in lowering the thermal conductivity of concrete. Normally, thermal conductivity of aggregate is higher than that of cement past. Hence aggregate is the responsible factor for the considerable variation of concrete thermal conductivity. Previous researches indicated that thermal conductivity of aggregate decreases by increasing temperature (NUREG/CR-7031 2010). Specific heat $C_{p,c}$ of concrete is increased when temperature is increased. Figure 2.8 and 2.9 illustrate the thermal conductivity and specific heat of concrete at elevated temperatures, respectively (CEN 2004; Gao et al. 2013).

Thermal expansion of concrete represents the change of concrete volume due to the change of temperature. The thermal expansion of concrete has an effect on the structural movement and thermal stresses, which can lead to cracking and spalling of the concrete at elevated temperatures (NUREG/CR-7031 2010). The thermal expansion of concrete increases with temperature, as shown in Figure 2.10 (CEN

2004). Moreover, due to drying, dehydration, disintegration and thermal expansion of concrete at elevated temperatures, concrete experiences a reduction in weight and density (Huang 1995).

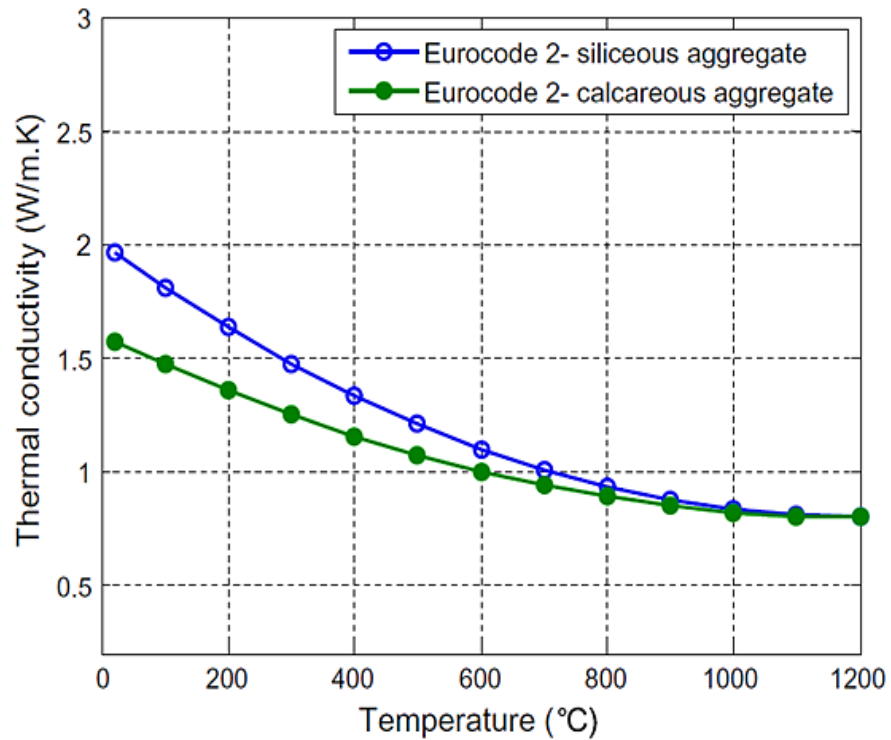


Figure 2.8 Thermal conductivity of concrete at elevated temperatures (CEN, 2004a)

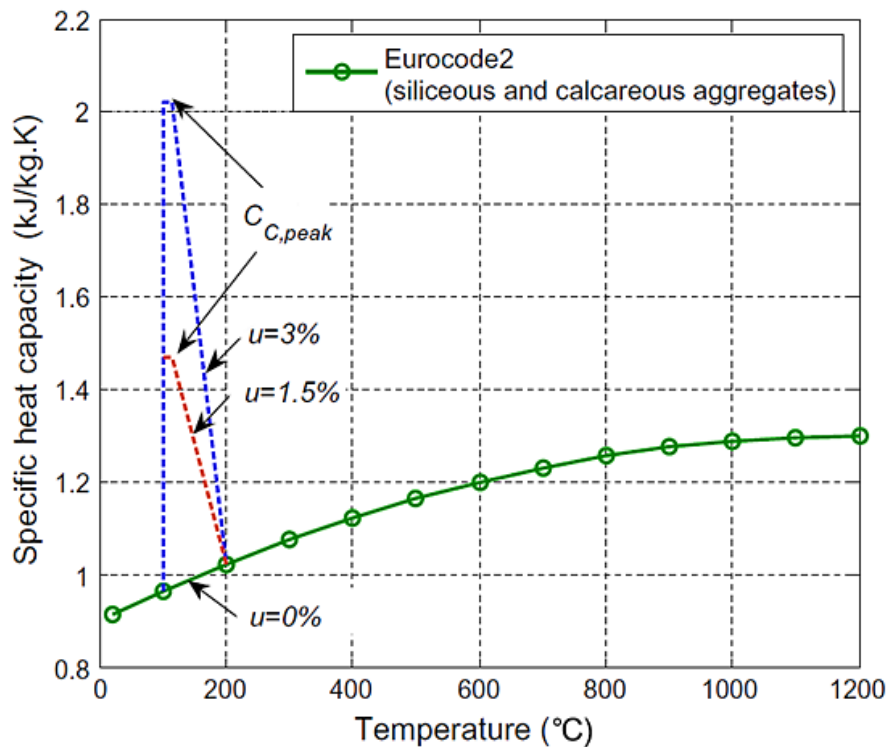


Figure 2.9 Specific heat capacity of concrete at elevated temperatures (CEN, 2004a)

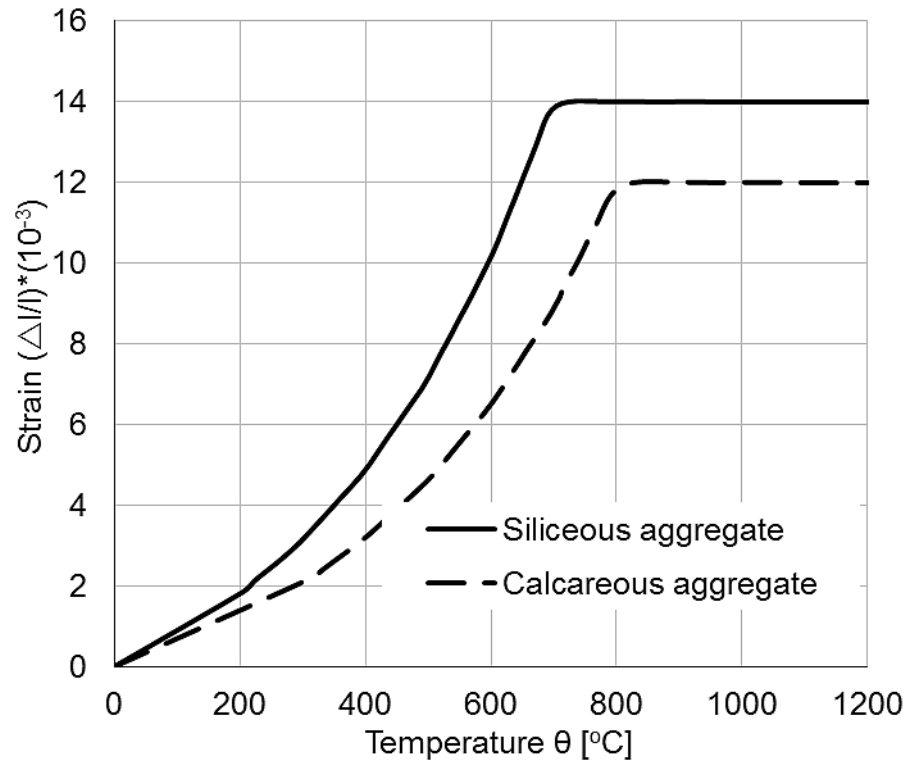


Figure 2.10 Thermal expansion of concrete at elevated temperatures (CEN 2004a)

2.5.1.2 Mechanical properties of concrete

The mechanical properties of concrete, such as strength and modulus of elasticity, are significantly affected by high temperature. Compressive strength of concrete is considerably reduced at elevated temperatures. This reduction is attributed to the degradation of the calcium silicate hydrate (C-S-H) because of water losing and dehydration of other components such as calcium hydroxide ($Ca(OH)_2$) and ettringite ($Ca_6Al_2(SO_4)_3(OH)_{12} \cdot 26H_2O$). Also different thermal expansion of aggregate and cement past is another important factor to initiate internal thermal stresses and form micro-cracks which can crumble the concrete (Arioz 2007).

Adding water to cement is necessary for hydration process, but adding extra water to increase the workability will result in increasing the water porosity (Rivera et al. 2016). Exposing the concrete to high temperature leads to generate a water vapour pressure inside the pores. This will result in concrete cracking, damaging concrete elements and explosive spalling of concrete, especially with high density and low porosity of the cement past.

The properties of concrete can be improved for resisting high temperature by using amelioration materials, such as fly ash and slag. The use of these materials can reduce the amount of chemical and physical sorbet water which can limit the interior stresses and spalling at elevated temperatures (Rivera et al. 2016).

As mentioned above, concrete can be decomposed due to the thermal incompatibility between aggregate and cement paste at high temperatures. Hence, the performance of concrete at elevated temperatures is considerably affected by the aggregate type due to the variation of thermal conductivity and thermal expansion of aggregates. The thermal conductivity of concrete affects the rate of heat transfer between the exposed surface and cool surface whereas the thermal expansion of concrete affects the cracking and spalling of concrete. Calcareous aggregates have more favourable thermal properties than siliceous aggregates due to less thermal expansion and thermal conductivity (Morley 1982). When concrete is exposed to high temperatures cement paste shrinks while the aggregate expands. Therefore, cracking of concrete can occurs due to the different volume changes between aggregate and cement paste.

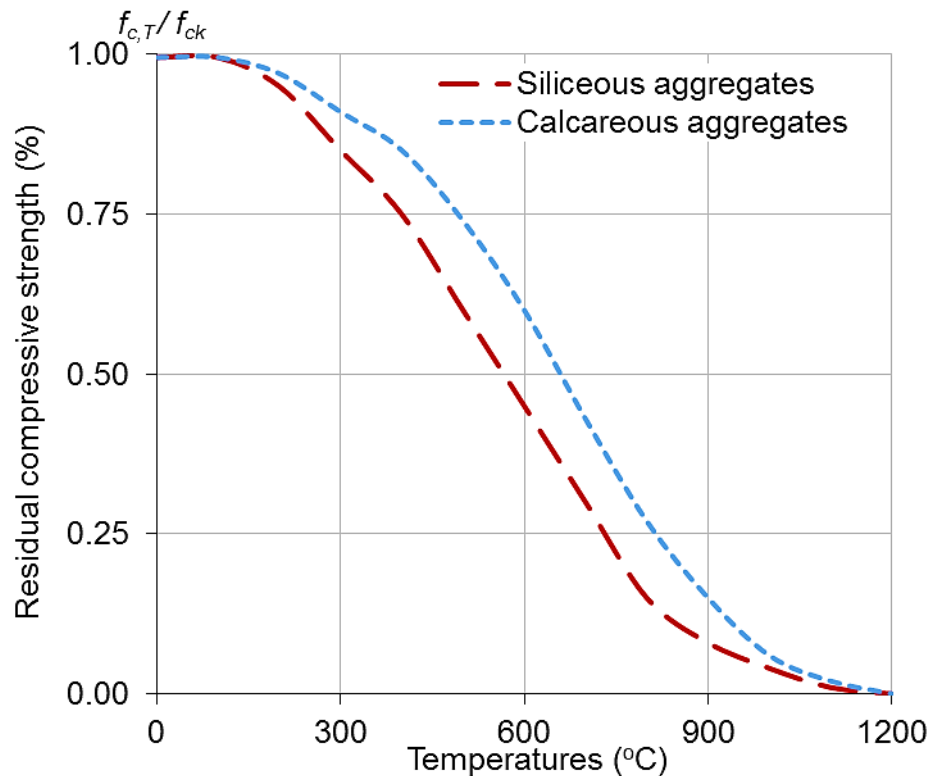


Figure 2.11 Degradation of concrete compressive strength at elevated temperatures (CEN, 2004a)

As a result from material degradation at elevated temperatures, loss of concrete strength and stiffness will occur. Figure 2.11 shows the degradation of concrete compressive strength under elevated temperatures (CEN 2004). Generally, softening behaviour of concrete at ambient temperature is not taken into consideration due to small value of the deformation of reinforced concrete members after loading. However, under extreme loading (such as fires) this softening becomes an important phase during structural analysis. Softening behaviour of concrete is affected by concrete confinement which can be provided by the transverse reinforcement, whereas confinement can increase the ductility and capacity of concrete (Legeron et al. 2005).

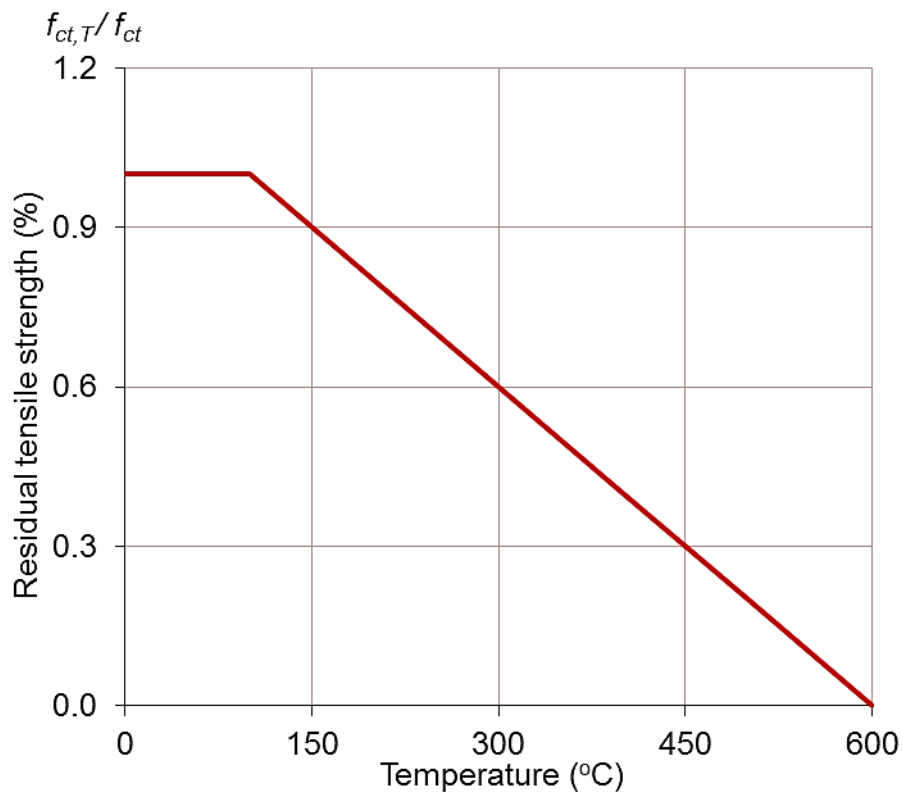


Figure 2.12 Degradation of concrete tensile strength at elevated temperatures

Concrete in tension is not considered in reinforced concrete design due to its brittle behaviour. Therefore, tensile stress in tension region of the member is transferred directly to the reinforcement, even the tension stiffening exists for concrete in tension as stated in (CEB-FIP Model code 90 1991). The degradation of concrete in tension under fire condition is greater than that in compression. Figure 2.12 shows the degradation of concrete tensile stress-strain curves at elevated temperatures as

stated in Eurocode 2 (CEN 2004). However, this degradation model proposed in Eurocode 2 has not been used in the bond models developed in this research because the concrete tensile strength becomes zero when temperature is above 600°C, as shown in Figure 2.12. Hence, the degradation of the tensile strength of concrete at elevated temperatures proposed by (Aslani & Bastami 2011) is adopted in this research. That is:

$$f_{ct,T} = f_{ct} \begin{cases} 1.02 - 0.00098 \times T & 20 < T \leq 300 \text{ } ^\circ\text{C} \\ 0.965 - 0.0001 \times T - 9 \times 10^{-7} T^2 - 3 \times 10^{-9} T^3 + 3.2 \times 10^{-12} T^4 & 300 < T \leq 900 \text{ } ^\circ\text{C} \\ 0.0 & T > 900 \text{ } ^\circ\text{C} \end{cases} \quad (2.3)$$

where $f_{ct,T}$ is the concrete tensile strength at temperature T , f_{ct} is the concrete tensile strength at ambient temperature.

2.5.2 The properties of reinforcement (steel bar and strand) at elevated temperatures

For the structural design of reinforced concrete structures in fire, it is important to identify the critical temperature for the steel reinforcement. The critical temperature for the steel can be defined as the temperature in which the steel tensile strength reaches to the actual stress within the reinforcement steel (Griffin & Beavis 1992). Generally, reinforcing steel recovers its strength after cooling when it is exposed to temperatures about 300-400 °C. In fact, even this recovery in strength can occur, prestressed strands may lose their prestress tension (relaxation effect) after cooling.

2.5.2.1 Thermal properties of reinforcement

The thermal properties of the reinforcing steel bars and strands (thermal expansion, specific heat capacity and thermal conductivity) change with temperature, as stated in Eurocode 2 (CEN 2002). At elevated temperatures, reinforcing steel and strands tend to expand as shown in Figure 2.13.

By increasing the temperature, thermal conductivity k_s of the steel decreases and specific heat increases (Huang 1995). Normally, the volume of reinforcing steel constitutes only with a small percentage of reinforced concrete members. Therefore,

the effect of steel reinforcement on the temperature distribution within the cross-section of concrete members can be neglected for thermal analysis (Bizri 1973).

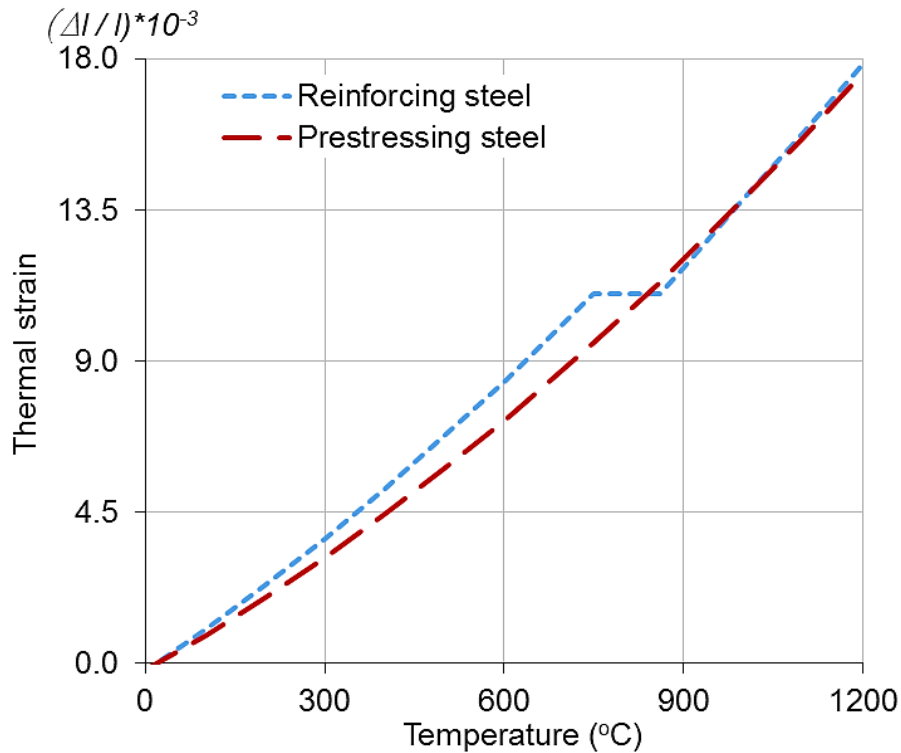


Figure 2.13 Thermal strains of reinforcing steel bar and strand

2.5.2.2 Mechanical properties of reinforcement

The reduction of steel strength and stiffness is significant under fire conditions. Cold work steel bars lose their strength more quickly than hot rolled steel bars during heating (see Figure 2.14). After cooling, the steel bars tend to recover their original strength. The residual strength of both types of steel bars remains unchanged up to 400 °C. However, at 600°C the steel bar will loss 10-15% of its original strength after cooling (Elghazouli et al. 2009). Exposing of reinforcement to high temperature leads to significant reduction in yield strength. As shown in Figure 2.14 (CEN 2004), steel can reach to the half of its original strength at the temperature of 550°C.

For the prestress steel, the loss of strength occurs at lower temperatures compared to normal steel bar. A considerable reduction can occur in prestress steel strength at temperatures 300–400 °C as illustrated in Figure 2.15 (CEN 2004). The steel bar as a polycrystalline material has an ordered microstructure consisting of iso-oriented crystalline regions or grains. Some defects and imperfections at the atomic scale

called as “dislocations” can be found in the crystalline structure. The creation, multiplication and interaction among the dislocations together with grain size explain why high dislocation densities and small-size grains improve yield strength of a material. At high temperatures the unstable microstructure undergoes a rearrangement of the dislocations leading to a final smaller dislocation density. The smaller dislocation density together with the formation of new grains which are larger than the original grains explains the observed sensitivity of the mechanical properties of the rebar to high temperature (Kumar et al. 2013).

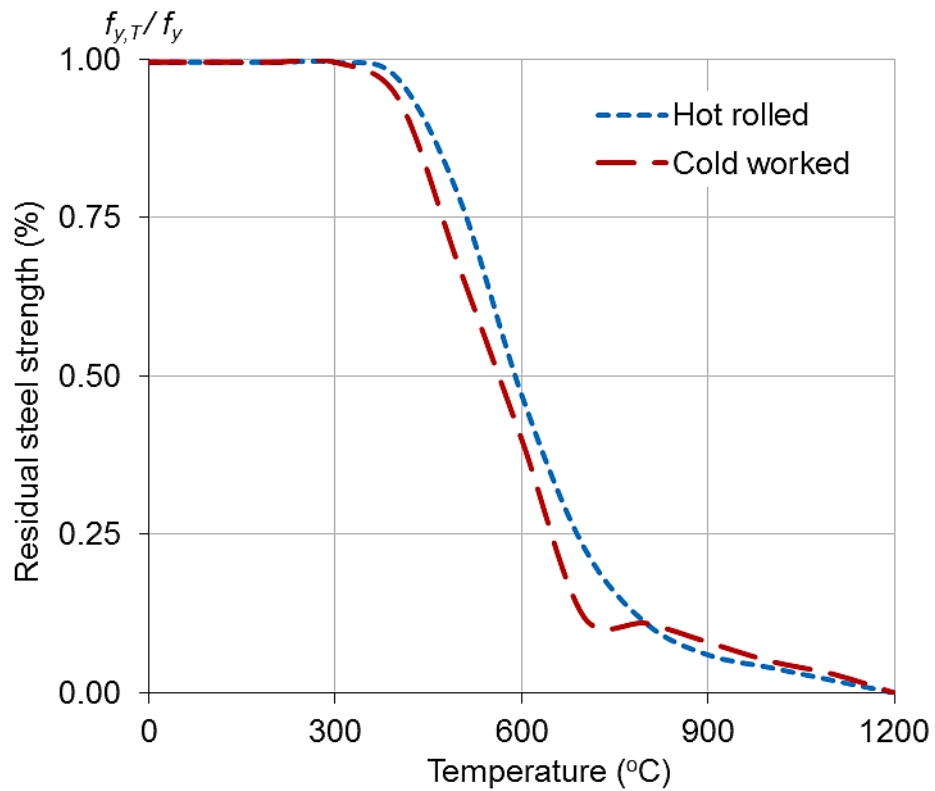


Figure 2.14 Degradation of steel bars strength at elevated temperatures (CEN, 2004a)

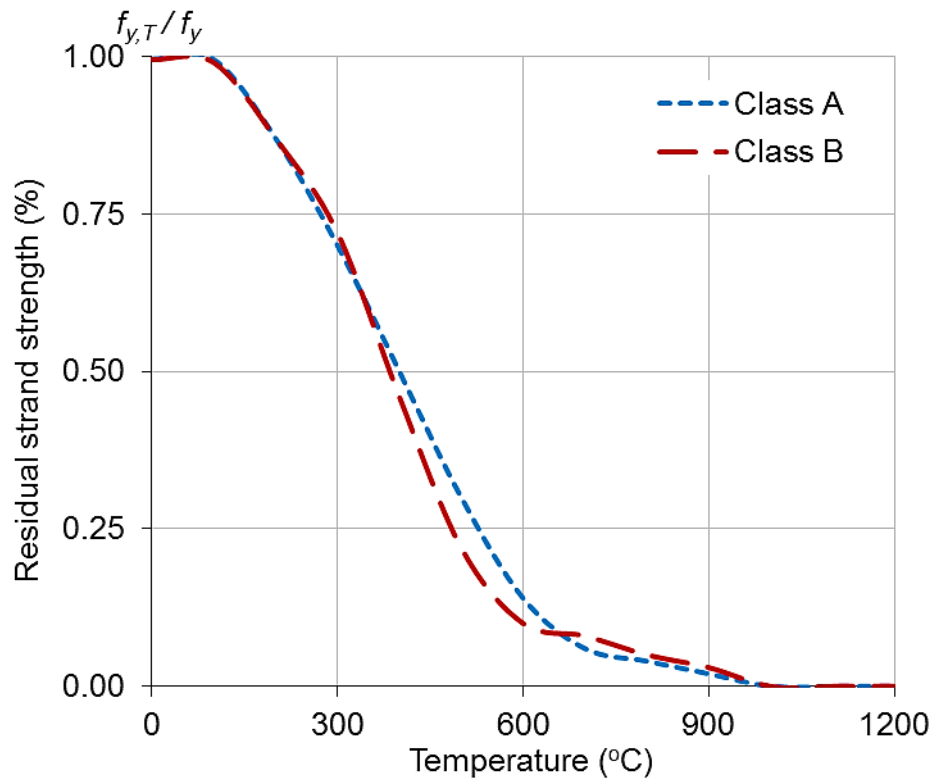


Figure 2.15 Degradation of strands strength at elevated temperatures (CEN, 2004a)

2.5.3 The bond behaviour at elevated temperatures

Reinforced concrete member undergoes many changes in its components (concrete and steel) after exposed to high temperatures. These changes significantly affect the interaction between steel reinforcement and concrete. Investigations on the behaviour of the bond between concrete and reinforcement at ambient temperature have been carried out over many years. However, for reinforced concrete members at elevated temperatures limited studies have been done due to complexity. Generally, previous researchers have drawn some conclusions about the bond strength under fire conditions. They indicated that the bond between concrete and steel reinforcement at elevated temperatures decreases with rising temperature and the rate of the reduction is greater compared with the reduction of concrete compressive strength. Also the reduction of the bond strength for plain bars at high temperature is more than that for ribbed bars and the bar diameter had little effect on the reduction of bond strength. Furthermore, the bond strength at elevated temperatures is influenced by the type of aggregate in concrete as well as the thickness of concrete

cover. Also, the bond strength at high temperatures is affected by the procedure used in experiment (Bazant & Kaplan 1996; Huang 2010).

At elevated temperatures, compressive stresses in the cement paste can occur due to the thermal expansion of the steel bar. These stresses act perpendicularly to the bar axis in the interface between the concrete and steel bar and the effect is radially reduced toward the concrete cover (Pothisiri & Panedpojaman 2012). On the other hand, similar stresses act in the cement paste surrounding the aggregates and these stresses depend on the aggregate type. The resultant from all these stresses is stresses called difference stresses. Based on Hertz (1982) study, these stresses are about 10-20 MPa at temperature 300°C for limestone concrete, but for quartz concrete they are less (Hertz 1982).

A study conducted by United State Nuclear Regulatory Commission (NUREG/CR-7031 2010) indicated that the bond strength is a function of three parameters: (I) concrete properties (water-cement ratio, type of cement and admixtures), (II) mechanical properties of steel bars (size and spacing of the ribs), (III) position of the bar within the concrete member (vertical bars have greater bond than horizontal bars).

An investigation about effect of using different types of steel bars on the bond strength at high temperatures was conducted by Diederichs & Schneider (1981). Cylindrical concrete specimens with concrete compressive strength of 48-60.9 MPa at 28 days (50.7-63.9 MPa at test time) were used in this investigation. The specimens were heated to the target temperature, and maintained at that temperature for three hours, and then pull-out tests were performed. Different types of steel bars were used in this investigation (ribbed bars, plain round bars and prestressing bars).

The effect of temperature on the bond-slip relationship are shown in Figures 2.16, 2.17 and 2.18, for 16 mm diameter deformed bars, 7.5 mm diameter prestressing steel bars and 8 mm round plain bars, respectively. Degradation of bond strength under elevated temperature is explained in Figure 2.19. The conclusions from the study were: the reduction rate of bond strength for ribbed bars was the same as the reduction rate of concrete compressive strength; the loss of bond strength for plain bars was greater than that in ribbed bars; rusted plain round steel bars exhibited better bond performance than fresh rolled plain steel bars (see Figure 2.19) (Diederichs & Schneider 1981).

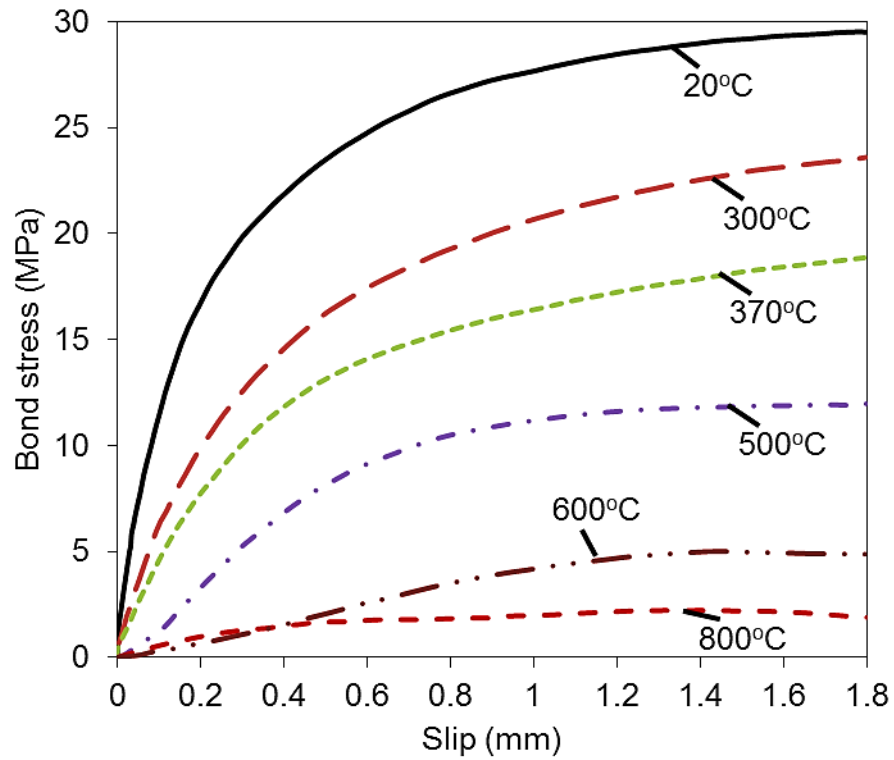


Figure 2.16 Bond stress-slip relationship of cold deformed steel at elevated temperatures (Diederichs & Schneider 1981)

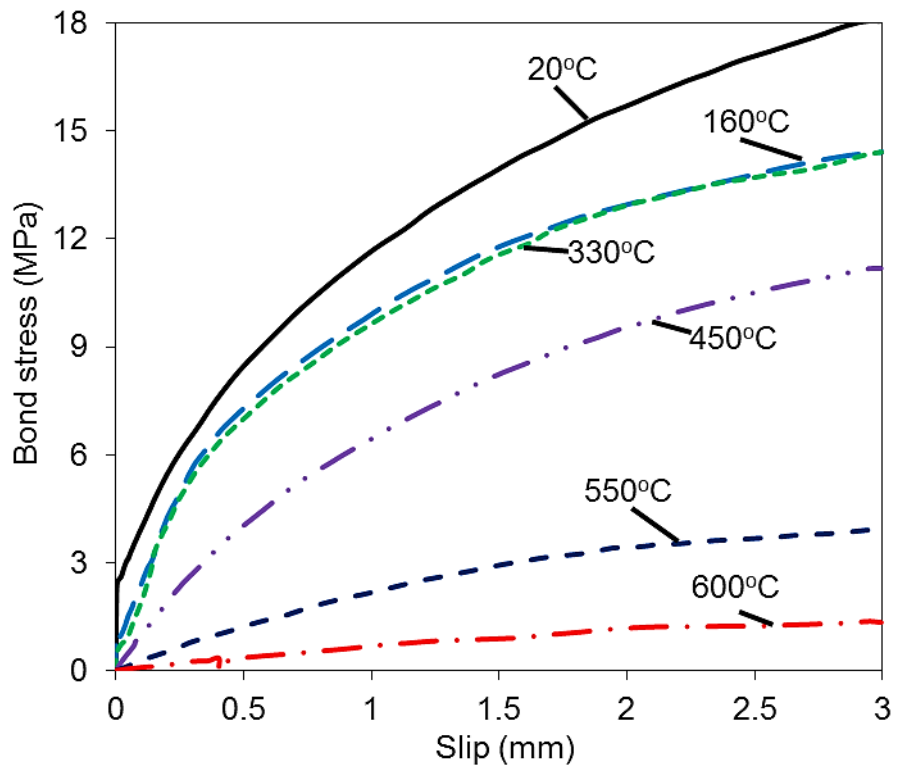


Figure 2.17 Bond stress-slip relationship of prestressing steel at elevated temperatures (Diederichs & Schneider 1981)

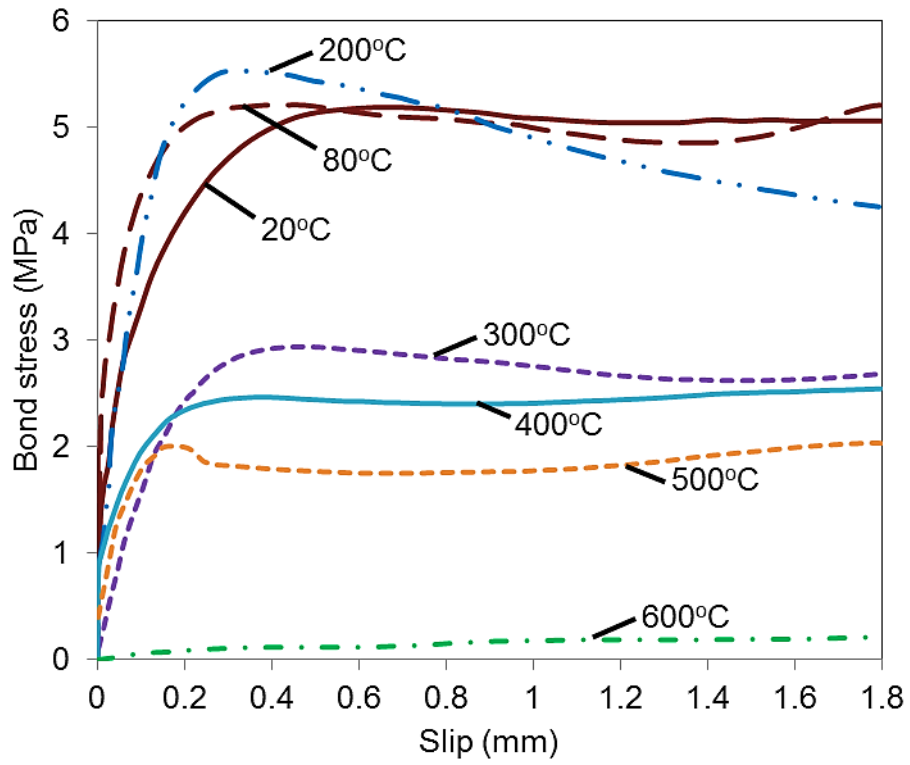


Figure 2.18 Bond stress-slip relationship of rusted plain round bars at elevated temperatures (Diederichs & Schneider 1981)

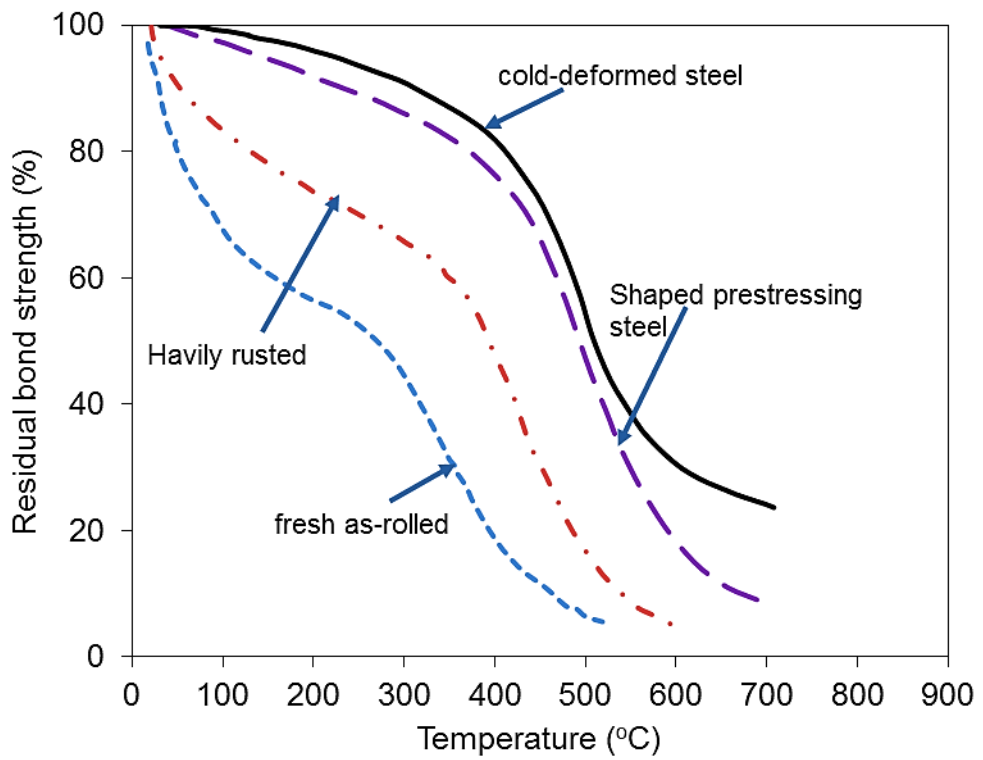


Figure 2.19 Relative bond strength of various reinforcing bars as a function of temperatures (Diederichs & Schneider 1981)

The residual bond strength after heating was experimentally investigated by Hertz (1982). Different bar's diameters (8-25 mm) with concrete compressive strength of 20 MPa were used in this study. The specimens were firstly subjected to temperatures up to 800°C, and held them at that temperature for two hours, then allowed them to cool slowly before the test. The bond strength was represented as the percentage of the concrete compressive strength to evaluate the residual bond strength. The study indicated that the residual bond strength for ribbed bars was greater than that for plain round bars.

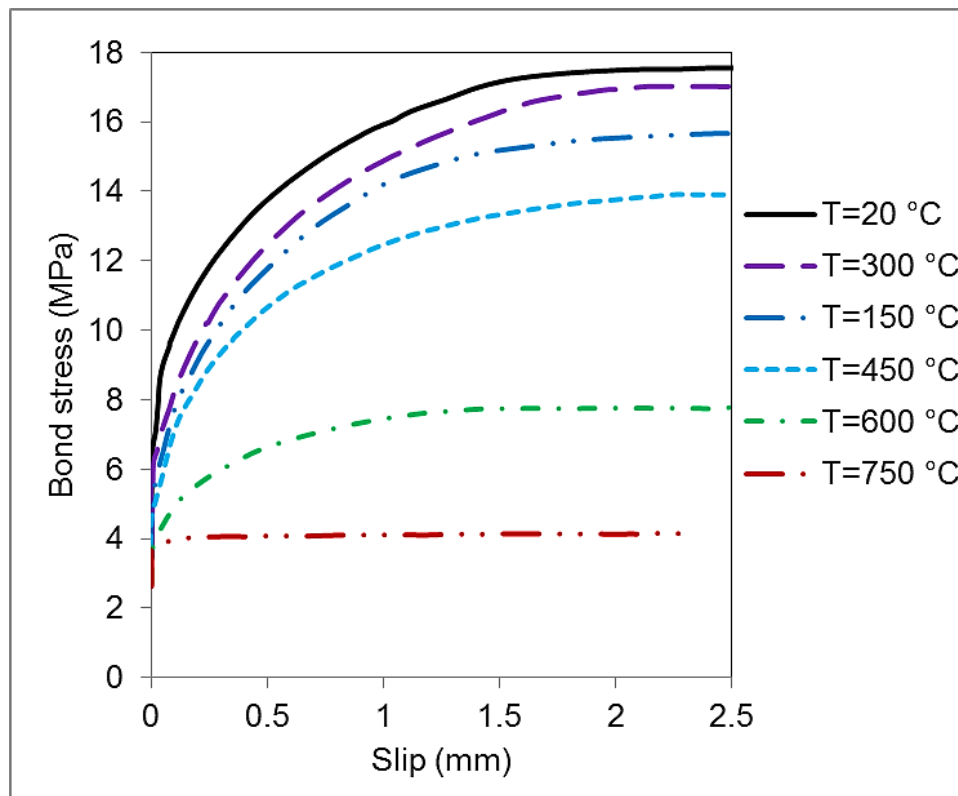


Figure 2.20 Residual bond stress-slip for various temperatures (16 mm steel bar diameter, 55 mm concrete cover and 3.7 MPa initial stress) (Morley & Royles 1983)

Another study about the bond behaviour at elevated temperatures was conducted by Morley and Royles (1983). Four cases were considered in this experimental investigation: (I) applied stress of 3.7 MPa during heating and loaded until failure while the specimen was hot, (II) applied stress of 3.7 MPa during heating and loaded to failure after cooling (residual stress), (III) loaded the specimens until failure while the specimen was hot without initial stress, and (IV) loaded the specimen until failure after cooling without initial stress (residual stress). High yield strength steel bars with diameter of 16 mm and concrete compressive strength of 35 MPa were

used in the study. Different concrete covers were utilized to consider the effect of concrete cover on the bond strength at high temperatures. The procedure used for heating was: heated the specimens at rate of 2°C/min to the required temperature, kept them at that temperature for one hour, then the specimens were loaded until failure while the specimens were hot. For finding the residual bond strength, the specimens were cooled down for one day before being tested. The test results for residual bond stress-slip with initial stress of 3.7 MPa (test condition II) is presented in Figure 2.20. Figure 2.21 shows the results for the specimens under test condition (III).

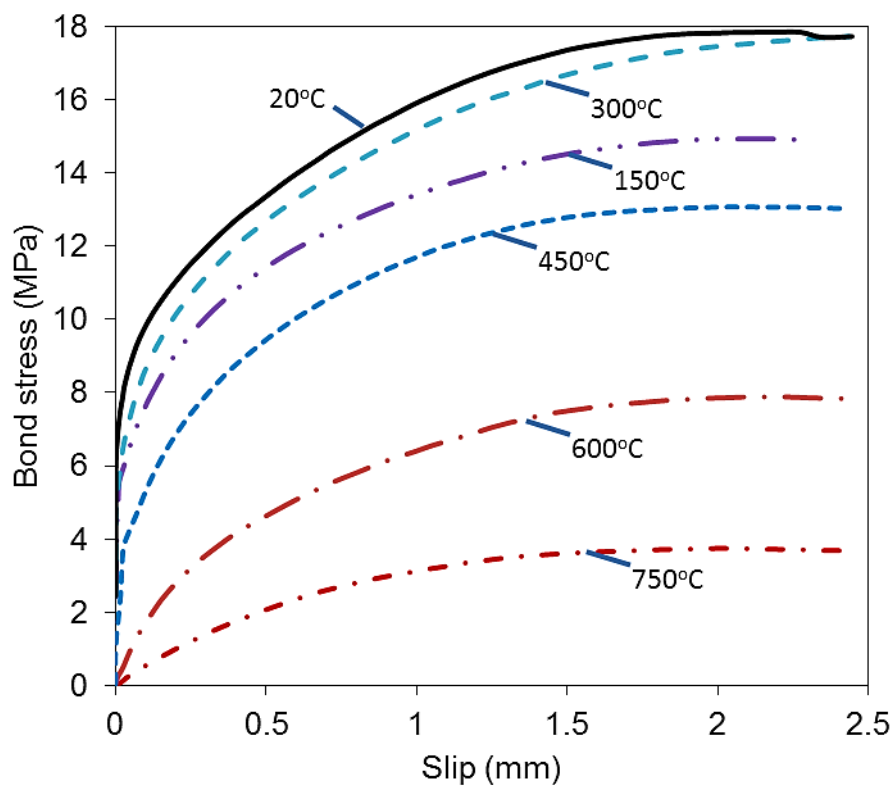


Figure 2.21 Bond stress-slip curves at various temperatures (16 mm deformed bar diameter, 55 mm concrete cover with no initial stress) (Morley 1982)

The effect of concrete cover was illustrated in Figure 2.22 and 2.23. The conclusions from this investigation were: the bond behaviour of the specimens stressed during heating performed better than those tested without stress; the reduction in bond strength at elevated temperatures was greater than the reduction of concrete compressive strength; The degradation of bond strength has a similar pattern compared with concrete compressive strength at high temperatures for large concrete

cover however, for small concrete cover the degradation of bond strength is similar to the concrete tensile strength.

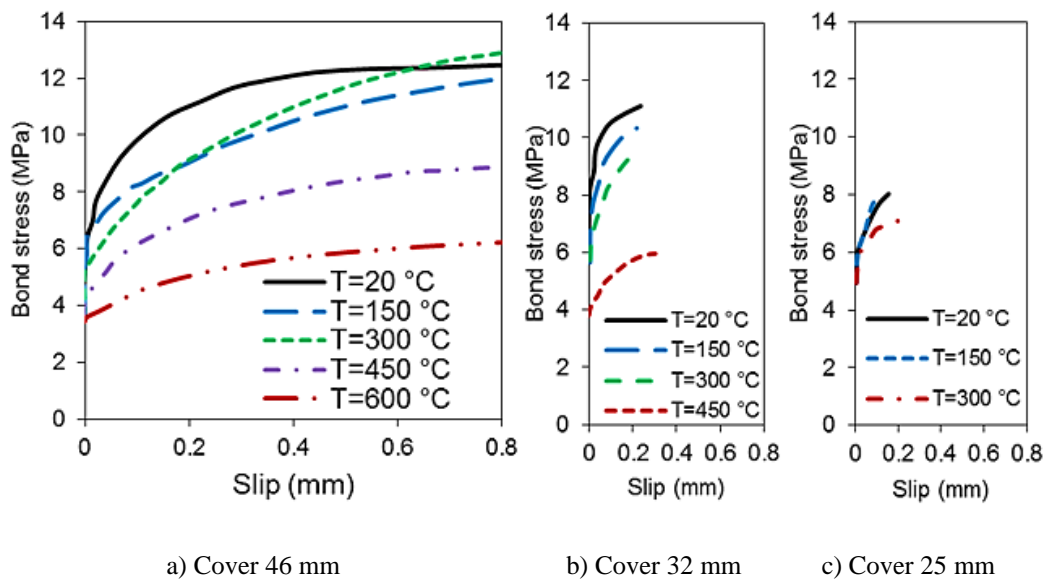


Figure 2.22 Residual bond stress-slip for different concrete cover and various temperatures

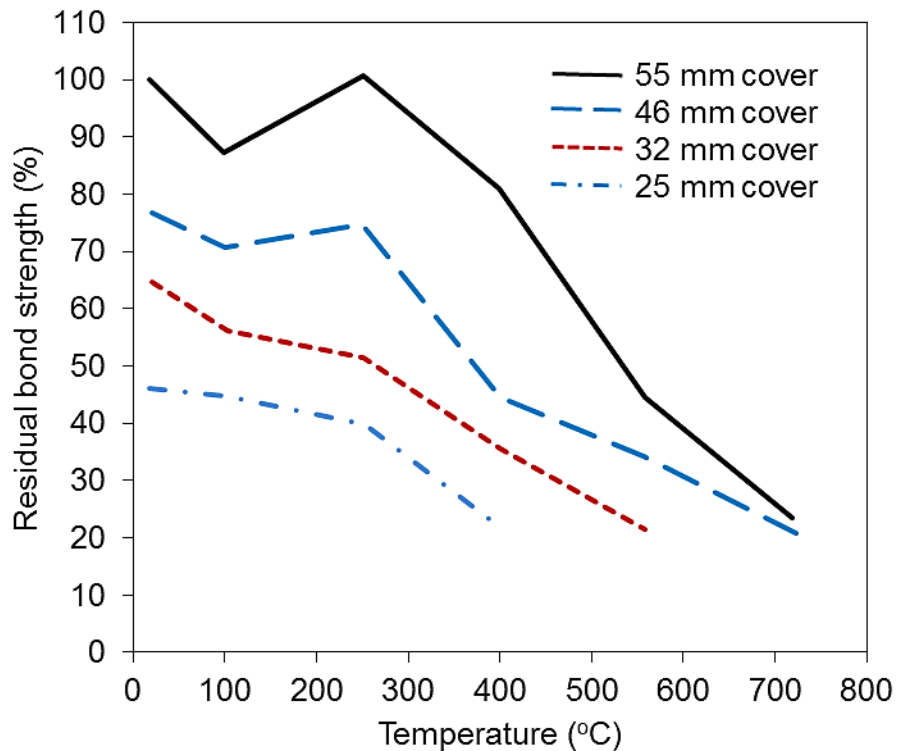


Figure 2.23 Variation of maximum bond stress with temperature for different covers (16 mm diameter of deformed bar) (Morley & Royles 1983)

Effect of using high strength pozzolanic concrete on the bond strength after exposing to high temperatures was investigated by Haddad and Shannis (2004). Four concrete

mixes were adopted using Portland cement and natural pozzolan as a cement replacement to give different concrete compressive strength (73.1, 66.0, 67.0, and 66.1 MPa). The specimens were heated to temperatures either 600°C or 800°C for one hour, and then allowed then to cool slowly down to ambient temperature. The results from this study indicated that using high strength pozzolanic concrete can reduce surface cracking at temperatures below 600°C without affecting the bond. Also, the study indicated that using 10% of natural pozzolan could reduce the cost of cement product and give an acceptable bond resistance against fire.

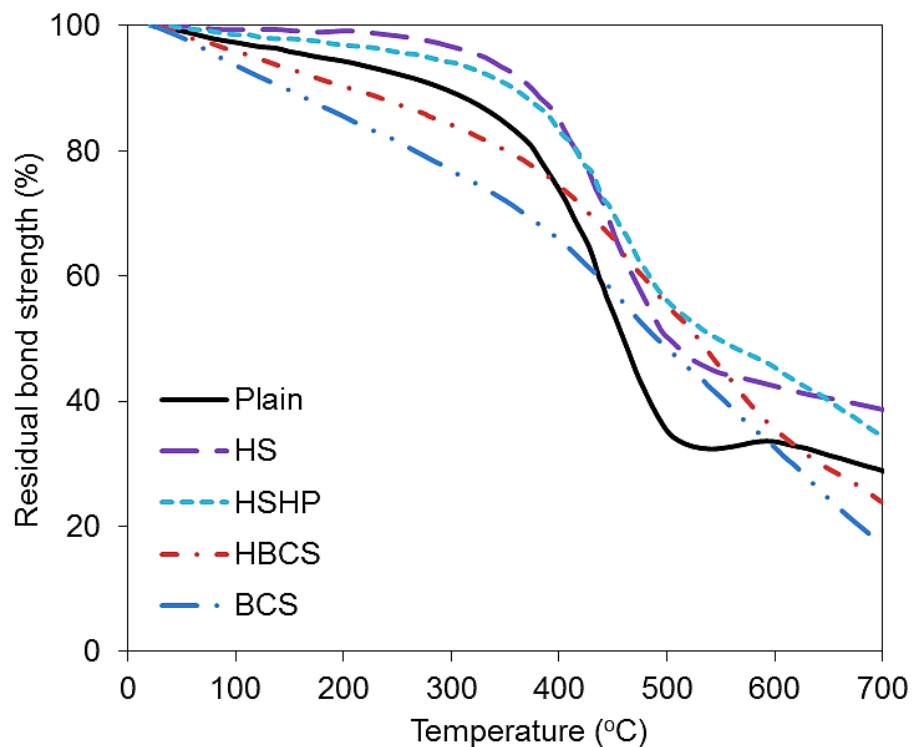


Figure 2.24 Residual bond strength versus temperature for modified specimens prepared with different FRC mixtures (Haddad et al. 2008)

The behaviour of the bond for fiber-reinforced concrete, after exposed to elevated temperatures, was studied by Haddad et al. (2008). Three types of fibers (hooked steel (HS), brass-coated steel (BCS), and high performance polypropylene (HP)) were used in the study. Concrete mixes contained different percentage of fiber to produce four types of concrete for the bond study (hooked steel fibrous concrete (HS), brass coated steel fibrous concrete (BCS), hooked steel-brass coated steel fibrous concrete (HBCS), and hooked steel-high performance polypropylene fibrous concrete (HSHP)). The effect of using fiber-reinforced concrete on the residual bond

strength at elevated temperature is shown in Figure 2.24. It can be concluded from the study that adding fibers to the concrete can limit concrete cracking and prevent spalling at temperatures below 600 °C, which can enhance the residual bond strength and bond ductility, especially when hooked steel fiber HS is used.

2.6 Finite element method

Finite element method is a powerful numerical technique for analysis of structural problems. Structural members are subdivided into finite number of individual components called ‘elements’. Types of these elements could be line elements (truss or beam elements), for plane elements (triangular or quadrilateral elements), or brick elements. These elements are connected by nodes, which are typically placed at the boundary of the elements. Finite element method was used only by the academics and mathematicians before the 1950s due to complexity, but later when the computers became available in 2000s, software are developed to carry out the structural analysis as well as the design (The Concrete Centre 2006).

2.6.1 Modelling the structures under fire conditions

The conventional approach for evaluating the structural fire resistance through fire tests is expensive, time consuming. An alternative to fire tests is the use of numerical modelling for evaluating fire resistance of reinforced concrete structures. Numerical methodology allows incorporation of various parameters in an efficient and cost-effective way. Hence, the tests data can be served for validating these models. At present, many programs have been developed to simulate the structural fire resistance, such as VULCAN, SAFIR, FEAST, ADAPTIC, FIREFRAME, ANSYS and ABAQUS. All these programs adopt the finite element procedures to model the structural behaviour under fire conditions (Lin 2014).

Numerous models have been developed to represent the behaviour of reinforced concrete structures under fire conditions, but none of these models have considered the interaction of bond between concrete and reinforcement (Huang 2010). Two common types of methods are used to simulate the bond between concrete and reinforcement: bond-link and bond-zone approaches. In the bond-zone approach, the properties of the contact surface between concrete and reinforcing bar is represented by the material law which considers the properties of the bond zone. The connection

between concrete and steel is assumed to be continuous within the contact surface. Therefore, using this approach to model the bond between concrete and reinforcement needs to apply more fine mesh within the bond zone area in order to achieve a reasonable accuracy. In the bond-link element approach, the bond can be modelled by connecting the nodes of the concrete elements with the nodes of the steel bar elements. This bond-link element has no physical dimensions in which the two nodes have the same coordinates at the beginning of the analysis (Huang 2010). The behaviour of bond-link element is defined based on a relationship between the bond stress and slip. The relationship in CEB-FIP Model Code 1990 was taken empirical as an average value of the bond stress based on a statistical methodology, as shown Figure 2.25. This bond-slip relationship is used at ambient temperature and highly dependent on the test data, which may limit their validity under different situations. Therefore, it is important to develop the models based on the constitutive equations of concrete, geometric properties of the steel bar and concrete cover to predict the bond behaviour of reinforced concrete members at elevated temperatures.

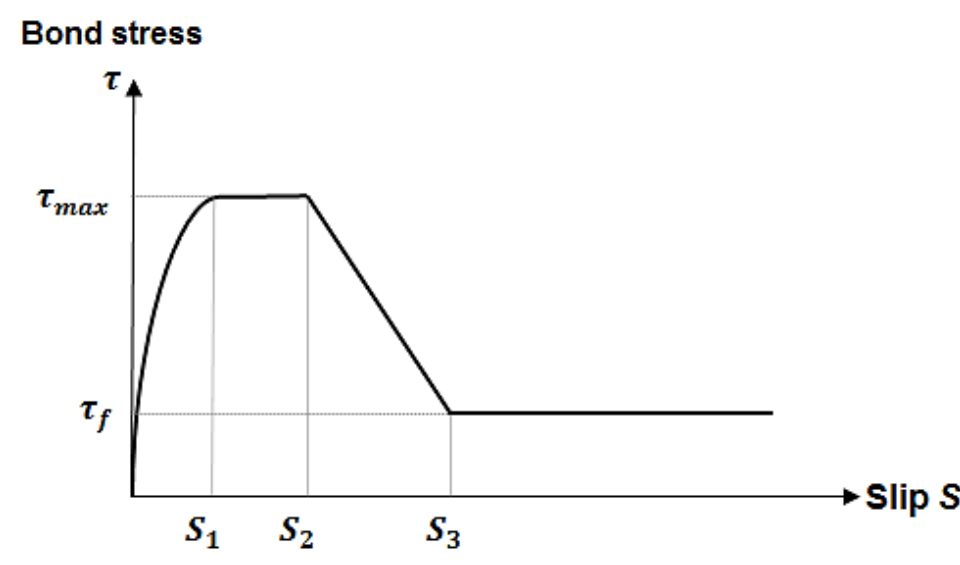


Figure 2.25 Average bond stress–slip curve defined by CEB-FIP Model Code 1990

2.6.2 Introduction to software VULCAN

VULCAN is a specialised finite element software for three dimensional non-linear analyses of steel and concrete structures under fire conditions (Huang et al. 1999; Huang et al. 2003a; Huang et al. 2009; Huang 2010). VULCAN software has been extensively validated versus available experimental results at each step of its

developments. Hence, this program provides a solid foundation for this PhD project for modelling the bond between concrete and reinforcement under fire conditions.

In this program, the reinforced concrete building is modelled as an assembly of finite plain beam-column elements, slab elements, reinforcing bar elements and bond-link elements. Each node from these elements is defined based on a common reference plane, which commonly coincides with the mid-surface of the concrete slab. The location of this reference plane is fixed during the analysis (Huang 2010).

For the beam-column and the steel bar elements, three-node line elements are used. The model takes into account the non-linearity of materials and geometric for the elements. The cross-section of the element is divided into a matrix of segments. This procedure gives opportunity for each segment within the cross-section to have different types of materials, mechanical properties and temperatures. This model considers the structural properties of the reinforced concrete at elevated temperatures, such as degradation of concrete strength and stiffness, concrete spalling, degradation of steel reinforcement, thermal expansion and failure of elements as a result of cracking and crushing of concrete segments or yielding steel bars (Huang et al. 2009).

The slab is modelled using non-linear layered finite elements procedure. The material and geometric non-linearity are taken into account in this model. The slab elements are divided into layers of plain concrete and reinforcing steel in order to consider the temperature distribution within the slab thickness, thermal strain, the degradation of the materials for each layer and concrete spalling, as well as considering the failure of each layer based on the level of the stress at Gauss points. Each layer can have different temperature, but within the layer the temperature is uniform (Huang et al. 1999; Huang et al. 2003a; Huang et al. 2003b).

The influence of bond between concrete and reinforcement at elevated temperatures is also modelled by using the bond-link element approach as illustrated in Figure 2.26. The bond-link element has two nodes with three translational degrees of freedom and three rotational degrees of freedom for each node. The node from the concrete elements is connected to the node from the steel bar elements by a two-node bond-link element. The slip between the reinforcement and concrete is assumed to be only in the direction of longitudinal axis of the rebar (Huang 2010). To consider the

bond between the concrete and reinforcement for the slab elements, the slab elements is modelled as an assembly of plain concrete slab elements and steel bar elements. Each node from the bar elements connects to other node from the slab element through the bond-link elements (Huang 2010).

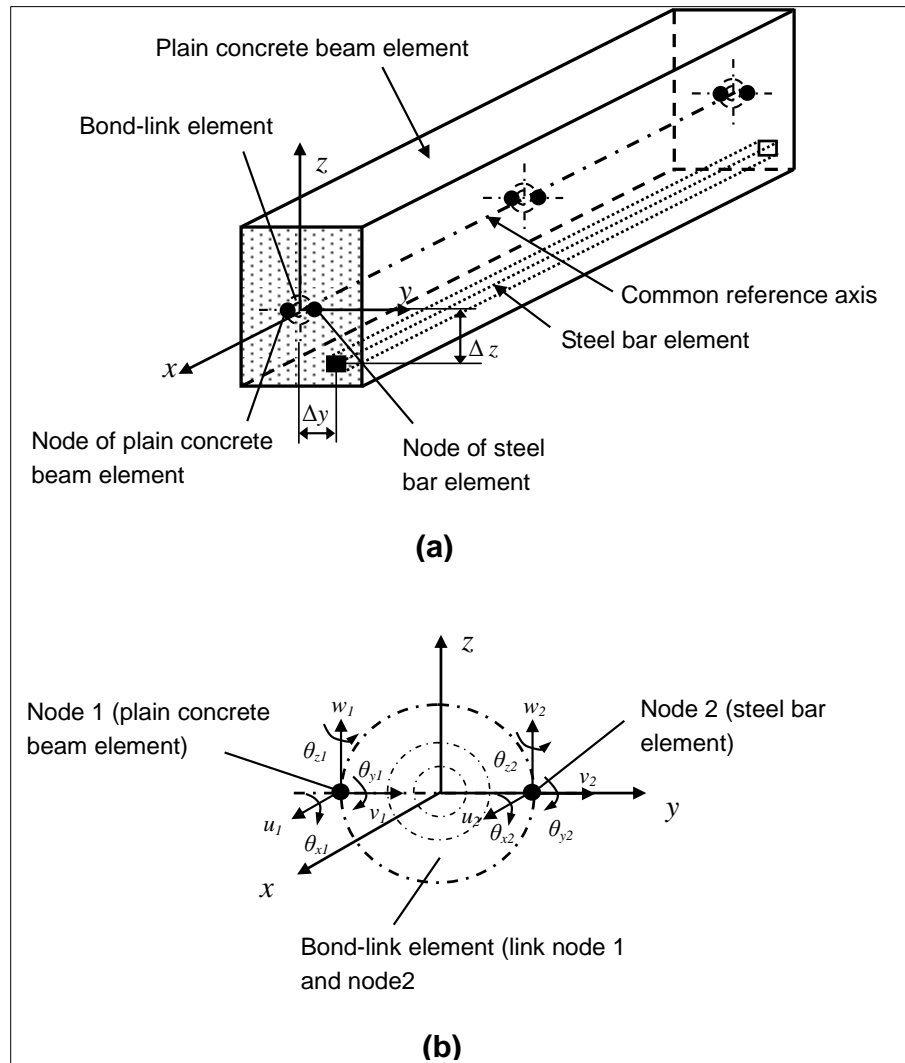


Figure 2.26 Reinforced concrete beam: plain concrete, reinforcing steel bar and 3D bond-link elements (Huang 2010)

Analyses of the structural members at elevated temperatures using VULCAN program undergo two phases. The first phase is to perform the thermal analysis for predicting the temperature distribution within the cross-section of structural members. The second phase is the structural analysis, which can be performed by using the predicted temperature history from the thermal analysis as temperature input data for the structural analysis.

Within this PhD project, two models have been developed for analysis of the bond stress-slip in normal and prestressed concrete structures under fire conditions. Then the models are incorporated into the bond-link elements within the VULCAN program for modelling normal reinforced concrete and prestressed concrete structures under fire conditions.

2.7 Conclusion

It can be concluded from this chapter that the bond between concrete and reinforcement is essential to provide the integration between concrete and rebar to build a composite material. The mechanism of bond stress-slip depends on the properties of the concrete and the reinforcement. The influence of high temperatures on these properties can affect directly on the bond strength. Also, there are many factors affect the bond strength. Some of these factors are related to the concrete and some of them are related to the steel bars. At elevated temperatures, concrete and reinforcement as well as the bond between them deteriorate dramatically. Therefore, it is very important to consider the influences of bond behaviour in order to ensure that there is sufficient fire resistance for the reinforced concrete structural members. It is evident from the review conducted in this chapter that computer modelling is an important tool for analysis and design of reinforced concrete structures under fire conditions.

Chapter 3 Analysis of bond-slip between concrete and steel bar in fire

The effect of the bond stress-slip on the structural behaviour of the reinforced concrete members at elevated temperature has been reviewed in Chapter 2. For analysis of reinforced concrete structures in fire, it is important to consider the influence of the bond between concrete and reinforcing steel bars. Therefore, in this chapter a new model will be developed to simulate the bond stress-slip between concrete and deformed steel bars at elevated temperature.

3.1 Introduction

Exposure of concrete structures to high temperatures leads to significant degradations in mechanical and physical properties of concrete and steel reinforcement as well as the bond characteristics between them. Degradation of bond properties in fire may significantly influence the load capacity or flexibility of the concrete structures. Therefore the bond behaviours need to be considered for the structural fire engineering design of reinforced concrete structures. At present, information about the material degradations of concrete and reinforcing steel bars at elevated temperatures are generally available. However, the research on the response of the bond characteristic between concrete and reinforcing steel bar at elevated temperatures is still limited (Diederichs & Schneider 1981; Pothisiri & Panedpojaman 2013).

Previous researchers indicated that when the reinforced concrete members are loaded, the stresses in the interface between concrete and steel bar increase. The capacity of the interface to transmit stress starts to deteriorate at the particular load level, and this deterioration becomes worse at elevated temperatures. The damage at the interface gradually spreads to the surrounding concretes. The development of this process results in a slip between the steel and concrete. The mechanism to transfer stresses between concrete and rebar can be represented by adhesion, mechanical interlock and friction. Adhesion can be defined as the chemical bond which is developed during the curing process of concrete. This bond is very small and can be lost in the early stages of loading or during exposure to fire. Hence, this kind of the

bond can be ignored in the modelling of bond characteristics in fire. In the case when deformed bars are used, stresses are transferred mainly by mechanical interaction between the rebar's ribs and adjacent concretes. Also, the friction does not occur until there is a slip between the steel bars and concrete (Tepfers 1979; Bigaj 1999; Wang & Liu 2003; Huanzi 2009).

There are two types of bond failure that can take place between the concrete and deformed bar. The first one is pull out failure (shear off) when the cover of concrete is very large and under high confinement. In this case, concretes are shearing off by wedging action of the ribs, and then concretes between the ribs are crushed gradually resulting in a pull-out failure. The second type of failure is splitting failure due to the cracks of the concrete cover surrounding the steel bar start to propagate radially. This type of failure is more common for pull-out tests of reinforcing steel bars in the real structures (Tepfers 1979; Huanzi 2009; Pothisiri & Panedpojaman 2013).

During the past decades, numerous models have been developed to calculate bond stress at ambient temperature (Tepfers 1979; Viwathanatepa et al. 1979; Bigaj 1999; Nielsen & Bicanic 2002; Wang & Liu 2003; Huanzi 2009). The majority of these models are empirical and developed based on a statistical methodology. Thus, these models are highly dependent on the test data, which may limit their validity in different situations (Huanzi 2009). Currently there are a limited number of numerical models available for modelling bond characteristics at elevated temperatures. Huang (2010) adopted the CEB-FIP (CEB-FIP Model code 90 1991) bond-slip model at ambient temperature and considered the degradation of bond strength at elevated temperatures by using the experimental results generated by Bazant and Kaplan (1996). Hence, the Huang's model is the first approximation of the bond characteristics in fire. Pothisiri and Panedpojaman (2013) have proposed a mechanical bond-slip model at elevated temperatures based on the theory of thick-wall cylinder and smeared crack approach of concrete in tension. The model has taken into account the variation of concrete properties with temperatures and the differential thermal expansion of rebar and concrete. However, the model was established to calculate the bond-slip based on the correlation between the experimental slip obtained from previous researches.

As indicated in (Huang 2010), due to the lack of robust models for considering the influence of the bond characteristics between concrete and steel bar at elevated temperatures, the majority of the numerical models developed for predicting the behaviour of reinforced concrete structures in fire were based on the full bond interaction. Hence, the main objective of this chapter is to develop a robust numerical model for predicting the bond-slip between concrete and steel bar under fire conditions. The model presented in this chapter is mainly based on the partly cracked thick-wall cylinder theory, and the smeared cracking approach is adopted to simulate the splitting failure of the concrete cover. In this numerical model, the calculation of the bond slip relationship is based on the constitutive equations of concrete and geometric properties of the rebar and concrete cover. The developed model can generate the bond stress-slip curve at elevated temperatures. The model can be used to calculate the bond radial pressure, bond stress versus slip. Also, this numerical model has been incorporated into the VULCAN software for 3D modelling of reinforced concrete structures under fire conditions.

3.2 Analytical model

The mechanical action between the rebar's ribs and surrounding concretes is explained in Figure 3.1. The transfer of the load between the reinforcing bar and concrete is achieved by the bearing of the ribs on the concrete. The resultant forces acting on the ribs are compressive forces which are generated due to the restraint of the surrounding concrete. The compressive forces acting on the ribs resulted from the pull out load are decomposed into two directions, parallel and perpendicular to the reinforcing steel bar. The reaction forces acting on the concrete, due to the perpendicular components of the compressive forces acting on the ribs, create circumferential tension stresses in the concretes surrounding the steel bar. If these tensile stresses exceed the tensile strength of concrete, splitting failure occurs (Wang & Liu 2003). Wang and Liu (2003) have established a model based on the theory of thick wall cylinder, that developed by Tepfers (1979), and taking into account the strain-softening of concrete in tension to calculate the maximum radial stress and maximum bond stress.

As mentioned above the bond-slip model developed in this chapter is mainly based on the partly cracked thick-wall cylinder theory and considering the smeared

cracking approach by taking the average stress-strain of concrete in tension (Tepfers 1979; Wang & Liu 2003). As shown in Figure 3.2, the magnitude of the pressure acting on the rebar P_T^i increases by raising the pull-out force acting on the steel bar. When P_T^i reaches to the maximum value, which is the capacity of the bond, the bond will fail after this point. Hence P_T^i starts to decrease with increasing the bond slip until R_i reaches to R_c , in which R_i is the radius of uncracked inner face and R_c is the radius of concrete cover including the radius on the steel bar (see Figure 3.2).

There are three stages can be considered for the response of partly cracked thick-wall cylinder to the internal pressure: the first stage is the uncracked stage; the second stage is the partly cracked stage and the third stage is the entirely cracked stage (Tepfers 1979; Uijl & Bigaj 1996; Bigaj 1999; Wang & Liu 2003).

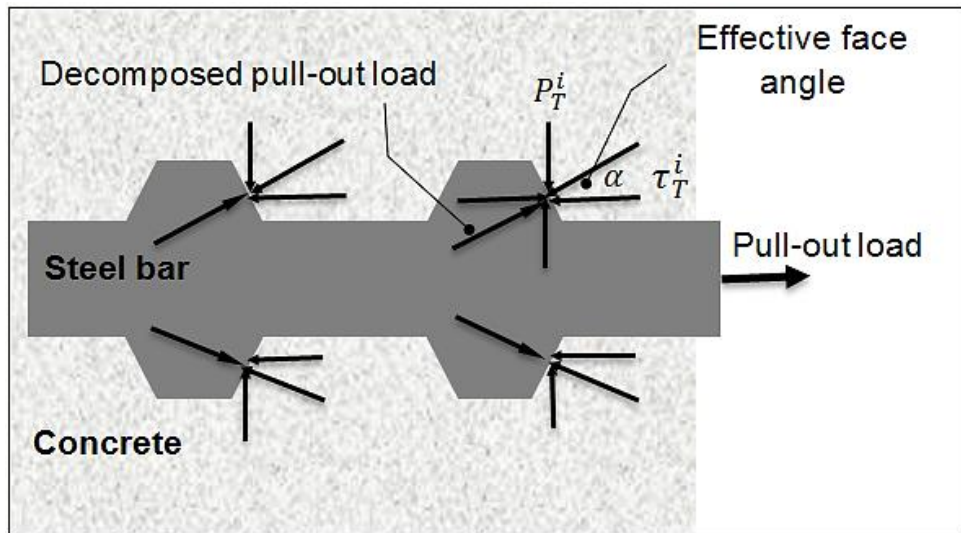


Figure 3.1 Mechanical action between the steel bar and concrete

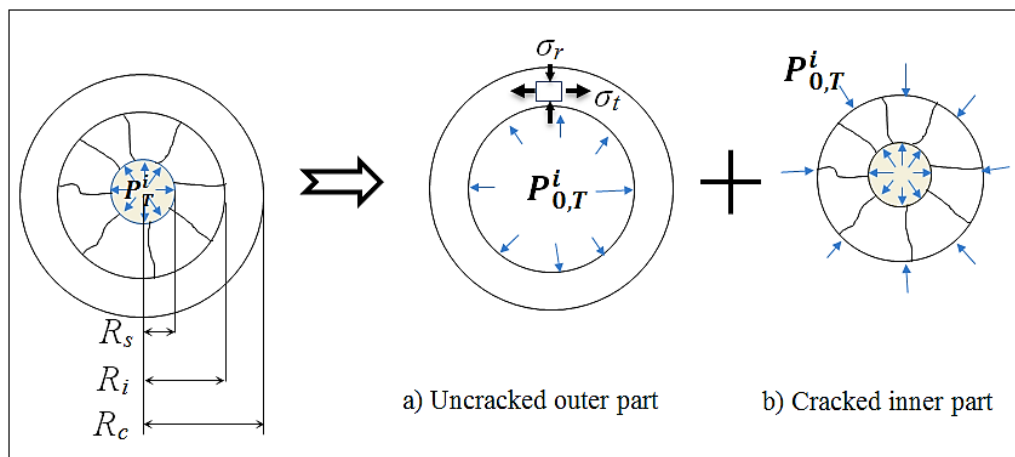


Figure 3.2 Partly cracked concrete cylinder

3.2.1 Uncracked stage

For uncracked outer part of the concrete cover (as shown in Figure 3.2 (a)) linear elastic behaviour of the concrete cylinder is assumed. Based on the theory of elasticity, the pressure at inner surface of uncracked outer part $P_{0,T}^i$ is a result from the compressive radial stress σ_r and the tensile tangential stress $\sigma_{t,T}$ as represented in (Timoshenko & Goodier 1951):

$$\sigma_r = \frac{R_i^2 P_{0,T}^i}{R_c^2 - R_i^2} \left[1 - \frac{R_c^2}{r^2} \right] \quad (3.1)$$

$$\sigma_{t,T} = \frac{R_i^2 P_{0,T}^i}{R_c^2 - R_i^2} \left[1 + \frac{R_c^2}{r^2} \right] \quad (3.2)$$

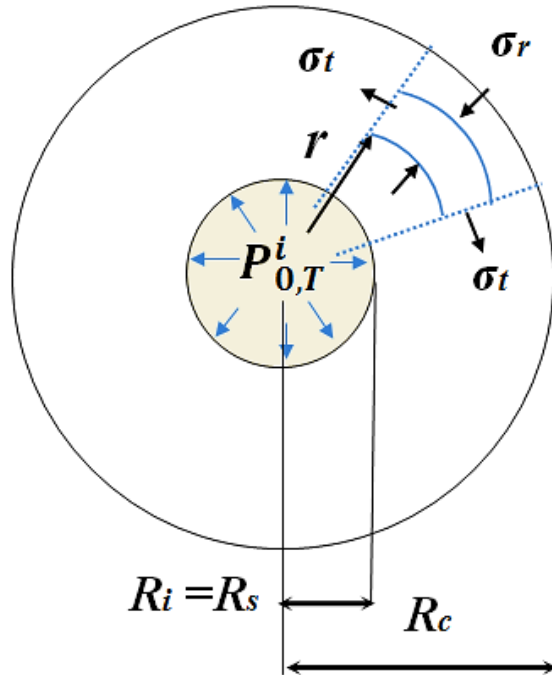


Figure 3.3 Uncracked elastic stage

For uncracked outer part of the concrete cover the tensile stress $\sigma_{t,T}$ cannot exceed the tensile strength of concrete at elevated temperatures $f_{ct,T}$. According to Equation (3.2), $P_{0,T}^i$ can be calculated when $R_i = R_s$ (see Figure 3.3) as:

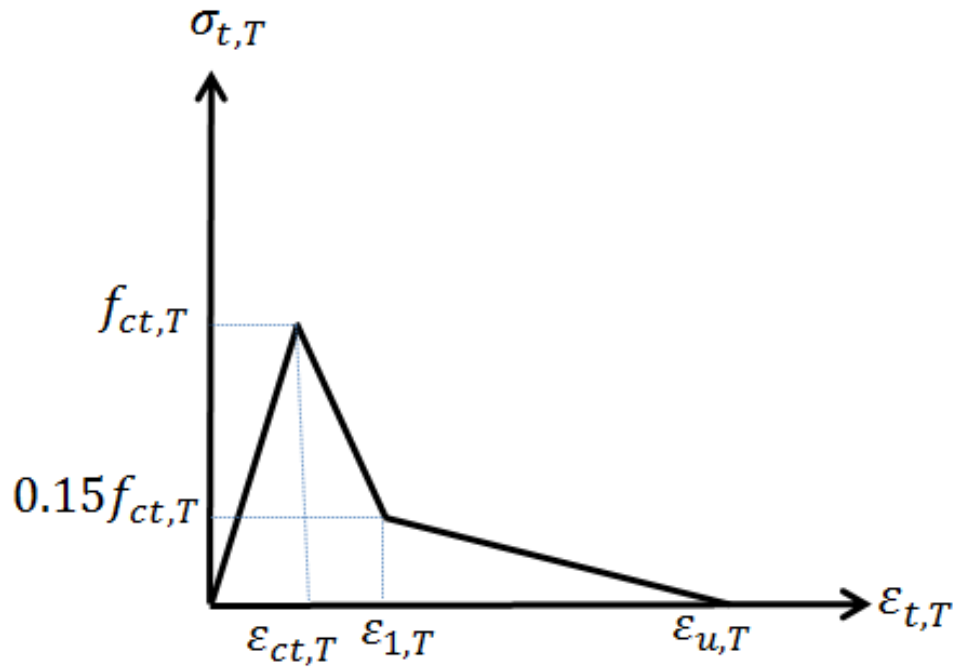
$$P_{0,T}^i = f_{ct,T} \frac{R_c^2 - R_i^2}{R_c^2 + R_i^2} \quad (3.3)$$

3.2.2 Partly cracked stage

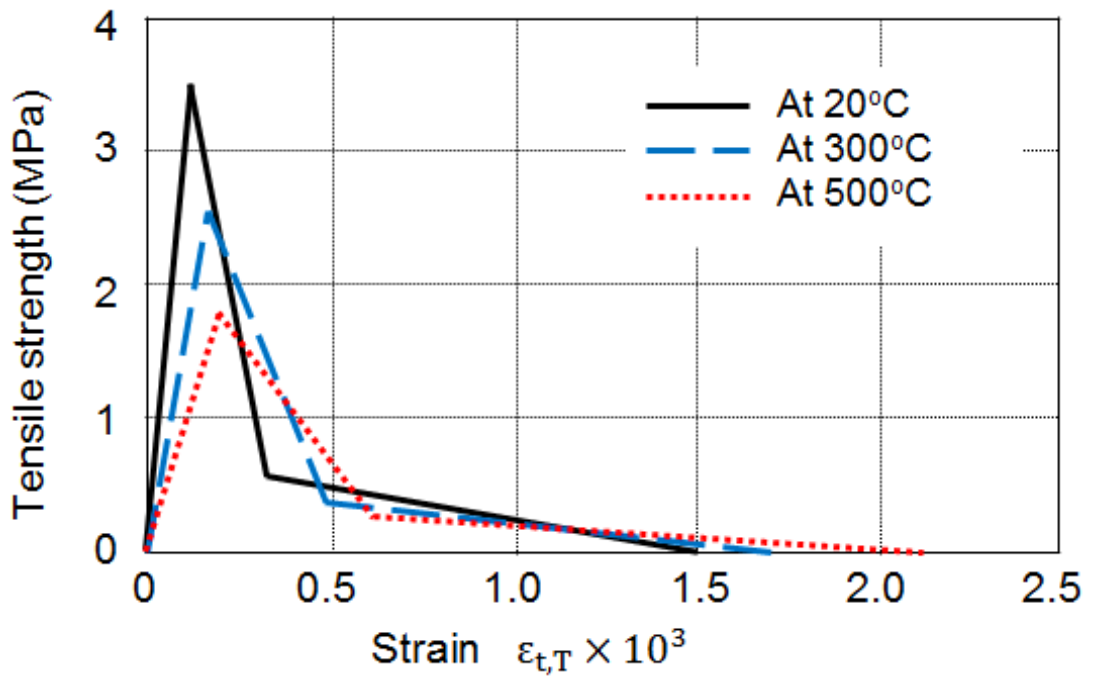
In this stage, the concrete cylinder is subdivided into an uncracked outer part and cracked inner part as shown in Figure 3.2. The contribution of uncracked outer part to the radial stress at the interface between concrete and steel bar at temperature T , $P_{0,T}^i$ is represented as:

$$P_{0,T}^i = \frac{R_i}{R_s} \left[f_{ct,T} \frac{R_c^2 - R_i^2}{R_c^2 + R_i^2} \right] \quad (3.4)$$

In this study, smeared cracks are assumed to form in radial direction when tangential stresses exceed the tensile strength of concrete $f_{ct,T}$. For the cracked inner part, softening behaviour of concrete in tension is considered in the current model, as shown in Figure 3.4(a) (CEB-FIP Model code 90 1991; Pantazopoulou & Papoulia 2001; Wang & Liu 2003). Previous researches indicated that the overall behaviour of concrete becomes more ductile when concrete exposes to high temperature (Fib Bulletin 46 2008), whereas the characteristic length of the concrete (l_{ch}) increases when the damage of the concrete at elevated temperatures diffuses. This can be happen due to increasing the fracture energy (G_F) and decreasing the tensile strength (f_{ct}) in which ($l_{ch} = G_F \frac{E_c}{f_{ct}^2}$) (Fib Bulletin 46 2008). This phenomenon is considered in the current model. Hence, smeared strain of concrete at elevated temperatures $\varepsilon_{u,T}$ increases by raising the temperature, as shown in Figure 3.4(b).



(a)



(b)

Figure 3.4 (a) Stress-strain curve of concrete in tension (b) Concrete tensile stress-strain curves at different temperatures

Therefore, the tensile stress of concrete $\sigma_{t,T}$ can be determined as:

$$\sigma_{t,T} = E_{0,T} \varepsilon_{t,T} \quad (\varepsilon_{t,T} \leq \varepsilon_{ct,T}) \quad (3.5)$$

$$\sigma_{t,T} = f_{ct,T} \left[1 - \frac{0.85(\varepsilon_{t,T} - \varepsilon_{ct,T})}{\varepsilon_{1,T} - \varepsilon_{ct,T}} \right] \quad (\varepsilon_{ct,T} < \varepsilon_{t,T} \leq \varepsilon_{1,T}) \quad (3.6)$$

$$\sigma_{t,T} = 0.15 f_{ct,T} \frac{\varepsilon_{u,T} - \varepsilon_{t,T}}{\varepsilon_{u,T} - \varepsilon_{1,T}} \quad (\varepsilon_{1,T} < \varepsilon_{t,T} \leq \varepsilon_{u,T}) \quad (3.7)$$

where $\varepsilon_{u,T}$ is the smeared strain of concrete at elevated temperatures when tensile stress equal to zero, and $\varepsilon_{u,T} = \beta \varepsilon_{ct,T}$. In order to determine the softening branch of stress-strain curve in tension, different values of β were used in previous researches. In the most cases, selection of the factor β was chosen based on the type of the problem and experiences of the researchers. The range of 10-25 can be adopted for the factor β based on a study by (Barzegar & Schnobrich 1986). For this reason, the sensitivity of factor β on the proposed model is explained in this research. Three values of factor β ($\beta=10, \beta=15$ and $\beta=25$) at temperatures of 300 °C and 500 °C are conducted. The results are shown in Figure 3.5. It can be seen from the figure that the value of factor β has an effect on the bond stress-slip curve at different temperatures. Therefore, it is reasonable to use $\beta=15$ as an optimum value in this research. Also $\varepsilon_{1,T} = \frac{2}{9} \varepsilon_{u,T}$ is used (Barzegar & Schnobrich 1986; Huang 1995).

$\varepsilon_{t,T}$ is the average tangential strain at a radial distance r , which can be expressed in terms of tangential elongation, δ_t as:

$$\varepsilon_{t,T} = \frac{\delta_t}{2\pi r} \quad (3.8)$$

When the tensile stress $\sigma_{t,T}$ reaches to the maximum tensile strength of concrete $f_{ct,T}$, just before the cracks form at a radial distance $r = R_i$ (see Figure 3.2 and Figure 3.3), by neglecting the effect of Poisson's ratio, the total elongation can be expressed as (Wang & Liu 2003):

$$\delta_i = 2\pi r \varepsilon_{i,T} \approx 2\pi R_i \varepsilon_{ct,T} \quad (3.9)$$

Substitute Equation (3.9) into Equation (3.8) to obtain:

$$\varepsilon_{i,T} = \frac{R_i}{r} \varepsilon_{ct,T} \quad (3.10)$$

At , $r = R_s$

$$\varepsilon_{i,0} = \frac{R_i}{R_s} \varepsilon_{ct,T} \quad (3.11)$$

where $\varepsilon_{i,0}$ is the smeared tangential strain of concrete at the rebar interface when $r = R_i = R_s$; $\varepsilon_{ct,T} = f_{ct,T} / E_{0,T}$, and $E_{0,T}$ is the initial modulus of elasticity of the concrete at elevated temperatures.

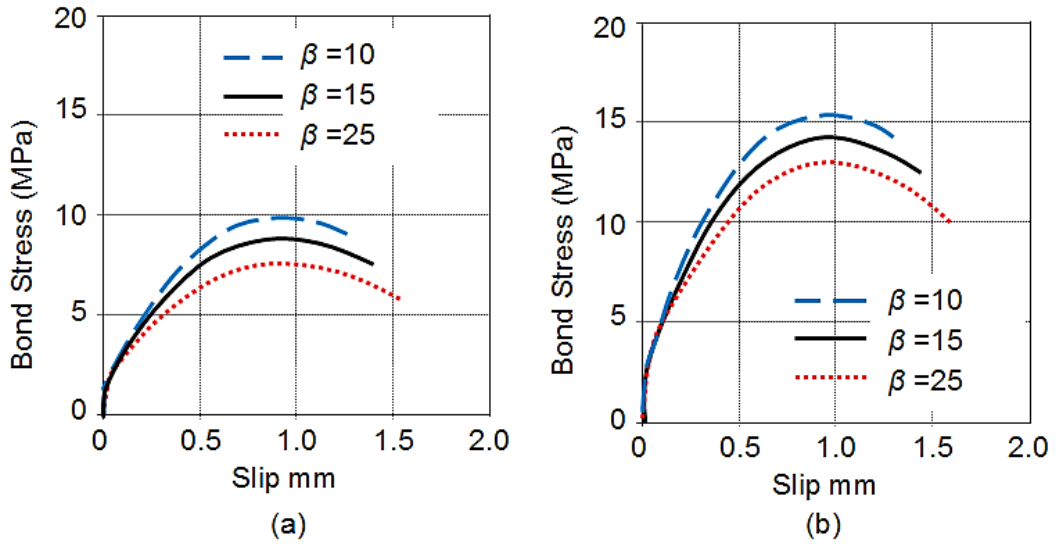


Figure 3.5 Influence of β on the current model at different temperatures: (a) At 500°C, (b) At 300°C

Now, the total radial stress at the interface between concrete and steel bar P_T^i equals to the contribution of uncracked outer part to the radial stress $P_{0,T}^i$ plus the contribution from the cracked inner part, in which the softening behaviour of concrete is taken into account. Hence, P_T^i can be calculated as:

$$P_T^i = P_{0,T}^i + \frac{1}{R_s} \int_{R_s}^{R_i} \sigma_{i,T}(r) dr \quad (3.12)$$

The integration in Equation (3.12) can be solved by using Equations (3.5)-(3.7) which can be expressed as (Wang & Liu 2003):

$$I = \int_{R_s}^{R_i} \sigma_{i,T}(r) dr = \frac{f_{ct,T}}{\varepsilon_{1,T} - \varepsilon_{ct,T}} \left[\frac{(\varepsilon_{1,T} - 0.15 \varepsilon_{ct,T})(R_i - R_s)}{0.85 R_i \varepsilon_{ct,T} \ln\left(\frac{R_i}{R_s}\right)} \right] \quad (\varepsilon_{ct,T} < \varepsilon_{i,T} \leq \varepsilon_{1,T}) \quad (3.13)$$

$$I = \int_{R_s}^{R_i} \sigma_{i,T}(r) dr = \left[\frac{0.15 f_{ct,T}}{\varepsilon_{u,T} - \varepsilon_{1,T}} \left(\frac{\varepsilon_{u,T} \frac{R_i \varepsilon_{ct,T} - R_s \varepsilon_{1,T}}{\varepsilon_{1,T}}}{R_i \varepsilon_{ct,T} \ln\left(\frac{R_i \varepsilon_{ct,T}}{R_s \varepsilon_{1,T}}\right)} \right) \right] + \left[\frac{f_{ct,T}}{\varepsilon_{1,T} - \varepsilon_{ct,T}} \left(\frac{(\varepsilon_{1,T} - 0.15 \varepsilon_{ct,T}) \frac{R_i (\varepsilon_{1,T} - \varepsilon_{ct,T})}{\varepsilon_{1,T}}}{0.85 R_i \varepsilon_{ct,T} \ln\left(\frac{\varepsilon_{1,T}}{\varepsilon_{ct,T}}\right)} \right) \right] \quad (\varepsilon_{1,T} < \varepsilon_{i,T} \leq \varepsilon_{u,T}) \quad (3.14)$$

3.2.3 Entirely cracked stage

In this stage, the concrete cover is completely cracked, the confining action of concrete is diminished and the splitting failure is occurred. Hence, the bond stress between the concrete and the steel bar becomes very little or negligible.

After calculation of Equation (3.12), the bond stress can be determined as (Tepfers 1979; Bigaj 1999; Pothisiri & Panedpojaman 2012; Pothisiri & Panedpojaman 2013):

$$\tau_T^i = P_T^i \cot(\alpha) \quad (3.15)$$

where α is the effective face angle (see Figure 3.1) which can be taken in the range of 30° to 45° (Tepfers 1979; Nielsen & Bicanic 2002). Hence, it is assumed that $\alpha = 42^\circ$ in the current model if α is not given in the test based on the rib face angle of the rebar.

In the current model, the effect of high temperature on the bond characteristics is considered by taking into account the degradation of concrete properties at elevated temperatures. The concrete properties at ambient temperature specified in Eurocode 2 EN 1992-1-1 (CEN 2004) are used. The elastic modulus of concrete at elevated

temperatures $E_{0,T}$ is calculated based on Eurocode 2 EN 1992-1-2 (CEN 2004). However, the degradation of the concrete tensile strength at elevated temperatures $f_{ct,T}$ specified in Eurocode 2 EN 1992-1-2 is not adopted in this model. This is mainly due to the Eurocode 2 EN 1992-1-2 (CEN 2004) assumed the concrete tensile stress reached to the zero $f_{ct,T} = 0$ when the concrete temperature is higher than 600 °C. Hence, the degradation of the tensile strength for concrete at elevated temperatures proposed by Aslani and Bastami (2011) is adopted in this study (see Equation (2.3)).

One of the main contributions of this research is to develop a procedure for calculating the slippage of the rebar and to establish a relationship between the bond stress and bond slip. In order to determinate the bond-slip relationship, the slip for the maximum bond S_{\max} (see Figure 3.6) that obtained from the bond stress-slip model in CEB- FIP Model Code 90 (CEB-FIP Model code 90 1991) is used with the maximum bond stress τ_{\max} that obtained from the partially cracked thick wall cylinder theory described above to form the bond-slip relationship. Hence, the slip of the rebar can be determined by considering the maximum slip S_{\max} at the maximum bond stress point τ_{\max} . In the current model S_{\max} equals to 0.6 mm for splitting failure at concrete cover $C = d_b$, and 1.0 mm for pull-out failure when concrete cover $C \geq 5d_b$ when good bond conditions are assumed (CEB-FIP Model code 90 1991), where d_b is the rebar diameter. By taking linear interpolation for $1 \leq C/d_b \leq 5$, S_{\max} can be determined for different values of concrete cover and rebar's diameters as:

$$S_{\max} = 0.6 + 0.1 \times \left(\frac{C}{d_b} - 1 \right) \quad (3.16)$$

Hence $0.6 \leq S_{\max} \leq 1.0$

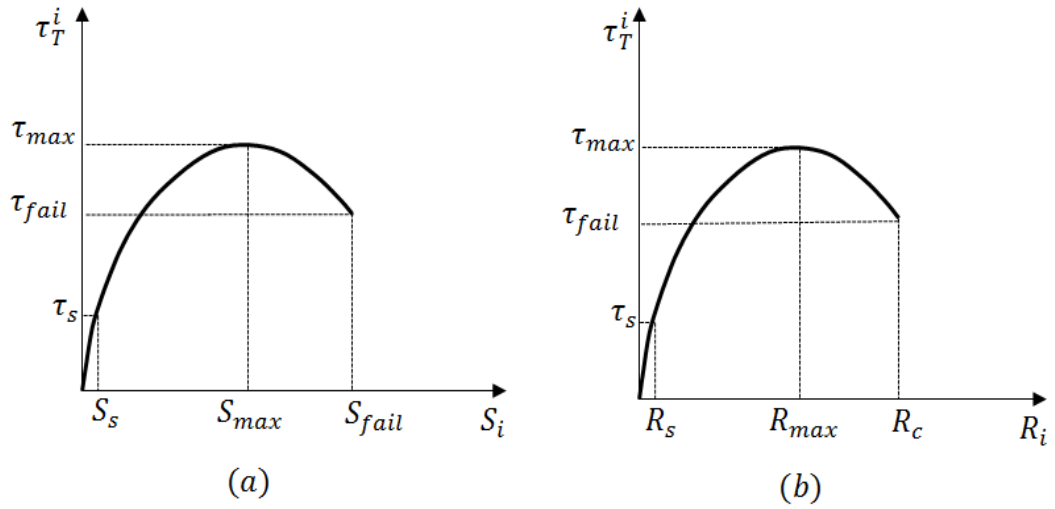


Figure 3.6 Proposed curves: (a) Bond stress-slip curve (b) Bond stress - R_i curve

As shown in Figure 3.6 (b) τ_{max} can be found when the tangent slop at the peak value of the bond stress- R_i curve equals to zero, that is:

$$\frac{d\tau_T^i}{dR_i} = \frac{\tau_T^{i+1} - \tau_T^i}{R_{i+1} - R_i} = 0.0 \quad (3.17)$$

The bond stress-slip curve (Figure 3.6 (a)) and bond stress - R_i curve (Figure 3.6 (b)) have two parts. The first part of the curves, where $0 \leq S_k \leq S_s$, where τ_s is the bond stress at $R_i = R_s$ and $\tau_s = \tau_T^{i=1}$ which can be calculated from Equation (3.15).

The slip S_s at τ_s can be calculated as:

$$S_s = \tau_{max} \left(\frac{\tau_s}{S_{max}} \right)^{1/\beta} \quad (3.18)$$

where β is assumed to be 0.4 (CEB-FIP Model code 90, 1991).

Then, the bond stress at elevated temperatures τ_T^k can be calculated as:

$$\tau_T^k = \tau_{max} \left(\frac{S}{S_{max}} \right)^\beta \quad (3.19)$$

For the second part of bond stress-slip curve and bond stress - R_i curve, where $S_i > S_s$ and $R_i > R_s$ respectively, the relationship between R_i and S_i can be

taken as a liner relationship (see Figure 3.7) (Sakai et al. 1999). The slop m of the line in Figure 3.7 can be calculated as:

$$m = \frac{\Delta R_i}{\Delta S_i} = \frac{R_{max} - R_s}{S_{max} - S_s} \quad (3.20)$$

Then, the slip for the second part S_i is:

$$S_i = \frac{R_i - R_s}{m} + S_s \quad (3.21)$$

where $i=1, 2, 3 \dots n$, and n is the total number of the steps at $R_i = R_c$, then $\tau_{fail} = \tau_T^n$ at the end of the numerical calculations.

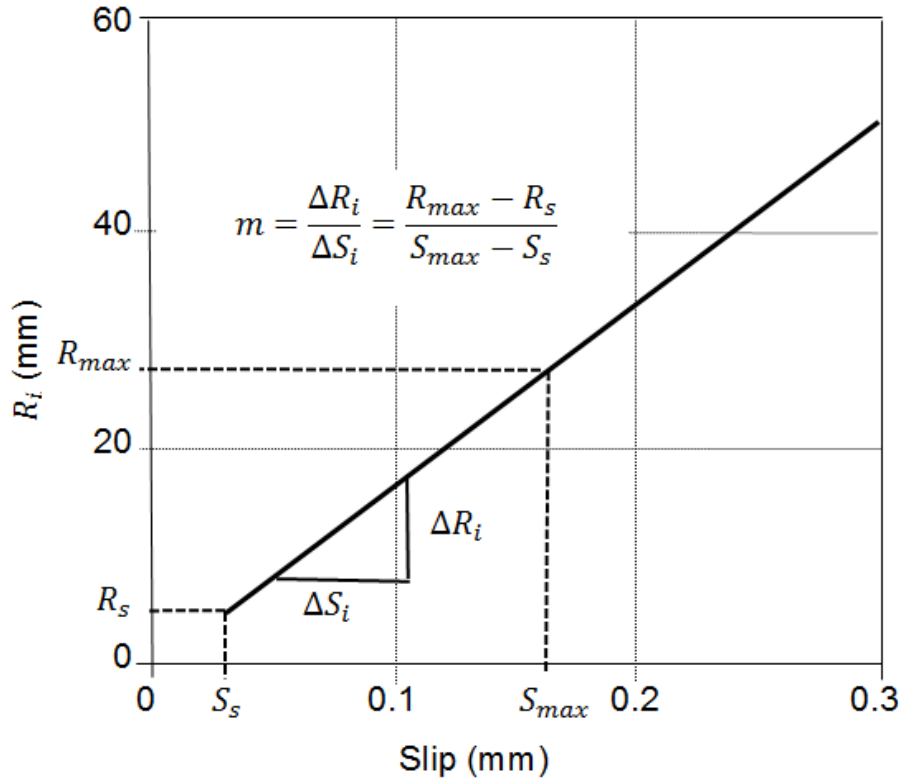


Figure 3.7 The relationship between the slip and R_i

The calculation procedure proposed in this model for determining the bond stress-slip curve at each temperature step can be summarised as following:

(1) Calculate the bond-stress τ_T^i and bond-slip S_i for the second part of bond stress-slip curve ($S_s < S_i \leq S_{fail}$ and $R_s \leq R_i \leq R_c$) (see Figure 3.6):

$$\Delta R = \frac{R_c - R_s}{n}$$

$i = 1, 2, 3, \dots, n$:

$$R_i = R_{i-1} + \Delta R$$

Calculate $P_{0,T}^i$ (Equation (3.4));

Calculate P_T^i (Equation (3.12));

Calculate τ_T^i (Equation (3.15))

Calculate τ_{max} and R_{max} (Equation (3.17))

Calculate S_s (Equation (3.18))

$i = 1, 2, 3, \dots, n$:

Calculate S_i (Equation (3.21))

(2) Calculate the bond-stress τ_T^k and bond-slip S_k for the first part of bond stress-slip curve ($0 < S_i \leq S_s$) (see Figure 3.6):

$$\Delta S = \frac{S_s}{n}$$

$k = 1, 2, 3, \dots, n$:

$$S_k = S_{k-1} + \Delta S$$

Calculate τ_T^k (Equation (3.19))

3.3 Incorporated bond stress–slip model into Vulcan software

In order to demonstrate the robustness and accuracy of the model proposed above, the developed bond stress-slip model has been incorporated into the VULCAN software (Huang et al. 2009) for simulating the bond characteristics between concrete and reinforcing steel bar at elevated temperatures. Huang (2010) has developed a two-node bond-link element within the VULCAN to consider the bond characteristics between concrete and steel bars under fire conditions. As shown in Figure 3.8, the bond link element has two nodes with zero length. Each node of the element has three translational degrees of freedom u, v, w and three rotational

degrees of freedom $\theta_x, \theta_y, \theta_z$, where x, y, z are the local coordinates of the steel bar in which x is the direction of longitudinal axis of the reinforcing steel bar element. It is assumed that the slip between reinforcing steel and concrete is related only to the longitudinal axis direction (x -direction) (see Figure 3.8 (a)). Hence, the bonding force $F_{T,x}$ between the concrete and reinforcing steel bar for the bond element is obtained as:

$$F_{T,x} = A\tau_T \quad (3.22)$$

where A is the contact area between the concrete and the reinforcing steel bar $A=UL$, where U is the perimeter of the steel bar and L is length of the steel bar which contributes to the node connected by the bond element.

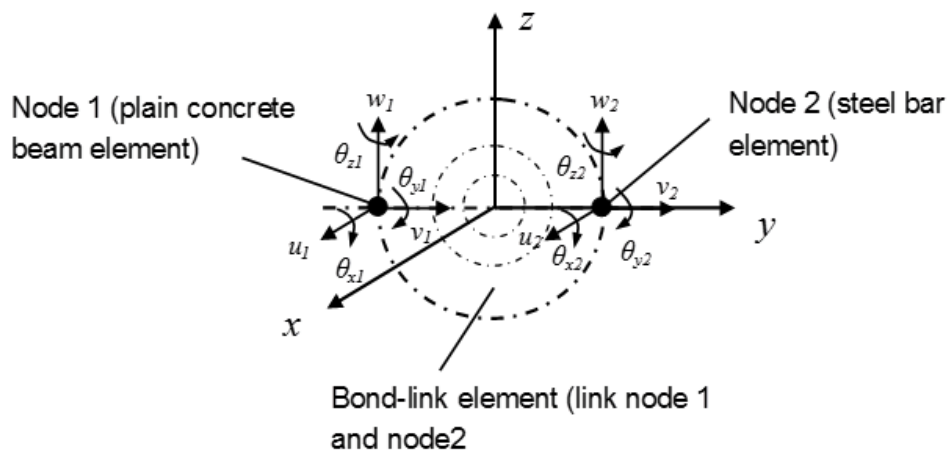
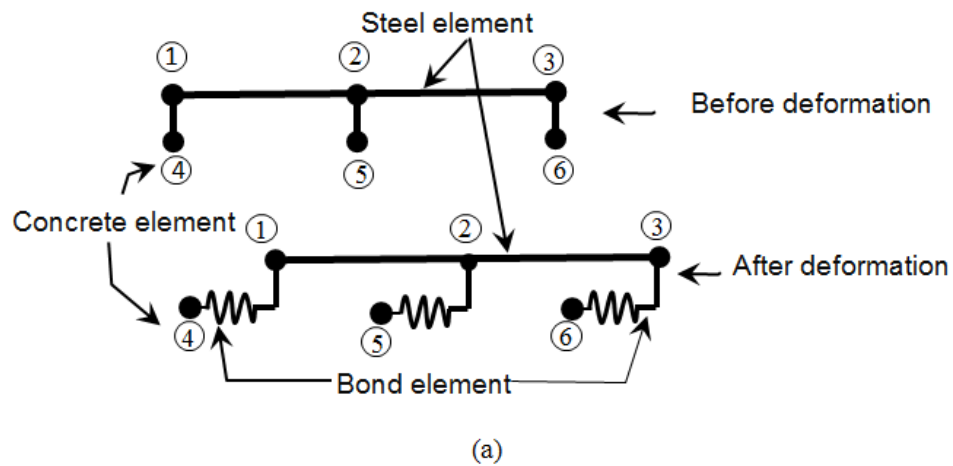


Figure 3.8 Bond-link element: (a) 2-D Coordinates (b) 3-D Coordinates

Hence, in the local co-ordinate (referenced to the reinforcing steel bar elements) the nodal force increment vector $\Delta \mathbf{F}$ of the element can be related to its nodal displacement increment vector $\Delta \mathbf{u}$ as:

$$\begin{Bmatrix} \Delta F_{x,1} \\ \Delta F_{y,1} \\ \Delta F_{z,1} \\ \Delta M_{x,1} \\ \Delta M_{y,1} \\ \Delta M_{z,1} \\ \Delta F_{x,2} \\ \Delta F_{y,2} \\ \Delta F_{z,2} \\ \Delta M_{x,2} \\ \Delta M_{y,2} \\ \Delta M_{z,2} \end{Bmatrix} = \begin{bmatrix} k_1 & 0 & 0 & 0 & 0 & 0 & -k_1 & 0 & 0 & 0 & 0 & 0 \\ 0 & k_2 & 0 & 0 & 0 & 0 & 0 & -k_2 & 0 & 0 & 0 & 0 \\ 0 & 0 & k_3 & 0 & 0 & 0 & 0 & 0 & -k_3 & 0 & 0 & 0 \\ 0 & 0 & 0 & k_4 & 0 & 0 & 0 & 0 & 0 & -k_4 & 0 & 0 \\ 0 & 0 & 0 & 0 & k_5 & 0 & 0 & 0 & 0 & 0 & -k_5 & 0 \\ 0 & 0 & 0 & 0 & 0 & k_6 & 0 & 0 & 0 & 0 & 0 & -k_6 \\ -k_1 & 0 & 0 & 0 & 0 & 0 & k_1 & 0 & 0 & 0 & 0 & 0 \\ 0 & -k_2 & 0 & 0 & 0 & 0 & 0 & k_2 & 0 & 0 & 0 & 0 \\ 0 & 0 & -k_3 & 0 & 0 & 0 & 0 & 0 & k_3 & 0 & 0 & 0 \\ 0 & 0 & 0 & -k_4 & 0 & 0 & 0 & 0 & 0 & k_4 & 0 & 0 \\ 0 & 0 & 0 & 0 & -k_5 & 0 & 0 & 0 & 0 & 0 & k_5 & 0 \\ 0 & 0 & 0 & 0 & 0 & -k_6 & 0 & 0 & 0 & 0 & 0 & k_6 \end{bmatrix} \begin{Bmatrix} \Delta u_1 \\ \Delta v_1 \\ \Delta w_1 \\ \Delta \theta_{x,1} \\ \Delta \theta_{y,1} \\ \Delta \theta_{z,1} \\ \Delta u_2 \\ \Delta v_2 \\ \Delta w_2 \\ \Delta \theta_{x,2} \\ \Delta \theta_{y,2} \\ \Delta \theta_{z,2} \end{Bmatrix} \quad (3.23)$$

The concrete prevents relative movement of reinforcing steel bars in the directions perpendicular to the longitudinal axis to the rebar. Therefore, it is reasonable to assume that common nodes of the concrete and reinforcing bar elements have identical rotations and movements in y and z directions. Hence, in this model k_2, k_3, k_4, k_5, k_6 in Equation (3.24) are assumed to have infinite magnitude such as (10^{15}) .

Coefficient k_1 is the tangent stiffness coefficients of the bond-link element related to the axis of the reinforcing steel bar element. At each temperature step j and for each iteration i , $k_1^{j,i}$ can be determined from the load-slip relationship as:

$$k_1^{j,i} = \frac{dF_{T,x}^{j,i}}{dS_x^{j,i}} = A \frac{d\tau_T^{j,i}}{dS_x^{j,i}} \quad (3.24)$$

For the first part of bond stress-slip curve, where $0 \leq S_j \leq S_s$, $k_1^{j,i}$ can be calculated as:

$$k_1^{j,i} = A \frac{\tau_{\max}^j}{S_{\max}^j} \left(\frac{S_x^{j,i}}{S_{\max}^j} \right)^{\beta-1} \quad (3.25)$$

For the second part of bond stress-slip curve, where $S_j > S_s$, a numerical differentiation method was used to calculate coefficient k_1^j .

$$k_1^{j,i} = A \frac{\tau_{i+1}^j - \tau_{i-1}^j}{S_{i+1}^j - S_{i-1}^j} \quad (3.26)$$

Using incremental analysis, the increment of bond force $\Delta F_{T,x}^{j,i}$ can be related to the increment of slip, $\Delta S_x^{j,i}$ using the tangent stiffness relationship, that is:

$$\Delta F_{T,x}^{j,i} = k_1^{j,i} \Delta S_x^{j,i} \quad (3.27)$$

in which

$$\Delta S_x^{j,i} = \Delta u_2^{j,i} - \Delta u_1^{j,i} \quad (3.28)$$

where $\Delta u_1^{j,i}$ and $\Delta u_2^{j,i}$ are the increments of displacement in the direction of $\Delta F_{T,x}^j$ at the nodes 1 and 2 of the bond-link element respectively.

As shown in Figure 3.8, in the current model a reinforced concrete member is represented as an assembly of plain concrete beam elements, reinforcing steel bar elements and bond-link elements. Both of the plain concrete beam elements and reinforcing steel bar elements are modelled using the 3-node beam element developed by Huang et al. (2009), in which the thermal expansions of concrete and steel bars are considered. Hence their effect in the direction of longitudinal axis of the reinforcing bar on the bond-link element developed in this project is taken into account. However, the thermal expansions of both concrete and steel in the radius direction of the steel bar have not been considered in the current model for simplicity. This is because the strain compatibility at the interface between steel bar and surrounding concrete is not always maintained when the pull-out load is applied (Pothisiri & Panedpojaman 2012), especially when the pull-out load reaches to the capacity of the bond. Also, the reduction in the steel bar's diameter due to the

Poisson's effect during the pull-out load could compensate the influence of the differential thermal expansion between the steel bar and concrete.

As mentioned above the plain concrete beam is modelled using the 3-node beam element. The cross-section of the beam element is subdivided into a number of segments to consider the temperature variation within the cross-section. Hence, in principle the temperature variation within the concrete rings around the bars (see Figure 3.2 and 3.3) can be considered in the current model. However, in the following validation section it is assumed that the temperatures of the concrete rings around the bars are uniform and equal to the temperature of the reinforcing bar for simplicity. This is a reasonable assumption for all pull-out tests (Pothisiri & Panedpojaman 2012).

3.4 Validations

The proposed model presented above was validated using a series of previous experimental results at both ambient and elevated temperatures. This section consists of two parts: the first part is to make a comparison between the predicted bond stress-slip curves and previous experimental pull-out test results at both ambient and elevated temperatures; the second part of the verification is to validate the response of VULCAN program after incorporation of the developed bond stress-slip model using bond-link element. In this case, reinforced concrete beams were modelled with full and partial bond between the concrete and steel bars to study the effect of bond on the response of the beam at ambient and elevated temperatures.

3.4.1 Validations of the bond stress–slip model

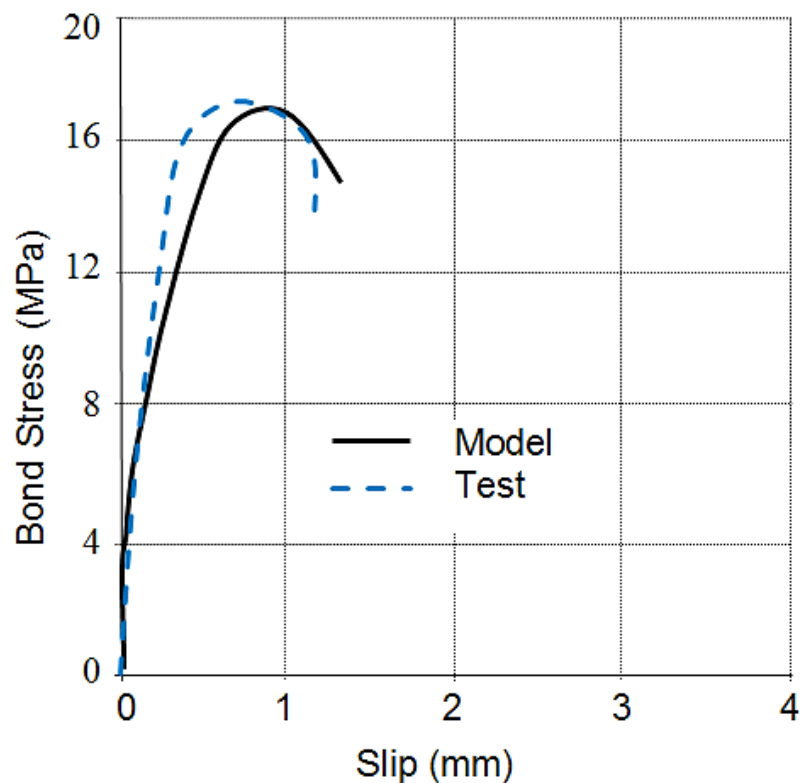
3.4.1.1 Bond stress–slip curve at ambient temperature

Table 3.1 gives information about the experimental tests carried out by Xiao and Falkner (2007), John and Bhupinder (2013) and Lee and Noguchi (2002) to study the bond-slip at ambient temperature. In the Table 3.1, l_b is the embedded length of the rebar inside the specimens and d_b is the diameter of the rebar. All material properties and geometric details of the specimens that mentioned in Table 3.1 were used as an input data for modelling the bond-slip in this section. Figure 3.9 (a) to (f) show the comparison of the predicted and measured bond stress-slip curves based on the tests.

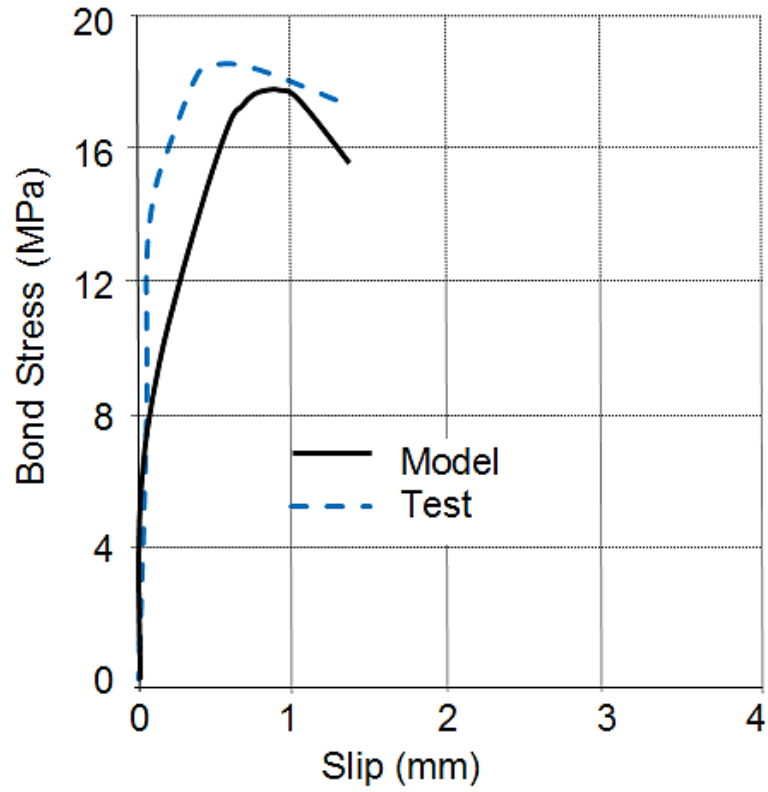
It is clear from the figures that there is an acceptable agreement between the predictions from the current model and the experimental results. This can confirm that the proposed model can be used for predicting the bond stress-slip curve between concrete and reinforcing steel bars at ambient temperature.

Table 3.1 Details of pull-out test in previous experiments at ambient temperature

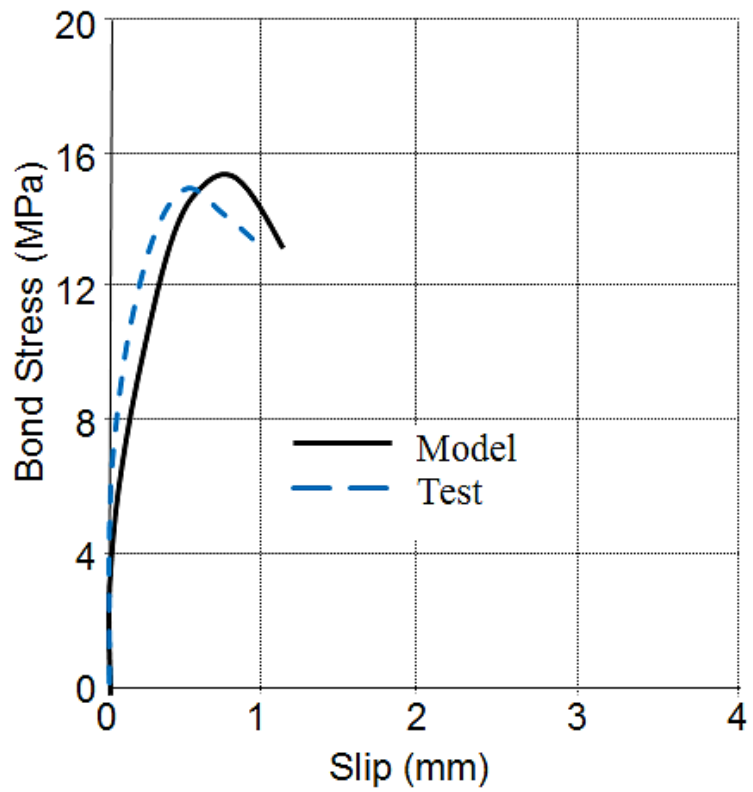
Reference	Specimens	$f_{ck,20^{\circ}C}$ (MPa)	Bar diameter d_b (mm)	R_c (mm)	C/d_b	l_b/d_b	Rib face angle (degrees)
(Xiao & Falkner, 2007)	RAC-II-0	34.0	10	50	4.0	5.0	55°
(John Robert Prince & Bhupinder, 2013)	A12R0	36.9	12	50	3.67	5.0	45°
	A16R0		16	50	2.6	5.0	36°
	A20R0		20	50	2.0	5.0	41°
	A25R0		25	50	1.5	5.0	51°
(Lee & Noguchi, 2002)	-	24.7	13	45	3.0	6.0	-



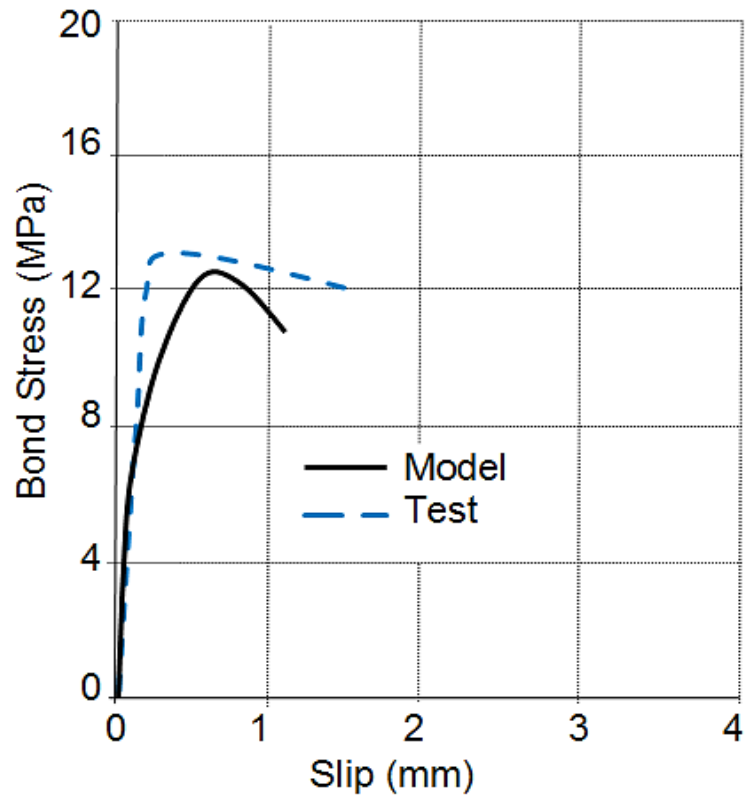
(a) Specimen RAC-II-0 (Xiao & Falkner 2007)



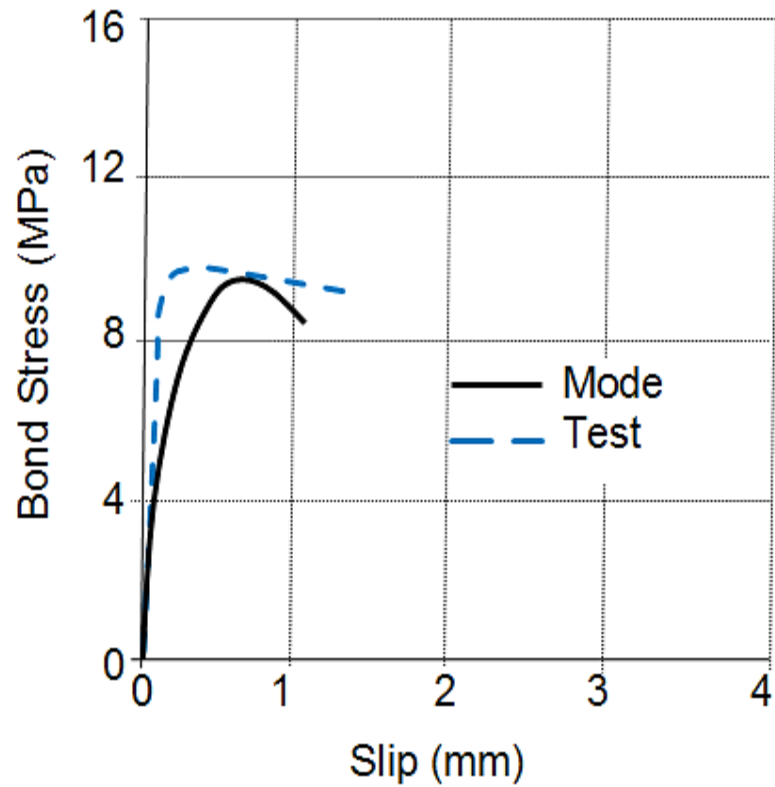
(b) Specimen A12R0 (John Robert Prince & Bhupinder 2013)



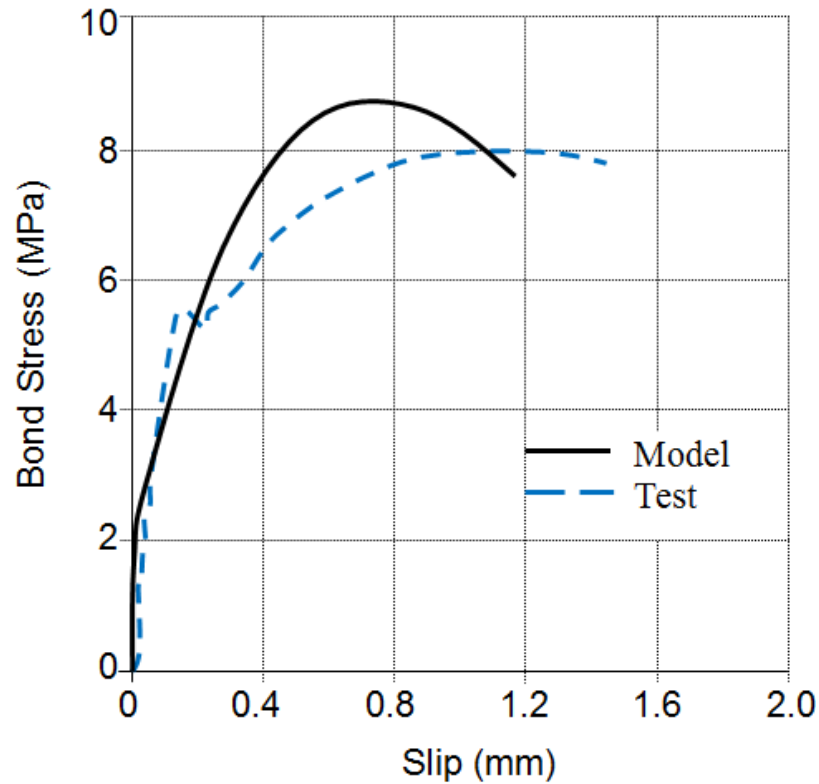
(c) Specimen A16R0 (John Robert Prince & Bhupinder 2013)



(d) Specimen A20R0 (John Robert Prince & Bhupinder 2013)



(e) Specimen A25R0 (John Robert Prince & Bhupinder 2013)



(f) Test conducted by (Lee & Noguchi 2002)

Figure 3.9 Comparison of predicted and measured bond stress-slip curves at ambient temperature

3.4.1.2 Bond stress–slip curve at elevated temperatures

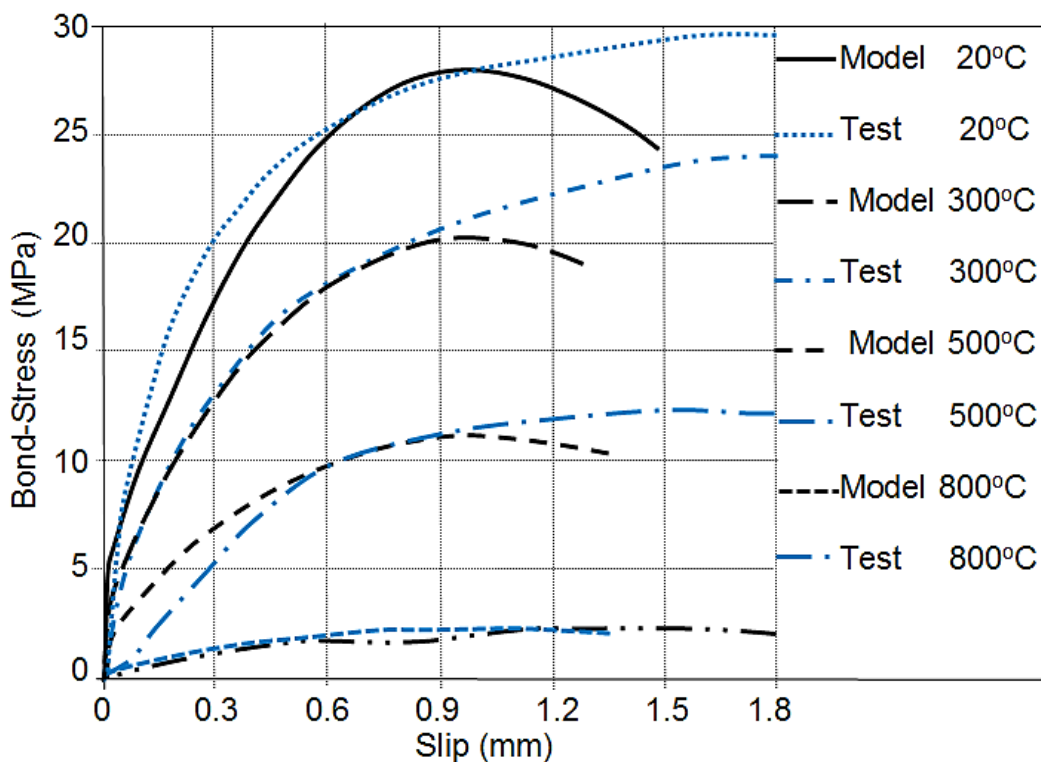
The details of pull-out tests at elevated temperatures used in this validation are summarised in Table 3.2. As mentioned before that the testes about the bond characteristics between the concrete and steel bars at elevated temperatures are limited. Hence, the proposed model was validated using the available experimental results of pull-out testes at elevated temperatures. All the material properties and geometries of the specimens in the tests were used as an input data for modelling the bond between the concrete and reinforcement at elevated temperatures.

The first test was conducted by Diederichs and Schneider (1981). This test was used for bond validation at elevated temperatures in this project. The details of the test were; deformed steel bar of 16 mm and the specimens were made with a bond embedded length of 80 mm and concrete cover of 78 mm. The temperatures within the test were in the range of 20 °C to 800 °C with heating rate of 1 °C/min. Figure 3.10 (a) illustrates the comparison of predicted and measured bond stress-slip

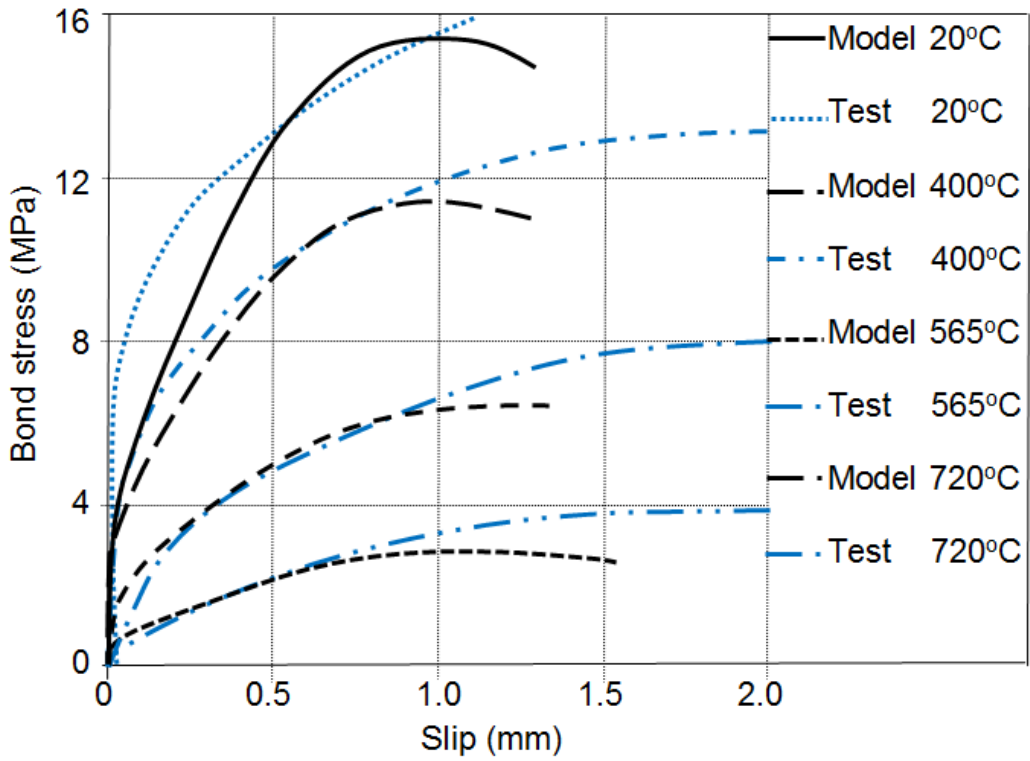
curves for different temperatures. It can be seen from the figure that a good correlation between the prediction from the model and the result from the tests was achieved. It is clear that the strength of the bond was degraded significantly by increasing the temperatures.

Table 3.2 Details of pull-out tests in previous experiments at elevated temperatures

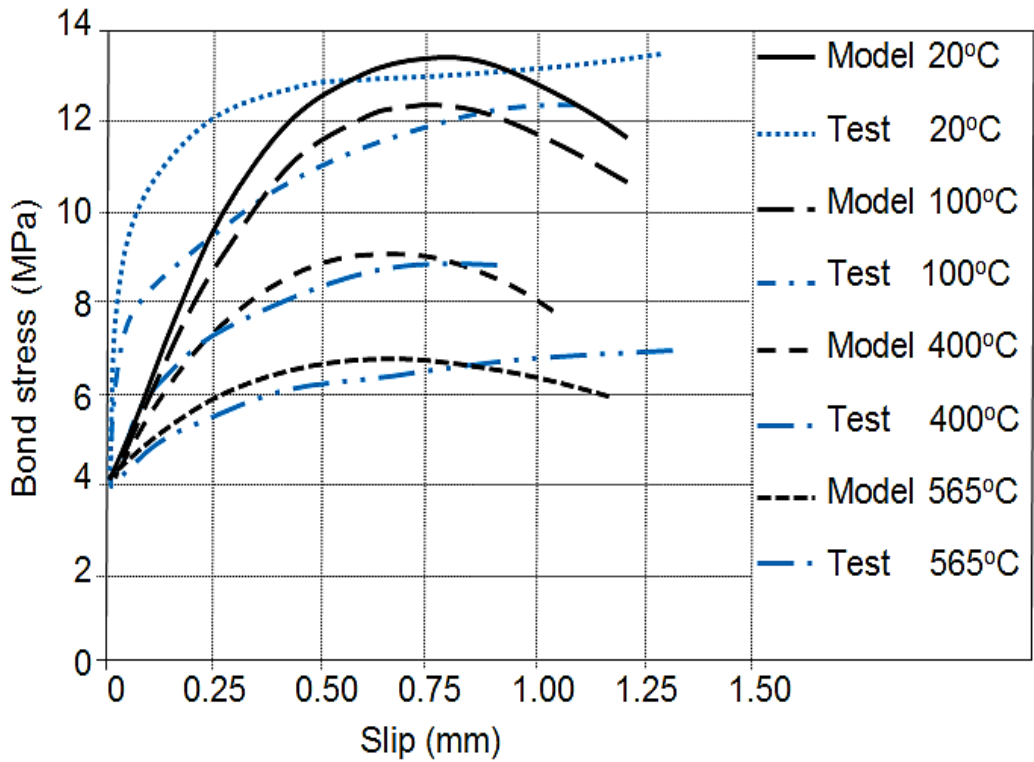
Reference	$f_{ck,20^{\circ}C}$ (MPa)	Bar diameter d_b (mm)	R_c (mm)	C/d_b	l_b/d_b
(Diederichs & Schneider, 1981)	45.0	16	86	4.88	5.0
(Morley & Royles, 1983)	29.0	16	63	3.44	2.0
		16	54	2.88	2.0
		16	40	2.0	2.0
		16	33	1.56	2.0
(Haddad & Shannis, 2004)	58.8	18	41	1.78	8.3
(Haddad, et al., 2008)	62.3	20	50	2.0	7.5



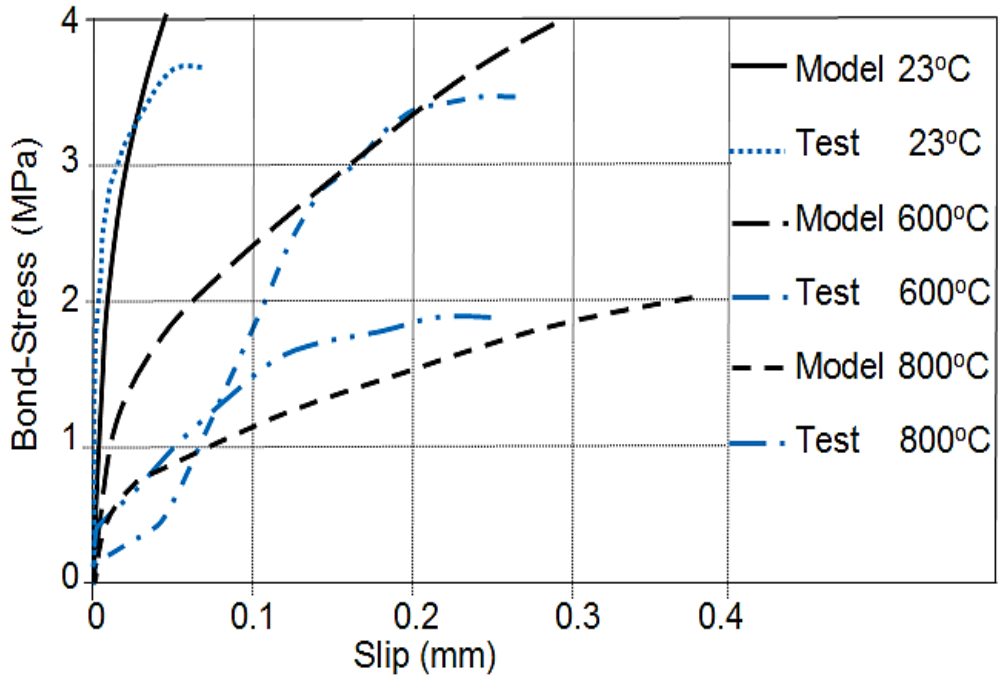
(a) Tested by (Diederichs & Schneider 1981)



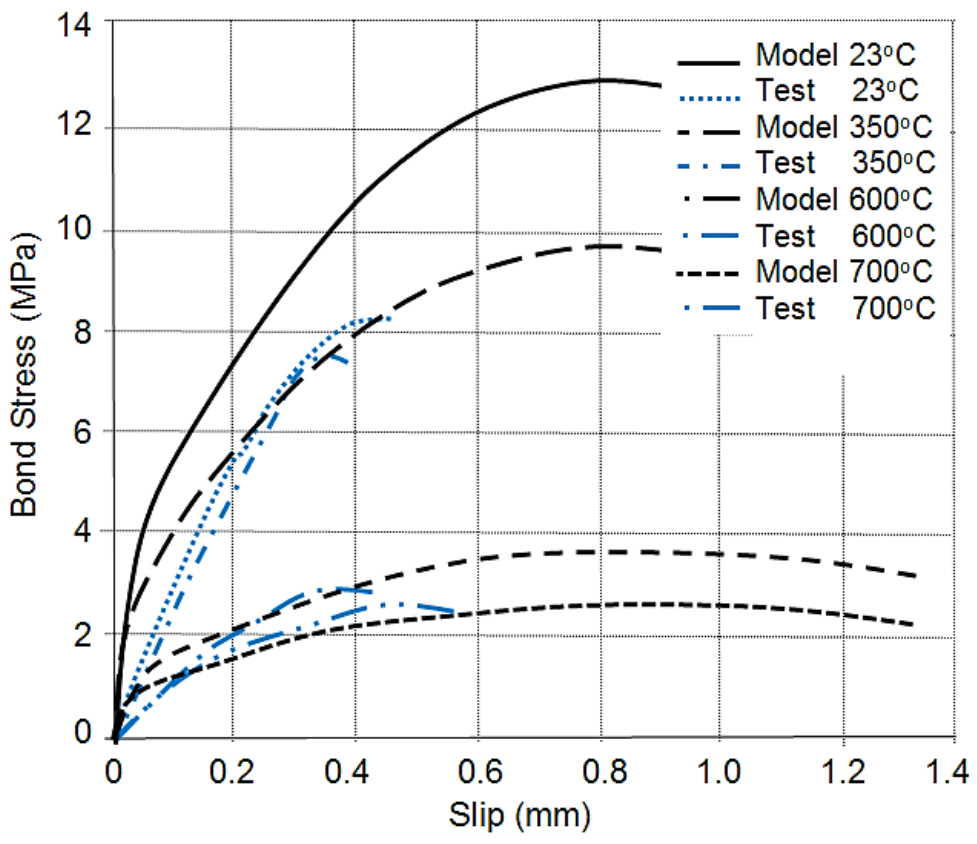
(b) Tested by (Morley & Royles 1983) ($d_b = 16\text{mm}$, concrete cover 55 mm)



(c) Tested by (Morley & Royles 1983) ($d_b = 16\text{mm}$, concrete cover 46 mm)



(d) Tested by (Haddad & Shannis 2004)



(e) Tested by (Haddad et al. 2008)

Figure 3.10 Comparison of predicted and measured bond stress-slip curves at elevated temperatures

The second test was carried out by Morley and Royles (1983). The temperatures within these tests were in the range of 20 °C-750 °C with heating rate of 2 °C/min. The lengths of the samples were 300 mm with a rebar embedded length of 32 mm. The details of the tests are given in Table 3.2. Figure 3.10 (b) and Figure 3.10 (c) show the comparison between the results from the testes and the predictions from the current model for concrete covers of 55 mm and 46 mm, respectively. It is evident that the predictions from current model are in the reasonable agreement with the testes data.

Another experimental test was conducted by Haddad and Shannis (2004) which was used for validation of the bond model at elevated temperatures. In these test, special cylindrical moulds of 82 mm diameter with a circular opening of 20 mm at the bases were used to cast the pull out specimens. The steel bar was 18 mm in diameter with imbedded length of 150 mm. The temperatures of the tests were 23 °C, 600 °C and 800 °C with heating rate of 20 °C/min. The details of the test are given in Table 3.2. A comparison between the current model and the results from the test is shown in Figure 3.10 (d). Again, reasonable agreement between the curves of the bond model and the curves from the testes were achieved.

Finally, a test was done by Haddad et al. (2008) has been adopted for further validation of the current model. The specimens in this test were in cuboid shape with dimensions of (100 x 100 x 400 mm). The steel bars of 20 mm with embedded length of 150 mm were used in this study. The range of the test temperatures was 23 °C to 700 °C. Figure 3.10(e) presents the comparison between the predictions from the current model and the results that achieved from the testes. It can be seen from the figure that the bond strength predicted by the current model is higher than the result from the teste at ambient temperature. However, there is very little difference between the tests at 23 °C compared with 350°C. This is contradicted with the tested results generated by other two researchers presented above.

3.4.2 Validations of the bond-link element with new developed bond stress–slip model

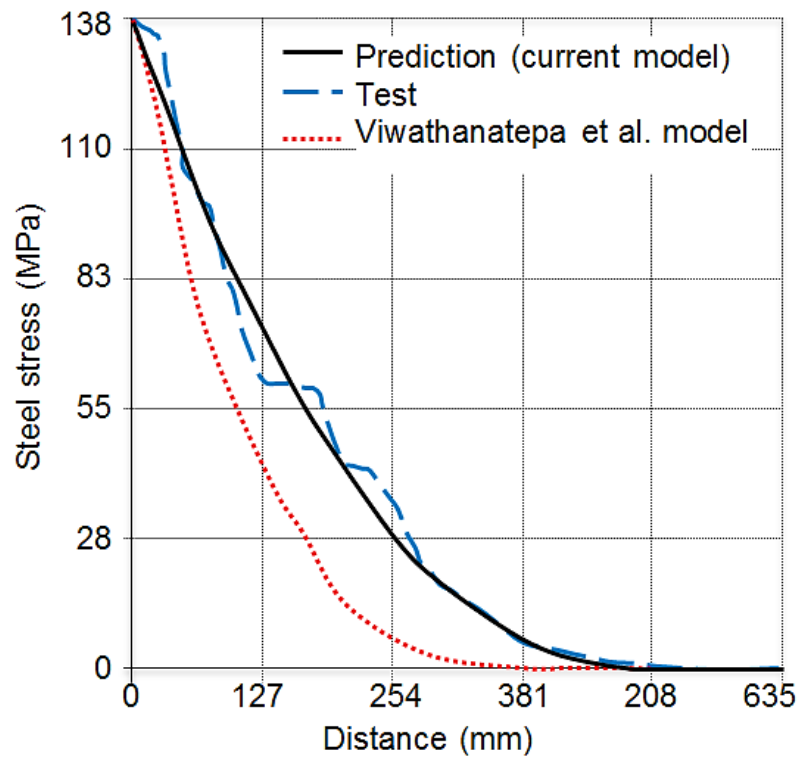
As mentioned in Section 3.3, the developed bond stress-slip model has been incorporated into the VULCAN software (Huang et al. 2009) for simulating the bond characteristics between concrete and reinforcing steel bar at ambient and elevated temperatures. In this section, three different types of tests were adopted to validate the response of the reinforced concrete members that modelled with full and partial interaction between the concrete and steel bar using bond-link element approach.

3.4.2.1 Modelling pull-out test at ambient temperature

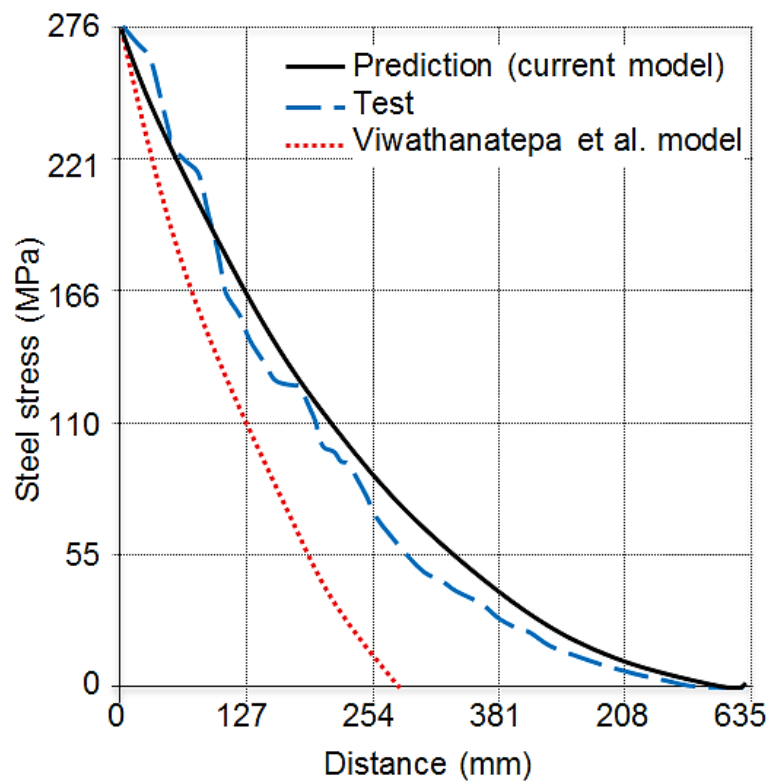
Viathanatepa et al. (1979) conducted several pull-out tests at the University of California in 1979. One specimen was used as a reference for validation. In this test, the reinforcing bar was 25 mm diameter with anchorage length of 635 mm through the concrete specimen. The specimen was subjected to a monotonic pull-out load under displacement control at one end only. The tested material properties of concrete and steel are as follows: the concrete cylinder compressive strength is $f_{ck}=32.4$ MPa, yield strength of the reinforcing steel bars is $f_y=468.4$ MPa. These material properties and the specimen details were used as an input data for the modelling the beam. The finite element mesh for modelling this test involved 4 three-node plain concrete elements, 4 three-node reinforcing steel bar elements. The nodes of the concrete elements were connected to the nodes of the steel bar elements by the two-node bond-link elements. Hence, total of 9 two-node bond-link elements were used in this case.

In this validation the predicted steel stresses from VULCAN output were compared with the teste data, as well as compared with the results from an analytical study generated by Viathanatepa et al. (1979). Figure 3.11(a) to (c) show the stress distribution along the anchored length of the reinforcing steel bar at three different load levels. It is clear from the figures that the results generated by the current model agree well with the teste results. To demonstrate the robustness of the current model, Figure 3.12 shows the predicted bond stress field along the anchored length for different loaded end slips. Also Figure 3.13 presents the predicted end slips versus total pull out load for the test. These results indicated that the strength of the bond

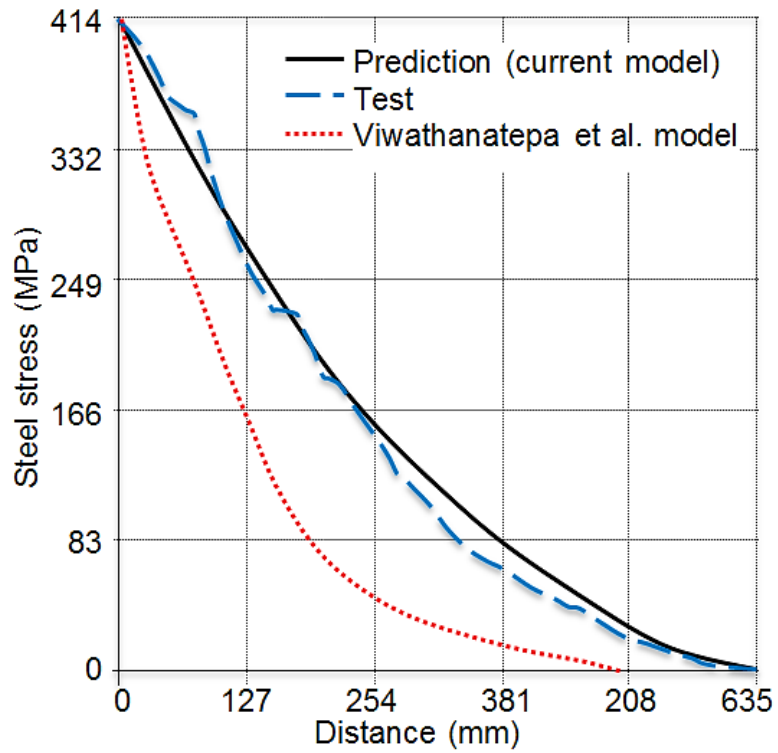
between concrete and reinforcing steel bar plays a very important role which can effect on the load capacity of reinforced concrete structural members.



(a) End stress=138 MPa



(b) End stress=276 MPa



(c) End stress=414 MPa

Figure 3.11 Comparison between the predicted and tested stress distributions along anchored reinforcing steel bar (Viwathanatepa et al. 1979)

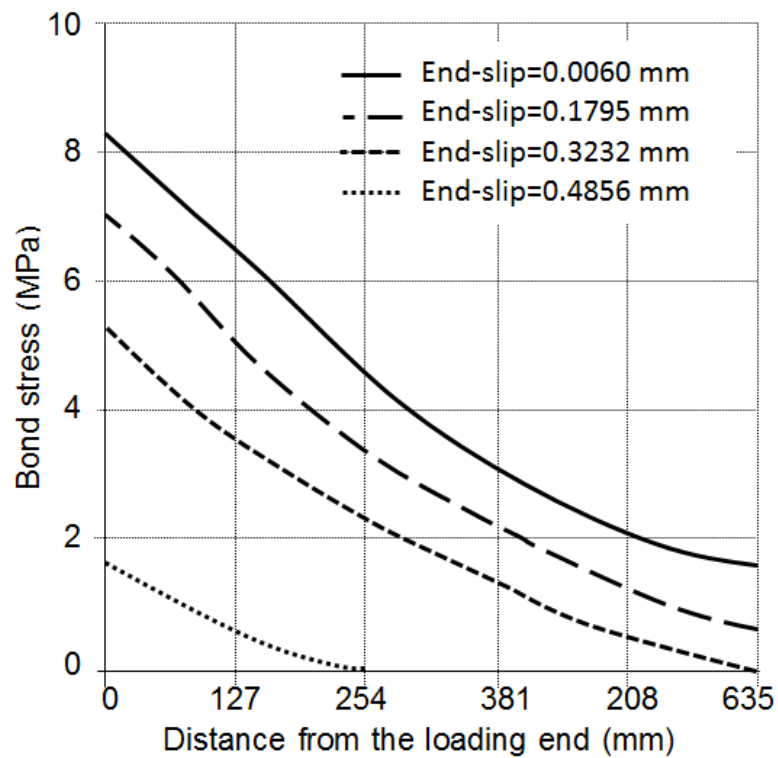


Figure 3.12 Predicted bond stress distributions corresponding to different end-slips for test (Viwathanatepa et al. 1979)

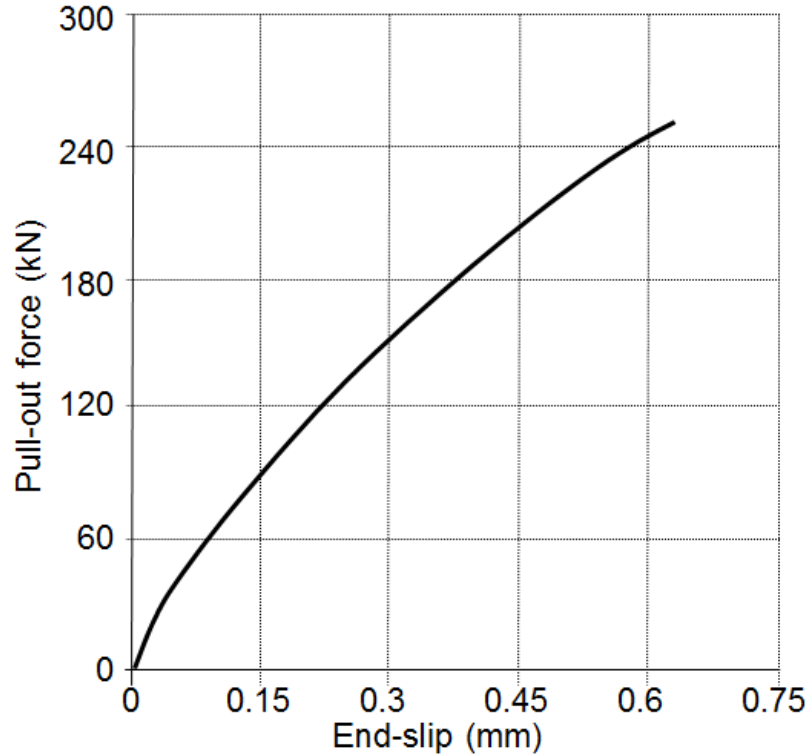


Figure 3.13 Predicted end-slips vs pull-out force for the test (Viwathanatepa et al. 1979)

3.4.2.2 Modelling simply supported RC beam at ambient temperature

In order to examine the capability of the developed model, a simply supported reinforced beam J4 tested by Burns and Siess (1962) was used for the validation. Figure 3.14 illustrates the details of J4 beam. The material properties of the concrete was $f_{ck}=33.34$ MPa and the reinforcing steel bars was $f_y=309.6$ MPa as a yield strength and elastic modulus of $E_s=203404$ MPa. The beam was modelled with 2 x 25.4 mm reinforcing steel bars. Those material properties were used as the input data for modelling the beam. Due to the symmetry of the beam, only half of the beam was modelled in this study. For modelling the beam J4, 4 three-node plain concrete elements, 8 three-node reinforcing steel bar elements with 198.2 mm off-set below the central reference axis and 63.5 mm right and left referenced to the central reference axis, and 18 bond-link elements were employed. Figure 3.15 shows the comparison of predicted and measured mid-span deflections of J4 beam with different bond conditions. In the figure, it was assumed for the case of perfect bond that there is no slip can occur between the steel bar and surrounding concrete, while the case of bond-slip the interaction between steel bar and concrete was considered

by using bond-link element that developed in this study. It is evident that the bond-slip of the reinforcing steel bars has a negligible effect on the load-deflection response at room temperature.

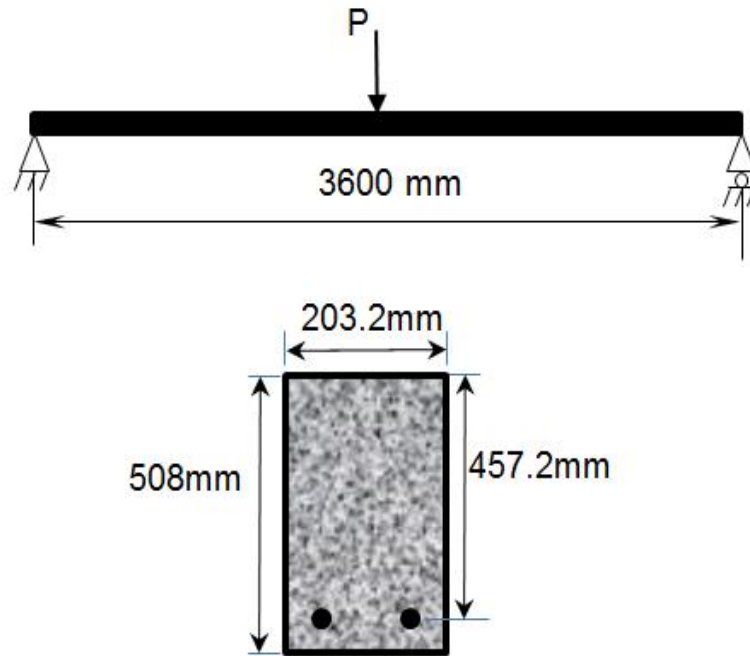


Figure 3.14 Details of J4 beam tested at ambient temperature (Burns & Siess 1962)

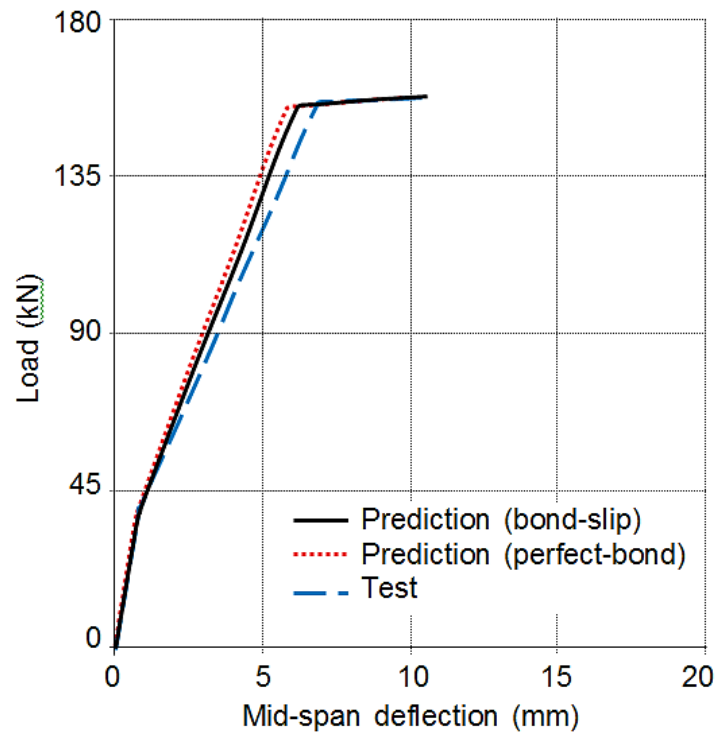


Figure 3.15 Comparison of predicted and measured mid-span deflections of J4 beam (Burns & Siess 1962)

3.4.2.3 Modelling fire tests of RC beams

Lin et al. (1987) carried out a series of tests on reinforced concrete beams under fire conditions. Two types of heating curves were adopted in these tests; ASTM standard fire curve and Short Duration High Intensity (SDHI) fire curve. In this validation, four beams of two groups were modelled. The first group Beam-1 and Beam-3 was heated using ASTM standard fire curve and the second group Beam-5 and Beam-6 was subjected to the SDHI fire. The details of the beam-1, beam-3, beam-5 and beam-6 used for modelling are shown in **Figure 3.16**. The concrete compressive strengths of beam 1, 3, 5 and 6 were $f_{ck}=27.68$ MPa, $f_{ck}=31.5$ MPa, $f_{ck}=33.37$ MPa and $f_{ck}=34.54$ MPa respectively. The yield strength of tested steel bars were $f_y=487.27$ MPa for the 22.2 mm steel bar diameter and $f_y=509.54$ MPa for 25.4 mm steel bar diameter. Degradation of the concrete compressive strength and the steel bars yield strength at elevated temperatures specified in EN 1992-1-2 (CEN 2004) were adopted for concrete and steel bar elements.

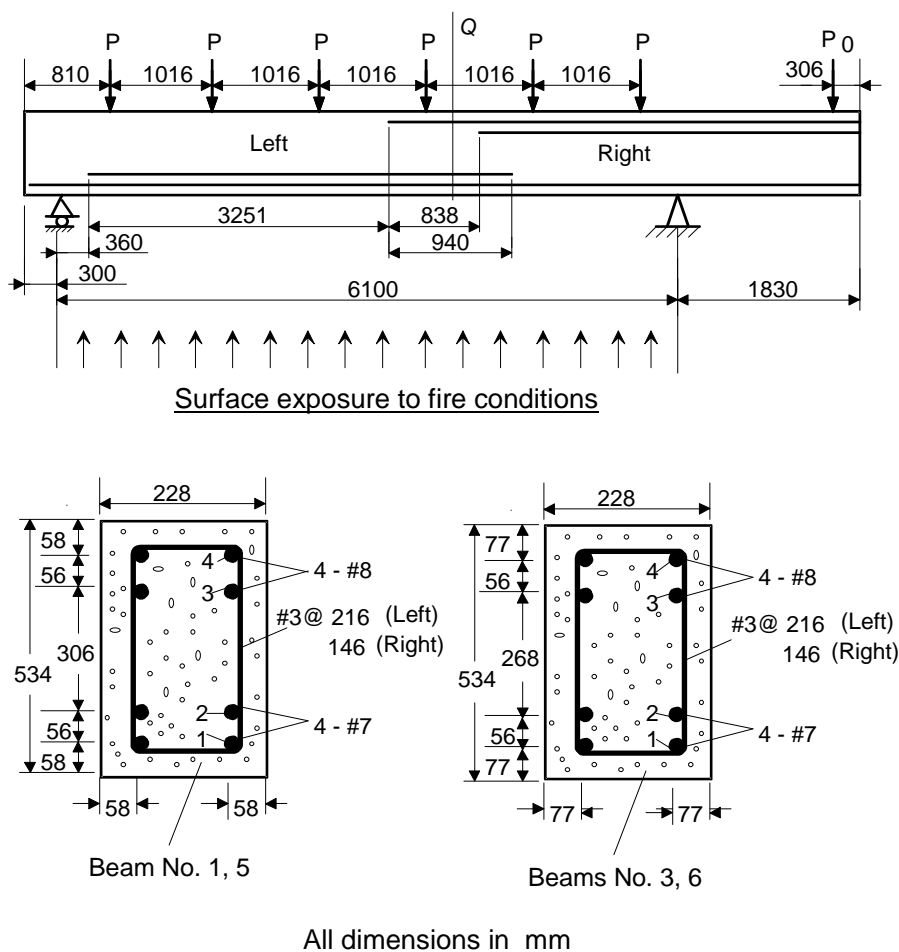


Figure 3.16 Details of tested beams in fire (Lin et al. 1987)

In order to model the tested beams using VULCAN software, two phases should be followed to perform the analysis. The first phase was to perform the thermal analysis. As shown in Figure 3.16 the arrangement of reinforcing steel bars in the tested beams varied along the length of the beam. To perform the thermal analysis in this study, the cross-sections of the beams were divided into 448 segments (28 rows x 16 columns). The steel bars were represented as steel segments within the cross-section of the beam and varied along the length of the beam based on the tested beams. The thermal analysis was conducted to predict temperature histories of each segment within the beam cross-sections. There are four layers of main reinforcing steel within the cross-sections as shown in Figure 3.16. For presenting the results of the thermal analysis, the reinforcing steel layers are denoted in sequence from bottom to top as layers 1 to 4. The predicted temperature histories of the main reinforcing steel layers for beams-1 and beam-5 are shown in Figure 3.17 and Figure 3.18 respectively. It is evident from the figures that reasonable agreements have been achieved from the thermal analysis by compare the temperature history of the test with the predicted temperature history for the steel bar layers.

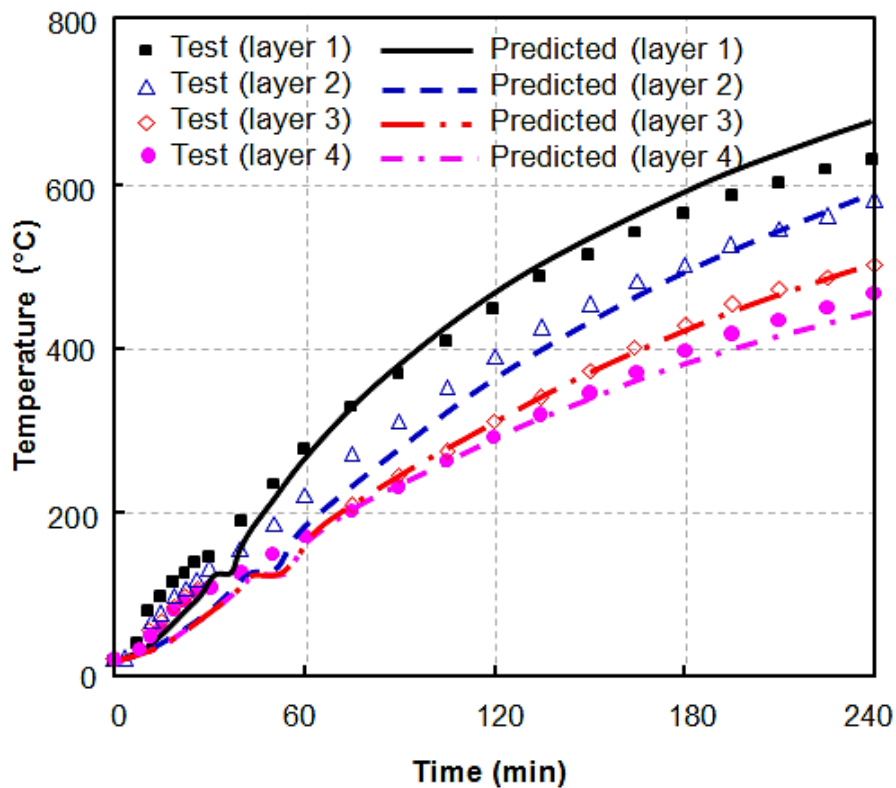


Figure 3.17 Comparison of predicted and measured temperatures of four main reinforcing steel layers for Beam 1 (Lin et al. 1987)

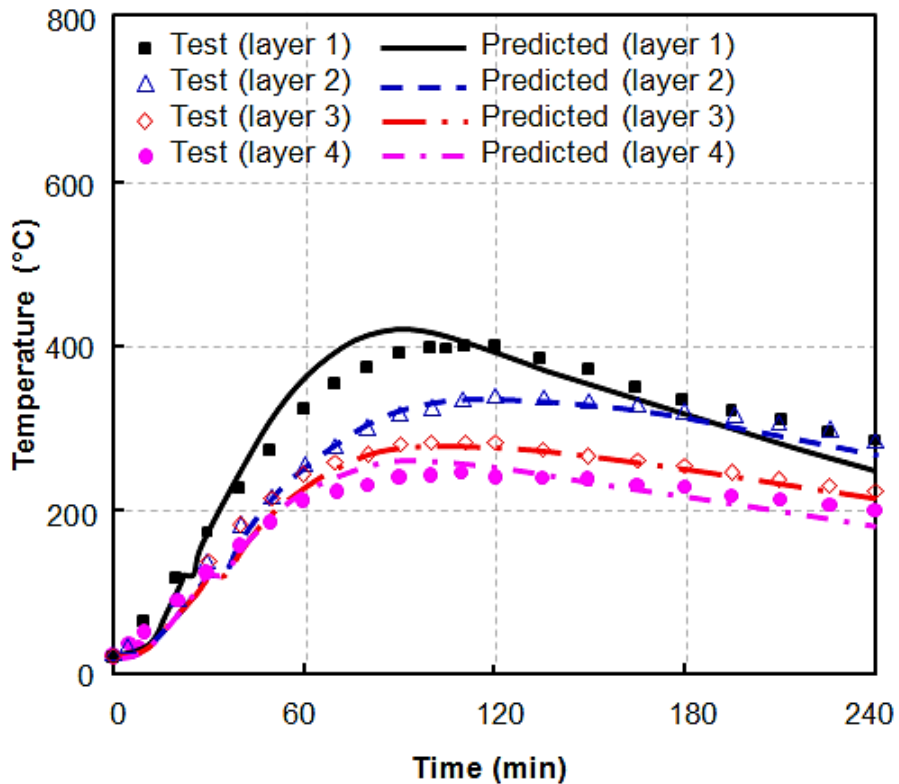


Figure 3.18 Comparison of predicted and measured temperatures of four main reinforcing steel layers for Beam 5 (Lin et al. 1987)

Predicted temperatures histories from the thermal analysis for each concrete and steel segment were used as the temperature input data for the structural analysis. Hence, same segmentations of the beams cross sections used in the thermal analysis were adopted for the plain concrete elements in the structural analysis, in which the volumes occupied by the steel bars were represented as void segments. The temperatures of the reinforcing steel bars were represented by the temperatures of the steel segments at related locations within the cross-section. In this analysis, a total of 10 three-node plain concrete elements with 448 segments, 48 three-node reinforcing steel bar elements with off-set from the central reference axis of the beam and 104 bond-link elements were employed for modelling the whole beam. As shown in Figure 3.16, the load P was kept constant at 44.48 kN during each fire test, although the cantilever force varied as the test progressed.

Due to the beam was continued over the right-hand support as shown in Figure 3.16, the maximum vertical deflection of the beam was formed around the position 2600 mm from the left-hand support. The comparison of predicted and measured maximum deflections of Beam 1 and Beam 3 under ASTM fire condition are shown

in Figure 3.19 and Figure 3.20 respectively. Again, these two beams were modelled twice to consider the case of perfect bond and bond-slip conditions. For the perfect bond condition, it was assumed that there is no slip can occur between the steel bar and surrounding concrete. However, partial interaction between reinforcing steel bar and concrete was considered by using current bond-link element for modelling the case of bond-slip condition. Under ASTM standard fire condition, it is evident from the figures that before 120 min test time the behaviours of the beams that modelled with full or partial bond conditions are almost identical. This is due to the average temperature at bond between concrete and reinforcing steel bar is less than 400°C (see Figure 3.17). Hence, the strength of the bond does not decrease significantly. As explained previously in section 3.4.1.2 the bond between the concrete and reinforcement decreases significantly at temperatures 400°C to 600°C. However, the influence of the bond became significant when the test time beyond 180 min in which the average temperature at the bond was above 500°C as shown the Figure 3.17.

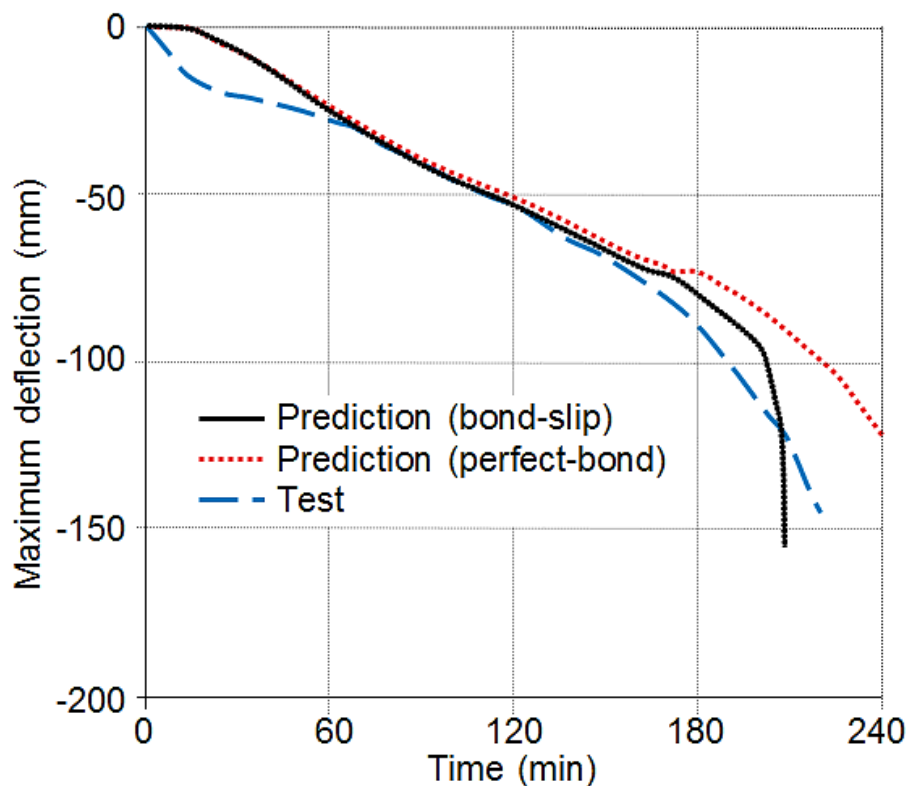


Figure 3.19 Comparison of predicted and measured maximum deflections of Beam1 (ASTM Fire)
(Lin et al. 1987)

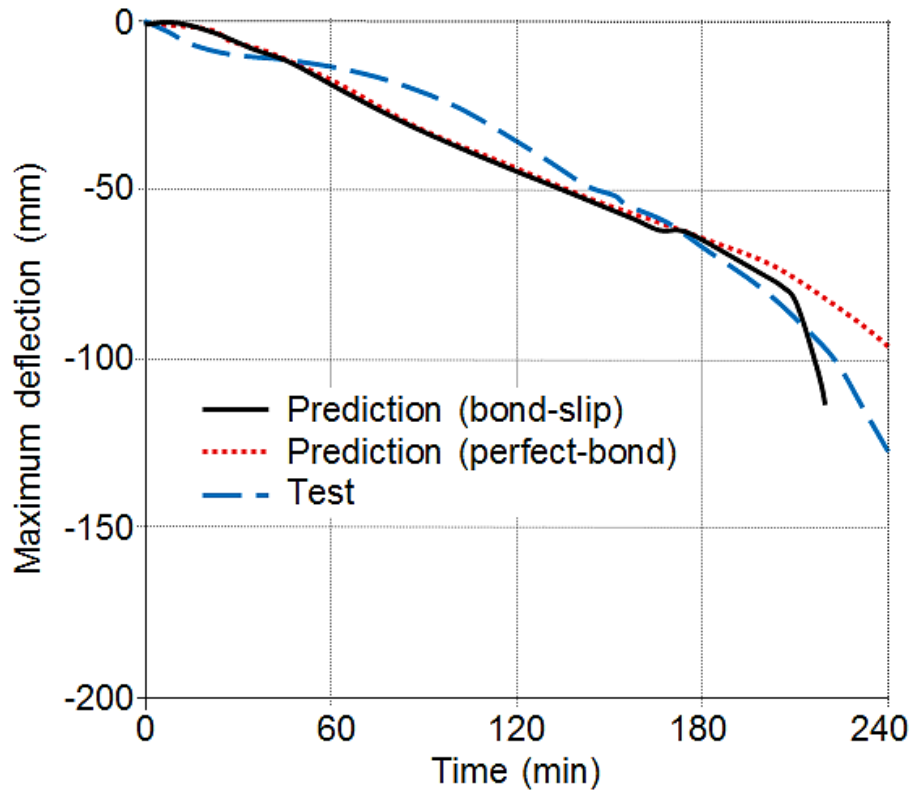


Figure 3.20 Comparison of predicted and measured maximum deflections of Beam3 (ASTM Fire)
(Lin et al. 1987)

Figure 3.21 and 3.22 illustrate the comparison between the predicted and tested maximum deflections of Beam 5 and Beam 6 under SDHI fire condition. It can be seen that the influence of the bond conditions is not significant. This is due to the maximum temperature of the bond is less than 400°C (see Figure 3.19). From the validations, it is evident that the new bond-link element with the developed bond stress-slip model is capable to consider the influence of bond characteristics between concrete and reinforcing steel bars on the structural behaviours of reinforced concrete structural members at ambient and under fire conditions. This study indicates that for fire resistance design of reinforced concrete structures the perfect bond assumption is un-conservative and it is important to consider the influence of bond within the concrete design under fire conditions.

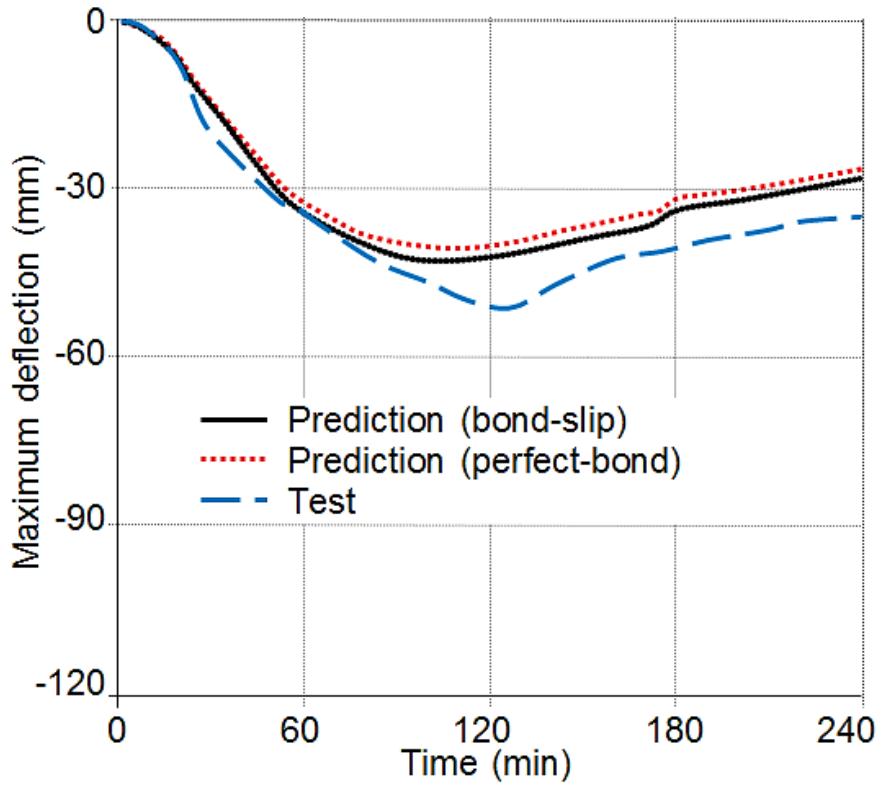


Figure 3.21 Comparison of predicted and measured maximum deflections of Beam5 (SDHI Fire) (Lin et al. 1987)

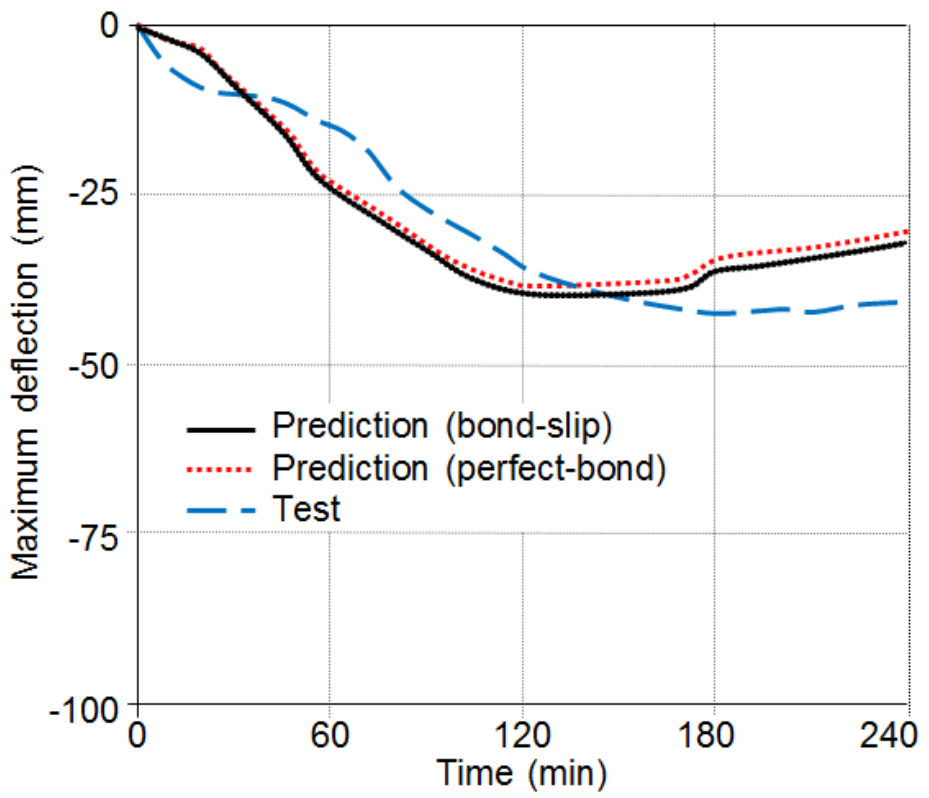


Figure 3.22 Comparison of predicted and measured maximum deflections of Beam6 (SDHI Fire) (Lin et al. 1987)

3.5 Conclusions

In this chapter a numerical model has been developed to simulate the bond-slip characteristic between the concrete and reinforcing steel bar at ambient and elevated temperatures. The model is based on the thick-wall cylinder theory with considering of the partially cracked concrete cover and the smeared crack of concrete in tension. Hence, the model takes into account the splitting failure of concrete cover. The degradation of the bond strength at elevated temperatures is related to the concrete material properties changed with temperature. The developed bond stress-slip model has been incorporated into VULCAN software using the two-node bond-link element approach to consider the influence of bond characteristic on structural behaviours of reinforced concrete structural members in fire. A series of validations have been conducted using the previous tested results generated by different researchers. Reasonable agreements have been achieved between the predicted results from the model and the experimental data. Based on this study, the following conclusions can be drawn:

- The model presented in this chapter is able to predict the bond-slip characteristic between the concrete and reinforcing steel bar at ambient and elevated temperatures. The model takes into account the variation of concrete properties, concrete covers and the geometries of rebar.
- The study indicated that the strength of the bond between concrete and reinforcing steel bars plays a very important role that can affect the fire resistance of reinforced concrete structures, especially when the temperature of the reinforcing steel bar is high (more than 400°C). Therefore, the assumption of the perfect bond condition for the analysis of reinforced concrete structures under fire conditions is un-conservative.
- For fire engineering design the failure of bond between concrete and reinforcing steel bar, particularly in beams with little or no continuity, can be the key criterion for fire resistance, but this clearly needs further parametric studies before general rules can be proposed.

Chapter 4 Behaviour of the bond between prestressed strands and concrete in fire

After understanding the effect of the bond stress-slip on the structural behaviour of the reinforced concrete members under fire conditions, it is important to study the bond stress-slip in prestressed concrete structures. Hence, this chapter is dedicated to develop a new analytical model to simulate the bond stress-slip between concrete and strands in prestressed concrete members at elevated temperatures. Influence of the bond-slip on the response of prestress concrete members under fire conditions is also investigated.

4.1 Introduction

Prestressed concrete (PC) members have obtained wide popularity in current building constructions. PC members can be constructed by utilizing unbonded or bonded strands with concrete. For bonded PC members, the bond is essential for the success of prestressing system. The bond in PC members may be categorized as transfer bond and flexural bond. During the manufacture of PC members, strands are initially prestressed using jacks at the ends abutments. The concrete is casted and cured then the strands are cut. Initial tensioning of the strand causes a reduction in the diameter of the strand due to Poisson's effect. After concrete reaches sufficient strength, the strands are released from the abutments, and the stress in the strands at the free ends of the members returns to zero. With this reduction of the strand stresses, the diameter of the strand expands along the transfer length. Therefore, wedging action between the strand and concrete will occur due to lateral expansion (called Hoyer effect). This effect leads to improve the bond performance over the transfer bond length (Abrishami & Mitchell 1993).

From the literature, to determine the bond for the flexural bond length, pull-out tests have been conducted by casting the concrete surround the strand then the strand is pulled-out from the concrete with measuring the pull-out force versus the slip. However, the bond for the transfer bond length can be obtained by applying initial prestress on the strand, and then casting the concrete until the time of test, then releasing the stress from the strand gradually with recording of stress released versus

the slip (Abrishami & Mitchell 1993; CEB-FIP-Bulletin10 2000). For the bonded PC structural members, transferring the force from the strand to the concrete is through the end anchors together with the bond between strand and concrete. Therefore, bonded PC beams are more robust structural members at ambient temperature. However, previous research indicated that compared to normal reinforcing steel, prestressed steel wires are more sensitive to elevated temperatures due to the stress level in prestressing wires is very high (Hou et al. 2015).

Structural fire safety is one of the most important considerations in building applications. In concrete beams, fire resistance is generally assessed by evaluating the bending failure only. However, bond failure can be dominated in bonded PC members. Concrete tensile strength is significantly affected by high temperatures results in a big reduction in the shear capacity of the concrete and bond strength. Also at high temperatures, internal stresses due to differential thermal elongations play a role on the occurrence of concrete cracks at the interface surrounding the rebar, which can decrease the bond stress (Fellinger, et al. 2003). The conventional approach of evaluating fire resistance through fire tests is expensive. Therefore, an alternative to fire tests is the use of numerical modelling for evaluating fire resistance of the prestressed concrete members. Numerical model allows the researcher to incorporate various parameters in an efficient and cost-effective way during the analysis (Kodur & Shakya 2014).

Previous research indicated that concrete structures begin losing strength rapidly when temperature reaches higher than 300°C (Rivera et al. 2016). For the prestress steel, the loss of strength occurs at lower temperatures compared to the normal steel rebar, in which a considerable reduction can be occurred in prestress steel strength at temperatures 300°C–400°C (ASHI Reporter 2007). At present, a number of investigations have been conducted to study the bond behaviour between prestressed strands and concrete at ambient temperature (Abrishami & Mitchell 1993; Lundgren 2002; Gustavson 2004; Galvez et al. 2009; Vázquez-Herrero et al. 2013). However, there are very limited researches conducted to investigate the bond-slip characteristic between prestressed strands and concrete at elevated temperatures. Hence, the main objectives of this chapter are to:

- Develop a robust model for modelling the bond-slip between concrete and strands for prestressed concrete structures in fire. This model can be used to predict the bond stress-slip for three wire and seven-wire strands with smooth or indented surface at elevated temperatures.
- Incorporate the bond-slip model into the 3D finite element program VULCAN to model prestressed concrete structures under fire conditions.
- Validate the model against previous test results.

4.2 Analytical model

In pretensioned concrete members, there are two distinct regions with different bond characteristics: the transfer length region and flexural length region. Figure 2.6 illustrates the behaviour of a prestress beam and the state of the strands stresses within the beam before and after applying the external load. Figure 2.6(a) shows the pretensioned reinforced concrete beam, and Figure 2.6(b) gives the variation of stresses in the pretensioned strand along an unloaded beam after the prestress is released from the strand and before applying the external load. Figure 2.6(c) shows the variation of stresses in the strand for the same beam after it is subjected to external load (Abrishami & Mitchell 1993). The transfer length l_t , as shown in Figure 2.6 (b) is the distance from the end of the beam where the strand stress is zero to the point where the strand stress reaches to the maximum level for unloaded beam. The transfer length l_t can be taken as $(50 d_s)$ (CEB-FIP-Bulletin10 2000). The flexural length l_f is the length that starts from the end of the transfer length to the point in which the ultimate stress can be developed after loading the beam (see Figure 2.6 (c)).

When concrete is casted around the strand in prestressed concrete structures, the concrete forms an envelope or sleeve surround the strand. The hardened concrete mimics the shape of the strand. When the strand is pulled through the concrete, movement is resisted by the concrete keys acting on the outside wires of the strand, as shown in Figure 2.6. This resistance is called mechanical interlocking (Russel & Burns 1993). The mechanisms that contribute to the bond between prestressed strand and surrounding concrete are chemical adhesion, friction and mechanical interlocking between strand's outer wires and concrete. The mechanical interlocking is the largest contributor to the bond, especially in cracked regions. When the cracks

are formed in the concrete surround the strand, the slip of the strand is occurred for some small finite distance on either side of the crack to preserve compatibility of the strand. When the bond's slip occurs, the mechanical interlocking is activated by the reaction of the interlocking of outside wires with the concrete envelope. The bond's slip is caused mainly by crushing of the concrete in front of the strand's ridges. The high pressure on the concrete in front of the ridges causes tensile stresses in the concrete surround the strand, which in turn create internal inclined cracks. These inclined cracks initiate at relatively low bond stresses at the contact point between the strand and concrete. Increasing the stress in the strand leads to increase the slip due to local crushing of concrete in front of the ridges of the strand. Then, shear cracks in the concrete keys between the strands ridges will initiate. At maximum bond resistance, these concrete keys are sheared off (Choi et al. 2010).

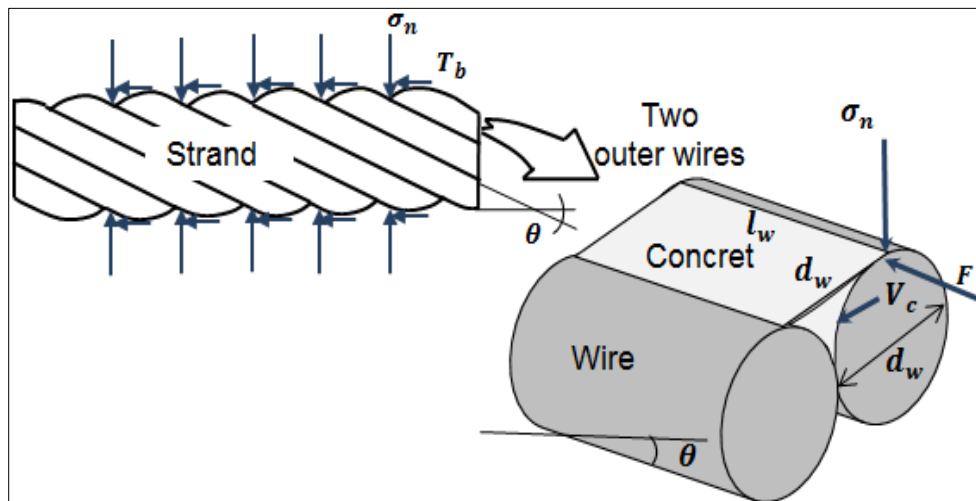


Figure 4.1 The interaction between the outer wires of the strand and concrete

In the proposed model, the shear force resistance (shear force capacity) of the concrete keys in front of strand ridges V_c (as shown in Figure 4.1) can be calculated as:

$$V_c = v_c A_{sh} n \quad (4.1)$$

where, v_c is the shear strength of the shear keys in the concrete mass (concrete shear capacity); n is the number of the outer wires and A_{sh} is the shear area of the cracked surface, which is the area of the concrete keys between two ridges of the strand, and

equals to the diameter of the outer wires d_w multiplied by the length of the wires l_w (see Figure 4.1) as:

$$A_{sh} = d_w l_w \quad (4.2)$$

The force F along the length of the outer wires of the strand (as shown in Figure 4.1) can be determined from two parts as:

$$F = F_1 + F_2 \quad (4.3)$$

The first part from Equation (4.3) can be calculated from the shear effect of concrete keys in front of the ridges of the strand as:

$$F_1 = \mu V_c \quad (4.4)$$

The second part of the force is achieved by considering the cohesion and the friction between the strand and concrete as:

$$F_2 = (0.6 \pi d_w) l_w (C + \mu \sigma_n) n \quad (4.5)$$

Where, C is the cohesion between the concrete and steel and μ is the coefficient of friction between the steel and concrete. Based on References (Brown et al. 1993; CEB-FIP-Bulletin10 2000; Bolmsvik & Lundgren 2006), the values of C and μ at ambient temperature can be assumed as stated in Table 4.1 below. Some researchers found that the coefficient of friction is independent on temperature, in which rising the temperature simultaneously produces a drop in the strength of the material and increase in the contact surface area, consequently the shear resistance as a whole remains unchanged (Bowden et al. 1942; Dzhafarov & Rozhenko 1968). Hence, in this proposed model, the value of μ is assumed to be the same at ambient and elevated temperatures, while the cohesion C is assumed to be zero when temperature $> 400^\circ\text{C}$.

Table 4.1 Values of C and μ used in the proposed model

Type of strand	Smooth		Indented	
	C	μ	C	μ
Three-wire strands	1.3	0.4	1.7	0.6
Seven-wire strands	1.3	0.4	1.6	0.5

The maximum bond force in the direction of the strand T_b (see Figure 4.1) is calculated as:

$$T_b = F / \cos(\theta) \quad (4.6)$$

where, θ is the pitch angle of the outer wires, which can be taken as ($\theta = 9^\circ$) (Russel & Burns 1993).

The shear strength of the concrete mass v_c in Equation (4.1) should not be assumed greater than $0.2 f'_c$ (Choi et al. 2010). The value of the shear strength of the concrete keys v_c can be calculated by using Parabolic Mohr Envelope (Curtis 2011). Figure 4.2 shows a parabolic fit to Mohr circles for uniaxial compression and tension test results (Curtis 2011). From Figure 4.2 the shear strength envelope is defined as follows:

$$\tau^2 = \left[f'_c - 2f_t \left(-1 + \sqrt{1 + \frac{f'_c}{f_t}} \right) \right] (\sigma_n + f_t) \quad (4.7)$$

where, σ_n is the normal stress perpendicular to the strand axis.

For the pull-out bond, which represents the bond for flexural length l_f (see Figure 2.6), $\sigma_n = 0$ then:

$$\tau = c = v_c = f_t \left(\frac{f'_c}{f_t} + 2 - 2 \sqrt{1 + \frac{f'_c}{f_t}} \right)^{1/2} \quad (4.8)$$

For the push-in bond, which represents the bond for transfer length l_t (see Figure 2.6), $\sigma_n \neq 0$; this means that there is a pressure affects normal to the axis of the

strand within the concrete. Hence, σ_n can be calculated based on the stress-strain relationship defined in Eurocode 2 (CEN 2004) for non-linear structural analysis as $\sigma_n = \sigma_c$; that is:

$$\sigma_n = \sigma_c = f_{cm} \frac{k\eta - \eta^2}{1 + (k-2)\eta} \quad (4.9)$$

$$\eta = \varepsilon_c / \varepsilon_{c1} \quad (4.10)$$

$$\varepsilon_{c1} = 0.7 f_{cm}^{0.31} \leq 2.8 \quad (4.11)$$

$$k = 1.05 E_{cm} |\varepsilon_{c1}| / f_{cm} \quad (4.12)$$

where, ε_{c1} is the strain at peak stress (Table 3.1 in Eurocode 2 (CEN 2004)) and ε_c is the concrete strain, which can be taken from Equation (4.15).

The normal pressure σ_n in prestressed concrete can be generated from the effect of Poisson's ratio (Hoyer effect). This normal pressure is generated due to the release of the prestressed strand after concrete casting; in which the nominal diameter of the strand will increase due to Poisson's ratio. This radial expansion generates normal stresses in the concrete surround the strand. These stresses provide an extra confinement to the strand, which leads to increase the bond stress between the strand and concrete. This expansion in diameter of the strand can be calculated as:

$$\frac{P_1}{A_s E_s} = \varepsilon_{s1} \quad (4.13)$$

$$\frac{P_2}{A_s E_s} = \varepsilon_{s2} \quad (4.14)$$

$$\varepsilon_c = \frac{P_1 - P_2}{A_s E_s} \nu = |\varepsilon_{s1} - \varepsilon_{s2}| \nu \quad (4.15)$$

Where, P_1 is the initial tension force on the strand (during the PC manufacture before applying the external loading) which is typically taken as 70-75% of the ultimate stress multiplied by the cross section area of the strand to give the force P_1 (Abrishami & Mitchell 1993; Vázquez-Herrero et al. 2013). P_2 is the force after the

stress released from the strand in which the effective force ΔP on the strand is $\Delta P = P_1 - P_2$, this can be applied for the pull-out test to study the behaviour of bond between the strand and concrete. However, in PC members when the strand is cut after the pretension, P_2 equals to zero, then the effective force ΔP equals to P_1 .

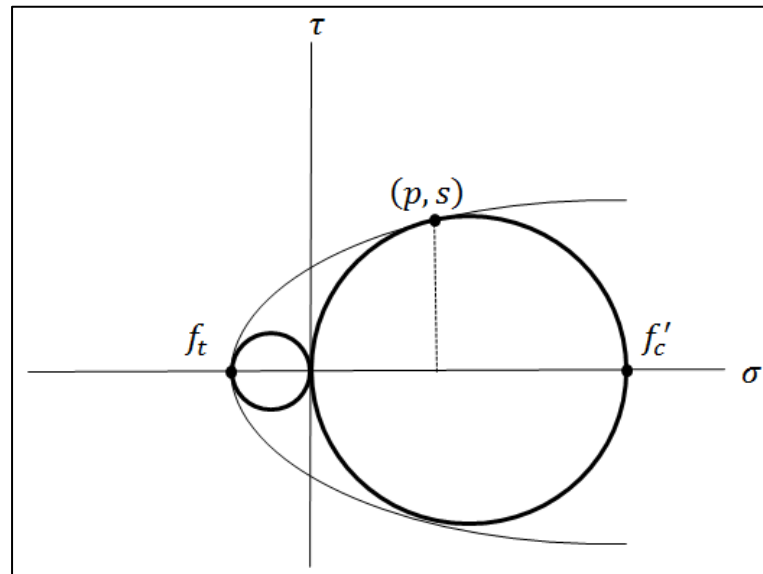


Figure 4.2 Parabolic Mohr Envelope (Curtis 2011)

The average bond stress-slip relationship between the concrete and deformed bar defined by CEB-FIP Model code 2010 (CEB-FIP 2010) has been adopted in this study as shown in Figure 4.3. In Figure 4.3, τ is the average bond stress; τ_{\max} is the maximum bond stress; S is the slip between strand and concrete.

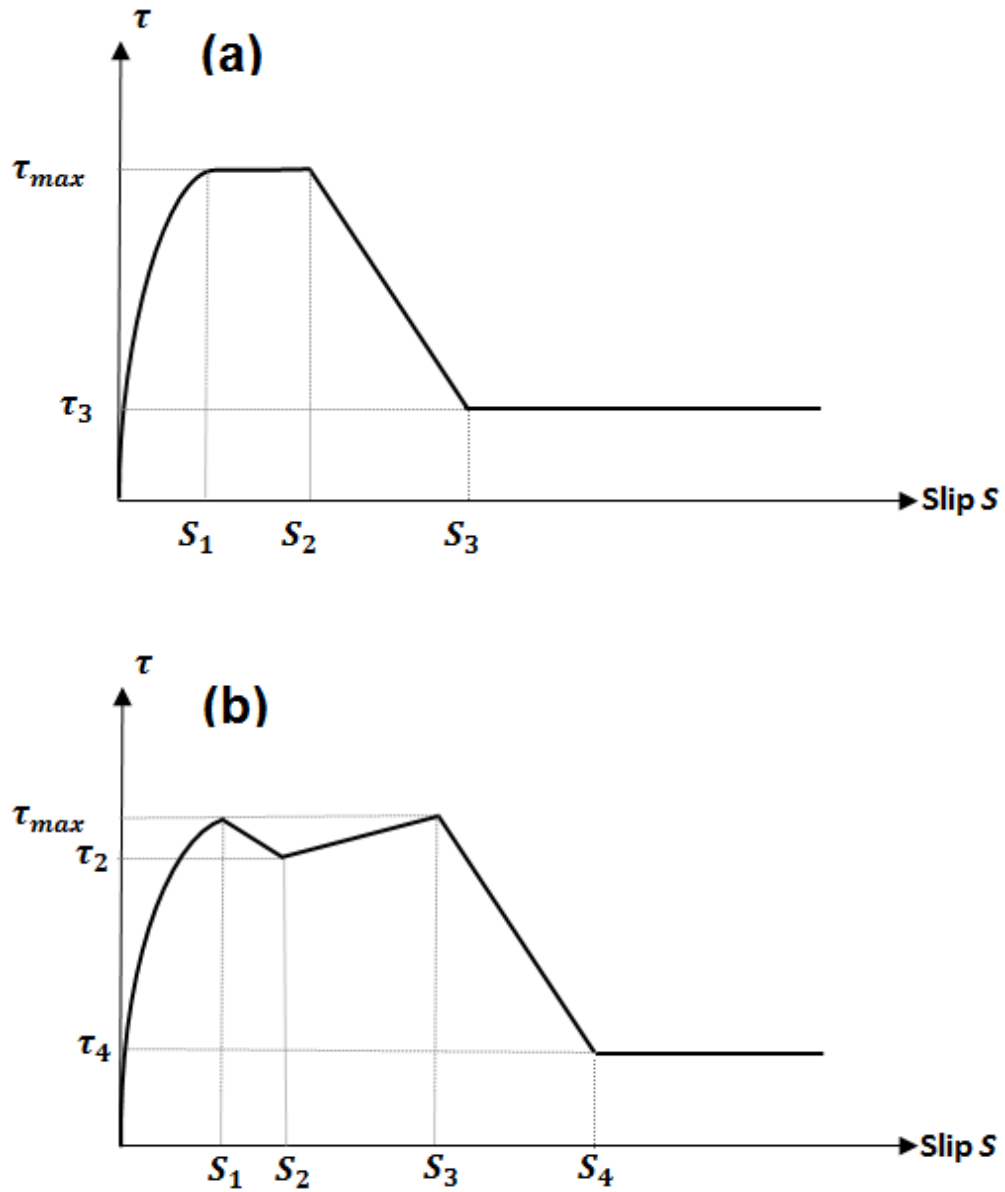


Figure 4.3 Bond stress-slip curve: (a) Three-wire strands and indented seven wire strands, (b) Seven-wire smooth strands

For three-wire smooth and indented, and seven-wire indented strands, the curve can be defined as follow (see Figure 4.3 (a)):

$$\tau = \left(\frac{S}{S_1} \right)^\alpha \quad \text{for } 0 \leq S \leq S_1 \quad (4.16)$$

$$\tau = \tau_{\max} \quad \text{for } S_1 \leq S \leq S_2 \quad (4.17)$$

$$\tau = \tau_{\max} - (\tau_{\max} - \tau_3) \frac{(S - S_2)}{(S_3 - S_2)} \quad \text{for } S_2 \leq S \leq S_3 \quad (4.18)$$

$$\tau = \tau_f \quad \text{for } S_1 \leq S \leq S_2 \quad (4.19)$$

For seven-wire smooth strands the curve is defined as (see Figure 4.3(b)):

$$\tau = \left(\frac{S}{S_1} \right)^\alpha \quad \text{for } 0 \leq S \leq S_1 \quad (4.20)$$

$$\tau = \tau_{\max} - (\tau_{\max} - \tau_2)(S - S_1)/(S_2 - S_1) \quad \text{for } S_1 \leq S \leq S_2 \quad (4.21)$$

$$\tau = \tau_2 + (\tau_{\max} - \tau_2)(S - S_2)/(S_3 - S_2) \quad \text{for } S_2 \leq S \leq S_3 \quad (4.22)$$

$$\tau = \tau_{\max} - (\tau_{\max} - \tau_4)(S - S_3)/(S_4 - S_3) \quad \text{for } S_3 \leq S \leq S_4 \quad (4.23)$$

$$\tau = \tau_f \quad \text{for } S > S_4 \quad (4.24)$$

In the current model, τ_{\max} is calculated as:

$$\tau_{\max} = \frac{T_b}{A_b} \quad (4.25)$$

where, T_b is the maximum bond force which is calculated from Equation (4.6) and A_b is the contact area between the strand and concrete as:

$$A_b = \pi d_s L_b \quad (4.26)$$

Where, d_s is the nominal diameter of the strand and L_b is the embedded length of the strand or the element length in finite elements.

The values of the slip parameters S_1 , S_2 , S_3 and S_4 are assumed based on statistical analysis of the experimental data from the previous researches (Abrishami & Mitchell 1993; Lundgren 2002; Gustavson 2004; Bolmsvik & Lundgren 2006; Vázquez-Herrero et al. 2013). These values are given in Table 4.2 and Table 4.3 for three-wire and seven-wire strands respectively.

Table 4.2 Three-wire strands parameters

Type of strand	Smooth	Indented
S_1	0.5	1.0
S_2	0.5	3.5
S_3	5.0	5.0
τ	$\tau_2 = 0.35\tau_{\max}$	$\tau_3 = 0.65\tau_{\max}$

Table 4.3 Seven-wire strands parameters

Type of strand	Smooth	Indented
S_1	0.25	1.0
S_2	0.5	3.5
S_3	3.5	6.0
S_4	8.0	-
τ	$\tau_2 = 0.75\tau_{\max}$ $\tau_4 = 0.35\tau_{\max}$	$\tau_3 = 0.35\tau_{\max}$

4.3 Effect of elevated temperatures on the bond strength

Exposing concrete structures to high temperatures leads to significant losses in mechanical and physical properties of concrete and strand, as well as the bond characteristics between them, as mentioned in Chapter 3. In this research the effect of high temperatures on the bond characteristics is considered by taking into account the degradation of concrete properties at elevated temperatures. As discussed in Chapter 3, the concrete properties at ambient temperature specified in Eurocode 2 EN 1992-1-1 (CEN 2004) are used. The compressive strength $f_{ck,T}$ and the modulus of elasticity of concrete $E_{c,T}$ at elevated temperatures are calculated based on Eurocode 2 EN 1992-1-2 (CEN 2004). The degradation of the tensile strength for concrete at elevated temperatures $f_{ct,T}$ proposed by Aslani and Bastami (2011) is adopted in this study. That is:

$$f_{ct,T} = f_{ct} \begin{bmatrix} 1.02 - 0.00098 \times T & 20 < T \leq 300^\circ\text{C} \\ 0.965 - 0.0001 \times T - 9 \times 10^{-7} T^2 - 3 \times 10^{-9} T^3 + 3.2 \times 10^{-12} T^4 & 300 < T \leq 900^\circ\text{C} \\ 0.0 & T > 900^\circ\text{C} \end{bmatrix} \quad (4.27)$$

where, f_{ct} is the concrete tensile strength at ambient temperature and T is the concrete temperature. The effect of elevated temperatures on the coefficient of friction between the strand and concrete and the cohesion was mentioned before. By considering the degradation of concrete properties at elevated temperatures, the bond stress τ and maximum bond stress τ_{\max} become temperature dependent in this model.

The procedure for calculating the maximum bond stress of prestressed concrete τ_{\max} can be summarised as follow:

- (1) Define the parameters for the concrete and strands (compressive strength and modulus of elasticity of the concrete; yield stress, Young's modulus, diameter, number of wires and surface condition of the strand), as well as, the initial force or the pretensioned stress effect on the strand.
- (2) Based on the strand's conditions, the values of C and μ can be defined from Table 4.1.
- (3) Calculate the material properties at elevated temperatures.
- (4) Calculate the radial strain of the concrete surround the strand ε_c (Equation (4.15)) and the radial stress σ_n (resulted from the effect of Poisson's ratio) from (Equation (4.9)).
- (5) Calculate the shear strength of the concrete keys v_c (Equation (4.8)).
- (6) Calculate the shear area of the cracked surface A_{sh} (Equation (4.2)).
- (7) Calculate the shear force capacity of the concrete keys V_c (Equation (4.1)).
- (8) Calculate the force along the length of the wires $F=F_1+F_2$ (Equation (4.3), Equation (4.4) and Equation (4.5)) respectively.
- (9) Calculate the maximum bond force T_b (Equation (4.6)) and the contact area A_b between the strand and concrete (Equation (4.26)).
- (10) Finally the maximum bond stress τ_{\max} can be determined from (Equation (4.25)).

4.4 Incorporating the bond stress-slip model into Vulcan software

The bond-slip model proposed above has been incorporated into VULCAN software in order to model prestressed concrete structures in fire. In recent years, a two-node bond-link element has been developed to simulate the effect of bond-slip between the reinforcing steel and concrete at elevated temperatures (Huang 2010). The framework of the bond-link element discussed in Section 3.3 has been used to incorporate the current model into VULCAN software for simulating the bond characteristic between the strand and concrete in PC members. For the bond element, the bonding force $F_{x,T}$ between the concrete and strand is obtained from Equation (3.23). In the local co-ordinate, referenced to the strand element, the nodal force increment vector, $\Delta \mathbf{F}$ of the element can be related to its nodal displacement increment vector $\Delta \mathbf{u}$ as given in Equation (3.24).

For the strand, apart from the slip along the longitudinal axis direction (x -direction) (see Figure 3.8) between concrete and strand, the concrete prevents the relative movement of the strand in other directions, which are perpendicular to the longitudinal direction of the strand. It is therefore reasonable to assume that common nodes of the concrete and strand elements have identical rotations and movements in y and z directions. Hence, in this model k_2, k_3, k_4, k_5, k_6 in Equation (3.24) are assumed to have infinite magnitude such as (10^{15}).

Coefficient k_1 is the tangent stiffness coefficients of the bond-link element related to the axis of the strand element, which can be determined from the force-slip relationship as:

$$k_1 = \frac{dF_{x,T}}{ds} = A \frac{d\tau}{ds} \quad (4.28)$$

The coefficient k_1 for three-wire smooth and indented strands and seven-wire indented strands can be obtained from derivatives of Equations (4.16) to (4.19) to form the tangent stiffness coefficients as follow:

$$k_1 = \frac{A\tau_{\max}}{s_1} \left(\frac{s}{s_1} \right)^{\alpha-1} \quad \text{for } 0 \leq s \leq s_1 \quad (4.29)$$

$$k_1 = 0.0 \quad \text{for } s_1 < s \leq s_2 \quad (4.30)$$

$$k_1 = -\left(\frac{\tau_{\max} - \tau_3}{s_3 - s_2} \right) \quad \text{for } s_2 < s \leq s_3 \quad (4.31)$$

$$k_1 = 0.0 \quad \text{for } s_3 < s \quad (4.32)$$

For seven-wire smooth strand, the coefficient k_1 can be calculated using the derivatives of Equations (4.20) to (4.24) to find the tangent stiffness coefficients as follow:

$$k_1 = \frac{A\tau_{\max}}{s_1} \left(\frac{s}{s_1} \right)^{\alpha-1} \quad \text{for } 0 \leq s \leq s_1 \quad (4.33)$$

$$k_1 = -\left(\frac{\tau_{\max} - \tau_2}{s_2 - s_1} \right) \quad \text{for } s_1 < s \leq s_2 \quad (4.34)$$

$$k_1 = \left(\frac{\tau_{\max} - \tau_2}{s_3 - s_2} \right) \quad \text{for } s_2 < s \leq s_3 \quad (4.35)$$

$$k_1 = -\left(\frac{\tau_{\max} - \tau_4}{s_4 - s_3} \right) \quad \text{for } s_3 < s \leq s_4 \quad (4.36)$$

$$k_1 = 0.0 \quad \text{for } s_4 < s \quad (4.37)$$

During the incremental analysis, the increment of bond force ΔF_x can be related to the increment of slip Δs multiplied by the tangent stiffness as:

$$\Delta F_{x,T} = k_1 \Delta s \quad (4.38)$$

In which,

$$\Delta s = \Delta u_1 - \Delta u_2 \quad (4.39)$$

Where, Δu_1 and Δu_2 are the increments of displacement in the direction of $\Delta F_{x,T}$ at the node 1 and node 2 of the bond-link element respectively (see Figure 3.8 (b) in Chapter 3).

The bond-link element used in this study permits modelling of full, partial and zero interaction at the interface between concrete and strands. In this non-linear incremental analysis procedure, the total slip of a bond element at any load level is calculated from the incremental slips of that bond element. The bond force corresponding to total slip is calculated from the incremental forces determined by Equation (4.38), and the tangent stiffness of the bond element is calculated using Equations (4.28) to (4.37).

As shown in Figure 3.8 (a) in Chapter 3, the prestressed concrete member is represented as an assembly of plain concrete beam elements, strands elements and bond-link elements in the current model. Both plain concrete elements and strand elements are modelled using a 3-node beam element, in which the thermal expansions of concrete and steel at elevated temperatures are considered. Hence their effect on the bond-link element developed in this project is taken into account. This effect related to the direction of longitudinal axis of the strand. However, the thermal expansions of both concrete and steel in radial direction perpendicular to the strand axis have not been considered in the current model. This is because the strain compatibility at the interface between the strand and surrounding concrete is not always maintained when the pull-out load is applied, especially when the pull-out load reaches to the capacity of the bond.

The plain concrete beam is modelled using the 3-node beam elements and the slab is represented as 9-node slab elements. The cross-section of the beam elements are subdivided into segments and the slab is divided into layers to consider the temperature variation within the cross-section for each segment or layer during the thermal analysis.

At ambient temperature, PC members incur initial camber due to prestressing. This initial prestressing effect is modelled in the current model by applying an initial tension strain on the strand's elements which can be calculated from the initial stress (usually about 70% of the strand ultimate stress) divided by the strand's young modulus.

4.5 Validations

In this section there are two sub-sections. In the first sub-section the bond stress-slip curves at both ambient and elevated temperatures are validated against the test data. The second sub-section of the validation is to consider the effect of bond-slip on the structural response of the prestressed concrete members at ambient and under fire conditions. The predictions of the current model are compared with previous experimental data.

In the current proposed model, the temperature variation within the concrete rings around the strand is considered. However, in the following validation section, it is assumed that the temperatures of the concrete rings around the strands are uniform and equal to the temperature of the strand for simplicity. This is a reasonable assumption for all pull-out tests.

4.5.1 Bond stress–slip curve at ambient and elevated temperatures

In this section, different cases of bond-slip curves have been adopted for validations. Three parts are conducted in order to validate the accuracy and capability of the proposed model. The first part is to examine the bond model within the transfer length and flexural length using push-in and pull-out tests, respectively. The second part is to verify the model in case of seven-wire strands is used by considering the smooth or indented surface conditions of the strand. The third part is to validate the model using three wire-strands and considering the smooth or indented surfaces of the strand.

4.5.1.1 Transfer and flexural bonds at ambient temperature

Abrishami and Mitchell (1993) conducted series of tests to study the bond stress-slip between seven-wire smooth strands and concrete. The tested material properties are as follow: cylinder concrete compressive strength was 25 MPa at the time of test, the prestressing steel were seven-wire strands with nominal diameters of 9.5, 13 and 16 mm. The strands with 9.5 and 13 mm diameter had an ultimate tensile strength of 1860 MPa and the 16 mm diameter strand had an ultimate tensile strength of 1760 MPa. Table 4.4 gives details of the specimens tested by push-in bond, as well as a comparison between the measured bond from the test and predicted bond results

from the model. Table 4.5 shows the details of the specimens tested by pull-out bond, as well as a comparison of the measured and predicted bond strengths. It can be seen from Tables 4.4 and 4.5 that the predicted results from the proposed model have good agreement in comparison with the test results in both cases (pull-out and push-in bond).

Table 4.4 Comparison between the predicted and measured bond stresses for push-in tests

Specimen	d_s mm	P_1 kN	P_2 kN	$\Delta P = P_1 - P_2$ kN	Bond strength MPa (test)	Bond strength MPa (predicted)
9.5-A-2	9.5	69	6	63.0	6.7	6.1
13-A-2	13	123	32	92.0	6.9	6.2
16-A-2	16	160	41	119.0	7.1	6.35

Table 4.5 Comparison between the predicted and measured bond stresses for pull-out tests

specimen	d_s mm	Bond strength MPa (test)	Bond strength MPa (predicted)
9.5-B-1	9.5	4.2	3.8
13-B-1	13	3.6	3.6
16-B-2	16	3.7	3.65

4.5.1.2 Bond stress–slip for seven-wire smooth and indented strands at ambient temperature

Vázquez-Herrero et al. (2013) carried out a test on the pull-out bond stress-slip between the smooth surface strand and concrete. The specimens in this test consist of seven-wire smooth strand and cylinder specimens made of normal concrete with dimensions of 150 mm diameter \times 300 mm length. The tested material properties for the concrete were: the compressive strength was 49 MPa and the tensile strength was 2.9 MPa. The properties of seven-wire smooth strand were: the nominal diameter was 15.2 mm, average elastic modulus was 197.4 GPa, breaking strength was 260 kN and the cross section area was 142 mm². Figure 4.4 shows the predicted bond stress-slip curve together with the test results. It is evident from the figure that good

agreement has been achieved between the predicted results from the model and test results.

Another pull-out test has been adopted in this section to validate the bond model using seven-wire indented strands. This test was conducted by Lundgren (2002) at Chalmers University of Technology. The diameter of the strand was 12.9 mm. The tested concrete compressive strength was 63 MPa and Young's modulus was 36 GPa. Figure 4.5 shows the comparison between the predicted and tested pull-out load versus bond slip curves. It can be seen from the figure that the model gives a good prediction in comparison with test results.

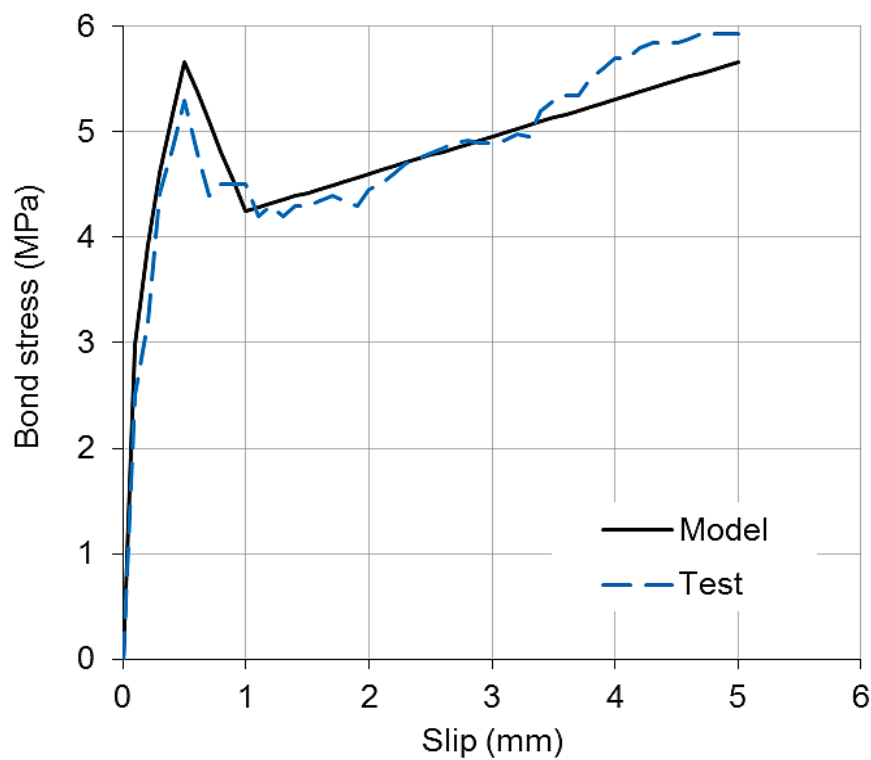


Figure 4.4 Comparison of predicted and tested bond stress–slip curves for the seven-wire smooth strand at ambient temperature (Vázquez-Herrero et al. 2013)

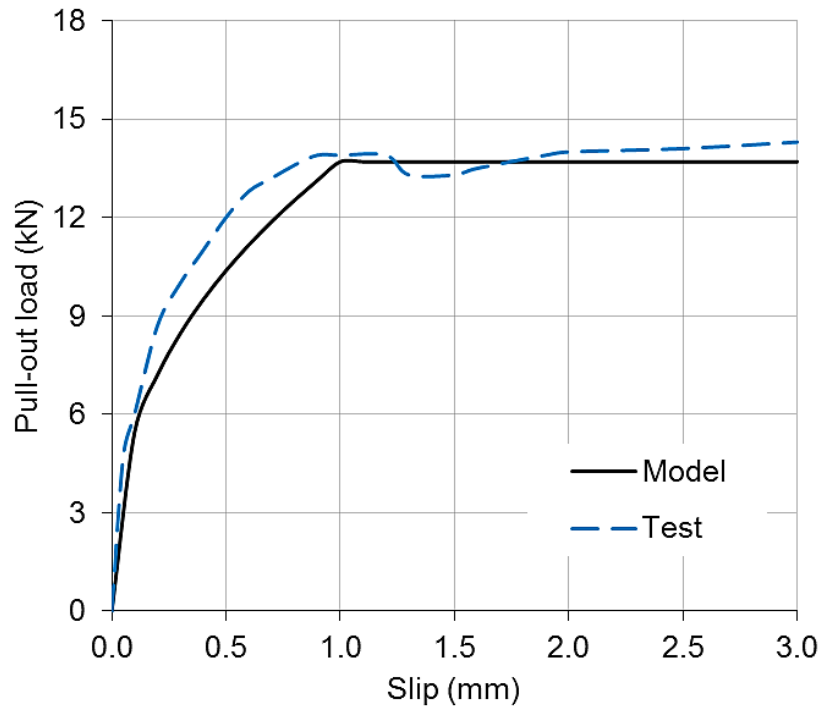


Figure 4.5 Comparison of predicted and tested load–slip curves for the pull-out seven-wire indented strands at ambient temperature (Lundgren 2002)

4.5.1.3 Bond stress–slip for three-wire indented and smooth strands at ambient temperature

Gustavson (2004) studied the bond characteristics of three-wire smooth and indented strands. In this study two types of bond tests were conducted, which were pull-out and push-in tests. For the push-in test, the indented strand was EU 138/6 with nominal diameter of 6.5 mm. The strand was prestressed with a force of 28 kN, corresponding to a prestress of 1320 MPa. The tested concrete compressive strength was 25 MPa. For the pull-out test, a smooth strand with 6.5 mm diameter and concrete compressive strength of 55 MPa were used in this test. Figure 4.6 shows the comparison of predicted and tested load–slip curves for the push-in test. Figure 4.7 illustrates the comparison of predicted and tested load-slip curves for the pull-out tests. It is clear from the figures that reasonable agreements can be obtained from the proposed model in comparison with test data in both cases.

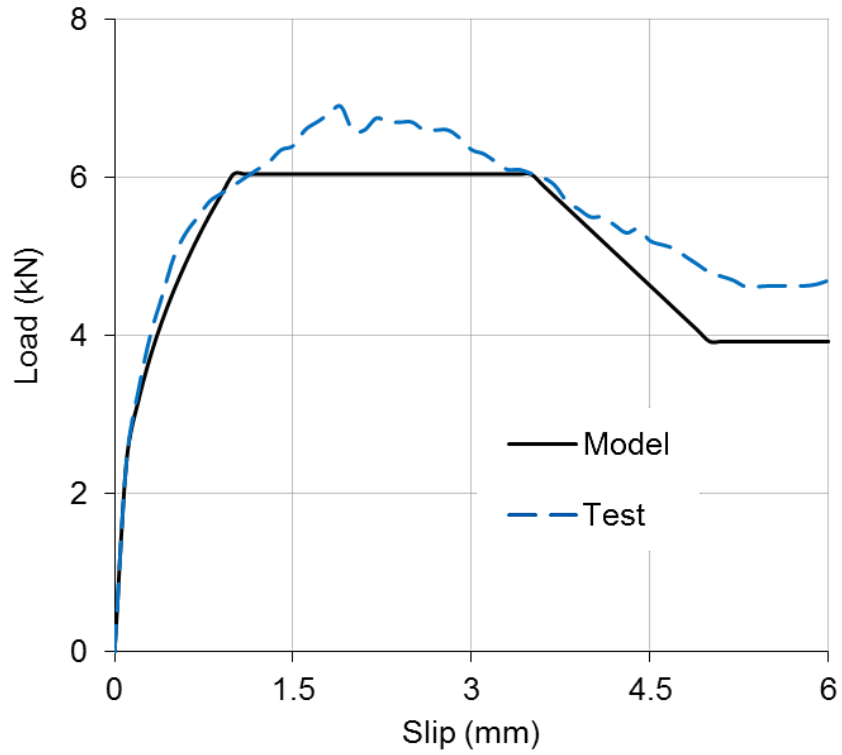


Figure 4.6 Comparison of predicted and tested load-slip curves for the three-wire push-in test at ambient temperature (Gustavson 2004)

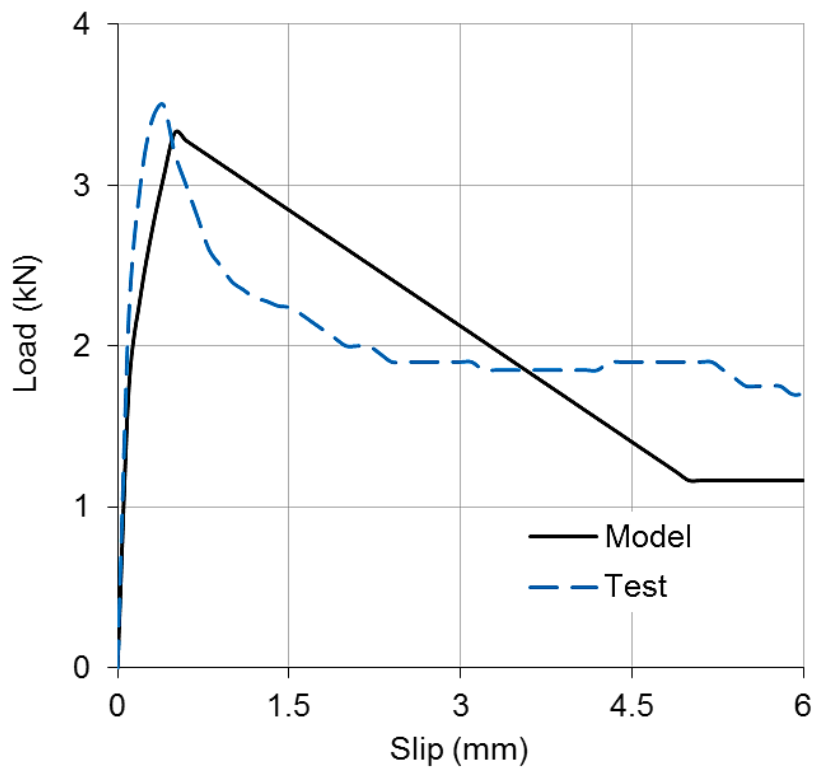
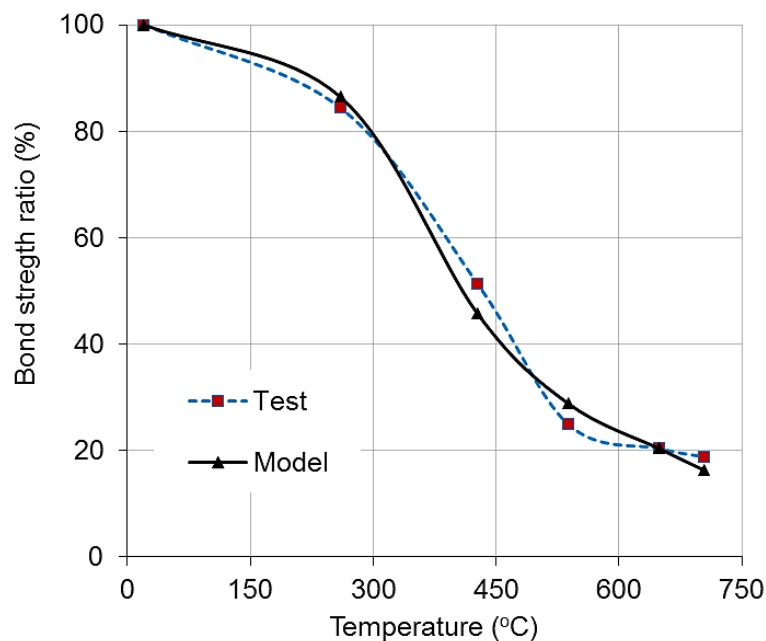


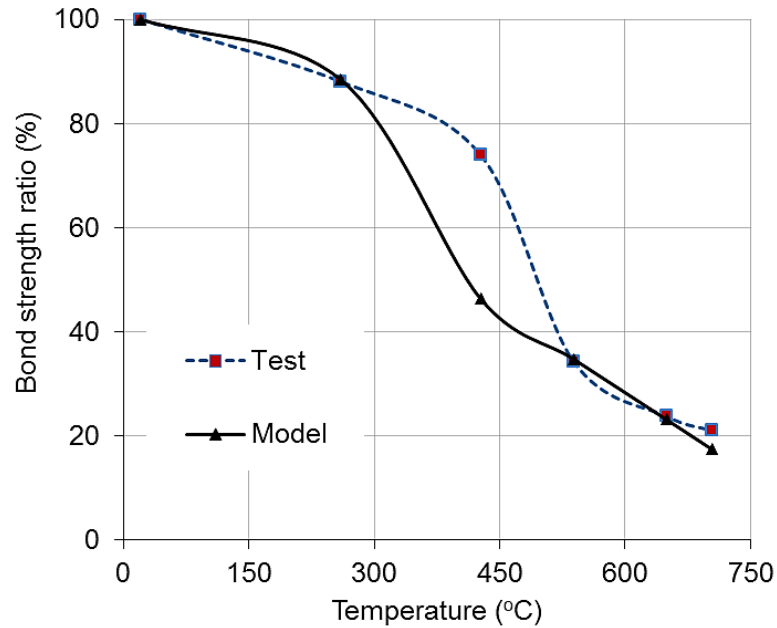
Figure 4.7 Comparison of predicted and tested load-slip curves for the three-wire pull-out test at ambient temperature (Gustavson 2004)

4.5.1.4 Bond stress–slip curves at elevated temperatures

Moore (2008) studied the bond-slip characteristics of strands at elevated temperatures. Seven-wire low relaxation strand with grade 270 was used in this investigation. The diameter of strand was 12.7 mm. Two types of concrete with different compressive strengths of 77.4 MPa and 98.8 MPa were used in the test. The dimensions of pull-out specimens were 152.4 x 152.4 x 101.6 mm with embedded length of 101.6 mm. The specimens were heated with a heating rate of 4.4 °C/min until the designated temperatures were reached, then held for 60 minutes in the furnace to obtain a uniform temperature for the specimens, and then the specimens were left outside the furnace for cooling. Six levels of temperatures were adopted in this study: 20 °C, 260 °C, 427 °C, 538 °C, 649 °C and 704 °C. In this validation, the degradation of the bond strength due to high temperatures was used for comparison between the proposed model and test results by taking ratio of the bond strength at elevated temperatures over the bond strength at ambient temperature. Figure 4.8 (a) and Figure 4.8 (b) show the degradation of bond strength versus temperatures using two values of concrete strength, and compare the predicted results from the proposed model with the teste results. It is clear from the figures that good results can be achieved by using the proposed model to predict the bond stress-slip for prestressed concrete members at elevated temperatures, especially when low concrete compressive strength is used.



(a)



(b)

Figure 4.8 Comparison of predicted and tested bond strength degradation with different concrete compressive strengths at elevated temperatures (Moore 2008): (a) 77.4 MPa; (b) 98.8 MPa.

4.5.2 Structural behaviour of prestressed concrete members

Two tests of simply supported PC beams and two tests of simply supported PC slabs at both ambient and elevated temperatures were used to validate the robustness of developed model in this section. In all cases of validation, both material and geometric non-linearity were considered. The predicted results from the VULCAN program, after incorporating the bond-slip model with it, have been compared with the experimental results to demonstrate the accuracy of the developed model.

4.5.2.1 Modelling of simply supported PC beams at ambient temperature

Two different experimental studies on simply supported PC beams have been adopted to validate the capability of the proposed model to simulate the bond-slip between the concrete and strands for prestressed concrete beams at ambient temperature.

The first experimental study was carried out by Cowen and VanHorn (1967). A prestressed concrete simply supported T-beam Z-1 was used in this study. The details of the tested beam are shown in Figure 4.9. The strands used in this study

were seven-wire 270K strands with diameter of 12.7 mm. These strands were located in the three layers within the cross-section of the beam, as shown in Figure 4.9.

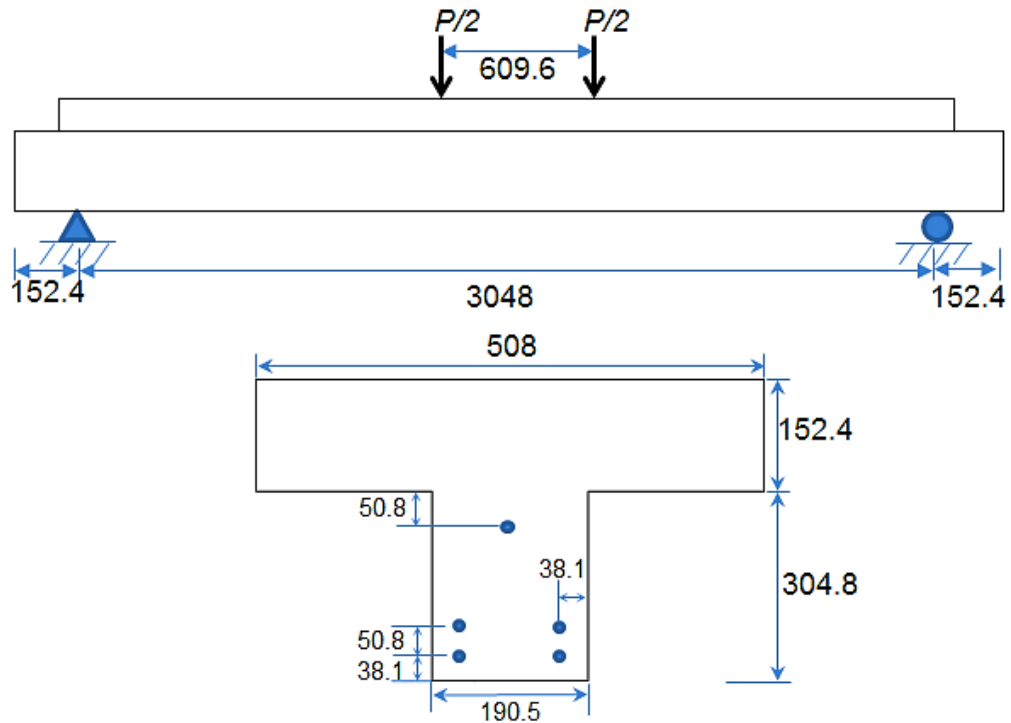


Figure 4.9 Details of tested T-beam Z-1 (Cowen & VanHorn 1967) (all dimensions in mm)

The strands were initially tensioned to a stress level of 70% of the specified ultimate stress (which was 1303 MPa) and the average effective prestress force at the time of the test was 128.5 kN. The concrete compressive strength at the time of the test was 42.4 MPa and the Young's modulus was 28.9 GPa. By applying the symmetry only half of the T-beam was modeled. In order to model the PC beam; 5 three-node plain concrete elements, 25 three-node strands elements and 55 bond-link elements were employed. By taking the value of $50 d_s$, the transfer length was 635 mm from the end of the beam. Therefore, the first 5 bond-link elements were modelled as transfer bond and the rest of 6 bond-link elements were represented as flexural bond for each strand, in which the total bond-link elements for five strands involved 25 transfer and 30 flexural bond-link elements. The initial prestressed force was 128.5 kN which can be applied as initial strain of 0.0055 on the strand's elements during the structural analysis. The predicted loads versus mid-span deflection curves are compared against the tested results as shown in Figure 4.10. It is clear from the figure that there

is a good agreement between the results from modelling the PC beam using the VULCAN program with bond-slip model in comparison with the results from the test data.

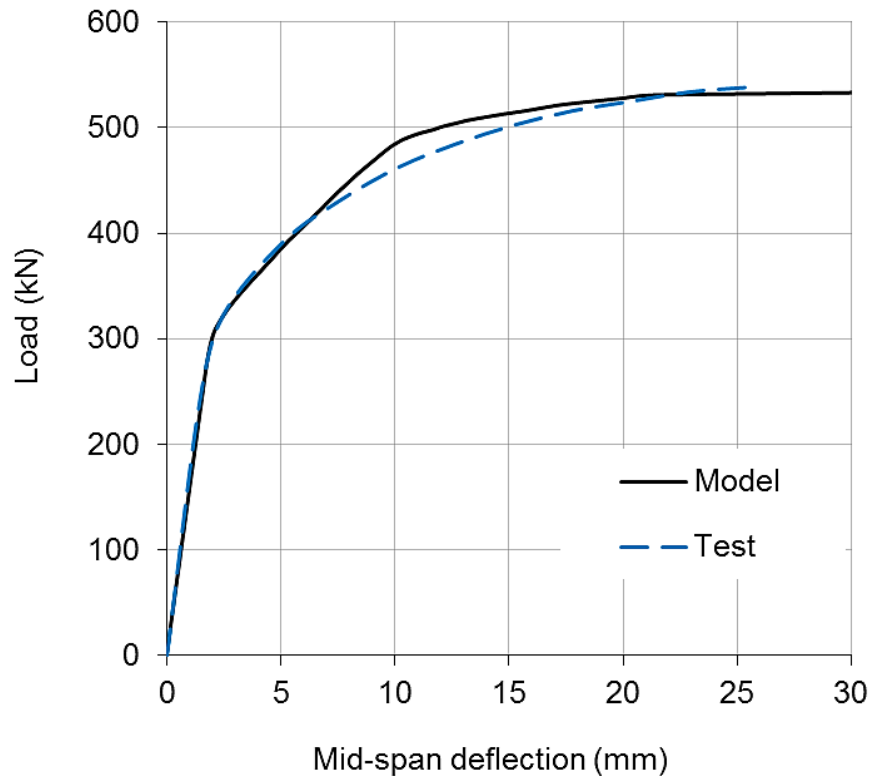


Figure 4.10 Comparison of the predicted and tested load versus mid-span deflections curves for T-beam Z-1 (Cowen & VanHorn 1967)

The second test was a simply supported T-girder (T-6-1.5h-A) of 8534.4 mm long. This test was done by Tadros and Morcous (2011) in America Transportation Centre. The materials used in this test were: Grade 270 low relaxation prestressing seven-wire strands with diameter of 17.78 mm, six strands were located in two rows with 50.8 mm concrete cover and strand spacing as shown in Figure 4.11. Concrete compressive strength at the time of the test was 62.0 MPa. Only half of the girder was modelled due to symmetry. 5 three-node plain concrete elements, 30 three-node strands elements and 66 bond-link elements were employed for modelling the girder. The transfer length was 889 mm from the end of the beam, thus 36 bond-link elements were modelled as transfer bond and the rest of 30 bond-link elements were represented the flexural bond. The initial prestress strain of 0.003 was applied on the strand's elements. Figure 4.12 shows the loads versus mid-span deflection curves for the test results from the experiment and compare that with the predicted results from

VULCAN program. Again, a good agreement can be achieved from modelling the beam with bond-slip in comparison with the test results.

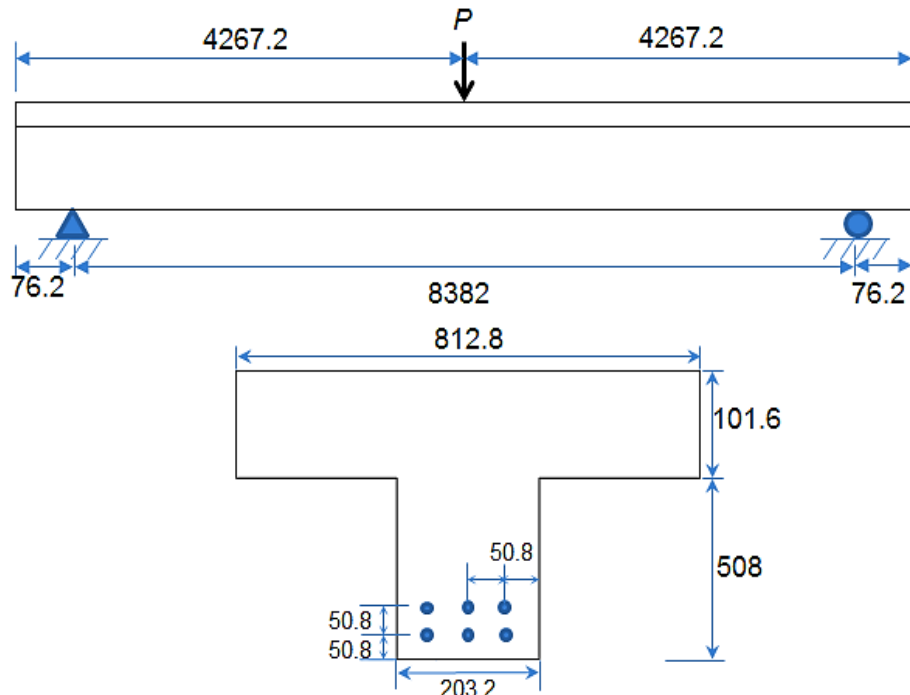


Figure 4.11 Details of the tested T-girder (T-6-1.5h-A) (Tadros & Morcous 2011) (all dimensions in mm)

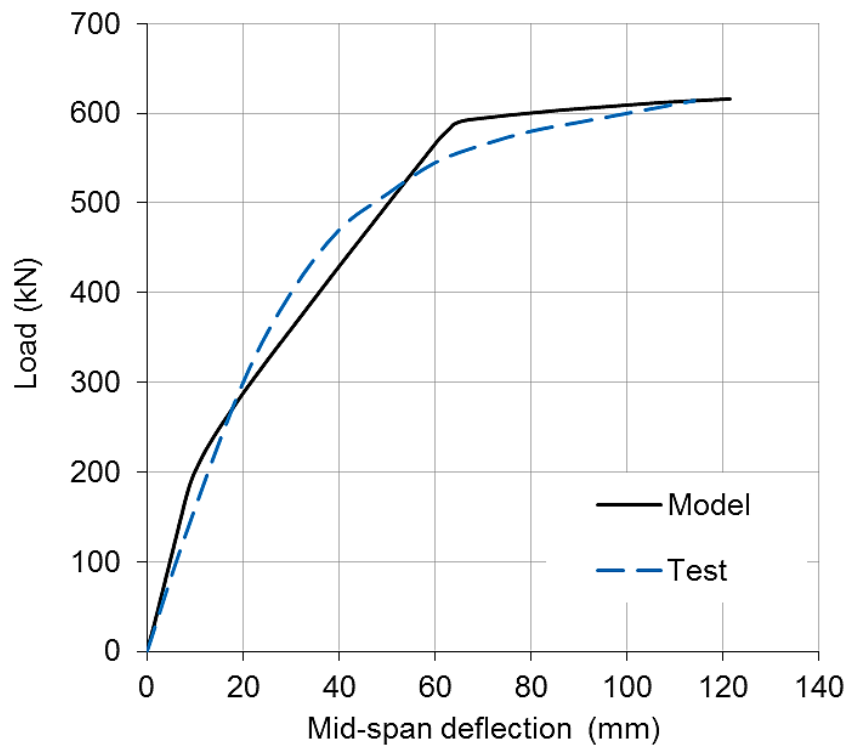


Figure 4.12 Comparison of the predicted and tested load versus mid-span deflections curves for the tested T-girder (Tadros & Morcous 2011)

4.5.2.2 Modelling fire tests of simply supported PC slabs

Two slabs have been adopted to validate the robustness and accuracy of the current model at elevated temperatures. The first slab was simply supported PC slab TB3 tested by Bailey and Ellobody (2009). The length of the slab was 4.0 m with 1.6 m width and thickness of 16 cm. Figure 4.13 illustrates the details of TB3 slab. The tested slab was subjected to the standard time-temperature curve specified in BS EN1991-1-2 (CEN 2002) by using gas furnace. The slab was heated over a middle length of 3.2 m out of its 4.0 m as shown in Figure 4.13. The tested concrete compressive strength at the time of test was 36.6 MPa. The strand was 15.7 mm seven-wire smooth strand of grad 270 with yield stress of 1675 MPa. These tested material properties were used as an input data for the modelling. Due to the symmetry of the slab, only half of the slab was modelled.

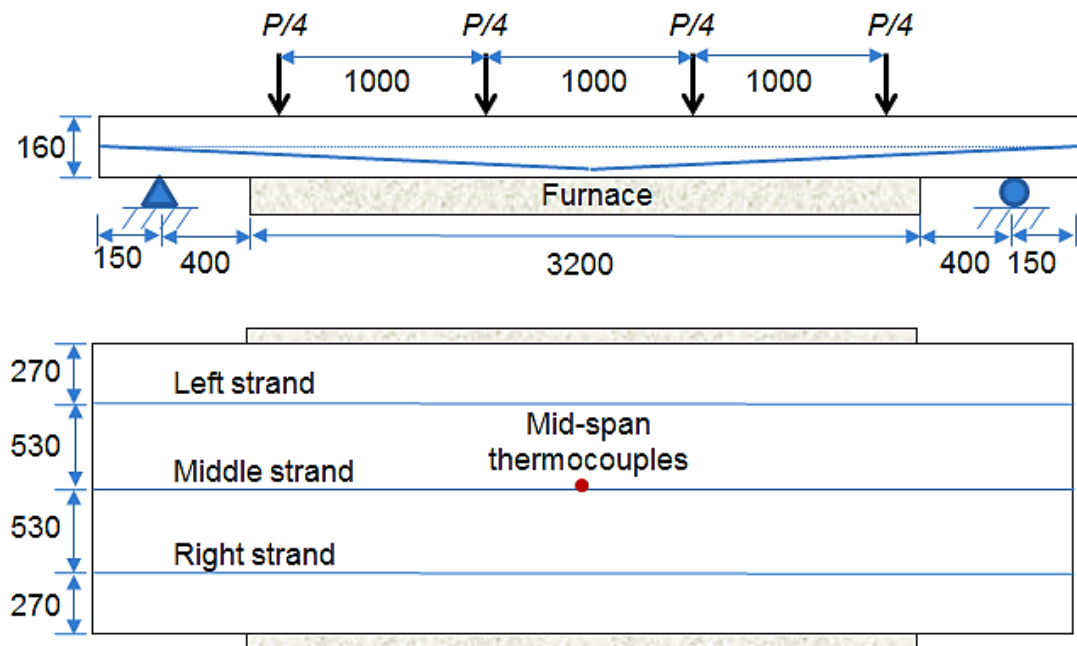


Figure 4.13 Details of PC Slab TB3 (Bailey & Ellobody 2009) (all dimensions in mm)

Two steps were followed for modelling the tested slab. In the first step, thermal analysis was performed by dividing the cross section of the slab into segments in order to predict the temperatures distribution within the cross-section of the slab. During the test, there was no evidence of concrete spalling on the heated surface; therefore, the spalling has not been considered in the thermal and structural analysis.

The predicted and tested temperature histories throughout the cross section of the slab at mid-span are shown in Figure 4.14; in which T represents the strands temperatures, HS refers to the hot bottom surface, MS for mid-height of the slab and CS represents the cold top surface of the slab. The predicted temperature histories of the strands and concretes from the thermal analysis were used as temperature input data for the structural analysis.

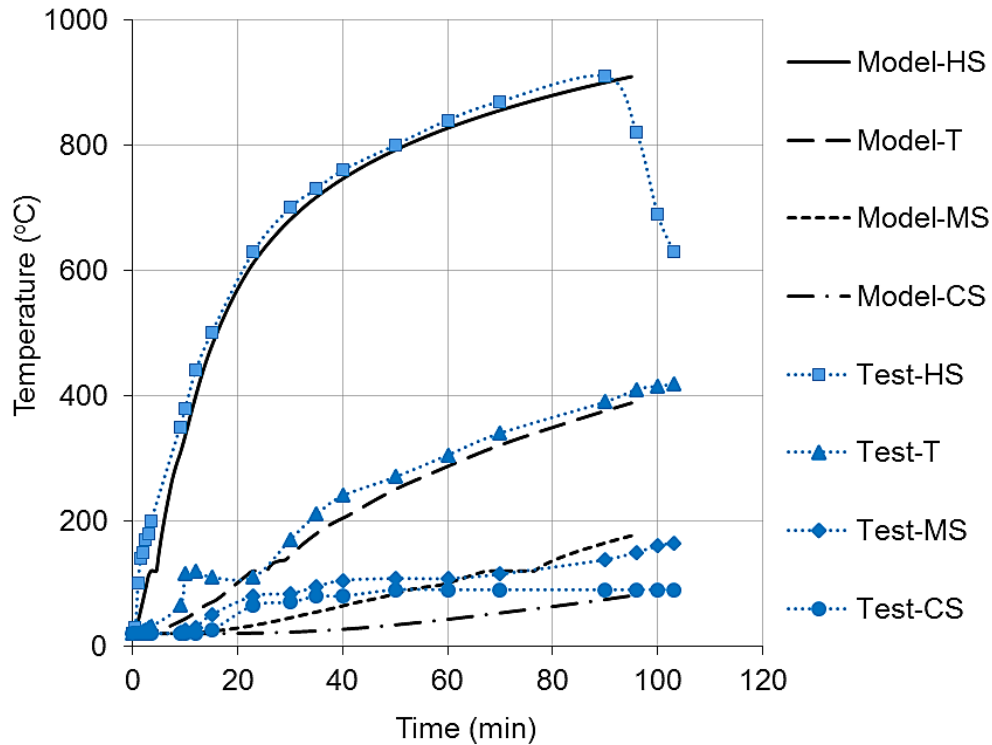


Figure 4.14 Comparison between the predicted and tested temperature histories (Bailey & Ellobody 2009)

Structural analysis was performed for the slab in the second step. The slab TB3 was modelled using 5 three-node plain concrete elements, 15 three-node strand elements and 33 bond-link elements. The transfer length of $50 d_s$ was 785 mm from the end of the slab, hence 9 bond-link elements were modelled as transfer bond and the rest of 24 bond-link elements were represented as flexural bond. In the structural modelling the reference axis was assumed to coincide with the central axis of plain concrete elements. In order to take into account the effect of strands curvature within the prestress system, the real positions of the strand elements within the cross-section of the slab and along the slab length were considered by offset the elements nodes based on the reference axis. The average applied design prestress force in the three

strands after pre-tension was 169 kN. This force can be modelled as an initial strain of 0.0045 to the strands elements to simulate the prestress on the strands. Same segmentation of the cross section of the slab that used in the thermal analysis was adopted for the structural analysis. The total vertical load of 41.6 kN (which represents 60% of the load capacity) was applied to the slab. This static load was kept constant during fire test.

Figure 4.15 shows the comparison of the predicted and measured mid-span deflections of the Slab TB3. The predicted and tested longitudinal expansions of the slab TB3 are shown in Figure 4.16. It is evident that the predictions using the current model agreed reasonably well with the test results.

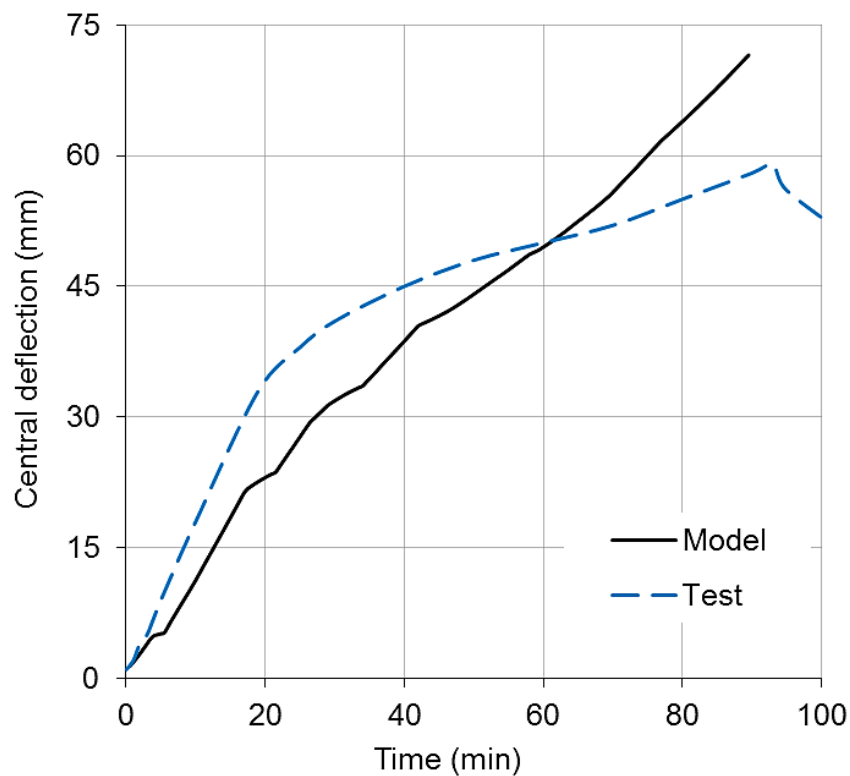


Figure 4.15 Comparison of predicted and measured mid-span deflections of Slab TB3 (Bailey & Ellobody 2009)

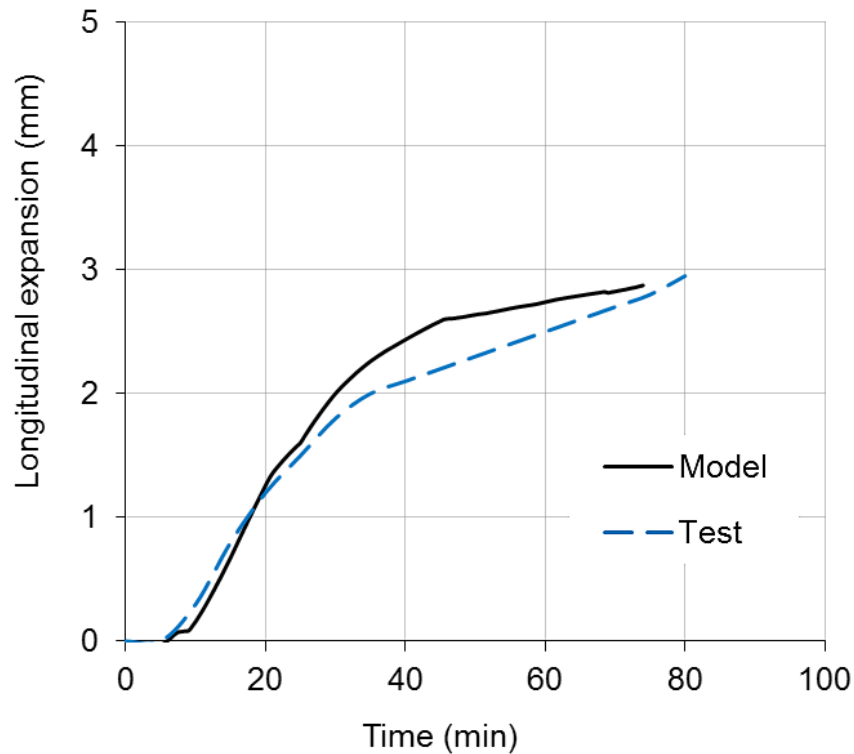


Figure 4.16 Comparison of predicted and tested longitudinal expansion for Slab TB3 (Bailey & Ellobody 2009)

The second fire test was conducted by Zheng and Hou (2008). One way simply supported prestressed concrete slab PSS-1 was selected for this validation. As shown in Figure 4.17, the dimensions of the slab were 5.3 m x 0.6 m x 0.09 m. The tested slab was subjected to the standard IOS 834 fire curve. However, the average measured furnace temperatures were lower than ISO 834 fire curve as shown in Figure 4.18. This measured time-temperature curve was used for the thermal analysis to predict the temperature distribution histories within the cross-section of the slab.

During the test, there were very little concretes spalled on the heated surface. Therefore, the spalling has not been considered in the thermal analysis for this test. In the thermal analysis, the cross-section of the slab was divided into 280 segments in order to consider the temperature history for each segment within the cross-section of the slab. Figure 4.19 shows the predicted and tested temperature histories at the position D1 (exposure surface to the fire) and position D2 (27 mm away from the exposure surface to the fire) within the cross-section of the slab. The predicted temperature histories for each segment within the cross-section of the slab were used as the input temperatures to perform the structural analysis.

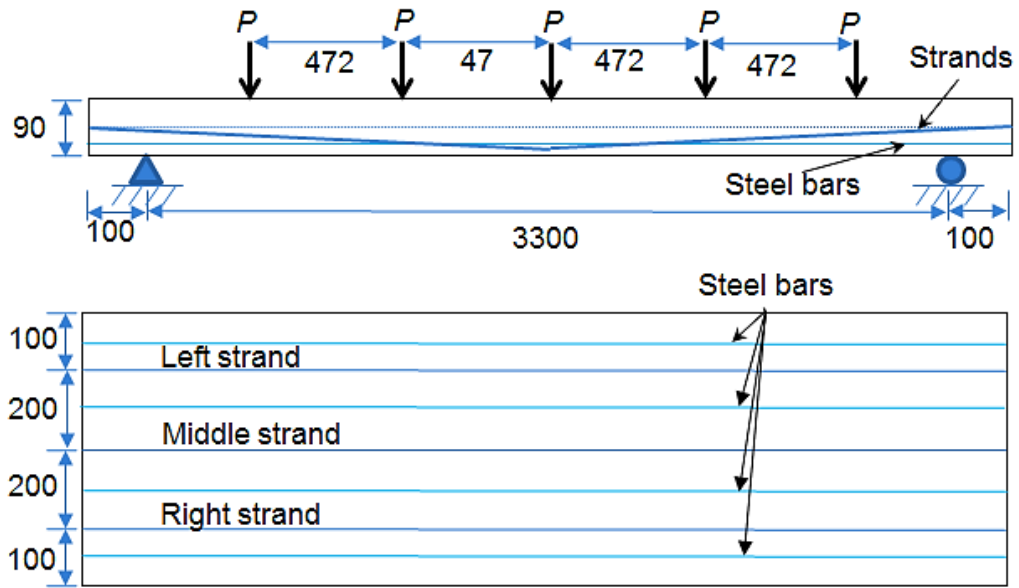


Figure 4.17 Details of PC Slab PSS-1 (Zheng & Hou 2008)

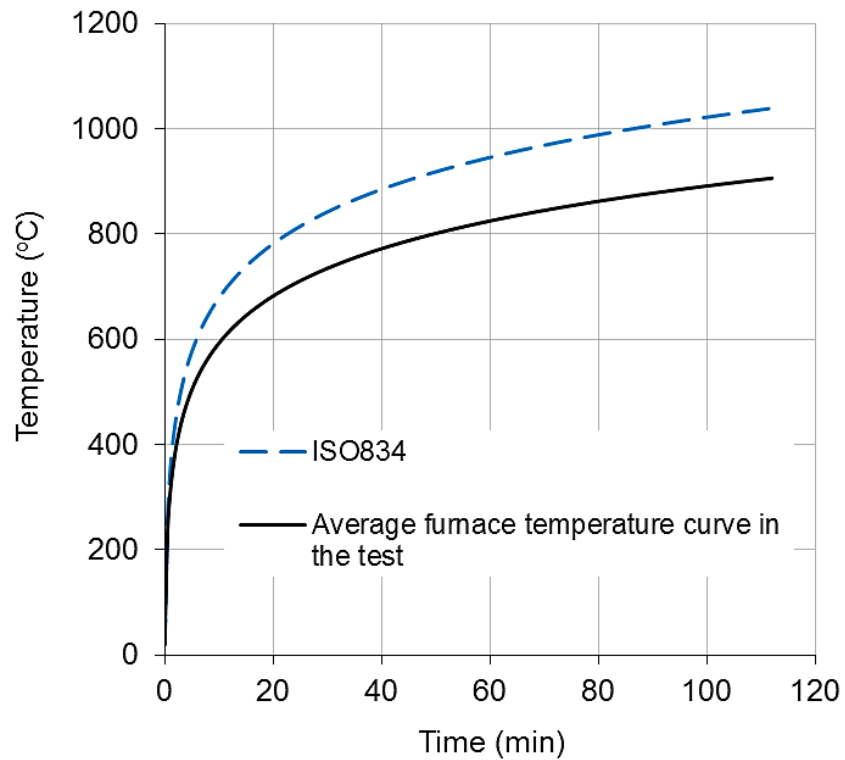


Figure 4.18 Heating curve used in the analysis (Zheng & Hou 2008)

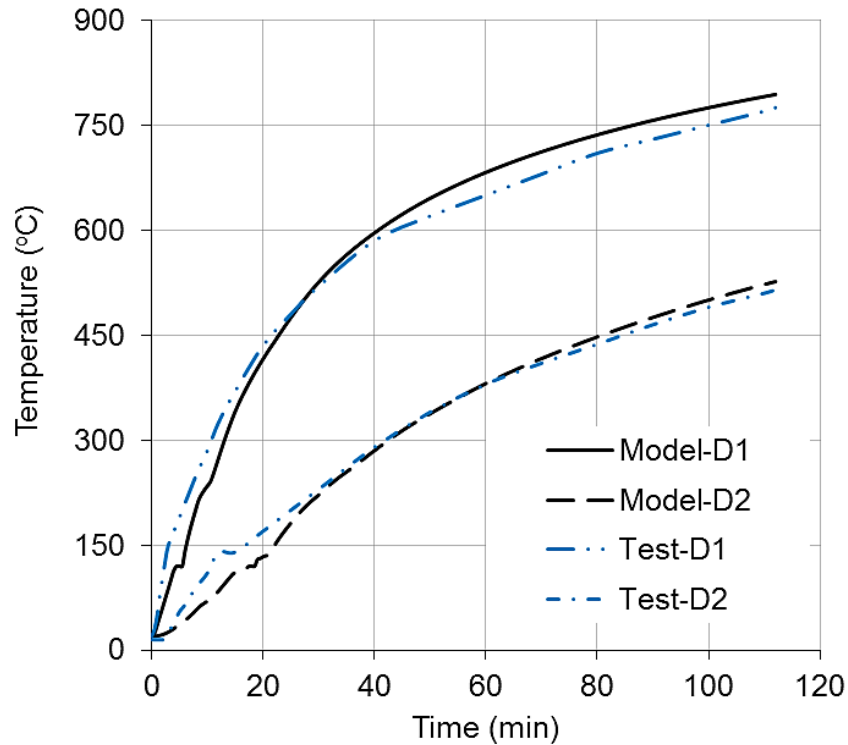


Figure 4.19 The predicted and tested temperature histories for Slab PSS-1 (Zheng & Hou 2008)

The tested concrete compressive strength at the time of test was 32.0 MPa, the strand was 5.0 mm seven-wire smooth strand with yield strength of 1498 MPa. The additional reinforcing steel bars were 6.5 mm with yield strength of 328 MPa, and 8.0 mm with yield strength of 320 MPa. Those tested material were used as the input data for modelling the slab.

For structural analysis, the slab PSS-1 was modelled using 8 three-node plain concrete elements, 24 three-node strands elements and 51 bond-link elements. The transfer length was 250 mm at both ends of the slab; hence 18 bond-link elements were modelled as transfer bond at each end of the slab and the rest of 33 bond-link elements were represented as flexural bond within the middle of the slab. Again the reference axis was assumed to coincide with the central axis of the plain concrete elements. The real positions of the strand elements within the cross-section of the slab and along the slab length were considered in the modelling to simulate the strand's curvature by offset the strands elements based on the reference axis. The prestress force in the strand for pre-tension was 70.7 kN. This force was applied as initial strain of 0.0046 to the strands elements to simulate the prestress on the strands in the model. The segmentations of the cross sections for the plain concrete elements

were the same as the thermal analysis. The applied load was five concentrated load of 1.53 kN (including the self-weight of the slab), which represents 0.35 of the load capacity of the slab. This static load was kept constant during the fire test. Figure 4.20 shows the comparison between the predicted and measured mid-span deflections of the slab PSS-1. It is clear from the figure that the predictions results from VULCAN software (after incorporating the current model) agree well with the test results.

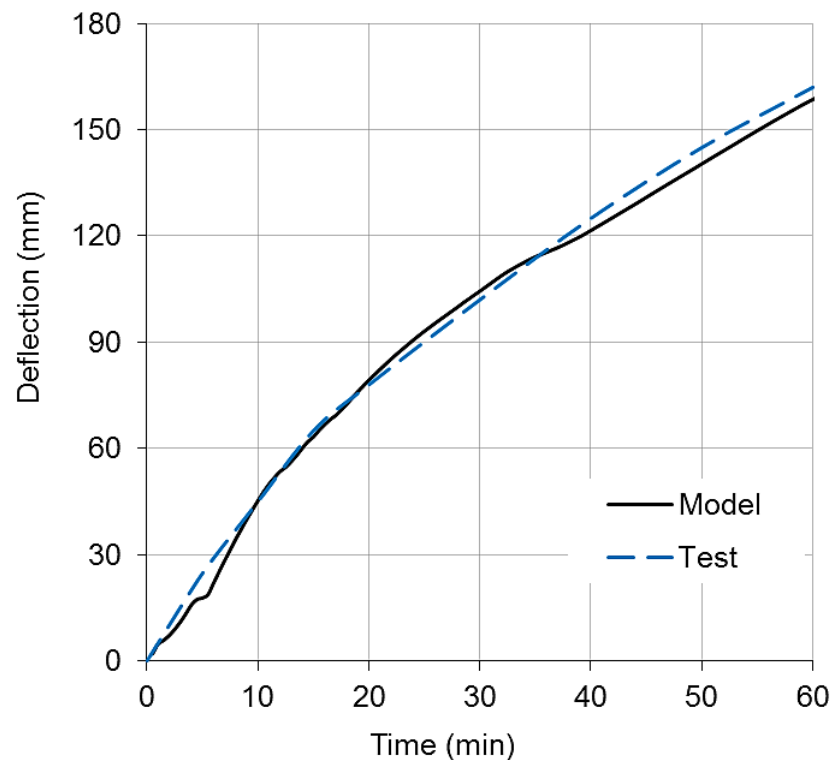


Figure 4.20 Comparison of predicted and measured mid-span deflections of Slab PSS-1 (Zheng & Hou 2008)

To summarise the validation in this section, two large scale PC beams at ambient temperature and two large scale PC slabs under fire conditions, which conducted by different researchers, were modelled to validate the model developed in this project. It is important to mention that the influence of bond stress-slip on PC structural members at ambient temperature is not significant due to high interaction between the concrete and strands. Hence, it is reasonable to assume the full interaction between concrete and steel strand for modelling PC members at ambient temperature. However, the effect of the bond at elevated temperatures is significant because of the degradation of bond stress due to high temperatures. As shown in

Figure 4.8, when the temperature is higher than 450°C, the bond strength reduces to 60% of the original strength at ambient temperature. Hence, for fire resistance design of PC structural member it is unconservative to assume fully bonded between concrete and steel strand as the bond can control the failure of PC members. Finally, It is evident from this study that the proposed bond-slip model can be used with reasonable accuracy for modelling the structural behaviour of PC members at both ambient and elevated temperatures.

4.6 Conclusions

In this chapter, a new analytical model has been developed to predict the bond stress-slip between strands and concrete for prestressed concrete members under fire conditions. The model is based on the mechanical interlocking between the prestressing steel strands and surrounding concrete as well as the effect of Poisson's ratio (Hoyer effect). The model takes into account the variation of the concrete properties and strands' geometries, as well as effect of the cohesion and friction between the strands and concrete. The degradation of the bond strength at elevated temperatures is related to the concrete material properties changed with temperature. The developed bond stress-slip model has been incorporated into the VULCAN software by using two-node bond-link element approach for analysing the structural behaviours of prestressed concrete structural members in fire. Series of validations have been conducted using the previous tested data generated by different researchers. Reasonable agreements have been achieved between the predicted results from the model in comparison with the tests results. The model presented in this chapter is able to predict the bond-slip characteristic between the concrete and strands for three-wire and seven-wire strands at both ambient and elevated temperatures. This model can be used to calculate the bond-slip for the transfer length (push-in bond) and flexural length (pull-out bond) within the prestressed concrete members. Also, the model is able to take into account different strand's diameters and different strand's surfaces (smooth or indented).

Chapter 5 Parametric study on the bond behaviour at elevated temperatures

As presented in Chapter 3, a new model for modelling the bond stress-slip between concrete and steel reinforcing bars at elevated temperatures has been developed. In order to understand the bond behaviour under different conditions, this chapter will dedicate to study the factors that can influence on the bond stress-slip under fire conditions. These factors are: influence of yielding the steel bars, effect of the concrete cover, influences of the concrete compressive strength and concrete spalling.

5.1 Introduction

Understanding the response of reinforced concrete members during loading is essential to design an efficient and safe structure. Experimental tests are commonly conducted to study the behaviour of an individual member under various factors. This method can provide actual behaviour of the structural members, however it is time consuming and expensive, especially for members subjected to fire conditions. Also, behaviour of individual member subjected to standard fire curve does not represent the real behaviour of building under fire condition, which makes it difficult for the designer to determine the appropriate level of safety for the structures.

Recently, finite element analysis is an alternative method that can be used to analyse the structural members or even whole building in fire. Finite element analysis provides an accurate prediction on the response of the structural elements that have different parameters, such as materials properties, element geometry, temperature and different types of loading. Elements geometry may change during loading in slender members like columns or for large deformable members. Therefore, non-linear analysis is a procedure that can be used to stimulate the inelastic behaviour of the elements (material and geometry) under different loading conditions (Badiger & Malipatil 2014).

Generally, researchers indicated that reinforced concrete structures have good fire resistance, better than steel structures. This assumption is correct if the cross-sections of the concrete members retain their integrity. However, spalling of concrete cover

causes severe damage to the reinforced concrete elements due to exposing steel bars directly to the fire (Bailey 2002).

At present, numerous models have been developed to study the behaviour of reinforced concrete members at ambient and elevated temperatures. But, the majority of these models were based on the assumption of full interaction between concrete and reinforcing bars (Huang 2010). However, the results presented in Chapter 3 and Chapter 4 indicated that the assumption of full bond between concrete and rebar at elevated temperatures is unconservative. The behaviour of the bond between concrete and steel bars has a considerable influence on the fire resistance of reinforced concrete members. Hence, the main objectives of this chapter are to:

- Conduct a parametric study to investigate the influence of the bond stress-slip on the response of reinforced concrete beam and slab members under fire conditions.
- Study the factors that effects on the bond stress-slip behaviour. These factors are: reinforcing steel bars' yielding; the thickness of concrete cover, concrete compressive strength and concrete spalling.
- Study the behaviours of different structural members within a whole building under different fire compartment conditions.

5.2 Modelling background

The behaviour of reinforced concrete structures under fire condition has been investigated by Huang (2010). The Finite element program VULCAN was used to simulate a reinforced concrete frame in fire. This frame (as shown in Figure 5.1) has been adopted in this research to perform the studies of the bond behaviour between concrete and reinforcement under fire conditions. As shown in Figure 5.2, the reinforced concrete structure is modelled as an assembly of finite plain beam-column and slab elements, reinforcing steel bar elements and bond-link elements. Each node from these elements is defined in a common reference plane. This reference plane is assumed to coincide with the mid-surface of the slab elements and its location is fixed throughout the analysis. Both materials and geometric non-linearity are taken into account in this model. The sophisticated behaviours of the structures under elevated temperatures such as thermal expansion, degradation of

stress–strain curves, failure of concrete segments due to cracking and crushing of concrete, failure of steel reinforcement by yielding or bar’s rupture are all considered in this model (Huang et al. 1996; Huang et al. 1999; Huang et al. 2009; Huang 2010).

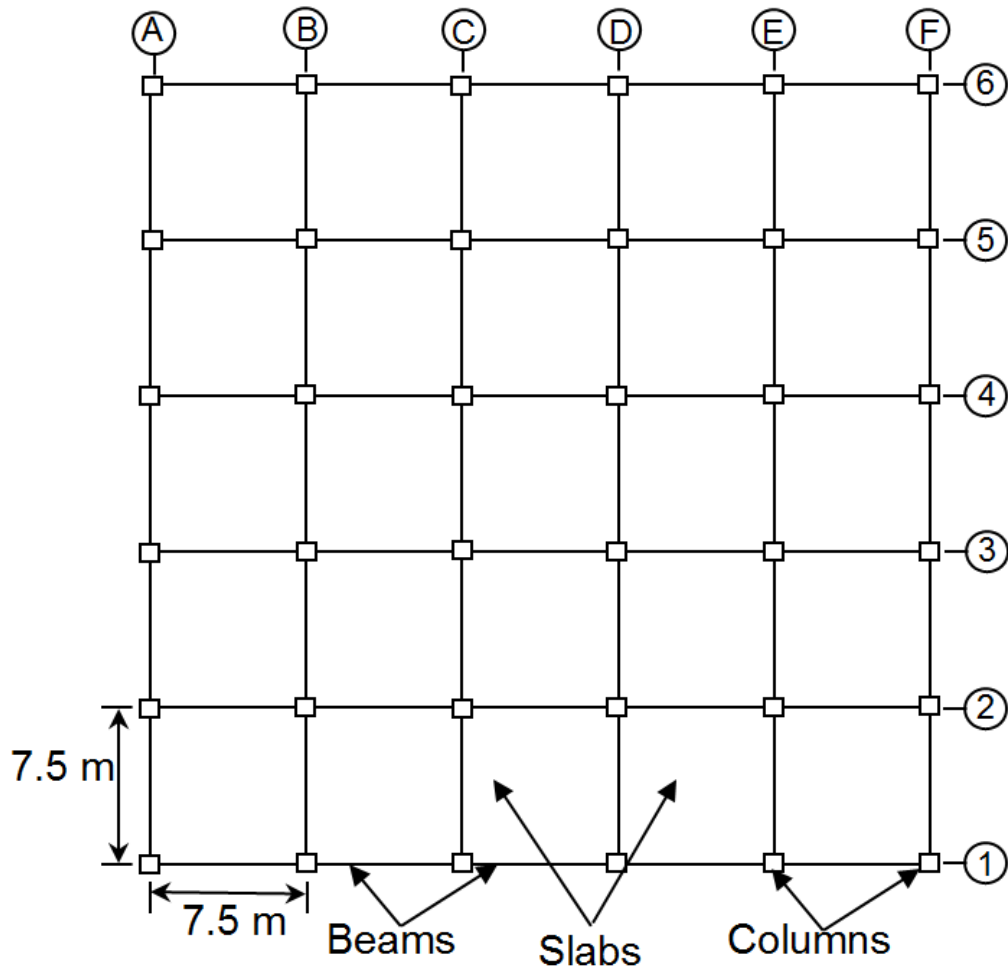


Figure 5.1 Whole floor layout of reinforced concrete structure

Analysis of the reinforced concrete members involves two phases: the first phase is to carry out the thermal analysis on the beam or slab. This thermal analysis can be achieved using two-dimensional non-linear finite-element computer program developed by Huang et al. (1996). In this program the thermal properties for concrete and steel given in Eurocode 2 (CEN, 2004a) are adopted. The second phase of the analysis is to perform structural analysis for the beam or slab members using VULCAN software. The output data from the thermal analysis are used as the temperature input data for the structural analysis.

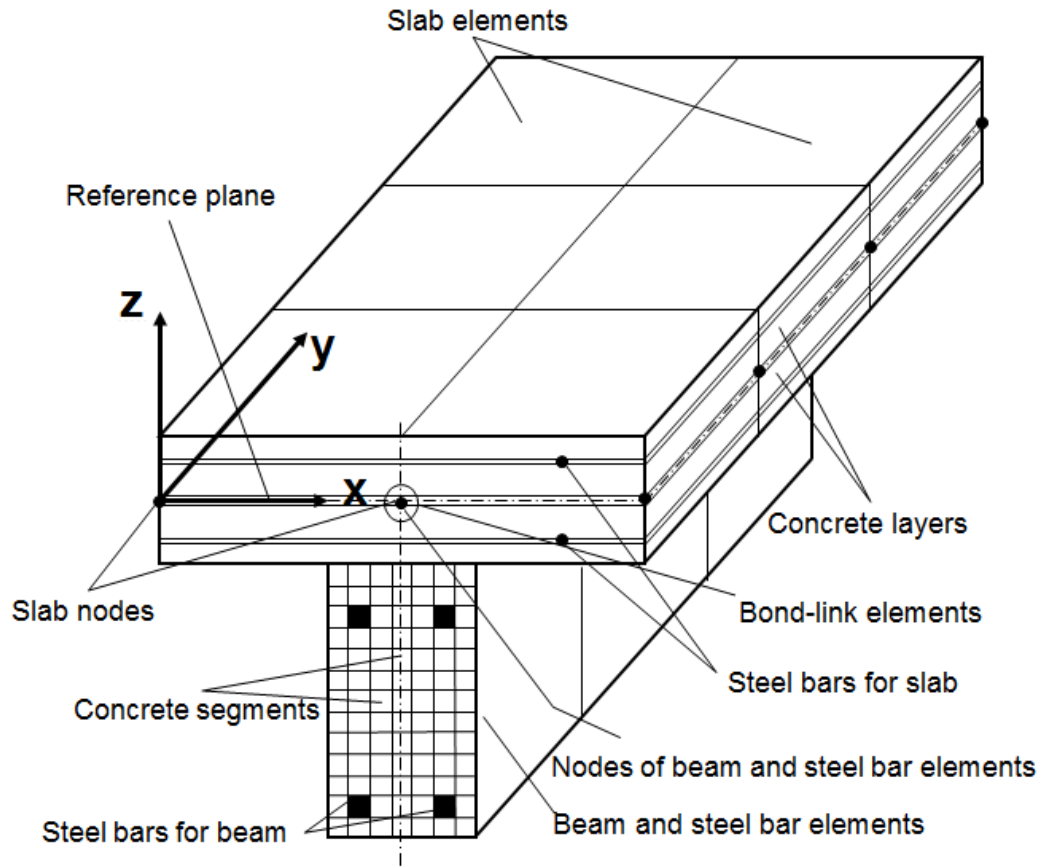


Figure 5.2 Division of reinforced concrete building into beam-column, slab, reinforcement and bond link elements (Huang 2010)

The cross-sections of beam-column elements are subdivided into a matrix of segments. Each segment can have different material properties and temperature profile (Huang et al. 2007). The non-linear layered procedure has been adopted in this software for modelling plain concrete slabs. Both material and geometric non-linearity are considered in the model (Huang et al. 1999; Huang et al. 2003a; Huang et al. 2003b). The slab elements are subdivided into layers (as shown in Figure 5.2) to consider the temperature distribution through the thickness of slab.

The bond-link element that developed in Chapter 3 is used to model the bond behaviour between concrete and reinforcement under fire conditions. Previous studies concluded that the behaviour of bond stress-slip depends on numerous factors such as: type of steel bar (ribbed or smooth bar), roughness of rebar (related to rib area), yielding of reinforcing steel bars, the concrete strength, position and orientation of the bar during casting, state of stress, the boundary conditions, the

concrete cover (CEB-FIP Model code 90 1991; CEB-FIP-Bulletin10 2000; CEB-FIP 2010; Huanzi 2009). Those factors are considered in this research.

Influence of concrete spalling on the thermal and structural behaviour of reinforced concrete members is also considered in this investigation. The effect of concrete spalling is represented by using void segments within the cross-section of beam and column, and void layers within the cross-section of slab. It is assumed that the void segments and void layers have zero mechanical strength, stiffness and thermal resistance. After spalling the outer parts from the concrete, the inner-parts will expose directly to the fire. In which the fire boundary moves within the cross-section of the concrete member. When the spalling reaches to the steel reinforcement, the bond strength will become zero in this region. A critical temperature is used as a criterion for the concrete spalling, in which the segment or the layer will be spalled when the temperature of this segment or layer reaches the 'critical temperature'. The spalling of concrete is assumed not to reach a point beyond the reinforcing cage of the member.

As shown in Figure 5.1, it is assumed that the building contains of ten floors with 4.5 m height of each story. Dimensions of each floor are 37.5 m x 37.5 m with five 7.5 m x 7.5 m bays in each direction. The building is subjected to ISO 834 standard fire (ISO-834 1975). The building represents a commercial office building and designed based on Eurocode 2 (CEN 2004a; CEN 2004b). The self-weight is 7.5 kN/m² for concrete density of 24 kN/m³. Raised floor involves: 0.5 kN/m² for ceiling, 0.5 kN/m² for services and 1.0 kN/m² for partitions with impose load of 2.5 kN/m². The total design load on the slab is 10.75 kN/m² at the fire limit state. The concrete compressive strength is 45 MPa with moisture content of 4% by weight and the yield strength of steel bar is 460 MPa. It is assumed that the building required two hours fire resistance with the slab cover of 25 mm. The floor slab thickness is 250 mm based on Eurocode 2 (CEN 2004b). The length of the beam is 7.5 m and exposed to fire from three sides as illustrated in Figure 5.3 and Figure 5.7. The cross-section's details of the beams are shown in Figure 5.4, which have dimensions of 500 x 350 mm and concrete cover of 30 mm.

5.3 Modelling isolated simply supported reinforced concrete beam

Figure 5.3 shows an isolated simply supported reinforced concrete beam heated by ISO 834 standard fire. The beam has the same dimensions and loading condition of the beams within the generic building (see Figure 5.1). Hence, the span of the beam is 7.5 m and the beam has two layers of reinforcing steel bars (three bars at the bottom and two bars at the top), as shown in Figure 5.4.

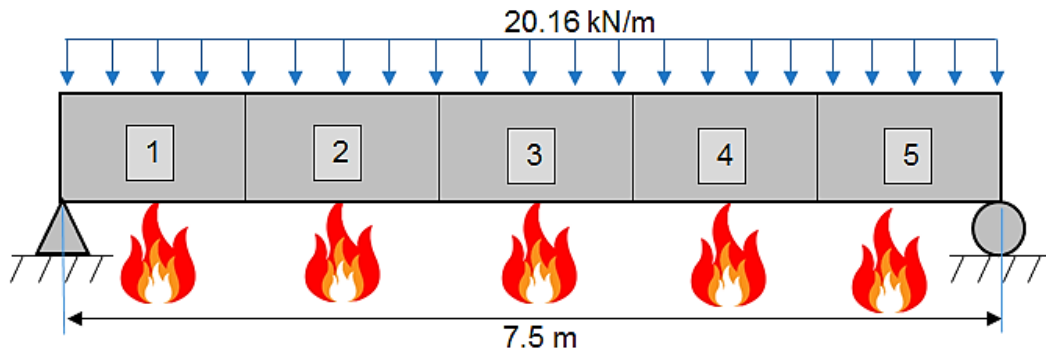


Figure 5.3 Isolated simply supported beam heated by ISO 834 standard fire

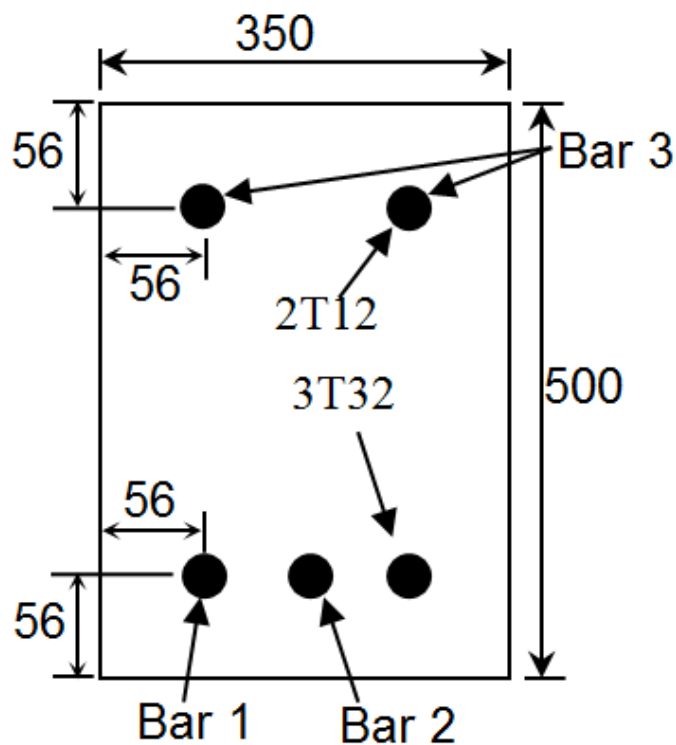


Figure 5.4 The cross-sectional details of the isolated reinforced concrete beam (all dimensions in mm)

As mentioned before, two steps should be followed in order to analyse the beam under fire condition. Firstly, the thermal analysis of the beam was conducted to calculate the temperature history within the cross-section of the beam. In this step, the cross-section of the beam was divided into 441 segments (21 x 21). Same segmentations were used within the cross-section of the beam for the structural analysis.

Spalling of the concrete was taken into account in this investigation to study the influence of spalling on the thermal and structural behaviours of the beam. Previous research indicated that the spalling of concrete is very likely to occur within the first 30 minutes of ISO 834 fire test and the range of the critical spalling temperature of concrete is between 200 °C to 400 °C (Huang 2010). Hence, the critical spalling temperature of concrete in this study is assumed to be 350°C. For assessing the influence of the bond on the behaviour of the beam, the beam with both of full or partial bond conditions between the concrete and reinforcement were modelled.

As mentioned before, the bond-stress slip relationship are affected by numerous factors such as steel bar roughness, thickness of concrete cover, concrete strength, position and orientation of steel bar during casting, boundary conditions, state of stress and yielding of reinforcing steel bars (CEB-FIP Model code 90, 1991; CEB-FIP-Bulletin10 2000). Hence, the factors considered for investigation here are: yielding of reinforcing steel bars, the concrete cover, the concrete compressive strength and concrete spalling.

Details of the reinforced concrete beam were given in Figures 5.3 and 5.4. The uniform line load acting on the beam was 20.16 kN/m, which is the same as the beam within the frame shown in Figure 5.1. The concrete compressive strength was 45 MPa and the yield stress of the steel bar was 460 MPa. The beam was modelled as an assembly of 5 three-node plain concrete beam elements and 25 three-node reinforced steel elements and 55 two-node bond link elements. Using the bond-link elements the beam can be modelled with full, partial or even zero interaction between concrete and reinforcing steel bars.

5.3.1 Yielding effect of reinforcing steel bars on the bond behaviour

The proposed model presented in Chapter 3 has been further improved in this chapter to take into account the yielding effect of steel bar on the bond behaviour. Yielding of the steel bar within the plastic range has an effect on the bond strength similar to the effect of splitting of concrete cover. A reduction in the steel bar diameter can occur due to steel bar's yielding. This contraction leads to a great reduction in the friction between concrete and rebar, and also affects the geometry of the bar ribs, which consequently reduces the bond stress (CEB-FIP-Bulletin10 2000).

In order to consider the yielding effect of steel bar on the bond behaviour, the bond stress τ should be modified by the factor Ω_y as follow (CEB-FIP 2010):

$$\tau_{\text{modified}} = \tau \cdot \Omega_y \quad (5.1)$$

$$\Omega_y = 1.0 \quad \text{for } \varepsilon_s \leq \varepsilon_{sy} \quad (5.2)$$

$$\Omega_y = 1.0 - \left[0.85 \cdot \left(1 - e^{-5ab} \right) \right] \quad \text{for } \varepsilon_{sy} < \varepsilon_s \leq \varepsilon_{su} \quad (5.3)$$

In which:

$$a = \frac{\varepsilon_s - \varepsilon_{sy}}{\varepsilon_{su} - \varepsilon_{sy}} \quad (5.4)$$

$$b = \left[2 - \frac{f_t}{f_y} \right]^2 \quad (5.5)$$

Where: ε_s is the steel strain; ε_{sy} is the yield strain of steel bar at the yield stress f_y ; ε_{su} is the ultimate steel strain, f_t is the steel stress and f_y is the yield stress of the steel bar. The yielding effect of the steel bar on the bond stress-slip curve is shown in Figure 5.5. This effect has been incorporated into the bond model developed in Chapter 3.

For demonstrating the influence of the yielding effect of reinforcing steel bar on the bond behaviour, the isolated beam was modelled using the bond models with and without the yielding effect of reinforcing steel bar. In the modelling, the concrete compressive strength was 45 MPa, the steel strength was 460 MPa and the concrete cover was 30 mm.

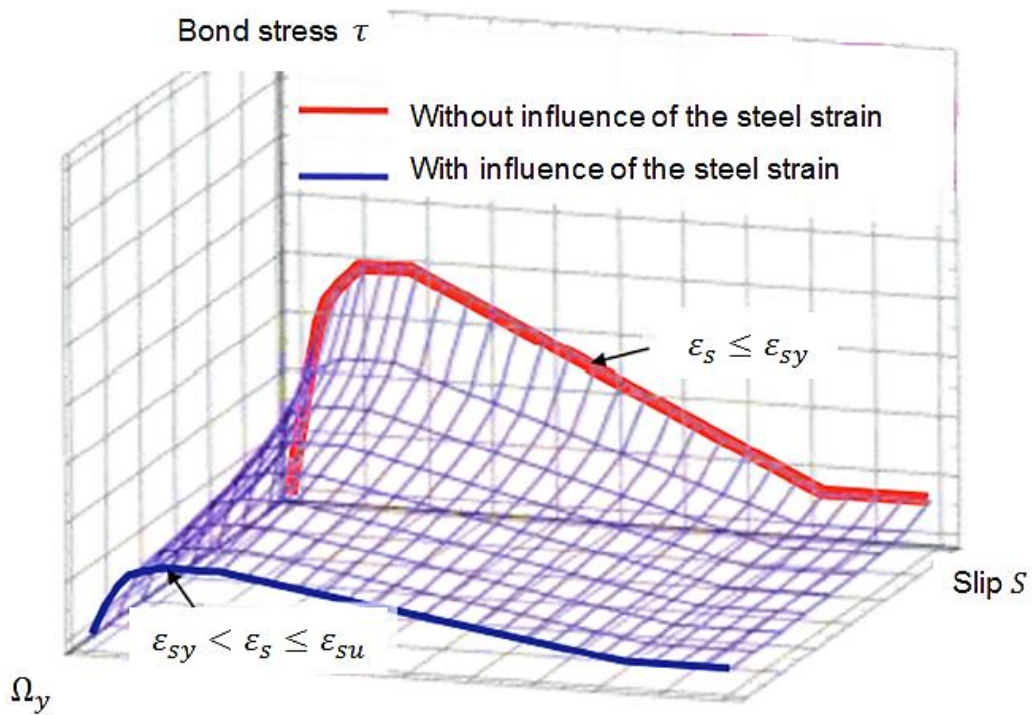


Figure 5.5 Influence of steel strains on local bond-stress slip relationship (CEB-FIP 2010)

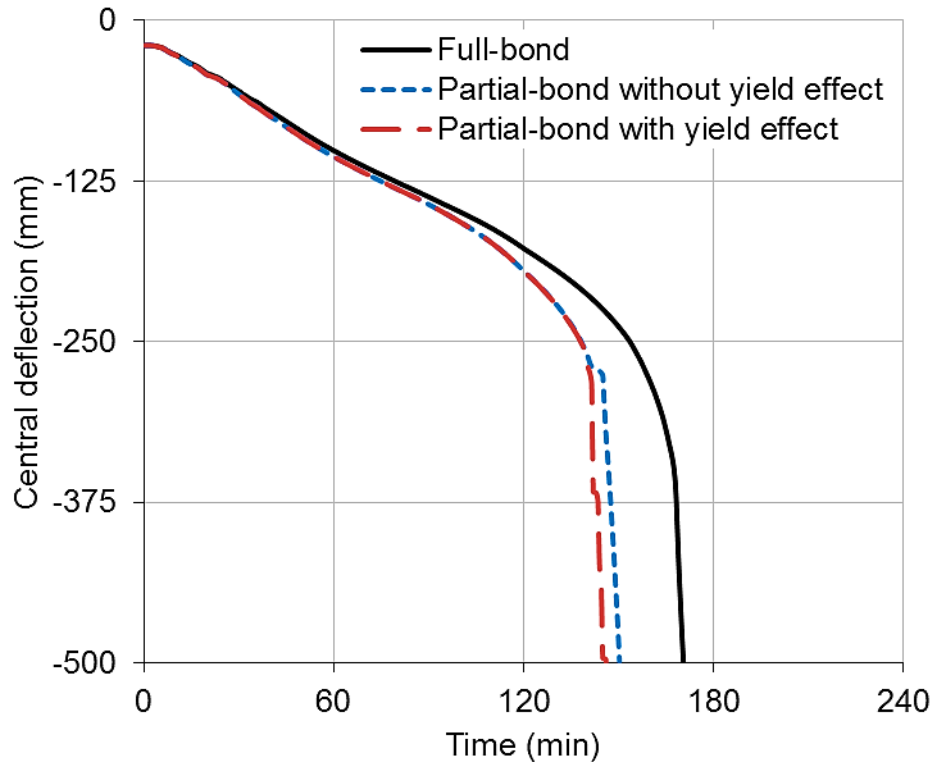


Figure 5.6 Yielding effect of reinforcing steel bar on the bond behaviour

Figure 5.6 shows the influence of yielding the steel bar on the central deflection of the beam under ISO 834 fire, together with the central deflection of the beam modelled with full bond interaction. As shown in Figure 5.6, the yielding effect of the steel bar has some degrees of influence on the bond behaviour but the influence is not significant. However, this demonstrated that the yielding effect of steel bar can reduce the bond strength between concrete and the steel bar.

5.3.2 The effect of concrete cover on the bond behaviour

Concrete cover is an important part for reinforced concrete members. Concrete cover provides the protection for the reinforcing steel bars from the outside attacks such as chloride, which can result corrosion for the steel bars. Also, the concrete cover gives isolation for the reinforcement from the high temperatures under fire conditions. Moreover, concrete cover provides the confinement for the steel bars to generate the bond between concrete and reinforcement.

Same isolated beam with concrete compressive strength of 45 MPa and steel strength of 460 MPa was used in this investigation. In order to investigate the sensitivity of the bond-slip model to the concrete cover of the beam at elevated temperatures, five

values of concrete cover thicknesses (10, 20, 30, 40 and 50 mm) were adopted in this study. The cross-section of the beam was subdivided into segments of concrete and steel, as shown in Figure 5.7. The same segmentation was used for both thermal and structural modelling of the beam. Also the beam was heated from three sides (see Figure 5.7).

Figures 5.8 to 5.10 show the temperatures of the reinforcing steel bars within the cross-section of the beam (Bar 1, Bar 2 and Bar 3 as identified in Figure 5.4) with different thickness of concrete covers. It is clear from the figures that the temperature of the steel bars decreases by increasing the concrete cover of the beam. Hence, the concrete cover can provide the protection to the reinforcing steel bars from the fire and reduce the effect of temperature on the steel bars and bond strength within the cross-section of reinforced concrete beams. It can be seen from the figures that after two hours (120 min) of exposing to ISO 834 standard time-temperature, the temperature for Bar-1 with cover 50 mm is less than that for cover 10 mm by about 47%, while for Bar-2 the temperature reduced by 49% and for Bar-3 the temperature reduced by 56%.

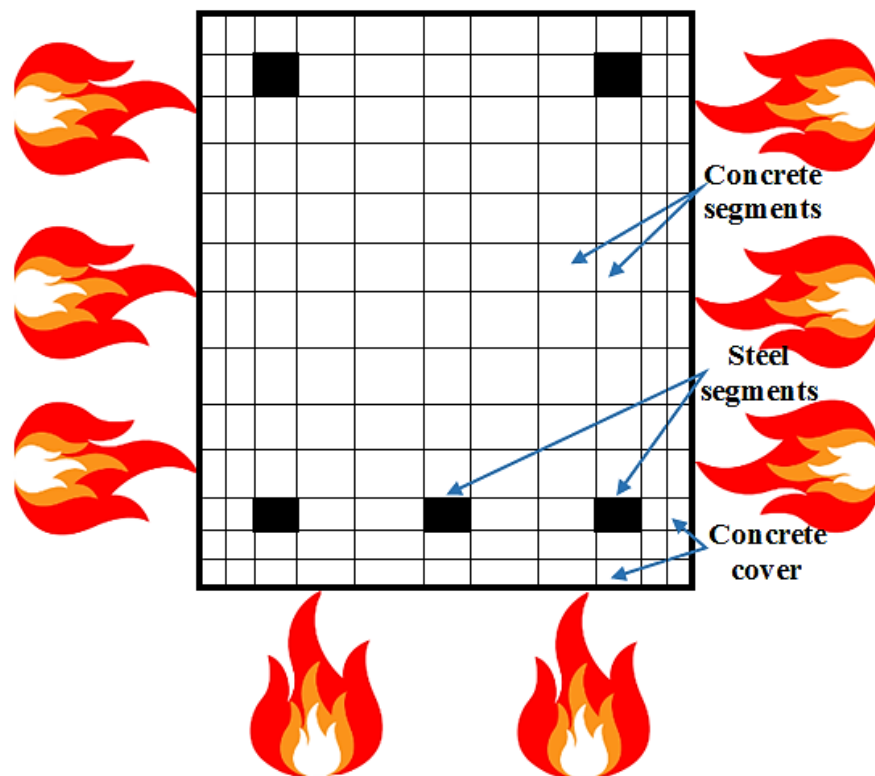


Figure 5.7 Segmentation of the beam cross-section

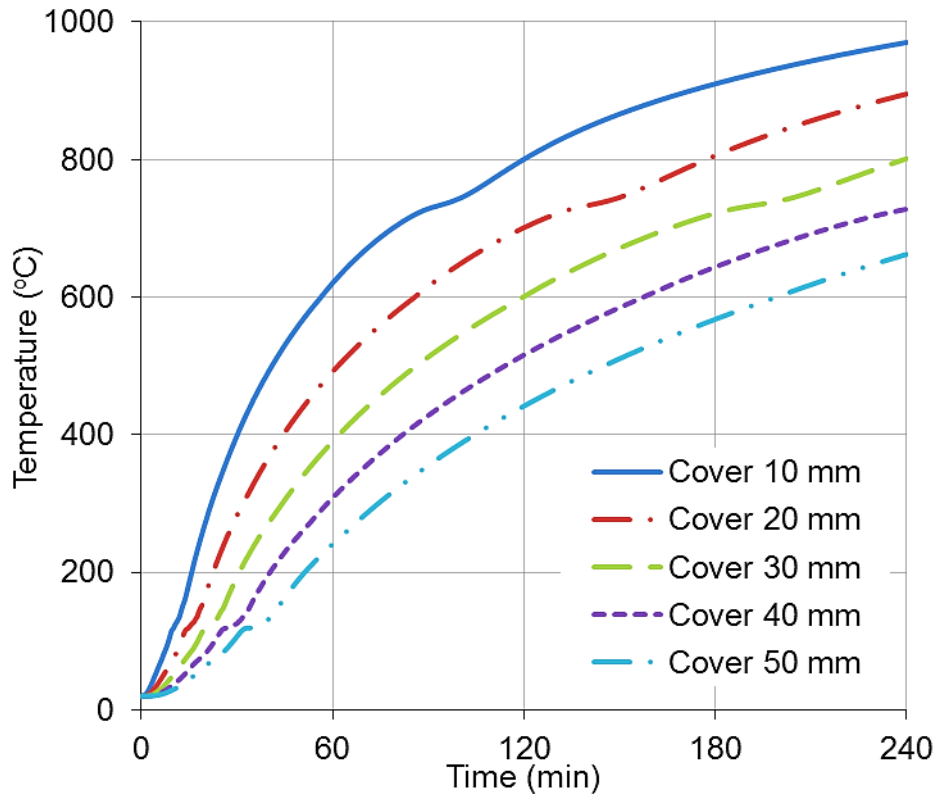


Figure 5.8 Temperature histories of the steel bar (Bar 1) for the beam subjected to ISO 834 standard fire with different thicknesses of concrete cover

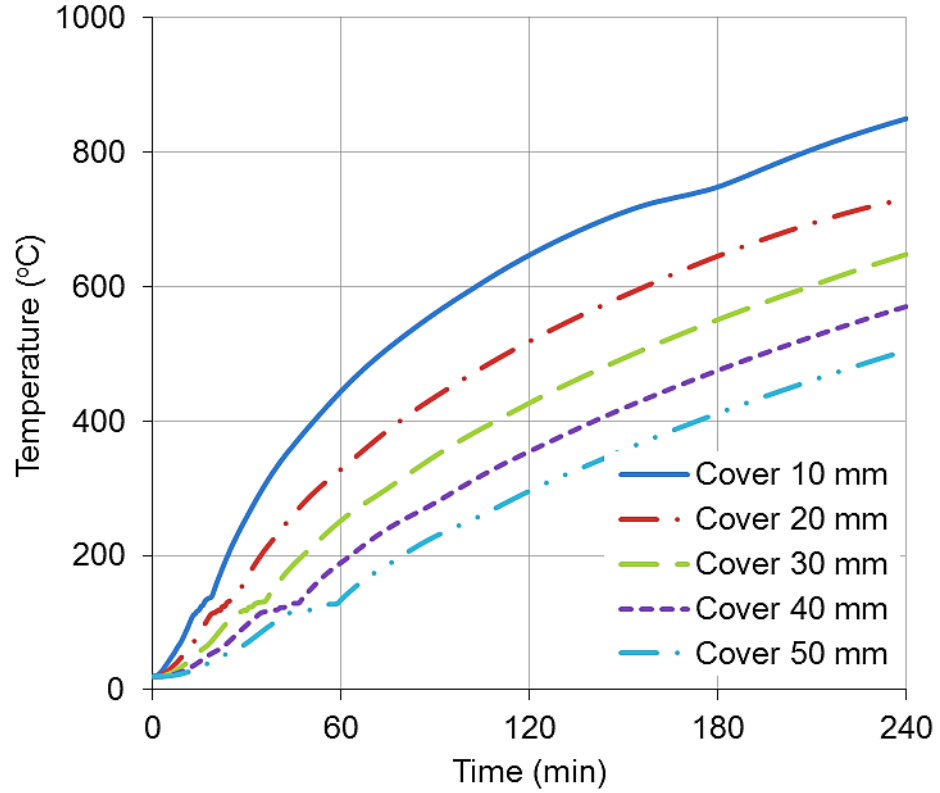


Figure 5.9 Temperature histories of the steel bar (Bar 2) for the beam subjected to ISO 834 standard fire with different thicknesses of concrete cover

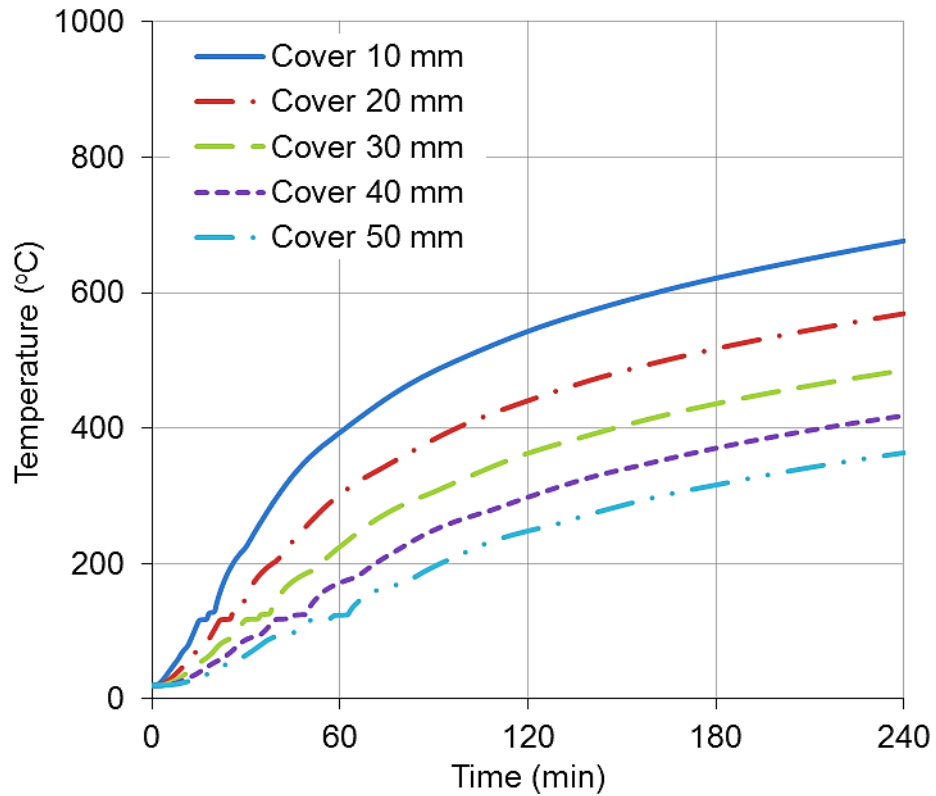


Figure 5.10 Temperature histories of the steel bar (Bar 3) for the beam subjected to ISO 834 standard fire with different thicknesses of concrete cover

Influence of concrete cover on the bond behaviour at elevated temperatures is presented based on the response of the beam to the high temperatures. Generally, degradation of the bond strength results in extra central deflection of the beam due to the bond deterioration. Figures 5.11 to 5.15 give comparisons between the case of full bond (full interaction between the concrete and reinforcement) and partial bond-slip between the concrete and steel bars for each thickness of concrete cover at elevated temperatures.

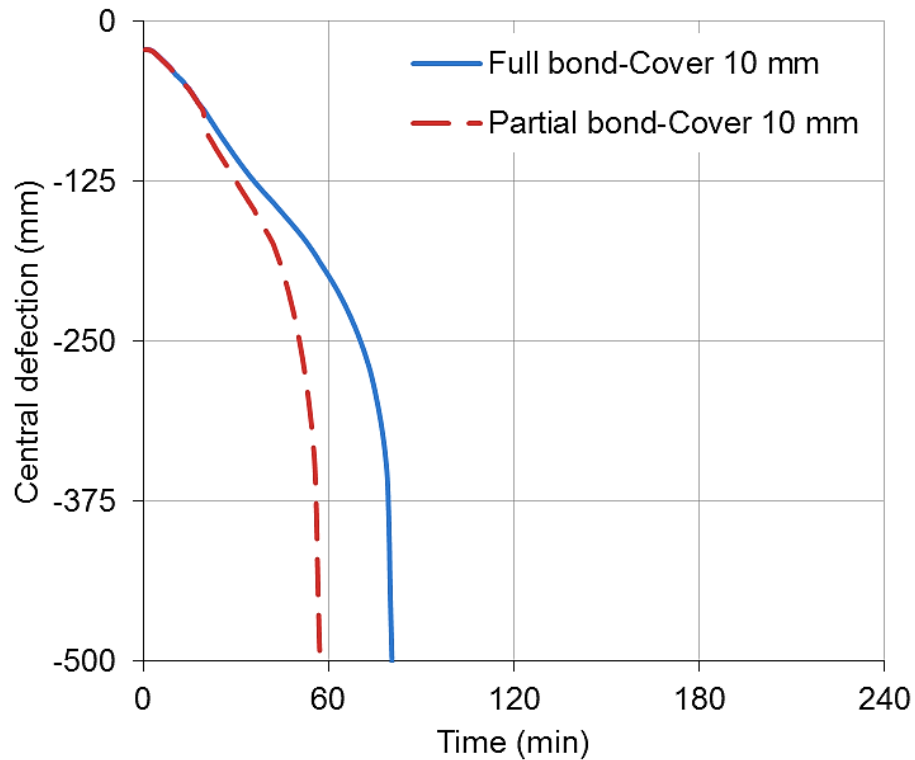


Figure 5.11 Comparison between full-bond and partial-bond for the concrete cover of 10 mm

It can be seen from the figures that the concrete cover has considerable effect on the behaviour of the beam with full or partial bond. As shown in Figure 5.11, for the case with the concrete cover of 10 mm, the behaviour of the two curves was identical until 40 min of fire exposure time. However, after that time a clear divergence between the two curves was observed. This difference between the two curves is attributed to the degradation of the bond, in which the temperatures of Bar 1 and Bar 2 become more than 400 °C (see Figure 5.8) and 350 °C (see Figure 5.9), respectively. However, for the case with concrete cover of 50 mm, the effect of bond becomes insignificant and identical behaviour of both curves can be seen due to low temperatures of the steel bars and high interaction between the concrete and rebar as shown in Figure 5.15.

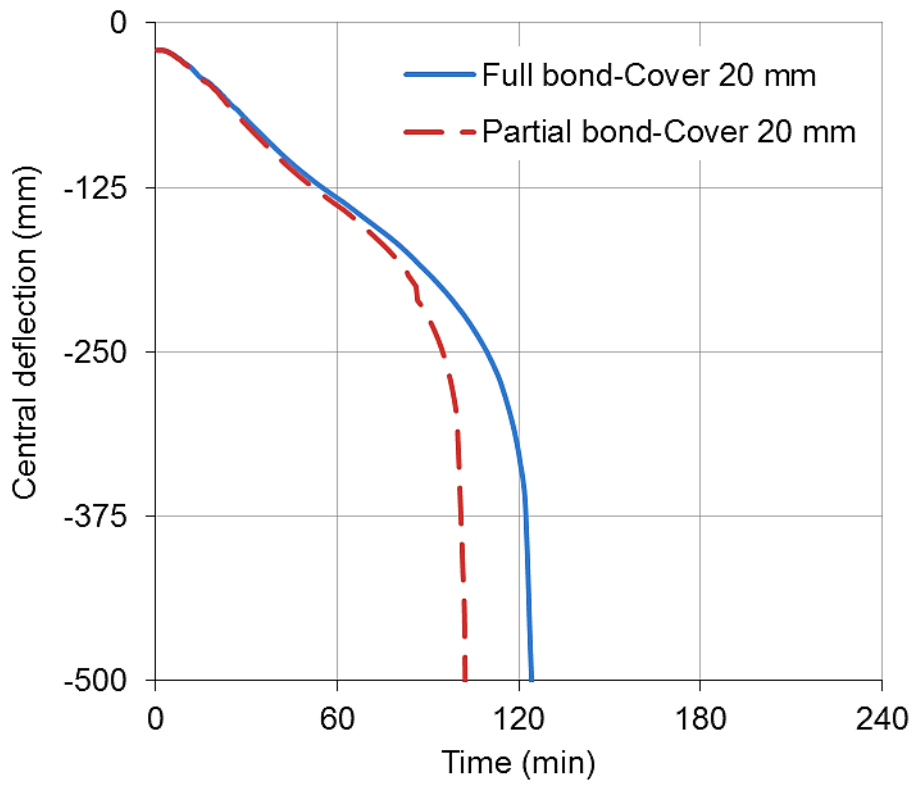


Figure 5.12 Comparison between full-bond and partial-bond for concrete cover of 20 mm

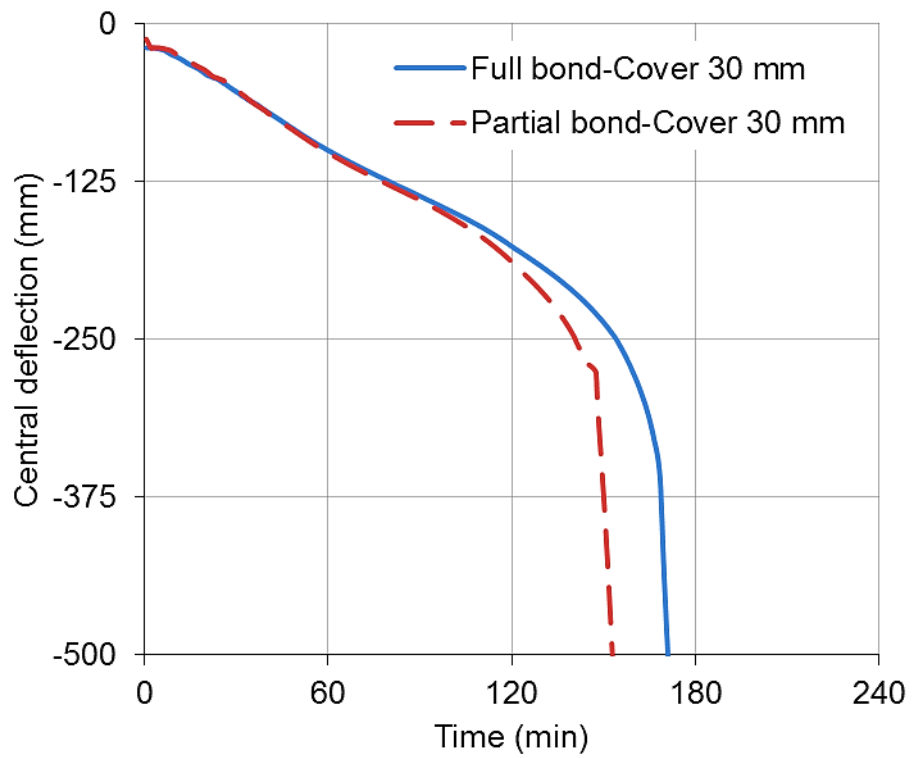


Figure 5.13 Comparison between full-bond and partial-bond for concrete cover of 30 mm

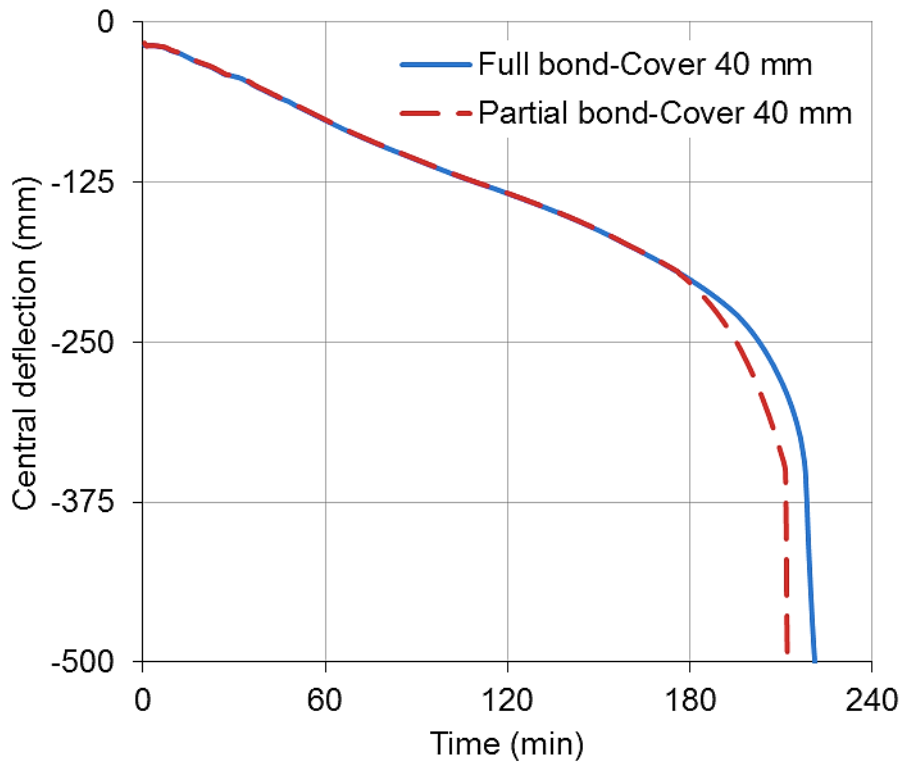


Figure 5.14 Comparison between full-bond and partial-bond for concrete cover of 40 mm

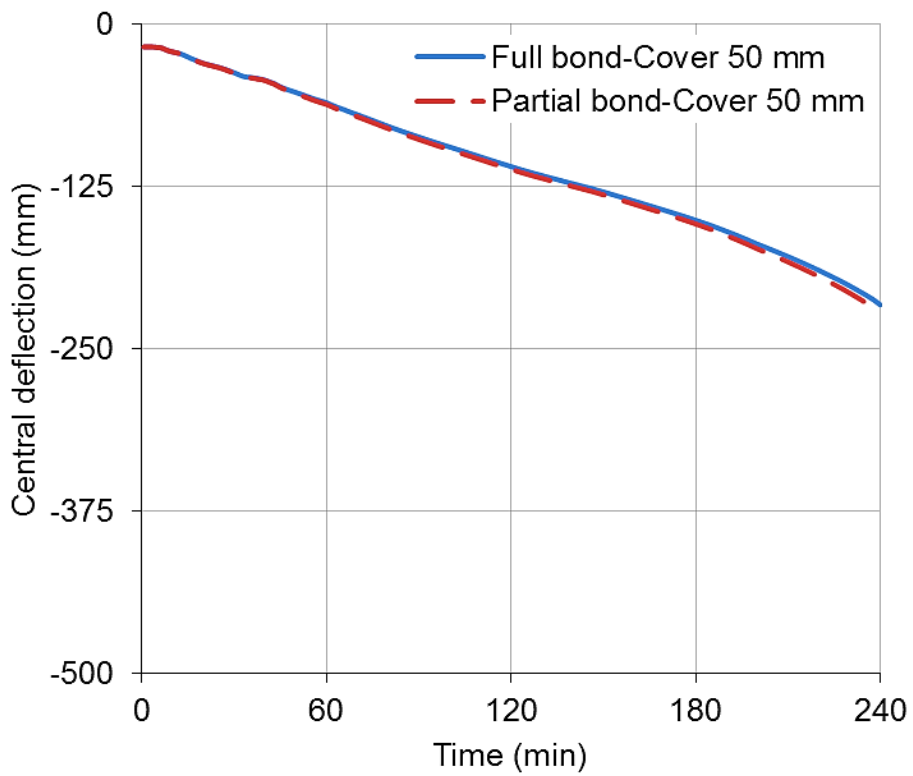


Figure 5.15 Comparison between full-bond and partial-bond for concrete cover of 50 mm

It can be concluded from the Figures 5.11 to 5.15 that, increasing the thickness of concrete cover has a great influence on the bond-slip, in which the degradation of the bond strength decreases with increasing the thickness of concrete cover. As mentioned before, the concrete cover is the main factor that can provide the protection to the steel bars and gives the confinement to the reinforcement for the bond strength. Therefore, the designer should carefully choose the proper concrete cover.

Finally, it is important to explain the type of failure based on the outputs of the VULCAN software. The failure of the beam with the concrete cover of 50 mm occurred mainly due to concrete cracking. For concrete covers of 40 mm, 30 mm and 20 mm the failure of the beam occurred due to concrete cracking, yielding the steel bars as well as the bond failure of some elements. For concrete cover of 10 mm the failure of the beam firstly occurred due to concrete cracking, then yielding the steel bars followed by rupture of some steel bars, also the failure of the most bond-link elements between the reinforcement and concrete.

The results generated from this study further support the claims of previous researchers that the concrete cover has a great influence on the bond strength by providing the confinement to the reinforcement. Hence, reduce the concrete cover is not only leads to increase the temperature of the reinforcement during fire, but also decreases the concrete confinement which can play a significant factor on the bond strength (CEB-FIP-Bulletin10 2000).

Figure 5.16 shows the influence of different concrete covers on the behaviour of the beam modelled with partial bond. It is evident that the concrete cover has a great influence on the behaviour of the beam. By considering the deflection criterion ($\text{span}/20$), the fire resistance for the beam is 77 min, 120 min, 167 min and 217 min for the concrete of 10 mm, 20 mm, 30 mm, 40 mm respectively. And more than four hours (240 min) fire resistance can be achieved when the concrete cover is 50 mm. Hence, increasing the concrete cover from 10 mm to 40 mm can increase the fire resistance of the beam for more than two hours.

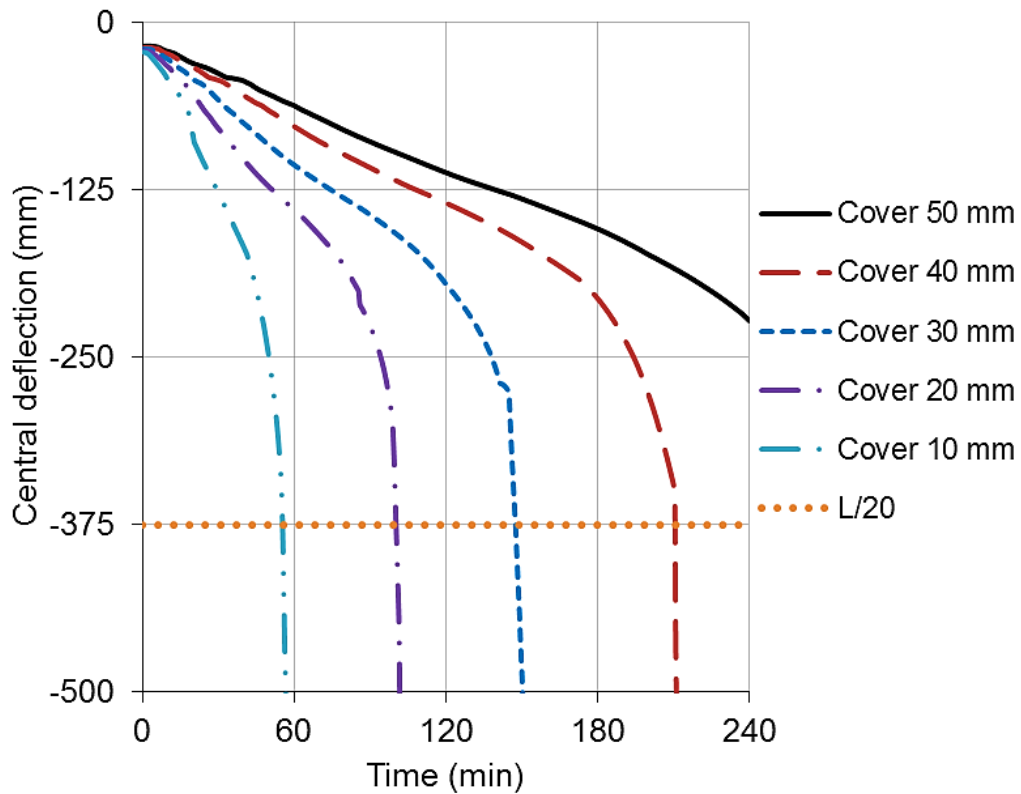


Figure 5.16 Influence of concrete cover on the structural behaviour of a simply supported beam modelled with partial bond

5.3.3 The effect of concrete spalling on the behaviour of the beam

Spalling of concrete in fire has a significant effect on the steel bars and the bond strength, which influence on the behaviour of reinforced concrete members. When the spalling of concrete occurs, the members will lose the concrete cover and the reinforcement will be exposed directly to the fire. Then, a great reduction in the strength and stiffness of steel bars can occur. Also, failure of the bond between the concrete and the rebar can happen due to losing the confinement of the concrete to the steel bar. The influence of spalling on a reinforced concrete beam was investigated by Huang (2010). The results from the study indicated that the influence of spalling for full-bonded member is significant, especially when the spalling occurs within the mid-span elements.

In this study the effect of concrete spalling on the bond behaviour was considered by modelling the beam using partial bond model. Same isolated beam has been used for this investigation. The beam has concrete compressive strength of 45 MPa, the steel bar yielding of 460 MPa and concrete cover of 40 mm. As shown in Figure 5.3, the

beam was modelled as an assembly of five plain concrete beam elements, 25 steel bar elements and 55 bond-link elements. In order to consider the effect of concrete spalling, void segments were used to represent the spalled concrete for the thermal and structural analysis. In this study, both full and partial bond were considered to investigate the effect of spalling on the behaviour of the beam. The time-temperature histories of the reinforcing steel bars for the cases of concrete spalling and no-spalling are illustrated in Figure 5.17. It is clear from the figure that the spalling of concrete cover has a great influence on the thermal behaviour of the beam. For instant, Bar 1 reached to temperature about 500 °C after 120 min with no-spalling of concrete, but with spalling Bar 1 reached to this temperature after just 24 min.

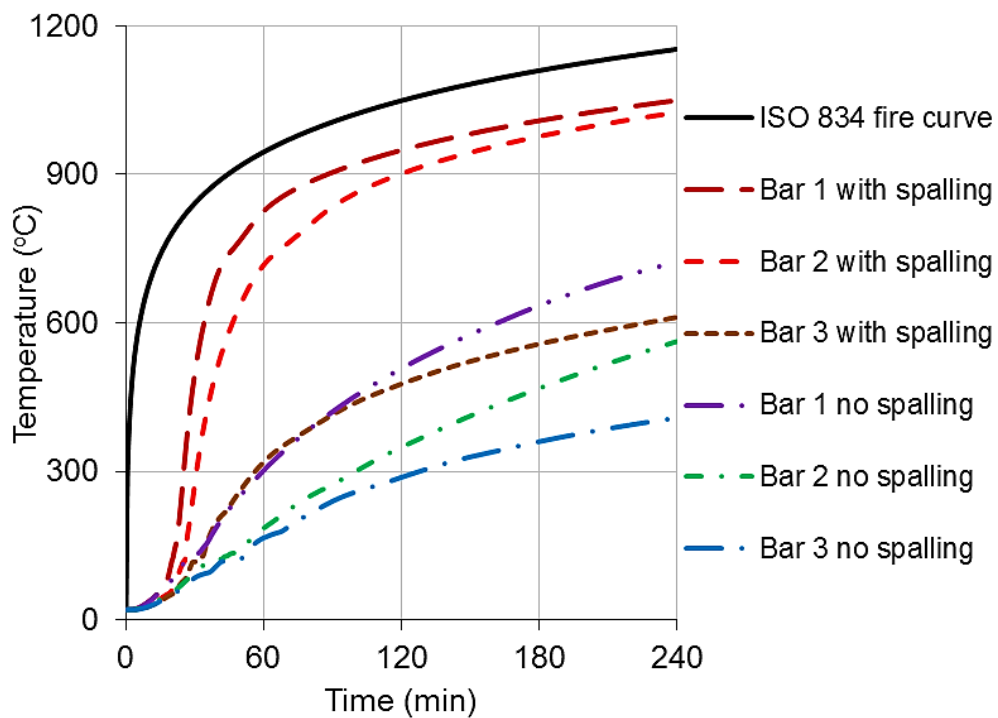


Figure 5.17 Temperature histories of the reinforcing bars for the beam exposed to ISO 834 standard fire

Figure 5.18 shows the influence of concrete spalling on the behaviour of the beam modelled as full or partial bond. It was assumed that all elements were subjected to concrete spalling. It can be seen that the impact of concrete spalling on the beam is very significant for both full bond and partial bond cases. However, the effect of spalling on the beam modelled with partial bond is greater than that modelled with full bond. Figures 5.19 to 5.22 give comparisons for the behaviour of the beam subjected to different concrete spalling and bond conditions.

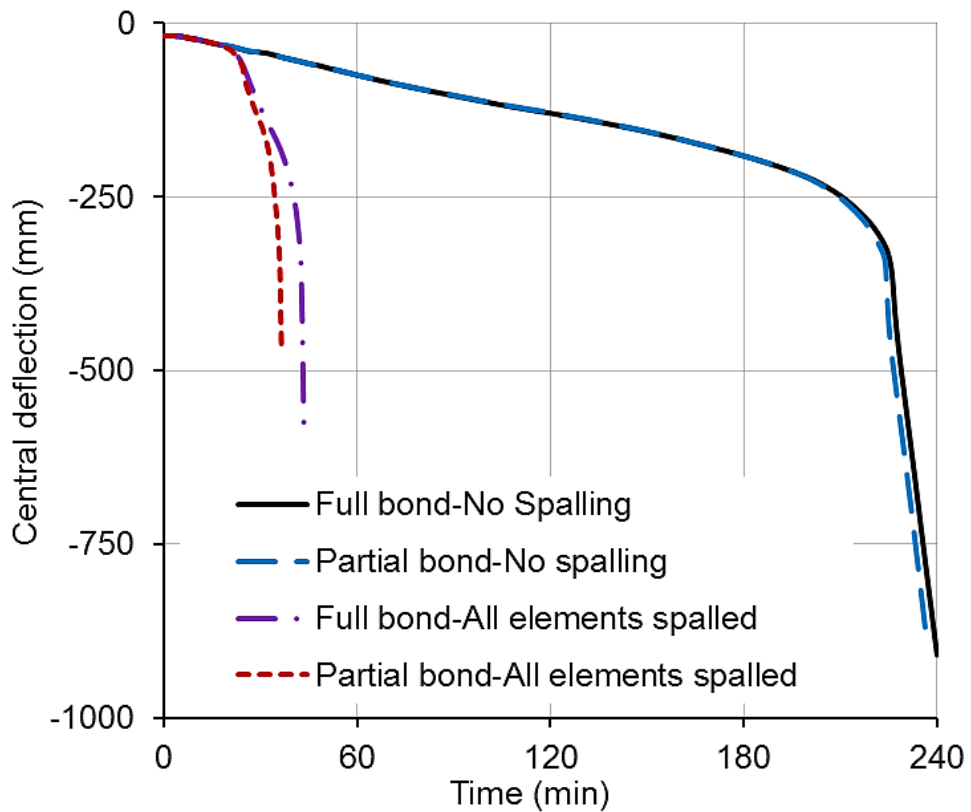


Figure 5.18 Influence of concrete spalling on the behaviour of the beam modelled as full or partial bond

Figure 5.19 shows the comparison of the behaviour of the beam modelled as full bond or partial bond in which all elements were spalled. It is clear from the figure that a big different can be seen between full bond and partial bond cases. From Figures 5.20 to 5.22, it is evident that the effect of spalling becomes more significant when elements 1&5 were spalled (see Figure 5.3 for element's positions) than the other elements. This can be justified as the bond stress at the end elements of the beam is higher than the bond stress at the middle elements, hence weaken the bond at the end elements has more influence on the response of the beam. It was observed from the VULCAN output files that the failure of the beam, when elements 1&5 were spalled, occurred due to bond failure and even bar rupture. While for other cases, the failure of the beam was dominated by yielding the steel bars.

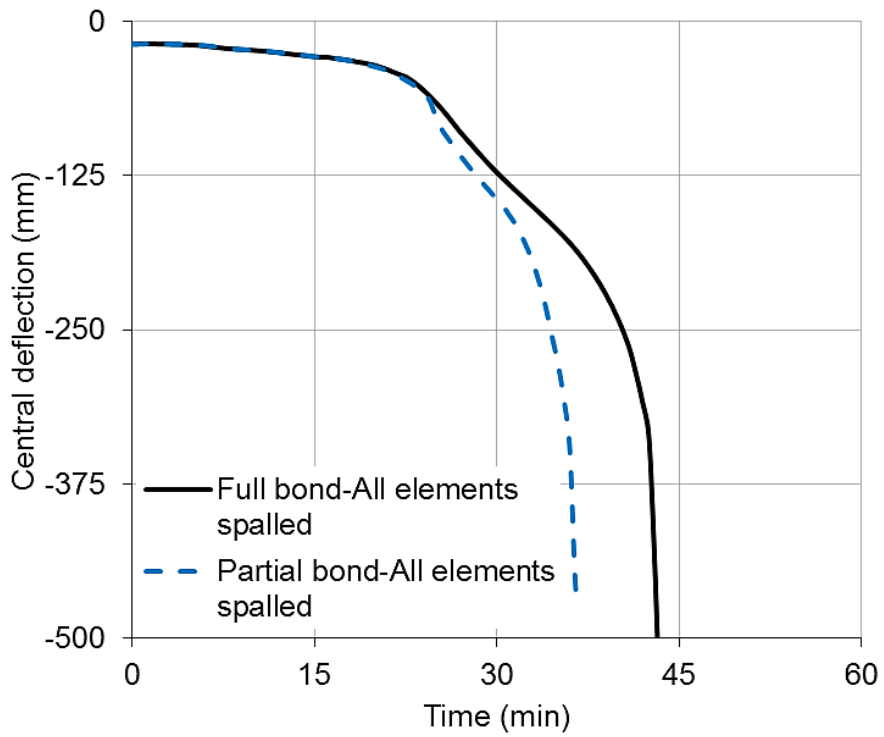


Figure 5.19 Comparison of the behaviour of the beam modelled as full bond or partial bond (all elements spalled)

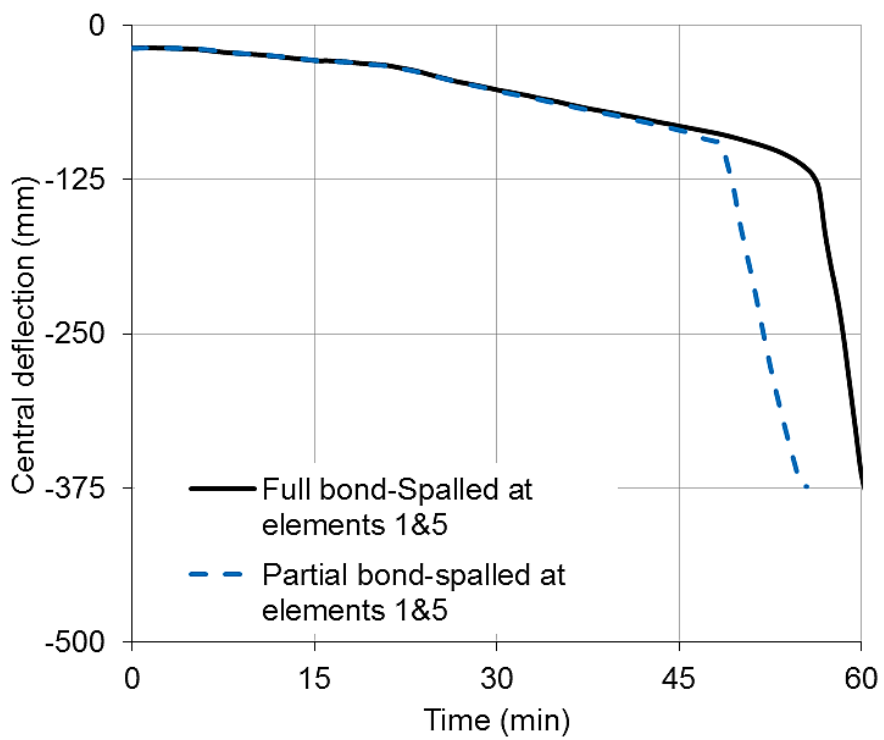


Figure 5.20 Comparison of the behaviour of the beam modelled as full bond or partial bond (elements 1&5 spalled)

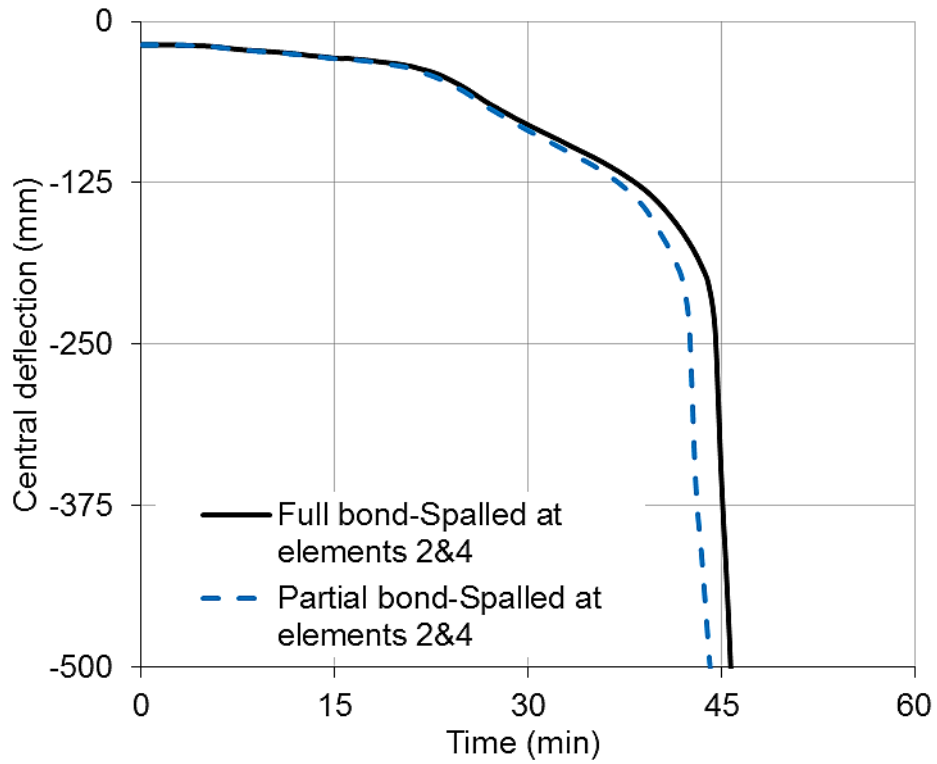


Figure 5.21 Comparison of the behaviour of the beam modelled as full bond or partial bond (elements 2&4 spalled)

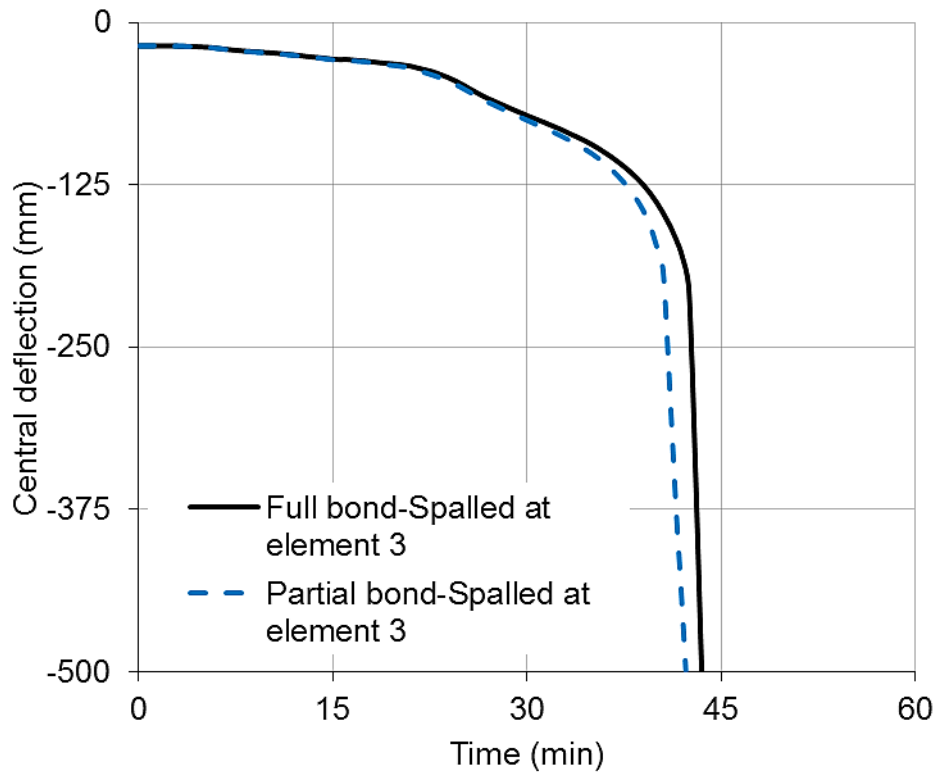


Figure 5.22 Comparison of the behaviour of the beam modelled as full bond or partial bond (element 3 spalled)

5.3.4 The effect of concrete strength on the bond

Concrete compressive strength is one of the factors that effect on the bond strength. The maximum bond strength τ_{\max} is related to concrete compressive strength as:

$$\tau_{\max} = a\sqrt{f_{ck}} \quad (5.6)$$

where: f_{ck} is the concrete compressive strength and a is a constant based on the bond characteristic (CEB-FIP Model code 90 1991; CEB-FIP 2010). Bond stress is a result from the shear strength of the concrete in front of steel bar ribs and the circumference tensile stress of the concrete surround the rebar. Therefore, degradation of the bond at elevated temperatures is directly linked to the concrete deterioration.

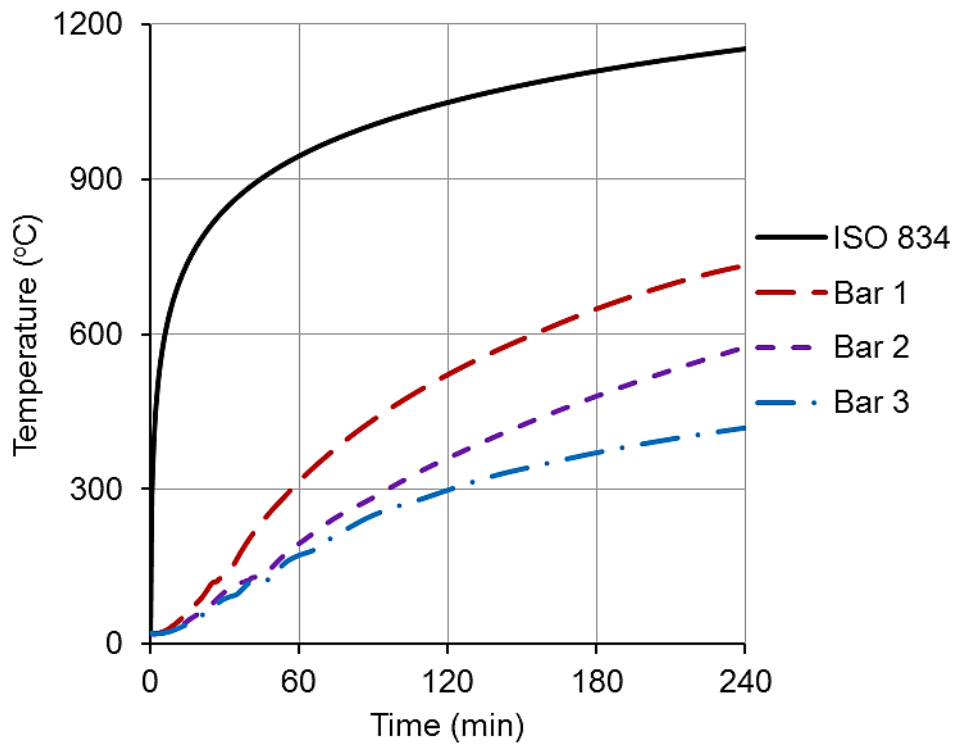


Figure 5.23 Time-temperature histories for the reinforcing steel bars of the beam subjected to IOS 834 standard fire

Same isolated beam with concrete cover of 40 mm and steel bar yielding strength of 460 MPa was used in this section to study the effect of concrete compressive strength on the bond behaviour. A range of concrete compressive strengths (20, 30,

40 and 45 MPa) were adopted in this investigation in order to examine the effect of concrete compressive strength on the bond characteristic between the concrete and the reinforcement. From the thermal analysis, the temperatures of the reinforcing steel bars are shown in Figure 5.23.

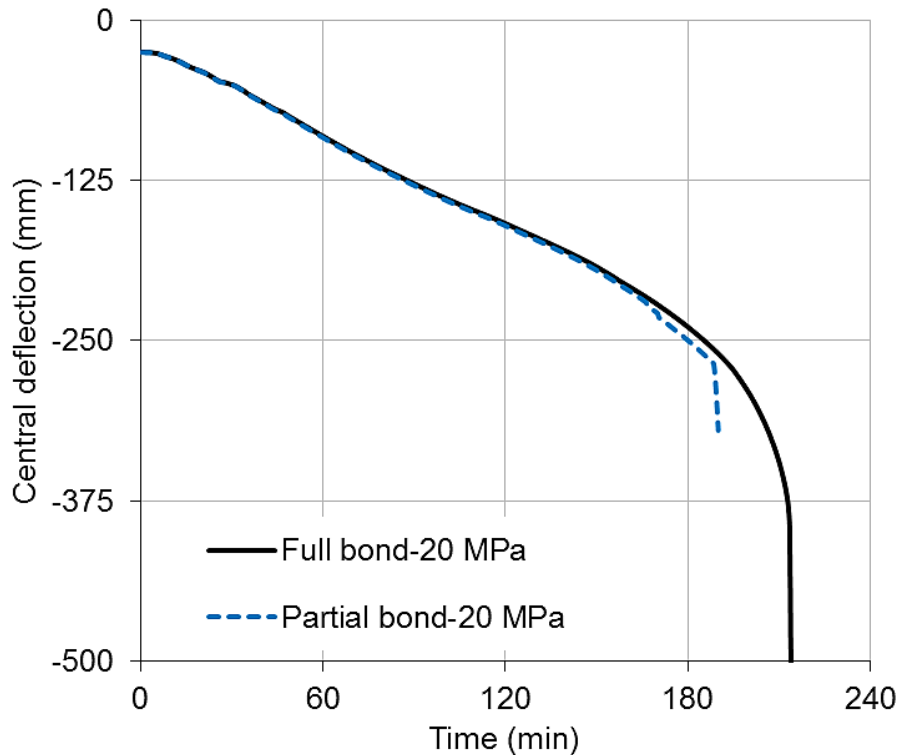


Figure 5.24 Comparison of the behaviour of the beam modelled with full bond and partial bond using concrete compressive strength of 20 MPa

The comparisons of the behaviour of the beam modelled with full bond and partial bond using different concrete compressive strength are presented in Figures 5.24 to 5.27. As shown from Figure 5.26 and Figure 5.27, the concrete compressive strength has no significant effect on the bond behaviour when the compressive strength is more than 40 MPa; and the behaviour of the beam modelled with full or partial bond is similar. However, great influence can be observed when the concrete compressive strength is less than 40 MPa, as shown in Figure 5.24 and Figure 5.25. This behaviour can be attributed to the considerable degradation of the bond strength.

Figure 5.28 shows the influence of concrete compressive strength on the behaviour of the beam modelled with full bond. It can be seen from the figure that there is no significant effect for concrete compressive strength on the behaviour of the beam modelled with full bond. However, as shown in Figure 5.29, there is a considerable

influence of concrete compressive strength on the behaviour of the beam modelled with partial bond, especially for lower concrete compressive strength.

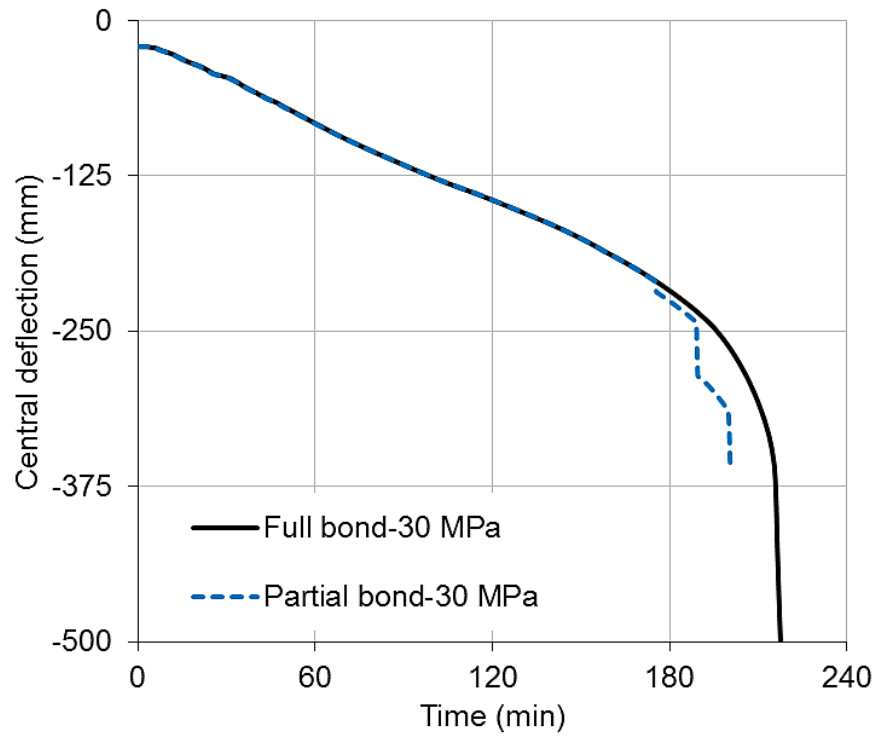


Figure 5.25 Comparison of the behaviour of the beam modelled with full bond and partial bond using concrete compressive strength of 30 MPa

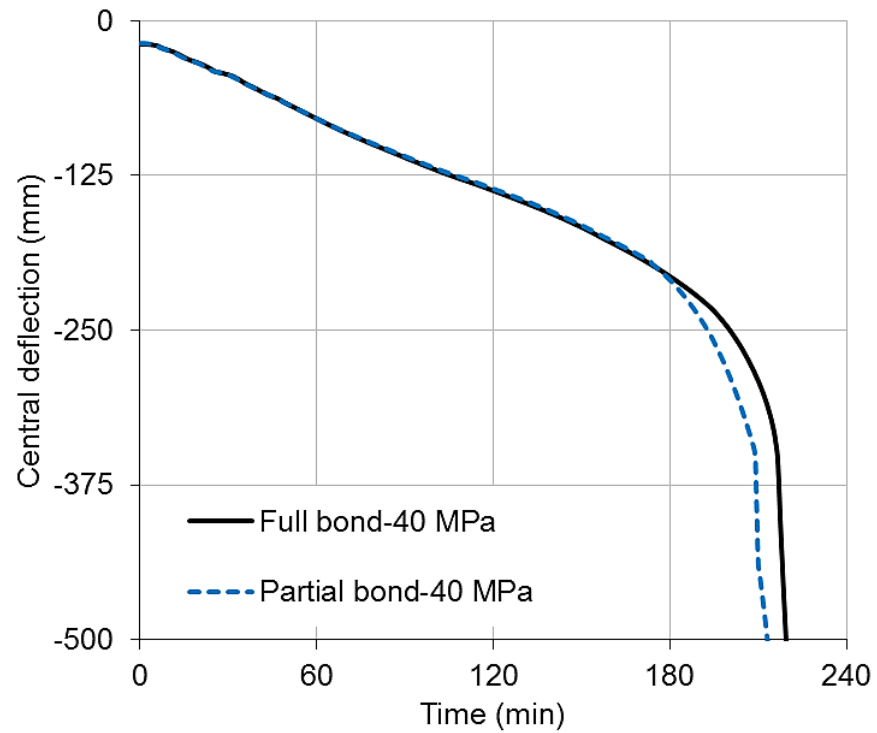


Figure 5.26 Comparison of the behaviour of the beam modelled with full bond and partial bond using concrete compressive strength of 40 MPa

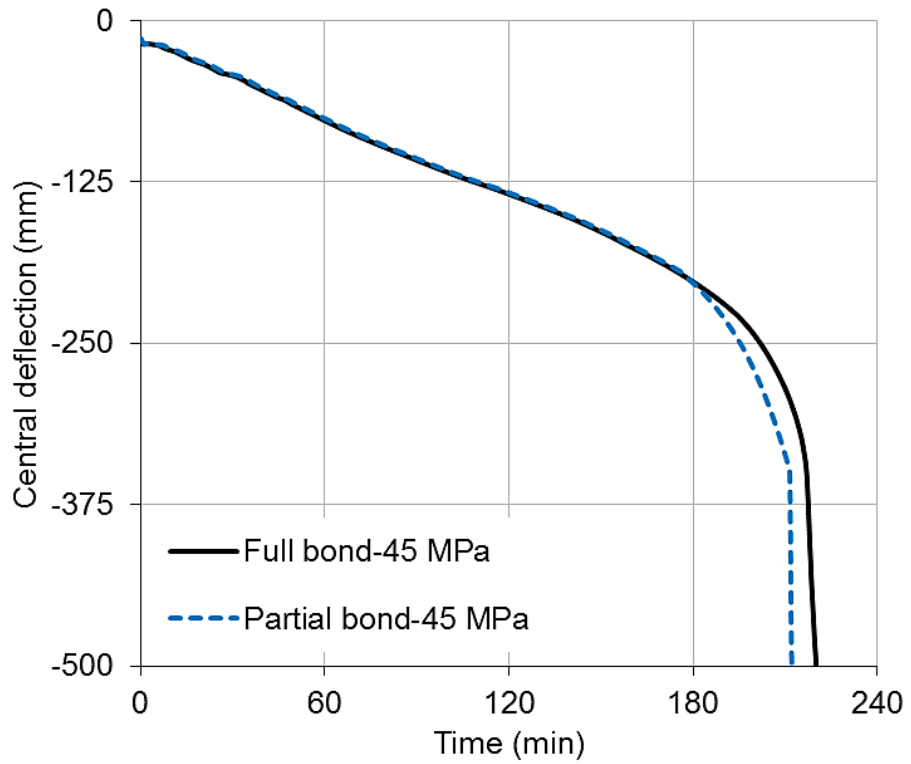


Figure 5.27 Comparison of the behaviour of the beam modelled with full bond and partial bond using concrete compressive strength of 45 MPa

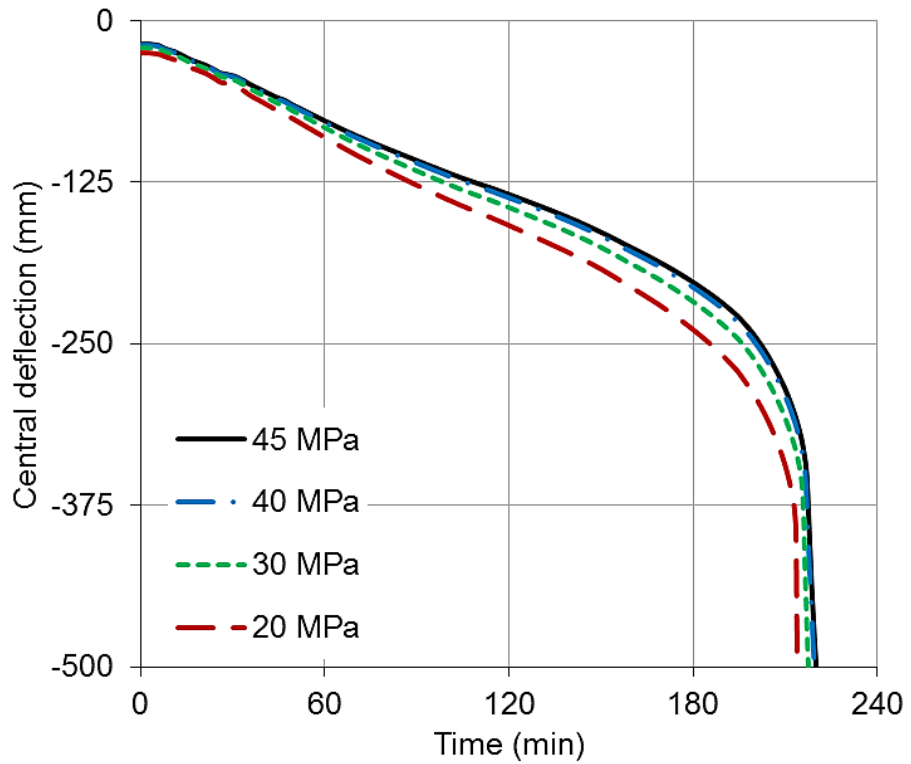


Figure 5.28 Influence of concrete compressive strength on the behaviour of the beam modelled with full bond

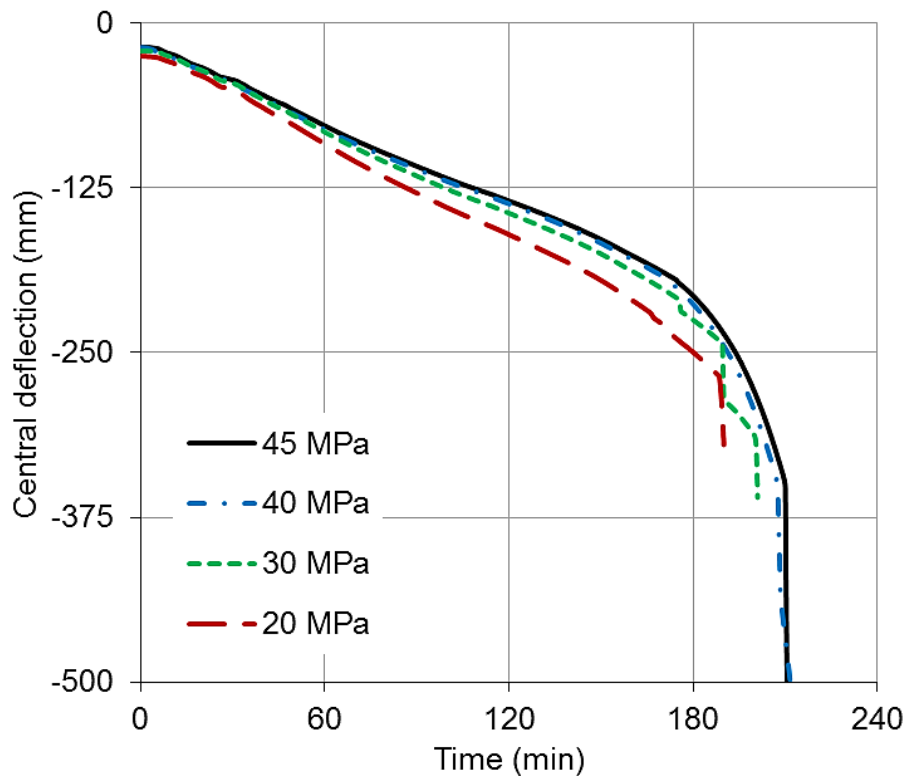


Figure 5.29 Influence of concrete compressive strength on the behaviour of the beam modelled with partial bond

5.4 Modelling isolated simply supported reinforced concrete slab

Figures 5.30 and 5.31 show an isolated simply supported reinforced concrete slab floor heated by ISO 834 standard fire. The slab has the same dimensions and loading condition of the slab floor within the generic building (see Figure 5.1). Hence, the dimensions of the slab are 7.5 m x 7.5 m and the load condition was 10.75 kN/m². Concrete compressive strength was 45 MPa and yield stress of the reinforcing steel bar was 460 MPa. The slab has two orthogonal reinforcing steel bar layers with steel area of 646 mm²/m for each layer.

As shown in Figure 5.30, the slab was modelled as an assembly of 25 nine-node plain concrete slab elements, 50 three-node reinforced steel bar elements (25 elements in each direction) and 85 two-node bond link elements which connected the plain concrete slab elements to steel bar elements. Hence, the influence of the bond between concrete and reinforcing steel bars can be modelled as partial or full bond conditions. The cross-section of the slab was subdivided into 14 layers in order to perform the thermal and structural analysis.

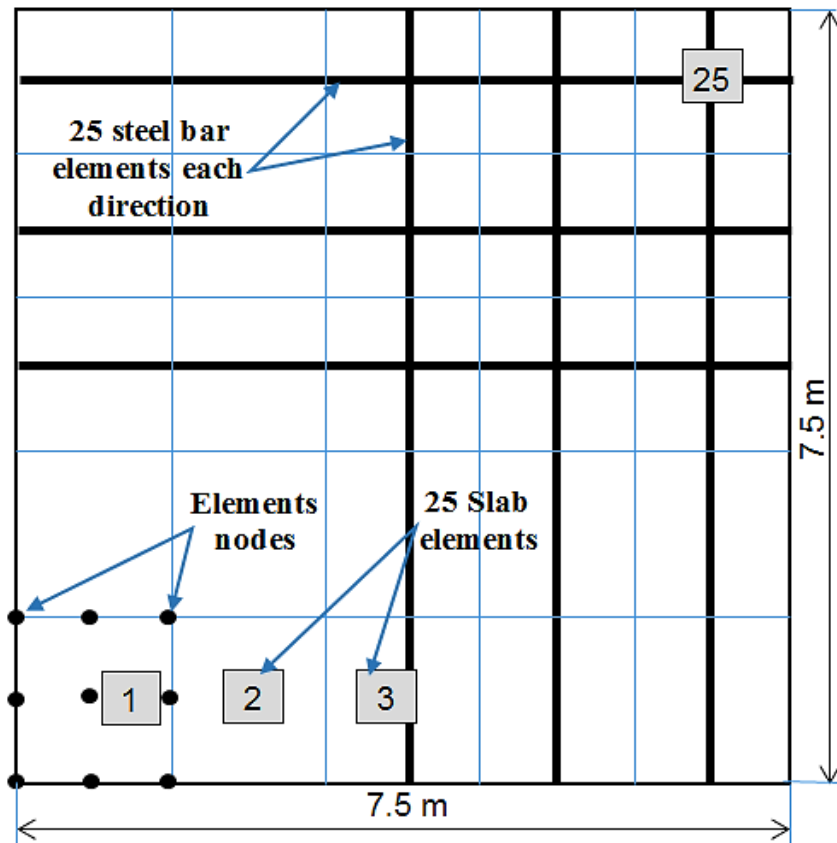


Figure 5.30 Details of the isolated slab modelled

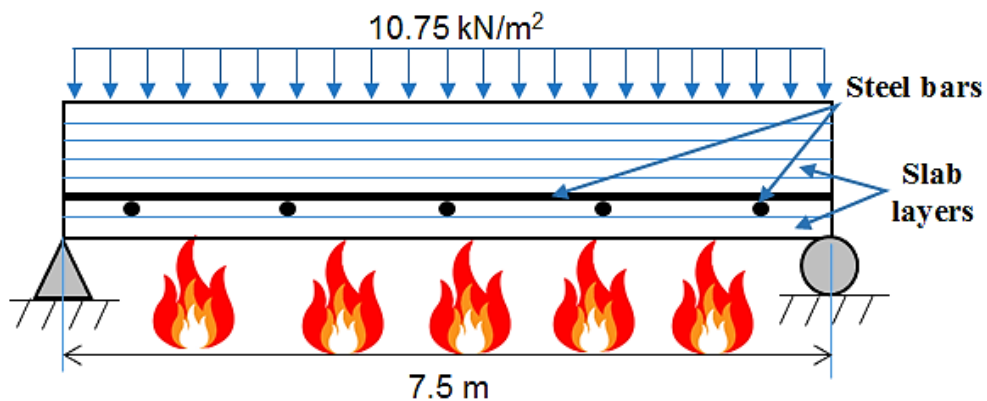


Figure 5.31 The cross-section of the slab modelled

5.4.1 The effect of concrete cover on the behaviour of the slab

As mentioned before, concrete cover is an important part of reinforced concrete members especially under fire conditions. Concrete cover provides a protection to fire exposure, as well as gives a confinement to the steel bars for anchorage. For considering the influence of concrete cover on the behaviour of the slab under fire

condition, five thicknesses of concrete cover (10, 15, 20, 25 and 30 mm) were adopted in this study. Figure 5.32 shows the temperature histories of the reinforcing steel bars for different thicknesses of concrete covers under ISO 834. It is evident that the temperatures of reinforcing steel bars are significantly affected by the concrete covers.

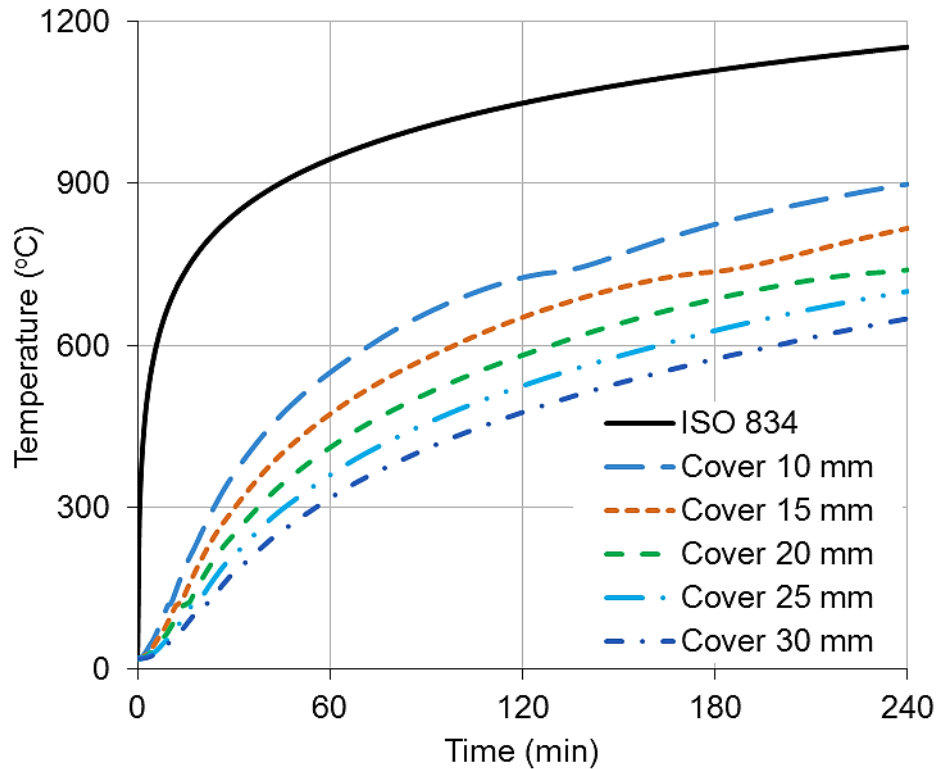


Figure 5.32 Time-temperature histories of the reinforcing steel bars with different concrete covers under ISO 834 fire

The structural analyses were carried out for each thickness of concrete cover using both full bond and partial bond conditions. Figures 5.33 to 5.37 present the comparison of the central deflections of the slab modelled as full bond or partial bond using different thicknesses of concrete cover.

It can be seen from Figure 5.37 that there is no big difference between the deflections of the slab modelled with full or partial bond when the concrete cover was 30 mm. However, when the slab cover was decreased to 25 mm and 20 mm, a clear different can be observed between the cases of full and partial bond, as shown in Figure 5.36 and Figure 5.35. This difference becomes greater when the concrete covers were 10 mm and 15 mm as illustrated in Figure 5.33 and Figure 5.34 respectively. This behaviour is mainly due to the increasing of the bond temperature

(see Figure 5.32). Based on the output data from the modelling, the failure of the slab with 10 mm concrete cover and full bond was due to rupture of many steel bars. This rupture of the steel bars is attributed to the full bond between concrete and the reinforcement in which the high steel strain was concentrated at some locations within the slab. However, when the slab was modelled with partial bond, just few elements were ruptured. This behaviour is attributed to the relative slips between the bars and concrete in which the steel strains within the steel bars can be more uniformly distributed along the length of the steel bars.

Similar behaviour was observed for 15 mm concrete cover with few bars ruptured, which leads to more divergence between the full and partial bond cases. In the case of 20 mm and 25 mm concrete covers, the slab failed mainly due to bond failure for partial bond, and also due to yielding of steel bars for full bond. For the slab with concrete cover of 30 mm, the failure of the slab with full bond was because of yielding of some steel bars while for partial bond just few bond elements failed. Figure 5.38 shows the influence of different concrete covers on the central deflections of the slab modelled as partial bond.

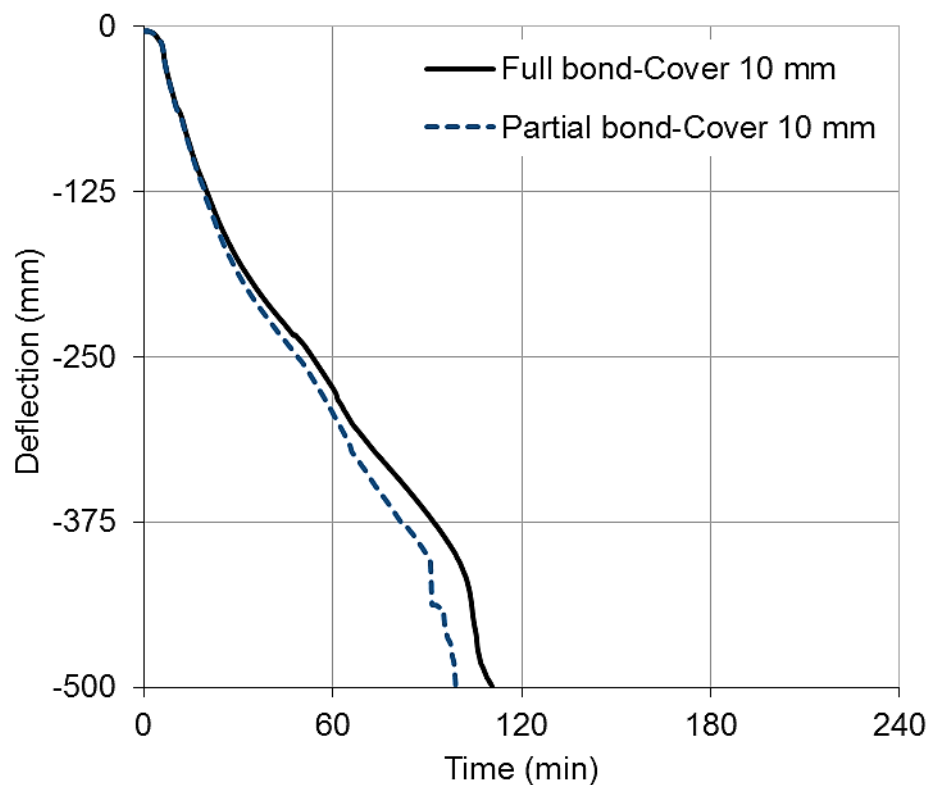


Figure 5.33 Comparison of the central deflections of the slab modelled as full bond or partial bond using concrete cover of 10 mm

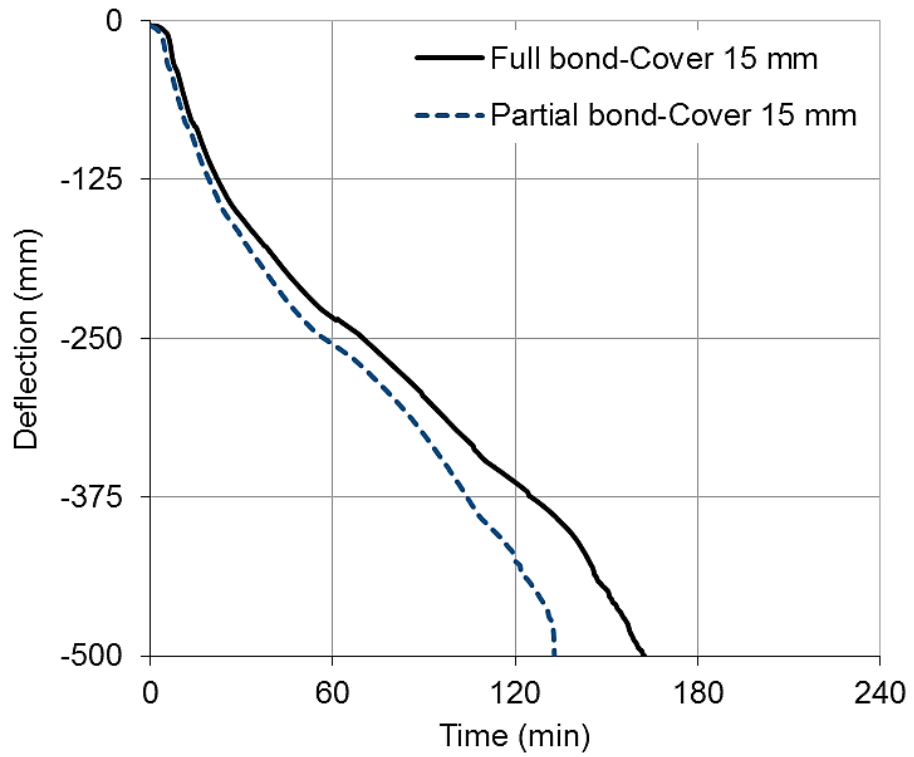


Figure 5.34 Comparison of the central deflections of the slab modelled as full bond or partial bond using concrete cover of 15 mm

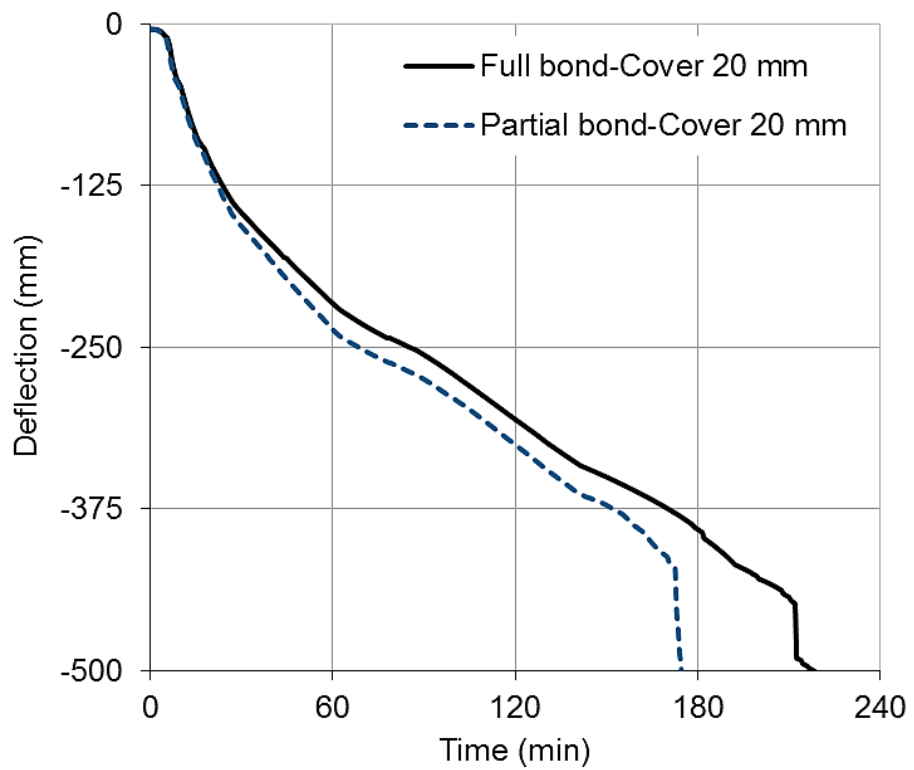


Figure 5.35 Comparison of the central deflections of the slab modelled as full bond or partial bond using concrete cover of 20 mm

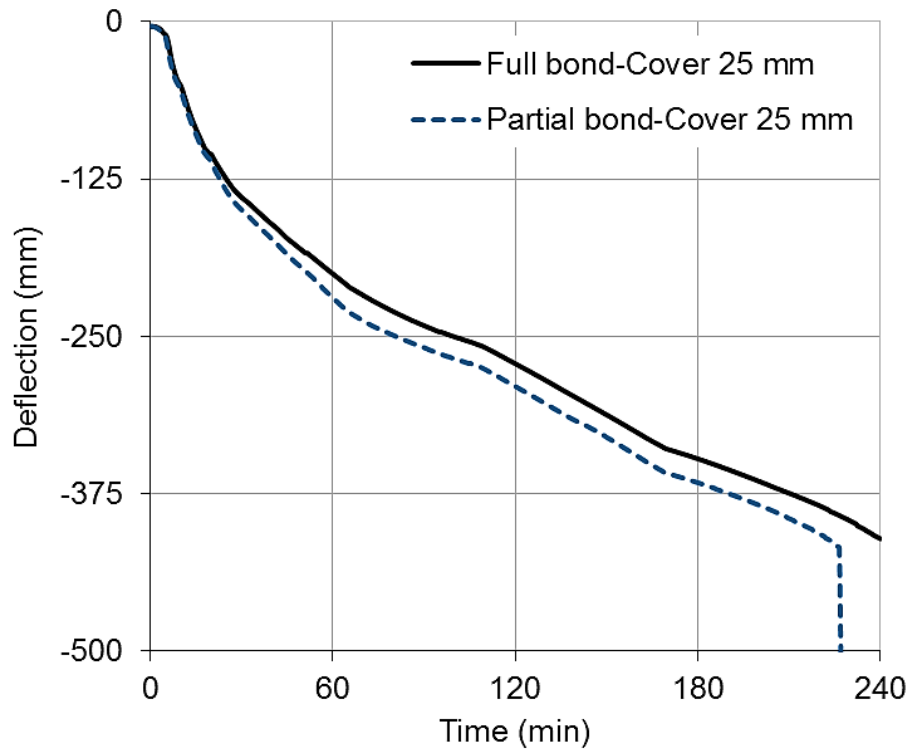


Figure 5.36 Comparison of the central deflections of the slab modelled as full bond or partial bond using concrete cover of 25 mm

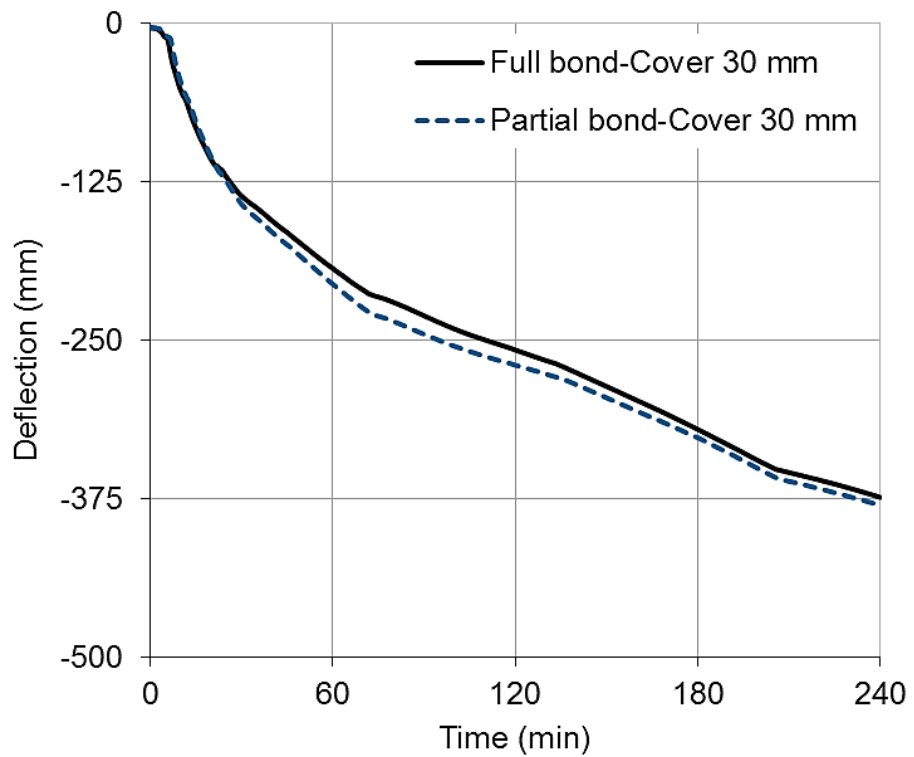


Figure 5.37 Comparison of the central deflections of the slab modelled as full bond or partial bond using concrete cover of 30 mm

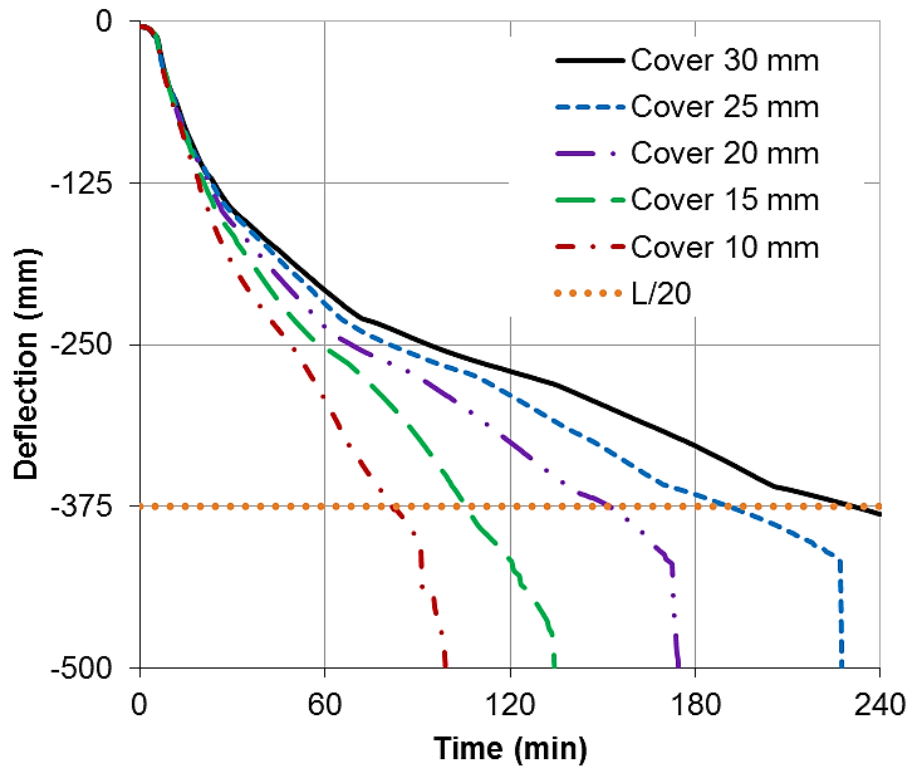


Figure 5.38 Influence of different concrete covers on the central deflections of the slab modelled as partial bond

5.4.2 The effect of concrete strength on the behaviour of the slab

To investigate the influence of concrete strength on the behaviour of the slab, the same isolated slab with concrete cover of 30 mm and steel bars yielding strength of 460 MPa was used. Four values of concrete compressive strength (20, 30, 40 and 45 MPa) were adopted in this study. The temperature history of the reinforcing steel bars mesh within the slab is shown in Figure 5.39.

The effect of concrete compressive strength on the response of the slab is shown in Figures 5.40 to 5.43. It can be seen from the figures that there was no great influence when the compressive strength was more than 40 MPa. However, the slab failed earlier when the compressive strength was less than 30 MPa. Generally, the effects of concrete compressive strengths on the behaviours of the slab were not significant, as shown in Figure 5.44.

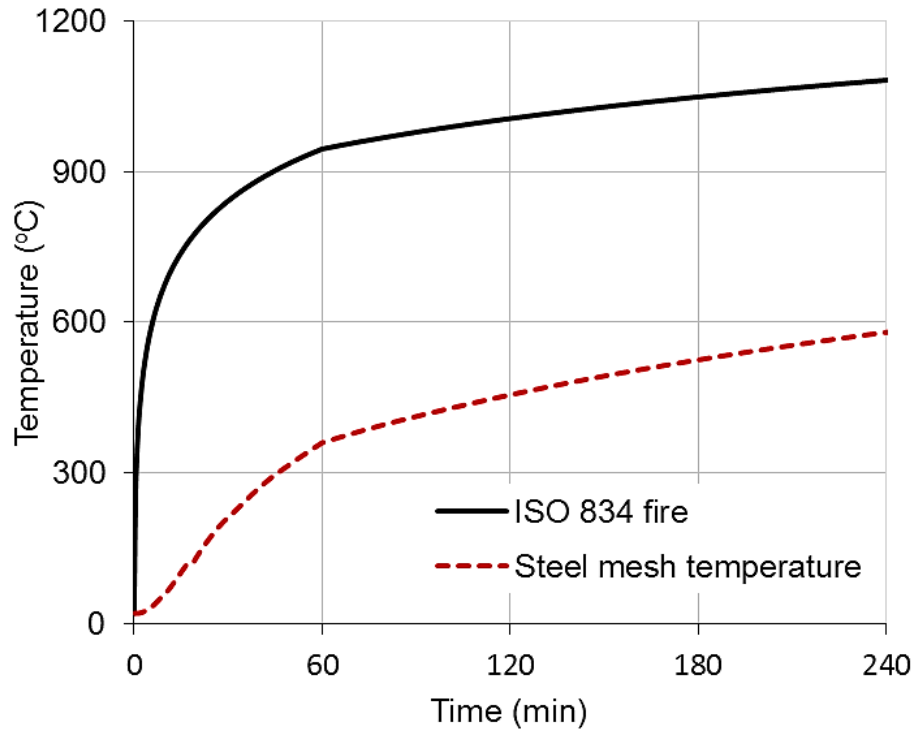


Figure 5.39 Time-temperature history of the reinforcing steel bars within the slab exposed to ISO 834 fire

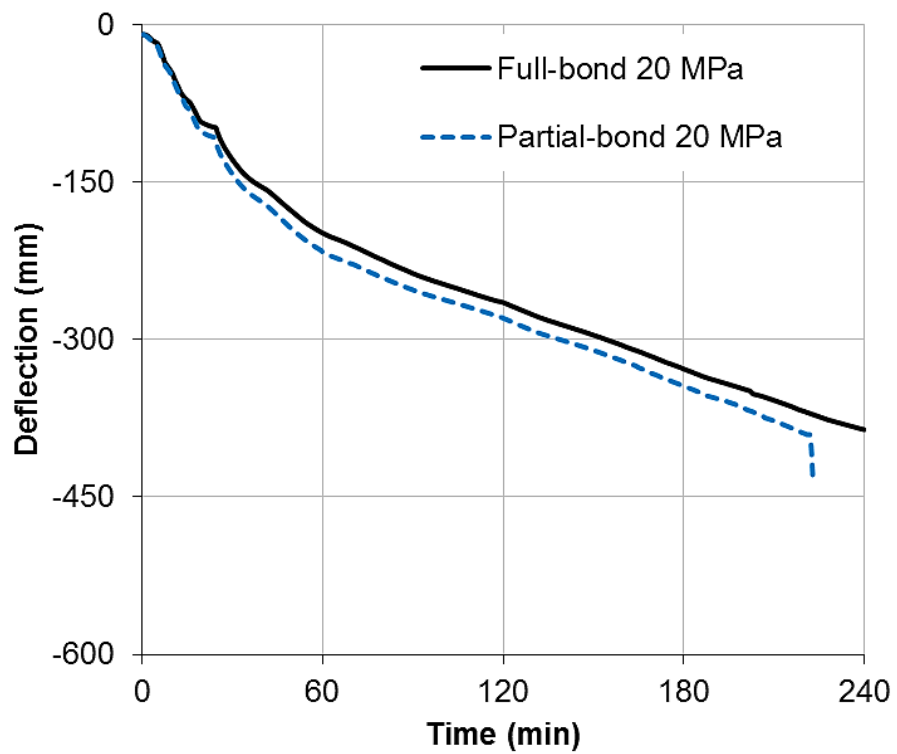


Figure 5.40 Comparison of the central deflections of the slab modelled as full bond or partial bond using concrete compressive strength of 20MPa

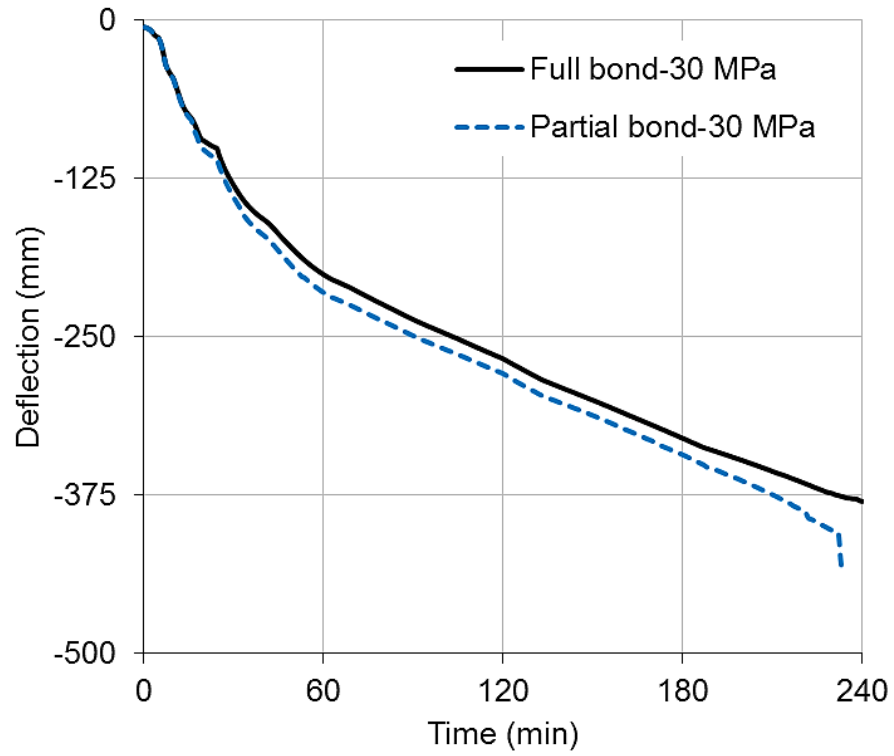


Figure 5.41 Comparison of the central deflections of the slab modelled as full bond or partial bond using concrete compressive strength of 30MPa

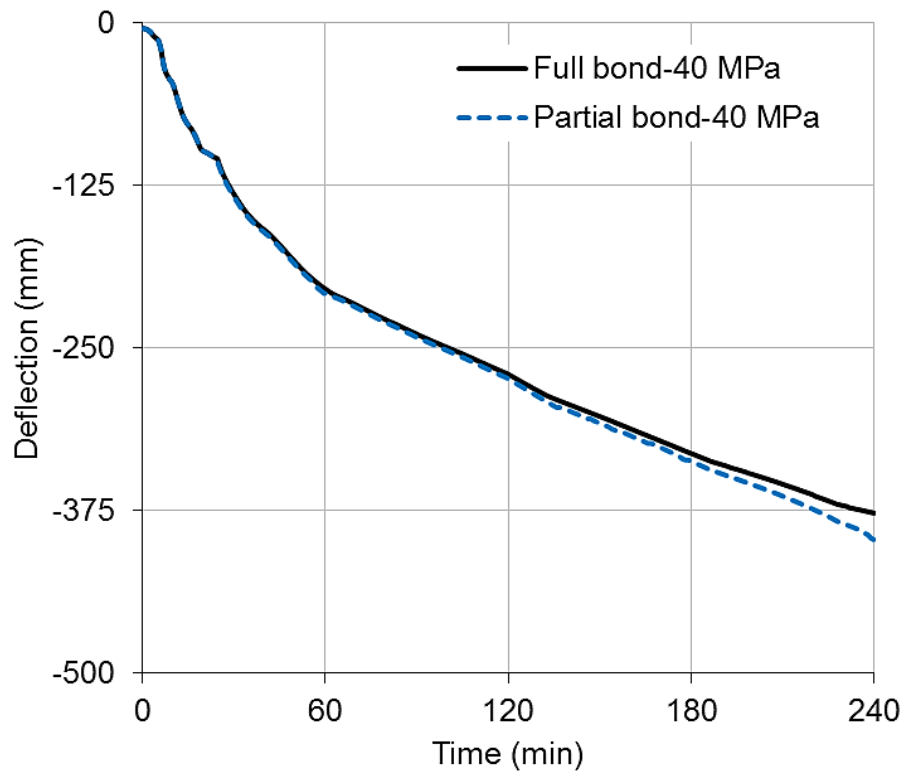


Figure 5.42 Comparison of the central deflections of the slab modelled as full bond or partial bond using concrete compressive strength of 40MPa

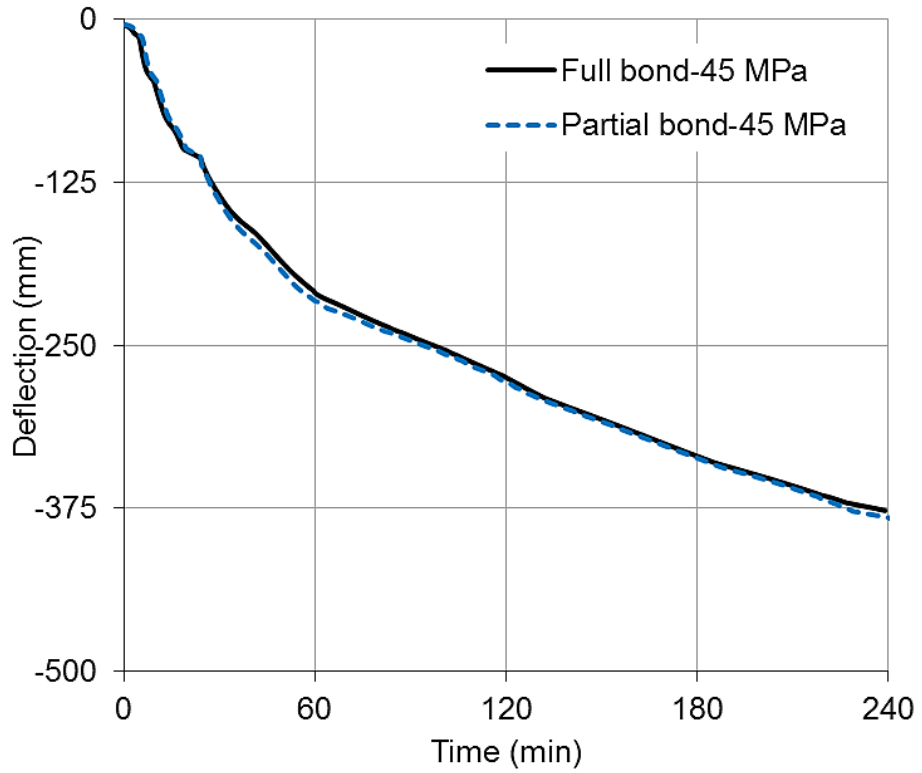


Figure 5.43 Comparison of the central deflections of the slab modelled as full bond or partial bond using concrete compressive strength of 45MPa

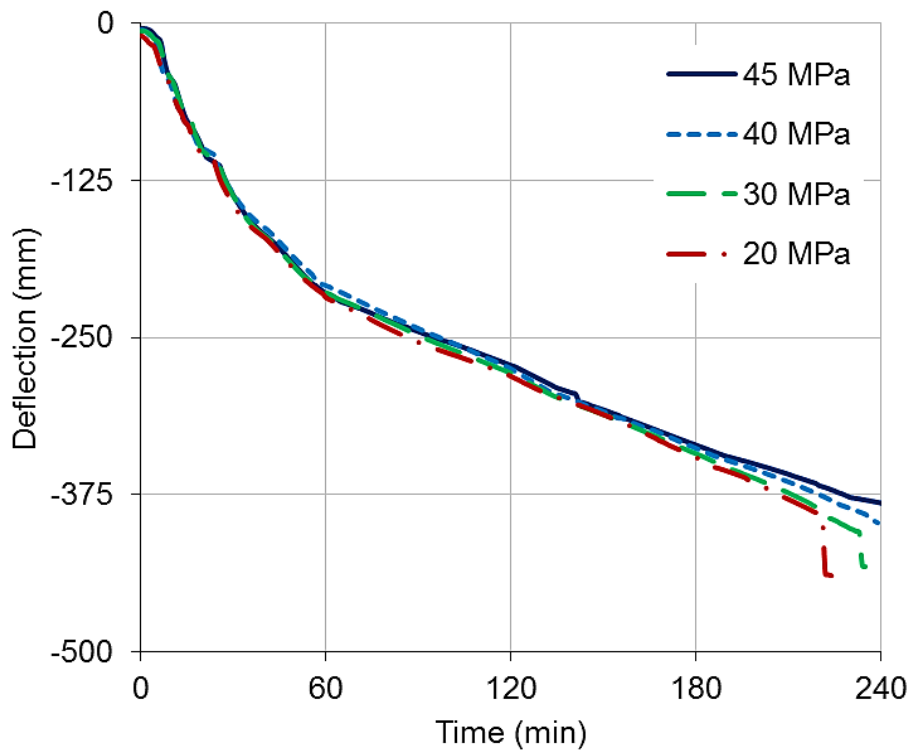


Figure 5.44 Influence of different concrete strengths on the central deflections of the slab modelled as partial bond

5.5 Modelling of reinforced concrete frame structure in fire

After conducting the studies on the behaviour of individual reinforced concrete members at elevated temperatures, it is important to investigate behaviour of these members within a building. The structural members within a real building behave differently compared to the isolated members. Fire in a building is normally localised in the areas called fire compartments. These fire compartments are surrounded by the cooling regions. The surrounding cooling structures can provide a considerable restraint to the members that effected by the fire. The behaviours of these members are influenced by the locations of the members within the building. Using isolated member subjected to standard fire curve gives the upper and lower limits of the member, but does not give the real behaviour of the member within the building.

Therefore, in this section a 3D reinforced concrete frame with floor slabs was modelled under different fire scenarios. It was assumed that concrete compressive strength was 45 MPa and the yield strength of the steel bar was 460 MPa. The details of the whole floor were shown in Figure 5.1. The same beam shown in Figure 5.3 and Figure 5.4, and the same slab shown in Figure 5.30 and 5.31 were used. The concrete cover of the beam was 30 mm, while the concrete covers of the slab and column were 25 mm. Due to very high computational power demanded, the frame was modelled using only full bond between concrete and reinforcement.

As shown in Figure 5.45, a quarter of the floor was modelled due to symmetry in this study. For the first case, it was assumed that the whole floor of the building was engulfed by ISO 834 standard fire. Figure 5.46 shows the deflections at positions a, b, and c (see Figure 5.45). It can be seen from the figure that the deflections at three positions of the floor slabs were approximately similar with little less deflection at position b. This is due to the continuity of the slabs and the restraint provided by some columns.

In order to investigate the influence of different locations of fire compartments on the structural behaviour of floor slabs. Six locations of fire compartments were investigated in this study. Figure 5.45 gives the locations of the fire compartments which were identified as FC-1, FC-2, FC-3, FC-4, FC-5 and FC-6. Only one fire compartment was exposed to ISO 834 standard fire while the rest of the structure

was assumed to be at ambient temperature. Figure 5.47 gives the central deflections of the floor slabs for different fire compartments. It can be seen from the figure that the lowest central deflection was the fire compartment FC-3 and highest central deflection was the fire compartment FC-1. The central deflections of the fire compartments FC-2 and FC-6 were similar. Also there were similar central deflections for the fire compartments FC-4 and FC-5.

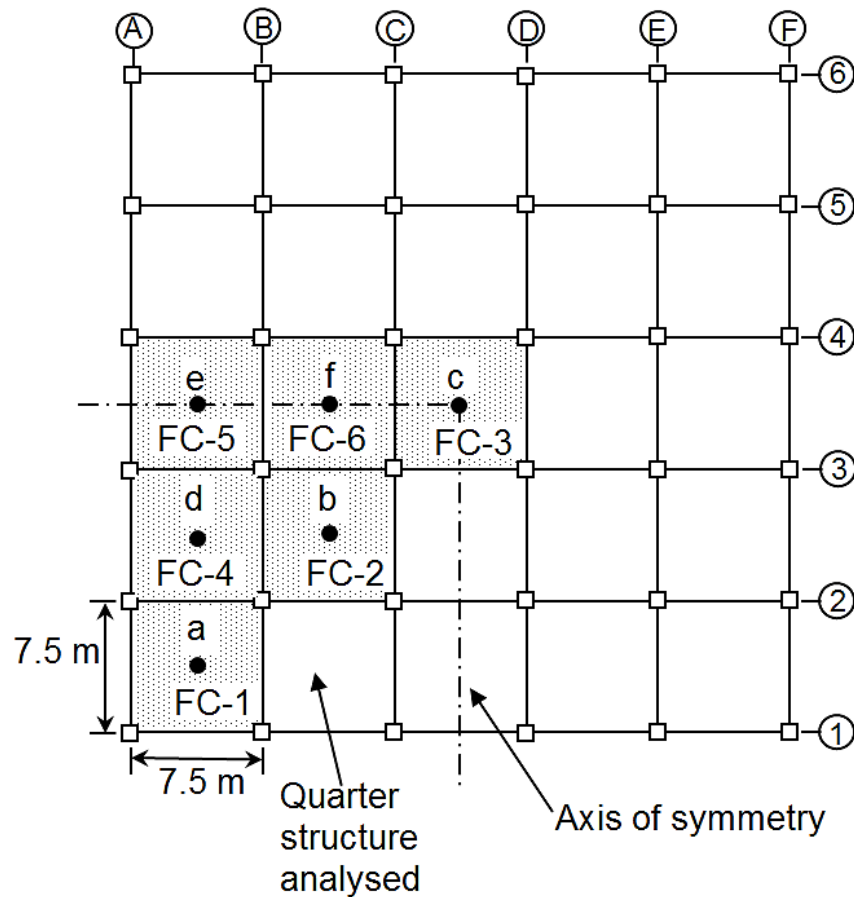


Figure 5.45 Floor layout of the building with different locations of the fire compartments

From this study it is clear that restraint provided by the cool structures surrounding the fire compartment has a positive effect on the fire resistance of the structural members within the fire compartment. The compressive membrane action may play important role to enhance the loading capacity of the floor slabs within the fire compartment. Figures 5.48 to 5.50 show the comparisons of the deflections at three locations for compartment fire and whole floor fire, together with the central deflection of isolated simply supported slab. It is evident from the figures that the deflections of the slabs subjected to whole floor fire were greater than the deflections of the slabs under compartment fires. This is because under whole floor fire only

very limited restraint was provided by columns for the floor slabs. It is also clear that the behaviour of isolated simply supported slab was considerably different with the slab within the structures.

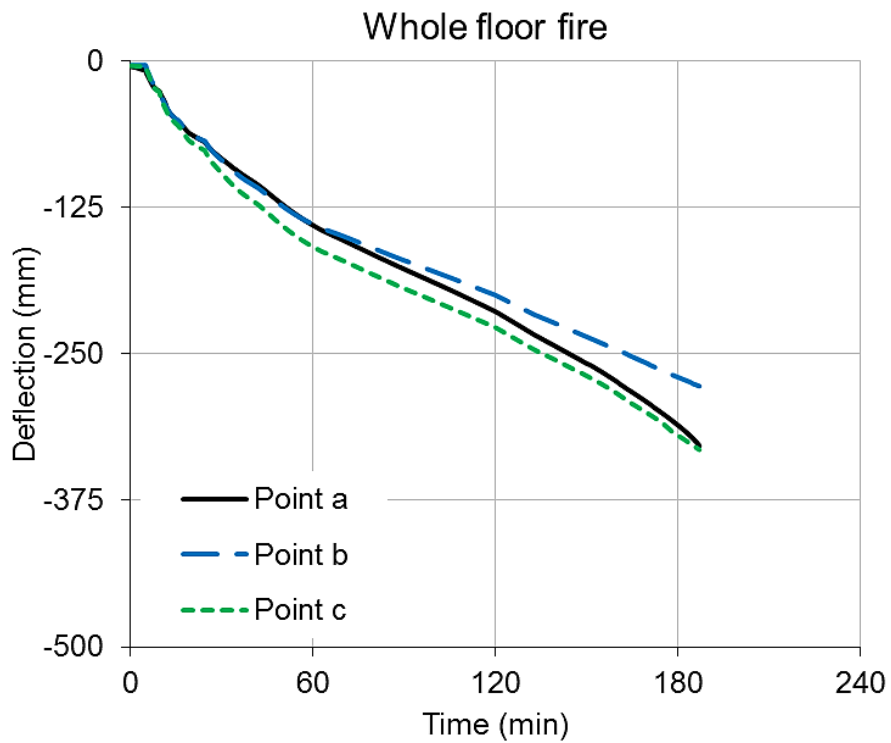


Figure 5.46 The deflections of the floor slabs at the position a, b and c under whole floor fire

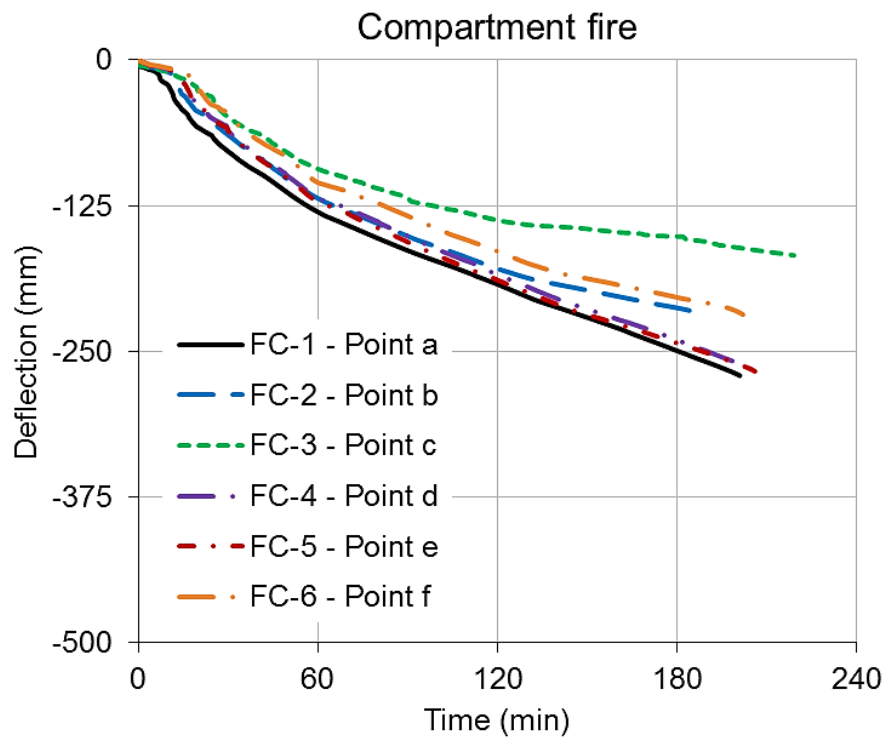


Figure 5.47 Comparison of the central deflections of the floor slabs for different fire compartments

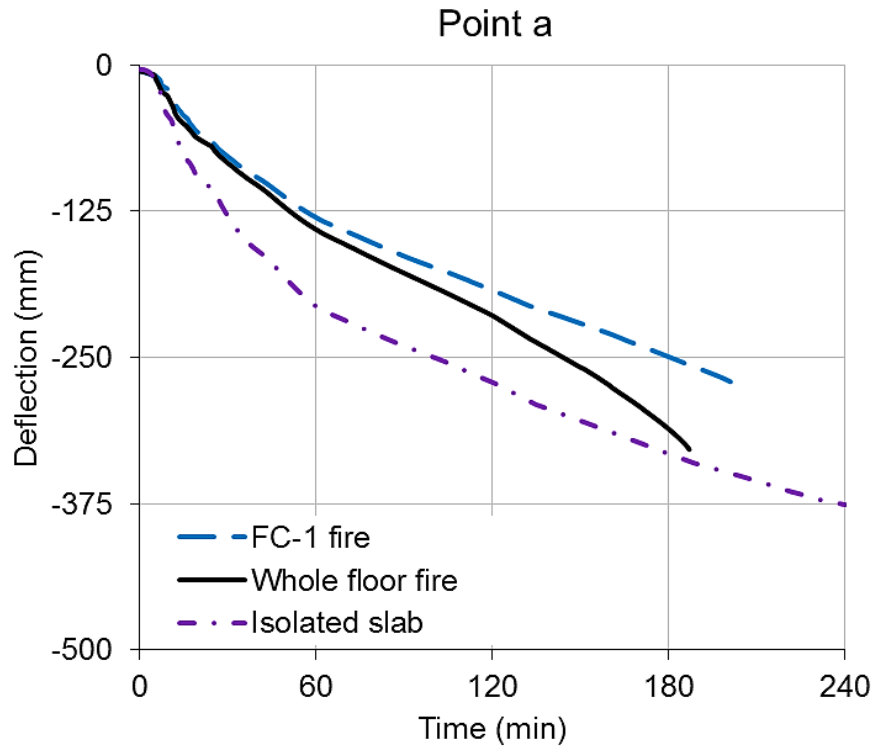


Figure 5.48 Comparison of the deflections at Position a for compartment fire FC-1 and whole floor fire, together with the central deflection of isolated simply supported slab.

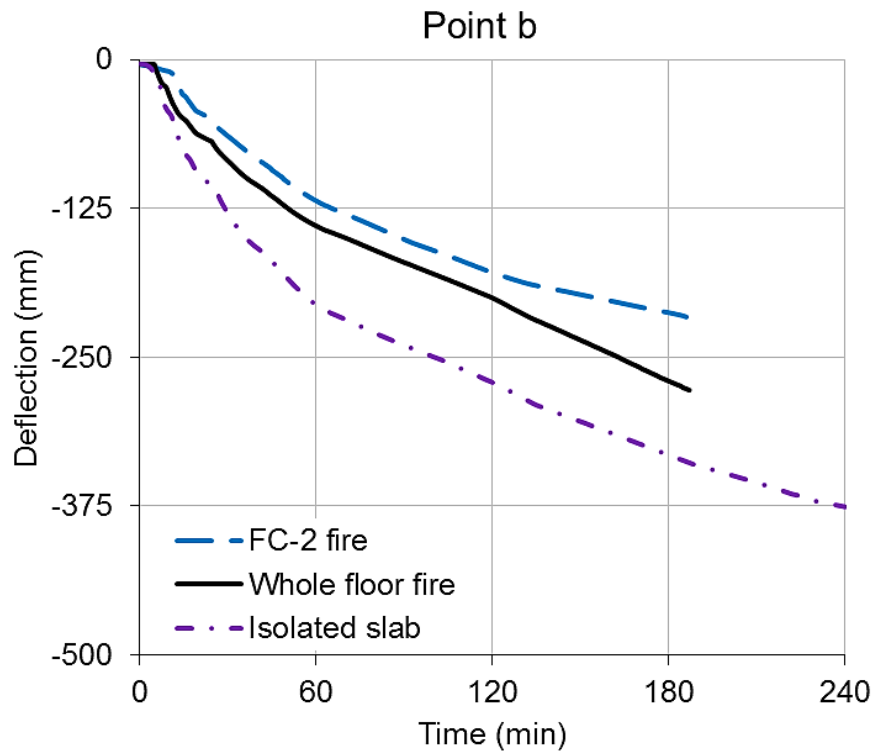


Figure 5.49 Comparison of the deflections at Position b for compartment fire FC-2 and whole floor fire, together with the central deflection of isolated simply supported slab.

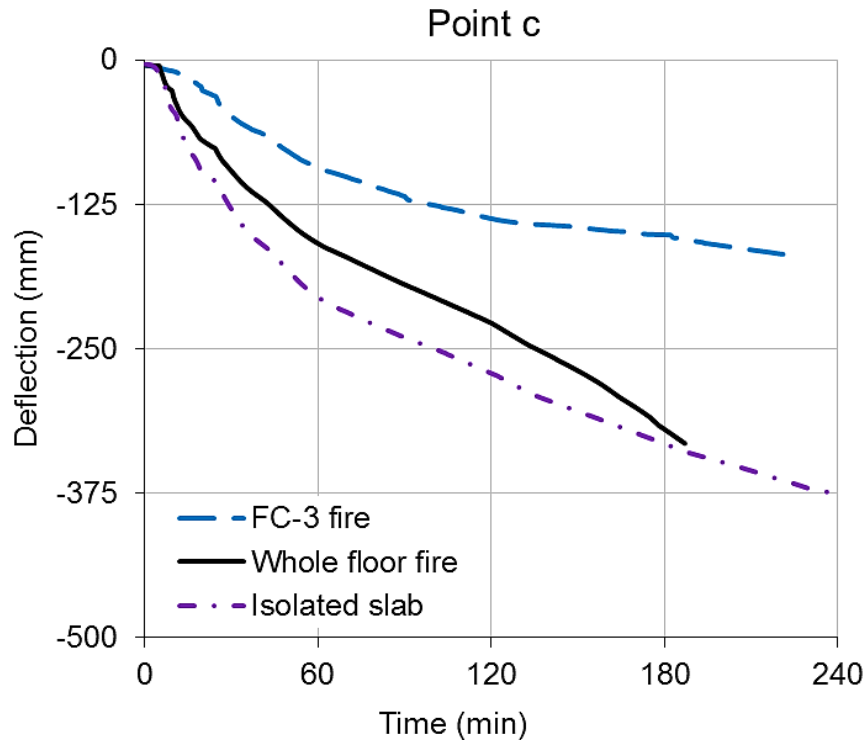


Figure 5.50 Comparison of the deflections at Position a for compartment fire FC-3 and whole floor fire, together with the central deflection of isolated simply supported slab.

5.6 Conclusions

In this chapter a parametric study has been conducted to investigate the effect the bond characteristic between concrete and steel reinforcement on behaviours of isolated simply supported reinforced concrete beams and slabs. Also a 3D reinforced concrete frame has been modelled under different fire scenarios. Based on the results some conclusions can be drawn as:

- The yielding effect of the steel bar has some degrees of influence on the bond behaviour of reinforced concrete beam. The yielding effect of steel bar can reduce the bond strength between concrete and steel bar within a beam, but the influence is not significant.
- The concrete cover has a great influence on the bond strength by providing the confinement to the reinforcement for both reinforced concrete beam and slab. Hence, reduce the concrete cover is not only leads to increase the temperature of the reinforcement during fire, but also decreases the concrete confinement which can play a significant factor on the bond strength.

- The impact of concrete spalling on the beam is very significant for both full bond and partial bond cases. However, the effect of spalling on the beam modelled with partial bond is greater than that modelled with full bond.
- For reinforced concrete beam it is clear that when the concrete compressive strength is more than 40 MPa, there is no significant effect on the bond behaviour. And the behaviour of the beam modelled with full or partial bond is similar. However, great influence can be observed when the concrete compressive strength is less than 40 MPa. This behaviour can be attributed to the considerable degradation of the bond strength. The influence of concrete compressive strength on the slab is less significant.
- The results generated from 3D modelling of concrete frame indicate that restraint provided by the cool structures surrounding the fire compartment has a positive effect on the fire resistance of the structural members within the fire compartment. The compressive membrane action may play important role to enhance the loading capacity of the floor slabs within the fire compartment. It is also clear that the behaviour of isolated simply supported slab was considerably different with the slab within the structures.

Chapter 6 Conclusions and recommendations for future works

For the last two decades considerable progress has seen made on our understanding of reinforced concrete structures under fire conditions. It is well known that the bond behaviours between concrete and reinforcing steel bars or strands have significant influences on the behaviours of reinforced concrete and prestressed concrete members. Conventionally, design of reinforced concrete structure is based on the assumption of the strain compatibility between concrete and steel bars. This assumption requires a good bond between concrete and steel bars. Current research indicates that bond strength between concrete and steel reinforcement plays an important role for assessing the fire resistance of reinforced concrete and prestressed concrete structures. The robustness of bounds is therefore vitally important to the fire resistance of reinforced concrete buildings. The development of effective bond models is a key issue in this research field. The PhD research reported here focused specifically on the development of robust models for modelling the bond characteristics between concrete and reinforcing steel or strands at elevated temperatures.

6.1 Summary of thesis contributions

6.1.1 Development of a robust model to simulate the bond stress-slip between concrete and steel bars at elevated temperatures

The first contribution of this PhD research is to develop a new model for predicting the bond stress-slip between concrete and reinforcing steel bars at elevated temperatures. The model is based on the thick-wall cylinder theory with considering of partially cracked concrete cover. In this model the smeared crack approach for concrete in tension is adopted. Hence, the model can take into account the splitting failure of the concrete cover. The degradation of the bond strength at elevated temperatures is related to the concrete material properties changed with temperatures.

The developed bond stress-slip model has been incorporated into VULCAN software using the two-node bond-link element approach for considering the influence of

bond characteristic on structural behaviours of reinforced concrete structural members at elevated temperatures. A series of validations have been conducted using the previous tested results generated by different researchers. Reasonable agreements have been achieved between the predicted results from the model and the experimental data.

6.1.2 Development of a new model to simulate bond stress-slip between the concrete and prestressed strands in fire

The second contribution of this PhD research is to develop a robust model to simulate the bond stress-slip between concrete and strands for prestressed concrete structures at elevated temperatures. The model was based on the mechanical interlocking between prestressing steel strands and surrounding concrete as well as considering the effect of Poisson's ratio (Hoyer effect). The model takes into account the variation of the concrete properties and strands' geometries, as well as effect of the cohesion and friction between the strands and concrete. The degradation of the bond strength at elevated temperatures is related to the concrete material properties changed with temperature.

The developed bond stress-slip model has been incorporated into the VULCAN software by using two-node bond-link element approach for analysing the structural behaviours of prestressed concrete structural members in fire. A series of validations have been conducted using the previous tested data. Reasonable agreements have been achieved between the predicted results from the model in comparison with the tests results.

6.1.3 Parametric study on the bond behaviour at elevated temperatures

The third contribution of this PhD research is to conduct a series of comprehensive parametric studies for investigating the influence of the bond stress-slip on the response of reinforced concrete beam and slab members under fire conditions. The main factors, which effect on the bond stress-slip behaviour, have been identified. These factors are: reinforcing steel bars' yielding, the thickness of concrete cover, concrete compressive strength and concrete spalling. Also a 3D reinforced concrete frame has been modelled under different fire scenarios. The behaviours of the

reinforced concrete structural members within a whole building have been compared to the behaviours of isolated members under the same fire conditions. Some interesting results have been generated.

6.2 Conclusions

Based on the validations of the developed bond models, the numerical studies, and a series of comprehensive parametric studies for investigating the influence of the bond stress-slip on the behaviour of reinforced concrete beam and slab members under fire conditions, the following conclusions can be drawn:

- (1) The validation results of the bond model for simulating the interaction between concrete and reinforcing steel bars show good agreement between the model predictions and experimental data. The developed model is able to predict the bond-slip characteristic between the concrete and reinforcing steel bar at elevated temperatures. The model takes into account the variation of concrete properties, concrete covers and the geometries of rebar.
- (2) The validation results of the bond model for predicting the bond stress-slip between strands and concrete for prestressed concrete members under fire conditions show reasonable agreements between the predicted results and tests results. The model is able to predict the bond-slip characteristic between the concrete and strands for three-wire and seven-wire strands at elevated temperatures. This model can be used to calculate the bond-slip for the transfer length (push-in bond) and flexural length (pull-out bond) within the prestressed concrete members. Also, the model is able to take into account different strand's diameters and different strand's surfaces (smooth or indented).
- (3) The research indicated that the strength of the bond between concrete and reinforcing steel bars plays a very important role that can affect the fire resistance of reinforced concrete structures, especially when the temperature of the reinforcing steel bar is high (more than 400 °C). Therefore, the assumption of the perfect bond condition for the analysis of reinforced concrete structures under fire conditions is un-conservative.
- (4) The yielding effect of the steel bar has some degrees of influence on the bond behaviour of reinforced concrete beam. The yielding effect of steel bar can

reduce the bond strength between concrete and steel bar within a beam, but the influence is not significant.

- (5) The concrete cover has a great influence on the bond strength by providing the confinement to the reinforcement for both reinforced concrete beam and slab. Hence, reduce the concrete cover is not only leads to increase the temperature of the reinforcement during fire, but also decreases the concrete confinement which can play a significant role on the bond strength.
- (6) The impact of concrete spalling on the beam is very significant for modelling both full bond and partial bond cases. However, the effect of spalling on the beam modelled with partial bond is greater than that modelled with full bond.
- (7) For reinforced concrete beam it is clear that when the concrete compressive strength is more than 40 MPa, there is no significant effect on the bond behaviour. And the behaviour of the beam modelled with full or partial bond is similar. However, great influence can be observed when the concrete compressive strength is less than 40 MPa. This behaviour can be attributed to the considerable degradation of the bond strength. The influence of concrete compressive strength on the slab is less significant.
- (8) The results generated from 3D modelling of concrete frame indicate that restraint provided by the cool structures surrounding the fire compartment has a positive effect on the fire resistance of the structural members within that fire compartment. The compressive membrane action may play important role to enhance the loading capacity of the floor slabs within the fire compartment. It is also clear that the behaviour of isolated simply supported slab was considerably different with the slab within the structures.

6.3 Recommendations for future studies

It is clear from this PhD research that there are questions to be addressed, regarding the behaviour of bond characteristics between concrete and steel bars or prestressed strands at elevated temperatures. In summary, it is recommended that the following areas should be considered for further works:

- (1) The developed models in this research consider monotonic loading conditions only. However, the frame works of the current proposed models can be further extended and developed to consider cyclic loading conditions

for the bond stress-slip of reinforced concrete and prestressed concrete structures subjected to dynamic or seismic loading conditions.

- (2) Experimental data on the bond behaviours of reinforced concrete and prestressed concrete members at elevated temperatures are still very limited. An extension of research to produce more test data is necessary for the validations and improvements of proposed models.
- (3) In this research the developed models only consider the confinement influence of concrete cover. However, the models can be further improved to take into account the confinement provided by stirrups or shear steels.
- (4) More experiments are needed to assess the influences of different concrete covers, different concrete compressive strengths. The further tested data can be used to compare the results generated from the parametric studies using current models.
- (5) Further numerical study is needed to investigate the bond behaviours of beam and slab members within the large frame structures under different fire conditions.

REFERENCES

- Abrishami, H. & Mitchell, D., (1993). Bond characteristic of pretensioned strand. *ACI Materials Journal*, 90(3), pp. 228-235.
- Arioz, O., (2007). Effects of elevated temperatures on properties of concrete. *Fire Safety Journal*, Volume 42, pp. 516-522.
- ASHI Reporter, (2007). *The effects of fire on structural systems*, s.l.: American Society of Home Inspectors.
- Aslani, F. & Bastami, M., (2011). Constitutive Relationships for Normal-and High-Strength Concrete at Elevated Temperatures. *ACI Material Journal*, 108(4), pp. 355-364.
- ASTM E119, (2000). *Standard test methods for fire tests of building construction and materials*. United States: ASTM Committee E05.
- Badiger, N. & Malipatil, K., (2014). Parametric Study on Reinforced Concrete Beam using ANSYS. *Civil and Environmental Research*, 6(8), pp. 88-94.
- Bailey , C., (2002). Holistic behaviour of concrete buildings in fire. *Proceedings of the ICE, Structures and Buildings*, 152(3), pp. 199-212.
- Bailey, C. & Ellobody, E., (2009). Fire tests on bonded post-tensioned concrete slabs. *Engineering Structures*, Volume 31, p. 686–696..
- Barzegar, J. F. & Schnobrich, W., (1986). *Nonlinear Finite Element Analysis of Reinforced Concrete Under Short Term Monatomic Loading*, s.l.: A report on a research project, University of Illinois at Urbana-Champaign, research series No.530.
- Bazant, z. & Kaplan, M., (1996). *Concrete at high temperatures*, s.l.: Longman Group.
- Benitez, J. & Galvez, J., (2011). Bond modelling of prestressed concrete during the prestressing force release. *Materials and Structures*, Volume 44, pp. 263-278.
- BIGAJ A. J., (1999). *Structural dependence of rotation capacity of plastic hinges in rc beams and slabs*, s.l.: s.n.

- Bisby, L., (2012). *Opportunities for performance-based fire resistance design of frp reinforced concrete slabs*, Edinburgh: BRE Centre for Fire Safety Engineering, The University of Edinburgh.
- Bizri, H., (1973). *Structural capacity of reinforced concrete columns subjected to fire induced thermal gradients*, Berkeley,: Structural Engineering Laboratory, Report No. 73-1, University of California,.
- Bolmsvik, R. & Lundgren, K., (2006). Modelling of bond between three-wire strands and concrete. *Magazine of Concrete Research*, 58(3), pp. 123-133.
- Bowden, . F. P., Moore, A. & Tabor, D., (1942). *The ploughing and adhesion of sliding metals*, s.l.: Council for scientific and industrial research, Bulletin no. 145.
- Brown, C. J., Darwin, D. & McCabe, S. L., (1993). *Finite Element Fracture Analysis of Steel-Concrete Bond*, Kansas: SM Report No. 36, University of Kansas Center for Research.
- Burkan, O. & Ghani, A., (2004). Finite element modeling of coupled heat transfer, moisture transport and carbonation processes in concrete structures. *Cement & Concrete Composites*, Volume 26, pp. 57-73.
- Burns, N. & Siess, C. P., (1962). *Load-deformation characteristics of beam-column connections in reinforced concrete*, Urbana: Civil engineering Studies SRS No.234, University of Illinois.
- CEB-FIP Model code 90, (1991). s.l.:Final draft ,Committe euro-international du beton. Bulletin d'information No.203-205.
- CEB-FIP, 2010. *CEB-FIP Model code (2010)*. First complete draft ed. s.l.:International Federation for Structural Concrete.
- CEB-FIP-Bulletin10, (2000). *Bond of Reinforcement in Concrete*. s.l.:s.n.
- CEN EUROPEAN STANDARD, (2004). *Eurocode 2: Design of concrete structures - Part 1-1 : General rules and rules for buildings*. London: British Standards Institution.
- CEN, (2002). *Eurocode 1: Actions on structures-Part 1-2 General actions – Actions on structures exposed to fire*. s.l.:BS EN 1991-1-2:2002.

CEN, (2004a). *Eurocode 2: Design of concrete structures - Part 1-2: General rules - Structural fire design*. London: BS EN 1992-1-2.

CEN, (2004b). *Design of concrete structures. Part 1.1: general rules and rules for buildings*. London: BS EN 1992-1-1.

Choi O.C. and Yang S.Y., (2010). Bond analysis model of deformed bars to concrete. *Fracture Mechanics of Concrete and Concrete Structures -Assessment, Durability, Monitoring and Retrofitting of Concrete Structures- B. H. Oh, et al. (eds), Korea Concrete Institute, Seoul, ISBN 978-89-5708-181-5.*

Choi, O., Choi, H. & Hong, G., (2010). *Bearing angle model for bond of reinforcing bars to concrete*, Seoul: Korea Concrete Institute, ISBN 978-89-5708-181-5.

Cowen, . H. S. & VanHorn, A. D., (1967). *End support on ultimate flexural bond in pre-tensioned beams.*, Pennsylvania: Bond in prestressed concrete progress report No. 3, Fritz engineering laboratory, Department of civil engineering, Lehigh University, Bethlehem.

Curtis, D., (2011). *Estimated shear strength of shear keys and bonded joints in concrete dams*. San Diego, California, 31st Annual USSD Conference.

Diederichs , U. & Schneider, U., (1981). Bond strength at high temperatures. *Magazine of concrete research*, 33(115), pp. 75-84.

Dzhafarov, Y. & Rozhenko, A. F., (1968). Effect of temperature on the friction characteristics of composite materials. *Institute of Materials Science* , 10(70), pp. 80-84..

Elghazouli, A., Cashell, K. & Izzuddin, B., (2009). Experimental evaluation of the mechanical properties of steel reinforcement at elevated temperature. *FireSafetyJournal*, Volume 44, p. 909–919.

Ervine, A., (2012). *Damaged reinforced concrete structures in fire*, s.l.: PhD thesis, University of Edinburgh.

Eunsoo Ch., Young-Soo Ch., Yeon-Wook K. and Joo-Woo K., (2010). Monotonic and cyclic bond behavior of confined concrete using NiTiNb SMA wires. *SMART MATERIALS AND STRUCTURES*, Volume 20.

Fellinger, J., Stark, J. & Walraven, J., (2003). *Bond model for prestressed strands in fire exposed concrete*. Reston, AV, American Society of Civil Engineers.

Fib Bulletin 46, (2008). *Fire Design of Concrete Structures-Structural Behaviour and Assessment*. s.l.: fib Fédération internationale du béton - Building, Fireproof.

Fu Y.F, Wong Y.L., Tang C.A. and Poon C.S., (2004). Thermal induced stress and associated cracking in cement-based composite at elevated temperatures—Part I: Thermal cracking around single inclusion. *Cement & Concrete Composites* , Volume 26, pp. 99-111.

Galvez , J. et al., (2009). Splitting failure of precast prestressed concrete during the release of the prestressing force. *Engineering Failure Analysis* , Volume 16, p. 2618–2634.

Gao, W., Jian-Guo Dai, J., Teng, J. & Chen, G., (2013). Finite element modeling of reinforced concrete beams exposed to fire. *Engineering Structures*, Volume 52, p. 488–501.

George S. and Mario B., (2010). Rebar pullout testing under dynamic Hopkinson bar induced impulsive loading. *Materials and Structures*, Volume 43, pp. 247-260.

Goto, Y., (1971). Cracks formed in concrete around deformed tension bars. *ACI-Journal*, pp. 244-251.

Griffin, B. & Beavis, M., (1992). *Fire resistance of prestressed concrete*, s.l.: University of Canterbury.

Gustavson, R., (2004). Experimental studies of the bond response of three-wire strands and some influencing parameters. *Materials and Structures*, Volume 37, pp. 96-106.

Haddad , R., Al-Saleh , R. & Al-Akhras, N., (2008). Effect of elevated temperature on bond between steel reinforcement and fiber reinforced concrete. *Fire Safety Journal*, Volume 43, pp. 334-343.

Haddad, R. & Shannis, L., (2004). Post-fire behavior of bond between high strength pozzolanic concrete and reinforcing steel. *Construction and Building Materials*, Volume 18, pp. 425-435.

- Hertz, K., (1982). The anchorage capacity of reinforcing bars at normal and high temperatures. *Magazine of Concrete Research*, Volume 34, pp. 213-220.
- Hou, X., Kodur, V. & Zheng, W., (2015). Factors governing the fire response of bonded prestressed concrete continuous beams. *Materials and Structures*, 48(9), pp. 2885-2900.
- Huang, Z., (1995). *The analysis of thermal and fire performance of cementitious building components*, s.l.: PhD Thesis, University of Central Lancashire.
- Huang, Z., (2010). Modelling of reinforced concrete structures in fire. *Engineering and Computational Mechanics*, Volume 163, pp. 43-53.
- Huang, Z., (2010). Modelling the bond between concrete and reinforcing steel in fire. *Engineering Structures*, Volume 32, pp. 3660-3669.
- Huang, Z., Burgess, I. & Plank, R., (2003b). Modelling membrane action of concrete slabs in composite buildings in fire. Part II: validations.. *Journal of Structural Engineering*, 129(8), pp. 1103-1112.
- Huang, Z., Burgess, I. & Plank, R., (2007). *Three-dimensional analysis of reinforced concrete beam-column structures in fire*, Sheffield: Department of Civil and Structural Engineering, University of Sheffield. Research Report DCSE/07/F/4..
- Huang, Z., Burgess, I. & Plank, R., (2009). Three-dimensional analysis of reinforced concrete beam-column structures in fire. *Journal of Structural Engineering, ASCE*, 135(10), p. 1201–1212.
- Huang, Z., Burgess, I. W. & Plank, R. J., (1999). Nonlinear analysis of reinforced concrete slabs subjected to fire. *ACI Structural Journal*, 96(1), pp. 127-135.
- Huang, Z., Burgess, I. W. & Plank, R. J., (2003a). Modelling membrane action of concrete slabs in composite buildings in fire. Part I: Theoretical development. *JOURNAL OF STRUCTURAL ENGINEERING*, 129(3), pp. 1093-1102.
- Huang, Z., Platten, A. & Roberts, J., (1996). Non-linear finite element model to predict temperature histories within reinforced concrete in fires. *Building and Environment*, 31(2), pp. 109-118.
- Huanzi, W., (2009). An analytical study of bond strength associated with splitting of concrete cover. *Engineering Structures*, Volume 31, pp. 968-975.

ISO-834, (1975). *Fire resistance test, elements of building constructions*. s.l.:International Standard ISO 834..

John Robert Prince M. and Bhupinder S., (2013). Bond behaviour of deformed steel bars embedded in recycled aggregate concrete. *Construction and Building Materials*, Volume 49, p. 852–862.

Kodur, V. & Shakya, A., (2014). Modeling of the response of precast prestressed concrete hollow-core slabs exposed to fire. *PCI Journal* , 59(3), pp. 78-94.

Kodur, V., (2014). *Properties of concrete at elevated temperatures*, s.l.: Hindawi Publishing Corporation,ISRN Civil Engineering,Article ID 468510.

Kumar, M. & Paulo, J., (2006). *Concrete microstructure, properties and materials*. Third Edition ed. United States: McGraw-Hill.

Kumar, V., Sharma, U., Singh, B. & Bhargava, P., (2013). Effect of temperature on mechanical properties of pre-damaged steel reinforcing bars. *Construction and Building Materials*, Volume 46, pp. 19-27.

Law, A., (2016). The role of modelling in structural fire engineering design. *Fire Safety Journal*, Volume 80, p. 89–94.

Lee, H. & Noguchi, T., (2002). Evaluation of the bond properties between concrete and reinforcement as a function of the degree of reinforcement corrosion. *Cement and Concrete Research*, Volume 32, p. 1313–1318.

Legeron, F., Paultre, P. & Mazars, J., (2005). Damage mechanics modelling of nonlinear seismic behaviour of concrete structures. *Journal of Structural Engineering*, 131(6), pp. 946-955.

Lin, S., (2014). *Development of robust connection models for steel and composite structures in fire*, s.l.: PhD Thesis, Brunel University London.

Lin, T., Ellingwood, B. & Piet , O., (1987). *Flexural and shear behaviour of reinforced concrete beams during fire tests*, s.l.: Report no. NBS-GCR-87-536. Center for Fire Research, National Bureau of Standards.

Losberg, A., (1964). *Anchorage of beam reinforcement shortened according to the moment distribution curve.*, s.l.: Seventh Congress of the IABSE, Final Report,<http://doi.org/10.5169/seals-7977>, pp. 383-392.

- Lundgren, K., (2002). *Steel-encased pull-through tests of seven-wire strands*, Sweden : Department of Structural Engineering Concrete Structures, Chalmers University of Technology, Report No. 02:13..
- Lutz, L., (1970). Analysis of stresses in concrete near a reinforcing bar due to bond and transverse cracking. *ACI-Journal*, pp. 778-787.
- Lutz, L., (1970). Information on the bond of deformed bars from special pull-out test. *ACI-Journal*, pp. 885-887.
- Malvar L. J., (1991). *Bond of Reinforcement Under Controlled Confinement*, California: Naval Civil Engineering Laboratory Port Hueneme, CA 93043-5003.
- Marti-Vargas, J., Serna, P. & Hale, W., (2013). Strand bond performance in prestressed concrete accounting for bond slip. *Engineering Structures*, Volume 51, pp. 236-244.
- Moore, W., (2008). *Performance of fire-damaged prestressed concrete bridges*, s.l.: Missouri University of Science and Technology, Masters Theses.
- Morley , P. & Royles, R., (1983). Response of the bond in reinforced concrete to high temperatures. *Magazine of Concrete Research*, 35(123), pp. 67 - 74.
- MORLEY P. D. and ROYLES R., (1979/80). The Influence of High Temperature on the Bond in Reinforced Concrete. *Fire Safety Journal*, pp. 243 - 255.
- Morley, P., (1982). *Effects of elevated temperature on bond in reinforced concrete*. s.l.:PhD Thesis, University of Edinburgh.
- Nielsen C. V. and Bicanic N., (2002). Radial fictitious cracking of thick-walled cylinder due to bar pull-out. *Magazine of Concrete Research*, 54(3), pp. 215-221.
- NUREG/CR-7031, (2010). *A compilation of elevated temperature concrete material property data and information for use in assessments of nuclear power plant reinforced concrete*. s.l.:U.S.NRC,Office of Nuclear Regulatory Research.
- ODBM, (2000). *The Building Regulations 2000: The Approved Documents:SI 2000/2531*, UK: s.n.
- Osterman, J., (1951). Proposed revisions to manual of standard practice for detailing reinforced concrete structures. *ACI-Journal*, pp. 349-351.

- Pantazopoulou S. J. and K. D. Papoulia K. D., Members, ASCE, (2001). Modeling cover-cracking due to reinforcement corrosion in rc structures. *Journal of Engineering Mechanics*, 127(4), pp. 342 - 351.
- Phan, L., McAllister, T., Gross, J. & Hurley, M., (2010). *Best practice guidelines for structural fire resistance design of concrete and steel buildings*, s.l.: National Institute of Standards and Technology, NIST Technical Note 1681.
- Pothisiri , T. & Panedpojaman, P., (2013). Modeling of mechanical bond–slip for steel-reinforced concrete under thermal loads. *Engineering Structures*, Volume 48, pp. 497-507.
- Pothisiri, T. & Panedpojaman, P., (2012). Modeling of bonding between steel rebar and concrete at elevated temperatures. *Construction and Building Materials*, Volume 27, pp. 130-140.
- Rehm, G., (1961). *On the fundamentals of steel-concrete bond*, Germany: s.n.
- Rivera, O. et al., (2016). Effect of elevated temperature on alkali-activated geopolymeric binders compared to portland cement-based binders. *Cement and Concrete Research* , Volume 90 , p. 43–51.
- Rombach, G., (2004). *Finite element design of concrete structures*. London: Thomas Telford.
- Russel, B. & Burns, N., (1993). *Design guidelines for transfer development and deboning of large diameter seven wire strands in pretensioned concrete girders*, Austin: The University of Texas, Research report 1210-5F.
- Sakai , T., Kanakubo , T., Yonemaru, K. & Fukuyama, H., (1999). *Bond splitting behavior of continuous fiber reinforced concrete members. Fiber Reinforced Polymer for Reinforced Concrete Structures.*, s.l.: ACI SP-188; 1131-1144..
- Tadros, M. & Morcous, G., (2011). *Impact of Large 0.7 in. Strand on NU-I Girders*, s.l.: Final Reports Technical Briefs from Mid-America Transportation Centre.
- Tepfers R., (1979). Cracking of concrete cover along anchored deformed reinforcing bars. *Magazine of concrete research*, 31(106), pp. 3-12.
- Tepfers, R., (1980). Bond stress along lapped reinforcing bars. *Magazine of Concrete Research*, 32(112), pp. 3-12.

- Tepfers, R., (1982). Lapped tensile reinforcement splices. *Journal of the Structural Division*, pp. 283-301.
- The Concrete Centre, (2006). *How to design reinforced concrete flat slabs using finite element analysis*, Surrey: The Concrete Centre, ISBN 1-904818-37-4.
- Timoshenko , S. & Goodier, J. N., 1951. *Theory of Elasticity*. s.l.:McGraw-Hill Book Company.
- Uijl, J. & Bigaj, A., (1996). *A bond model for ribbed bars based on concrete confinement*, s.l.: Delft university of technology, HERON, 41(3), ISSN 0046-7316.
- Valcuende M. and Parra C., (2009). Bond behaviour of reinforcement in self-compacting concretes. *Construction and Building Materials*, Volume 23, pp. 162-170.
- Vázquez-Herrero, C., Martínez-Lage, I. & Aguilar, G., (2013). Evaluation of strand bond properties along the transfer length of prestressed lightweight concrete members. *Engineering Structures* , Volume 49, pp. 1048-1058.
- Viwathanatepa, S., Popov, E. & Bertero, V., (1979). *Effects of generalized loadings on bond of reinforcing bars embedded in confined concrete blocks*, Berkeley: Earthquake Engineering Research Center, University of California, Report No EERC 79-22.
- Wang , X. & Liu, X., (2003). A strain-softening model for steel-concrete bond. *Cement and Concrete Research*, Volume 33, pp. 1669-1673.
- Watstein, D., (1947). Distribution of bond stress in concrete pull-out specimens. *ACI-Journal*, pp. 1041-1052.
- Welsh, W. & Sozen, M., (1968). *Investigation of prestressed reinforced concrete for highway bridges, Part V: Analysis and control of anchorage-zone cracking in prestressed concrete*, Urbana: University of Illinois.
- Xiao J. and Falkner H., (2007). Bond behaviour between recycled aggregate concrete and steel rebars. *Construction and Building Materials*, Volume 21, p. 395–401.
- Yu, X., Huang, Z., Burgess, I. & Plank, R., (2005). *Concrete spalling in fire: a review of the current state of knowledge.*, Sheffield: Department of Civil and Structural Engineering, University of Sheffield. Research report DCSE/05/F/04..

Zheng, W. & Hou, X., (2008). Experiment and analysis on the mechanical behaviour of PC simply-supported slabs subjected to fire. *Advances in Structural Engineering*, 11(1), pp. 71-89.